AGARD-AR-269

AGARD ADVISORY REPORT No.269

Fluid Dynamics Panel Working Group 12 on Adaptive Wind Tunnel Walls: Technology & Applications

(Les Souffleries à Paroi Adaptable: Technologies et Applications)

NORTH ATLANTIC TREATY ORGANIZATION

ADVISORY GROUP FOR AEROSPACE RESEARCH AND DEVELOPMENT

(ORGANISATION DU TRAITE DE L'ATLANTIQUE NORD)

AGARD Advisory Report No.269

Fluid Dynamics Panel Working Group 12

on

Adaptive Wind Tunnel Walls: Technology & Applications

(Les soufflerles à paroi adaptable: technologies et applications)

This Advisory Report was prepared at the request of the Fluid Dynamics Panel of AGARD.

The Mission of AGARD

According to its Charter, the mission of AGARD is to bring together the leading personalities of the NATO nations in the fields of science and technology relating to aerospace for the following purposes:

- Recommending effective ways for the member nations to use their research and development capabilities for the common benefit of the NATO community;
- Providing scientific and technical advice and assistance to the Military Committee in the field of aerospace research and development (with particular regard to its military application);
- Continuously stimulating advances in the aerospace sciences relevant to strengthening the common defence posture;
- Improving the co-operation among member nations in aerospace research and development;
- Exchange of scientific and technical information;
- Providing assistance to member nations for the purpose of increasing their scientific and technical potential;
- Rendering scientific and technical assistance, as requested, to other NATO bodies and to member nations in connection with research and development problems in the aerospace field.

The highest authority within AGARD is the National Delegates Board consisting of officially appointed senior representatives from each member nation. The mission of AGARD is carried out through the Panels which are composed of experts appointed by the National Delegates, the Consultant and Exchange Programme and the Aerospace Applications Studies Programme. The results of AGARD work are reported to the member nations and the NATO Authorities through the AGARD series of publications of which this is one.

Participation in AGARD activities is by invitation only and is normally limited to citizens of the NATO nations.

Published April 1990

ISBN 92-835-0558-1

Printed by Specialised Printing Services Limited
40 Chigwell Lane, Loughton, Essex IG10 3TZ

Preface

This report presents the results of a study by Working Group 12 of the Fluid Dynamics Panel of AGARD on adaptive-wall wind tunnels. The participants in WG12 represented Canada, France, Germany, Italy, Netherlands, Turkey, United Kingdom and United States.

The driving force in the development of adaptive-wall wind tunnels is the improvement of the accuracy of experimental results obtained in a wind tunnel of given size by virtually eliminating wall interference. This is achieved by the shaping of impermeable walls or adjusting the distribution of flow through ventilated walls to conform as nearly as possible to a stream-surface of the associated unconfined flow. Wall adaptation has become realistic through the development of fast computers. It represents an outstanding example of the symbiosis of experiment and computation.

Wall interference is most critical in the transonic speed range, on which, accordingly, the Working Group has concentrated its activities. The scope of WG12 is to review the history and state of the art of adaptive-wall technology, with regard to both the various streamlining algorithms and the existing adaptive-wall facilities; to discuss limitations and open questions of adaptive-wall methods and to compare them with passive-wall correction techniques; to assess residual wall interferences; to present the prospects for high-productivity and unsteady flow testing with adaptive walls; and to make recommendations for future developments.

The Working Group was first proposed by M.Laster (AEDC) and H.Hornung but, by the time it was approved, Laster was just leaving the Fluid Dynamics Panel. Unfortunately, it was also not possible to extend the membership of R.Kilgore (NASA Langley RC), who would have made an ideal chairman for the Working Group and has given extensive support to it throughout its term. The chairmanship thus devolved on H.Hornung, who was persuaded to stay on the Panel as a member for Germany for the duration of WG 12's activities, though he had moved to Caltech almost at the beginning.

The Working Group derived considerable benefit from the existence of the Newsletter "Adaptive Wall" published by NASA Langley RC. Clearly, this has provided an important vehicle for interchange of ideas in this field and it is hoped that it will continue to play this invaluable role.

The Working Group has held four meetings:

October 1987	Göttingen, Federal Republic of Germany
April 1988	Toulouse, France
October 1988	Ankara, Turkey
April 1989	Hampton, VA, United States

The participants were

J.P.Chevallier	France
C.Ciray	Turkey (FDP member)
J.C.Erickson, Jr	United States
H.Försching	Federal Republic of Germany (SMP member)
M.J.Goodyer	United Kingdom
H.G.Hornung	Federal Republic of Germany (FDP member, chairman)
C.L.Ladson	United States
A.Mignosi	France
M.Mokry	Canada
G.P.Russo	Italy
J.Smith	Netherlands
E.Wedemeyer	Federal Republic of Germany

Avant-Propos

Ce rapport présente les résultats de l'étude effectuée par le groupe de travail 12 du Panel AGARD de la Dynamique des Fluides sur les souffleries à paroi adaptable. Ont participé à ce groupe des représentants du Canada, de la France, de la Republique Fédérale d'Allemagne, de l'Italie, des Pays Bas, de la Turquie, du Royaume-Uni et des Etats Unis.

Le but recherché dans le développement des souffleries à paroi adaptable est d'améliorer la précision des résultats expérimentaux obtenus par une soufflerie d'une taille donnée en éliminant pratiquement tous les effets de paroi. Ceci est obtenu soit par le profilage de parois étanches, soit par la modulation de l'écoulement à travers des parois ventilées afin de reproduire au mieux une surface de courant de l'écoulement associé non confiné. L'adaptation de la paroi est devenue une possibilité grâce à la mise au point des ordinateurs rapides. Elle représente un exemple remarquable de la symbiose entre l'expérimentation et le calcul.

Les effets de paroi sont les plus critiques dans la plage des vitesses transsoniques et par conséquent, la plupart des activités du groupe de travail ont porté sur ce domaine. Le mandat du groupe de travail No.12 est le suivant:

- faire le point de l'historique et de l'état de l'art de la technologie des parois adaptables en particulier en ce qui concerne les différents algorithmes utilisés pour le calcul des lignes de flux.
- discuter des limitations imposées et des questions qui restent à résoudre dans le domaine des méthodes à parois adaptables, et d'en faire la comparaison avec les techniques de correction à parois passives.
- évaluer les effets de paroi résiduels.
- présenter les perspectives en ce qui concerne l'optimisation du rendement ainsi que la réalisation d'essais en écoulement instationnaire au moyen de parois adaptables.
- et faire des recommandations concernant les futurs travaux.

Le groupe de travail a été proposé à l'origine par M.Laster (AEDC) et M.Hornung mais l'approbation n'a été obtenue que tardivement au moment où M.Laster allait quitter ses fonctions auprès du Panel de la Dynamique des Fluides. Malheureusement, il n'a pas été possible non plus d'obtenir la prolongation du mandat de M.R.Kilgore (NASA Langley RC) qui eut été un président idéal et qui a soutenu ce groupe d'ailleurs tout au long de son existence. La présidence de ce groupe a donc été confiée à M.Hornung qui a été persuadé de rester au Panel en tant que membre représentant le RFA pendant la durée des activités du groupe de travail No.12, et ceci bien qu'il ait eu à assumer ses fonctions à Caltech conjointement avec le début des travaux du groupe.

Le groupe de travail a puisé librement dans le bulletin "Adaptive Wall" publié par NASA Langley RC. Cette publication sert de forum pour un échange de connaissances dans ce domaine et il est à espérer qu'elle continue à jouer ce rôle de toute première importance.

Le groupe de travail s'est réuni quatre fois:

octobre 1987	Göttingen, Republique Fédérale d'Allemagne
avril 1988	Toulouse, France
octobre 1988	Ankara, Turquie
avril 1989	Hampton, VA, Etats Unis

Les participants étaient:

J.P.Chevallier	France
C.Ciray	Turquie (FDP membre)
J.C.Erickson, Jr	Etats Unis
H.Förshing	Republique Fédérale d'Allemagne (SMP membre)
M.J.Goodyer	Royaume-Uni
H.G.Hornung	Republique Fédérale d'Allemagne (FDP membre, président)
C.L.Ladson	Etats Unis
A.Mignosi	France
M.Mokry	Canada
G.P.Russo	Italie
J.Smith	Pays Bas
E.Wedemeyer	Republique Fédérale d'Allemagne

Contents

1. The Aims and History of Adaptive Wall Wind Tunnels

Editor: M.J. Goodyer

Other Contributors: J.P. Chevallier, J. Erickson, M.C. Lewis (University of Southampton), P.B.S. Lissaman, H.H. Pearcey (NPL), E.W.E. Rogers (NPL), W.F. Hilton (NPL)

1.1 Introduction

The adaptive wall test section has its roots in the era when flight speeds were beginning to approach transonic on the level or in dives, that is the 1930's. The engineers who were charged with looking ahead to the aircraft designs of the near future, designs drawing on the most advanced technologies available, among their various challenges had to provide data on aerodynamic performance at the high speeds of projected military aircraft.

By the mid 1930's there was already a fund of experience available to some countries and design teams, notably arising from the Schneider competiton series which had just concluded, during which time fuels, piston engines with propellers, airframe structures and aerodynamics, had all advanced to a remarkable extent under the stimulus of competition. This is evidenced by the world speed record increasing by 50% during the decade to 1935, from Mach 0.38 to Mach 0.58 in level flight, with the record held much of the time by sea planes. In addition, although the records were set exclusively by piston engine powered propeller aircraft, various forms of jet propulsion were under consideration which were to emerge very soon in military service, such as the gas turbine based jet engine, the pulse jet and the rocket. Speed was a prime goal with war increasingly in prospect. The aerodynamicists had to attempt to provide experimental data at appropriately high speeds, speeds which varied between projects from high subsonic to supersonic.

During the following few years this climate spawned a variety of new wind tunnels. Quite quickly and relatively easily (albeit at rather a small scale because of the cost implications of the high levels of drive power) the supersonic needs were satisfied at Mach numbers upwards from about 1.4. The lower bound was set by the dual problems of wave reflection from the walls of the test section and the difficulty of starting a tunnel when using reasonably sized models. Tests at subsonic speeds in the main were carried out in tunnels of conventional design, that is in tunnels having convergent contractions and closed test sections. The upper limit in Mach number in these tunnels was typically around Mach 0.8, set by choking. Thus a dilemma emerged: a desire to acquire test information in a speed range, the transonic range, which evidently was unobtainable in the closed wind tunnel.

The unobtainable band of Mach number, say from 0.8 to 1.4, arose because of effects of the proximity of straight test section walls.

Rarely is there the absolute block to progress just suggested. The aerodynamicist could, and did, turn to several alternatives which were free from boundary restrictions, such as free-flight testing of various kinds, and the testing of models mounted on high speed sleds. However the quality of data thus derived was not of a high order and neither was it easily or cheaply obtained. There was strong pressure to modify the wind tunnel to allow tests to be performed at higher speeds than normal, in particular on aircraft models at speeds significantly above those reached by the latest fighters.

The decade following 1935 was punctuated by the appearance of a variety of designs of test section intended to make this upward extension.

The open-jet tunnel was quite commonly used in low speed testing and, when driven up to transonic speeds, was free from the choking phenomenon and therefore could reach the desired speeds in the airstream ahead of the model. However it did suffer a boundary interference, opposite in sign to that caused by a closed test section, arising from the finite size and boundary condition of the jet which introduced undesirable errors into the data. Furthermore the flow at the model was too unsteady and the technique was abandoned for application to this speed range.

1.2 The Emergence of the Adaptive Wall Test Section

The obvious alternative was to devise a test section which had boundaries which could be controlled so as to provide the required approximation to the free-air streamtube. This is what is now called the adaptive-wall test section, which made its appearance in the late 1930's as a direct result of the aerodynamic difficulties already described.

The object of this historical review is to place on record the more important steps in the evolution of the adaptive-wall test section in its various forms from these early times up to about 1975 when the first examples of all of the modern varieties were well on their way. Histories are always incomplete and inaccurate for a variety of reasons. For instance the volume of material to hand forces a distillation; facts are overlooked or become lost with the passage of time; the experience, information available to and the opinions of the author colour the choice of material to be presented. However it must be said that hitherto the reporting of the history of adaptive-wall wind tunnels has been characterised by more than its share of factual inaccuracies, but more seriously by errors of omission. It is hoped that this Chapter, assembled with the help of several of those closely involved in almost all stages of the evolution, will be judged to form a balanced and accurate record.

The development of adaptive-wall technology falls into two distinct and roughly 20-year-long eras, the first spanning the period from the mid 1930's to the mid 1950's, the second beginning around 1970 and continuing to the present.

The initial development took place among a group of engineers and scientists at the National Physical Laboratory in England, with the origins of the design traceable back at least to 1936. In that year a brief report appeared [Reference 1.1] in which the author, Dr. Gough of the Engineering Division of NPL, advocated the use of two flexible walls as means for reducing blockage effects in the high speed testing of two-dimensional aerofoil models. He reported that in a parallel-walled test section where Mach 0.95 had been reached when empty, the maximum was only 0.76 with a model present. Furthermore the Mach number

in the flow downstream of the model was noticeably higher. With some success he experimented with the use of fixed contoured liners in the test section to relieve the blockage, reaching Mach 0.83 upstream and downstream. To quote an important paragraph from the report on the work, "It would appear that a different modification of the tunnel profile would be required for each different aerofoil section and for each air speed. This suggests that it would be useful to employ flexible walls on two opposite sides of the tunnel. Flexible walls would also enable speed control to be exerted by means of a variable throat downstream of the model .....". A more expanded description of the tunnel and the experiments which led to this conclusion appeared in a widely available form [1.2] in February 1937. The tunnel was duly fitted with flexible walls and the first reports on tests appeared in November 1937 [1.3] and September 1938 [1.4].

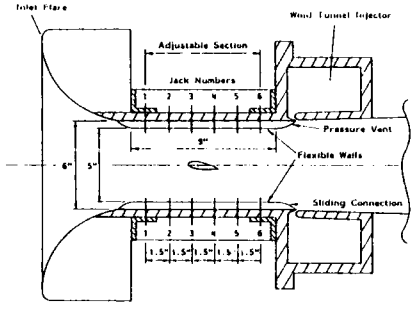

FIGURE 1.1 THE ORIGINAL ADAPTIVE WALL WIND TUNNEL, THE 5 INCH X 2 INCH TRANSONIC TUNNEL AT THE NPL, ENGLAND IN 1938

The first adaptive wall test section was 2 inches wide and 5 inches deep, the tunnel running at atmospheric stagnation conditions and driven by a compressed air injector. The narrower walls were made from flexible steel, 0.01 then later 0.015 inches thick, controlled by six equally spaced jacks on each wall. The developed form of this test section is sketched on Figure 1.1. During the first model tests, on three aerofoils with the walls crudely streamlined (evidently streamlining criteria had not yet been established), reference or free air Mach numbers up to 0.97 are recorded at zero incidence. As a result of experience with this small tunnel, opinions were formed on geometrical features including the desirable length of the test section and the jack spacing. The engineers not only showed that higher speeds could be obtained with a given model in a flexible tunnel rather than in a rigid tunnel, but also that the Mach number returned to the free air value downstream of the model. They noted and quantified a thickening of the wake [1.4] with increase of Mach number, in various tests from Mach 0.73 to 0.97, as evidenced by the size of the sonic throat which they were forming with the downstream jacks. The tunnel continued in use for many years and finished its days at Southampton University [1.5].

Almost immediately NPL built a larger adaptive wall tunnel, also induction driven, called the 20 by 8 inch and fitted with flexible walls along the 8 inch sides. In fact the test section was nominally 17.5 inches deep by 8 inches wide. This tunnel became a workhorse [1.6] and was running by May 1941 [1.7]. Most of the testing was of two-dimensional aerofoils. The standard model had a 5-inch chord and tests typically went up to Mach 0.85. Usually the measurements were of aerofoil pressure distributions and wake surveys, supplemented by shadowgraph, schlieren, and surface flow visualization. Under pressure of war they carried out an impressive amount of high speed aerodynamic work in this tunnel. To offer some perspectives, among the many jobs was a test on a section fitted with a 25 percent control surface where about 1000 complete pressure distributions were obtained, representing a considerable effort for the time. Work on 37 aerofoil sections is covered in 24 wartime reports [1.6].

Tests on various three-dimensional models are reported [1.6, 1.8], including bombs and the Meteor WWII jet fighter. The test arrangement for the fighter model is shown on Figure 1.2, and testing was concerned with the interaction of the flow from the wing brake-flaps with the horizontal stabilizer. To quote from the text covering this topic, "The flexible walls of the tunnel were used in each experiment to give conditions approximating to the free-air case".

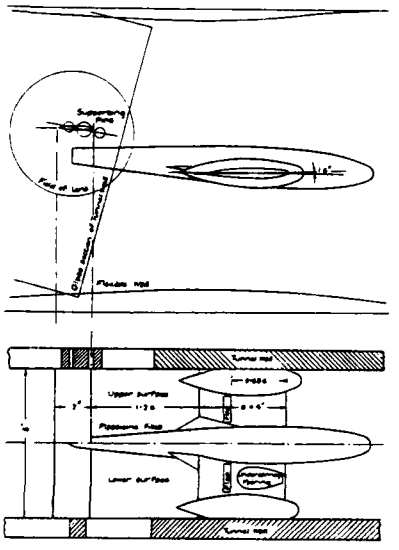

FIGURE 1.2. A GLOSTER "METEOR" WWII JET FIGHTER MODEL IN THE 20 X 8 ADAPTIVE WALL TRANSONIC TUNNEL AT NPL, ENGLAND

NPL also constructed a low speed flexible walled wind tunnel, having a 4-foot test section [1.9], which was running by 1944, evidently to gain large scale experience for an even larger tunnel which was never built.

The 20 by 8 inch transonic adaptive wall wind tunnel continued in service until around 1954 when it was supplanted by ventilated types, which were becoming the standard partly because ventilation was then believed to offer an interference-free environment and partly because, by adjusting automatically to changes of model or flow, they were much more convenient to use. It is interesting to note that in tests reported in 1951 [1.10], leading to the adoption of ventilation by NPL, the 20 by 8 inch tunnel was used as the standard by which the new ventilated designs were judged, because the blockage in the adaptive wall tunnel ".... is thought to be negligible."

As has already been suggested, the hypothesis underlying the adaptive wall test section is that a model is free from wall interference when tested inside a finite streamtube which coincides with a streamtube in free air around the same model. In two-dimensional flow in an impervious test section a pair of walls needs to follow a convenient pair of streamlines.

At the formative stage NPL were concerned with two-dimensional tests as has been seen, and the process of choosing a pair of wall contours which could be accepted as

representing streamlines in free air required the development of a convenient and practical streamlining algorithm. Their introduction by NPL seems to have progressed through three stages. The first was that used in the very earliest tests in the 5" by 2" tunnel [1.4] where the method of streamlining the walls, when the test section was empty or contained a model, was to adjust the contours " ... so as to give the least possible variation in static pressure near the walls, this being taken to represent a near approach to free-air conditions." The principal aim of the adaptive wall test section at this time was to relieve blockage, solid and wake.

This algorithm was replaced [1.7] by a method somewhat later attributed [1.11] to an unpublished theory by Sir Geoffrey Taylor. To quote [1.7] "It is intended to adjust the walls, when making measurements on an aerofoil, to positions half way between the taper that gives uniform pressure in the empty tunnel and that giving uniform pressures in the presence of the aerofoil. Theoretically - though not allowing for compressibility effects which may be assumed second order, at least until shock waves supervene - the walls should then very nearly correspond to streamlines surrounding the aerofoil in free air."

The third stage is detailed analytically in a 1944 report [1.12] under "Original Method for Finite Lift." The modification to the second method arose because the necessary step of adjusting for constant equal pressures along both walls was only possible, when lift was present, by bending the axis of the tunnel through a finite angle. This was not possible with their geometry of test section and the alternative scheme was adopted of adjusting the walls to constant pressures differing on the two walls by an amount depending on lift. The walls were then set to positions half way between these contours and the straight. The fourth stage of development is given in the same report [1.12] under "Revised Method of Wall Setting" where the principal change was to set 0.6 of the mean constant-pressure displacement from straight, modified by an amount calculated to allow for the deflection of the infinite flowfield by the lift. The lift was obtained from model pressure plotting or from wall pressures.

It should be mentioned here that two researchers who were heavily involved with using the 20 by 8 tunnel from around 1942 onwards (Dr. E.W.E. Rogers and Professor *H.H. Pearcey*) stated in recent discussions that they did not recall the use of the fourth stage. Their recollection was of the third stage algorithm, but with the walls moved 0.6 of the way towards constant pressure.

The streamlining criteria used by NPL were based on the outcome of analyses of potential flowfields. Computations of imaginary flowfields coupled with the iterative convergence to streamlines, a feature of most modern adaptive wall operations, would have been too laborious to contemplate. It is ironic that binary code electronic digital computers were in regular use for deciphering at that time just 50 miles away at Bletchley Park, but were highly classified and not available for general use.

The aim of these researchers, to make the walls of the test section follow closely the streamlines which would have existed in their locations when the model was immersed in an infinite flowfield, forms a common and principal thread throughout the development of adaptive wall techniques. Further, as aerodynamic testing is taking place because viscous flows cannot be computed reliably, no attempt is made to compute the shapes of streamlines around a model.

Several of those at NPL during this period (Dr. Rogers, Professor Pearcey and Dr. W.F. Hilton) drew attention to a constructional feature of the 20 x 8 tunnel which, with the benefit of hindsight, can be seen to have had an aerodynamic consequence. The two flexible walls were each formed from three longitudinal strips of steel, 0.02 inches thick. The ability of this material to withstand an aerodynamic load was recognised as being limited and therefore some pressure relief was built into the design of the tunnel. Thus, in practice, the test section region was vented to plenum chambers lying behind the flexible walls, and the venting took the form of longitudinal slots, 0.02 inches wide [1.13], between each strip and also along the edges where the flexible walls approached the rigid sidewalls. The four slots thus formed had an open area ratio of about 1%. It was noted [1.14] that the choking Mach number with straight walls was higher than expectation but at that time the phenomenon was not associated with the existence of the slots. Their significance in this respect became apparent only after slotted test sections emerged for transonic testing.

It was discovered at the end of the war that a large transonic wind tunnel had been built in Germany (at Ottobrunn near Munich) variously described as having a 3 metre [1.15], 9 foot [1.16] and 7 foot [1.17] test section with flexible walls at the top and bottom, adjusted by screw jacks. The second of these references states that "Although the possibility of modifying wind tunnel corrections in this way had been borne in mind, the main object of the Munich tunnel was rather to control the position of the shock-wave to a point in the tunnel well downstream of the model, by introducing a throat there. In this way, speeds much nearer the speed of sound at the model were anticipated ...". The tunnel was complete but had run only for five hours, reaching Mach 0.85. From the foregoing it seems possible that, given time, the users of this tunnel might have gradually developed interference-alleviation methods.

In France a small wind tunnel [1.18] was operated using more-or-less adaptive principles. The sonic wind tunnel of the Fluid Mechanics Institute of Lille (IMFL), built in 1948, had a rectangular test section (0.04m x 0.24m x 0.6m) equipped with deformable top and bottom walls (seven jacks for each wall).

To be used in the transonic range this wind tunnel was fitted with two slotted walls and two deformable counter-plates behind them to control the secondary flow in the plenum chamber. To determine the best adjustment of the counter-plate shape, two similar models were used. During a first test with a small model, a great number of pressure measurements on the lateral wall gave the Mach number distribution on the line corresponding to the wall relative position for a larger model. During a second test with the large model in the test section, jack positions may be found to obtain the same Mach number distribution along the floor and ceiling.

The same device and this method are also used in a wind tunnel of the St. Cyr Institute.

While the NPL adaptive wall tunnels continued in service for another ten years until the mid 1950's, as far as the evolution of adaptive wall techniques is concerned there is little more to report aside from some NPL tests, at Mach numbers up to unity, on swept wing panels spanning the test section [1.19, 1.20].

1.3 The Beginnings of the Modern Era, c.1970 to 1975

Between the two periods of activity on adaptive walled wind tunnels there were about 15 years when the ventilated designs were used exclusively and very widely in transonic testing. Work of any kind with the flexible walled wind tunnels was discontinued. However the early hopes for zero wall interference with ventilated test sections were not realised and the practice developed of estimating and applying corrections to the measured data. Sometimes the corrections were disturbingly large in the light of the uncertainties of the boundary conditions, notably in tests near to the speed of sound with three dimensional models and more generally in two dimensional testing. Simultaneously the standards desired from tunnel data were rising and the various sources of imperfection in the test environment came under scrutiny, including high turbulence and noise, low Reynolds number, support interference as well as wall interference. In two research establishments at least, [1.21, 1.22], there was also concern over the volume of the plenum chamber which is a feature of ventilation. This environment led to the emergence of the Adaptive Wall.

The aims of the new designs of test section were now somewhat different, coloured by the experiences of recent times. The dominant aim remained the control of wall interference at high subsonic speeds which drove NPL to the adaptive wall in the first instance, but in some cases the aims now included new but lower priority features. The elimination of the plenum is one example. The reduction of turbulence by the elimination of ventilation is another. In all cases the groups devised new wall streamlining algorithms based on the computational methods now available, which allowed the quantification as well as the reduction of interference.

The development of new test sections proceeded with two-dimensional models as test articles, in test sections having two plane walls and two walls modified to the adaptive mode.

In reading the following accounts of events the total dominance at that time of the ventilated test section should be borne in mind, also that the generation of aerodynamicists which had struggled with alternatives before adopting ventilation and who were familiar with some of those alternatives, had moved on, quite often into retirement. It may not be excusable but the younger researchers addressing the above problems were not aware of the other transonic test section design options which had already been investigated. They began to reinvent. This despite the fact that unclassified material was readily available describing the alternatives. It seems likely that genuine reinvention occurred in several places over a few years centered on about 1970, more-or-less simultaneously and more certainly independently. That is not to suggest that the modern tunnels do not feature any originality, quite the contrary. A common feature of the modern wind tunnels was the computation of inviscid flowfields exterior to the test section, a subject which is expanded upon in Chapters 3 and 4.

At that time there were various phrases used to describe the concepts but which have now fallen from use, such as Self Correcting and Self Streamlining. From hereon in this report the concepts will be grouped under the more familiar Adaptive Wall heading.

In the light of the independence of actions it is not proposed to explore the contentious issue of claims for which person or which organisation was the "first", partly because a claim would depend on the measure, such as the first to propose or the first to build. It appears that six researchers were involved as principals in this period. Following is a brief chronology of events derived from discussions and publications. The order in which they are presented is alphabetical. The institutions are those with which they were associated at the time.

J.P. CHEVALLIER, ONERA

In 1970 the AGARD expert's meeting on "engine airplane interference in transonic tests and wind tunnel wall interference for airplane with lift in transonic tests" showed clearly the state of the art and its drawbacks.

Working on this subject Professor Chevallier tried to overcome the Mach number limitation inherent to the linear theory by using a small transonic perturbation code, following the publications of Murman and Cole [1.23], Krupp [1.24], it was provided by Chattot and published later [1.25].

To compute the perturbation field due to the wall, the difference between the streamlines in the unlimited and limited flows was introduced at the wind tunnel boundary [1.26]. This promised to take into account the real behaviour of the transverse component of the flow even with the development of boundary layers along perforated walls, but it became evident that an active control of the transverse flow was necessary to reduce the interference. Since the code used to compute the airfoil field provided numerically the functional relationship between the two perturbation components as well in an external flow field extended without limits, the complete concept of the active boundary control was proposed in a short internal note in July 1972 [1.27].

The different means for applying the new concept with perforated or solid walls was discussed but without any proof of convergence of the iterative adaptation process.

During the end of 1972 and the beginning of 1973, as it was requested to demonstrate the feasibility of transonic tests with adaptation, a numerical simulation was attempted and almost a year was devoted to this tedious task, since the internal flow field computations had a poor convergence.

From the end of 1973 to mid 1974 a small wind tunnel (S4LCh-ONERA Chalais-Meudon) was equipped with two deformable walls [1.28]. The tests performed during autumn 1974 on an existing model (NACA 64A010 at M = 0.866) led to positive conclusions.

These encouraging results were presented at an AGARD Mini-Laws Group Symposium on the transonic test section (ONERA - France 5-6 Sept. 1974) [1.29], and also at the "Groupe Sectoriel Franco-Sovietique Aeronautique" in November and during a technical discussion on 10 December 1974.

From the end of 1974 to mid 1975 more experience was acquired by using in S4LCh the NACA 64A010 airfoil at 6^{o} of angle of attack and different Mach numbers and the following topics were studied: how to define the reference conditions without an empty tunnel calibration, how to work with an internal supersonic region extending from wall to wall, what are the consequences of some defects of adjustment.

In October 1975, J.P. Chevallier presented the paper "Soufflerie transsonique à parois auto-adaptables" at the AGARD Symposium on Wind Tunnel Design and Testing Techniques in London [1.28]. This paper included all the results of the initial demonstration experiments.

Antonio FERRI, New York University

An AGARD report of December 1972 contains the statement [1.30 p22] by Ferri that he proposed a concept of adaptive walls in 1970, the statement suggesting that he might have in mind the notion of variable porosity. To quote " we can change locally the porosity at the wall in order to decrease the interference, provided we are capable of analyzing what happened " This was made at a point in a discussion where attention had been drawn to the severe interference existing in ventilated test sections at speeds close to Mach 1, which was limiting the size of models and therefore attainable Reynolds numbers. Reduction of interference was seen as a way to relieve the problem.

In January 1973 an article appeared in the AIAA Journal [1.31] in which he gave the theoretical outline of a general correction method for ventilated transonic test sections. He forecast two alternative applications: the determination of porosity characteristics which eliminate interference or the calculation of wall corrections. The application of the analysis would require the experimental determination of streamline deflection and pressure near the tunnel walls.

In February 1973 Ferri and his co-workers issued a preliminary report [1.32] on tests carried out in a 15-inch square slotted test section at the Flight Dynamics Laboratory, under contract to the AFOSR and ONR. Two-dimensional circular arc sections were tested at zero angle of attack and the Mach numbers of 0.91 and 0.95, with measurements of their pressure distributions. Measurements were also made of static pressure and flow angularity using probes positioned inside the test section near the walls. The data allowed estimates to be made of the required wall porosity, or the variation in tunnel cross sectional area, required for interference-free flow. The research effort was continued [1.33], still using ventilation by means of longitudinal slots, with the test conditions extended to include lifting cases.

The wall interference was modified by adding strips of tape to approximate to a contour calculated from measurements to give zero interference at zero angle of attack

Michael J. GOODYER, NASA Langley Research Center and Southampton University

Magnetic suspension systems for wind tunnels were in use at small scales at that time for testing three dimensional models at subsonic speeds and up to hypersonic speeds but excluding the transonic range above about Mach 0.8. A group at Langley Research Center were reviewing future work on the development of magnetic suspension and addressed transonic testing. A major concern with the transonic speed range was the size and cost of the levitating electromagnets positioned around the test section These dominate system cost which becomes a strong function of the air gap between the magnets and the model, and the dynamic pressure of tests. The plenum chamber, associated with all transonic tunnels at that time, increased the air gap and therefore cost predictions at a time when the testing community was striving for much higher Reynolds numbers, itself driving up scale, dynamic pressures and cost.

Goodyer reviewed the reasons for the slotted test sections in use at Langley Field and came to the conclusion that they and their plenum chambers could be replaced in principle by suitably contoured solid walls, thus allowing the electromagnets to be positioned more closely to the model The idea was quickly embodied in the simpler alternative of two-dimensional testing for immediate experimental exploitation, the ideas being placed on record at Langley Field during July 1972 ("Transonic Test Section Design", 10 July 1972, and "Self-Adapting Flexible Test-Section Walls", 14 July 1972 [1.34]).

An existing low speed wind tunnel having a square test section was modified during the first part of 1973. The modifications were for two-dimensional tests and comprised the installation of two flexible walls top and bottom inside the normal walls, controlled by manual jacks, and the addition of a suitable contraction to the flexible walls. Wall streamlining was performed first for the flow around a high blockage (22%) circular cylinder in June 1973 then around a lifting aerofoil during July 1973, using an HP desktop computer for the streamlining computations. A photograph taken of the aerofoil model and streamlined walls during this series of tests has been published [1.35].

In the period 1973 to 1975 the tunnel continued to be used, and modified in the light of experience, for aerofoil testing and for tests with a higher blockage (29%) circular cylinder [1.21]. NASA built a two-dimensional aerofoil model of NACA 0012-64 section and 5.4 inch (13.72cm) chord. This was tested at appropriate Mach and Reynolds numbers in the 7½-feet (228 6cm) deep Low Turbulence Pressure Tunnel to provide interference-free performance data. The model was then used at Southampton in tests in the much shallower 6 inch (15.2cm) adaptive wall tunnel. During this period also a tunnel was built [1.36] for creating cascade flow around a single turbine blade, and plans were laid to commence the construction of an automated two-dimensional transonic tunnel under NASA Grant. The low speed experiences were summarised at the AGARD 1975 meeting [1.37].

Peter LISSAMAN, Northrop Corporation

From around 1967 Dr. Lissaman had been considering the problems of wall interference at low and transonic speeds. He formed the opinion that some form of control over boundary conditions was required which led him to produce a research proposal [1.38].

In this document he reviewed older ideas (but evidently was unaware of the NPL work) and drew attention to a Louvre scheme for use in the relief of jet/wall interference [1.39]. He listed as difficult to correct (or impossible in severe circumstances) several flow types including strong separation, reflected waves and multi-energy flows. He proposed streamlining criteria for infinite flowfields as well as the less conventional circumstances of the sheared wing, cascade, ground effect and free jet. He discussed in analytic terms the outlines of methods to determine, in an iterative manner, the adjustment of the shape of an impervious test section leading progressively to low levels of interference. His research proposal was for a paper study of the methods initially, followed in due course by phases of further development leading to two and three dimensional experimentation. He seriously considered the prospects for patent protection.

There is no evidence available suggesting that the contract was awarded. However the documentation does serve very well to highlight the fact that the adaptive wall test section ideas which emerged in this era were far from being confined to any one person.

Paul RUBBERT, The Boeing Company

The motivation behind Rubbert proposing the adaptive wall test section was a 1970 aircraft project at Boeing, the Advanced Transonic Transport designed for around Mach 0.98. He was aware of the poor test data emerging from ventilated tunnels at this Mach number and wished to employ a new principle.

He concerned himself mainly with three-dimensional testing, this being the prime interest of his employer. A draft of a paper outlining his proposals entitled "A General Concept for Elimination of Wind Tunnel Wall Interference with Emphasis on STOL" (22p, 9 Figs.) emerged in 1972 and is held on record by NASA at Langley Field. In the report he outlined the need for active control of the tunnel wall contour, or the inflow distribution for a permeable wall. He discussed applications to STOL, high subsonic and transonic three-dimensional testing, and high lift and transonic airfoil testing, and gave streamlining criteria.

Rubbert visited Langley Field in 1973 and gave a presentation with viewgraphs (also held by NASA) extending his ideas particularly with respect to two-dimensional testing. Notable among the ideas presented was the outline of a method for rapidly converging impermeable walls to streamlines in two-dimensional testing, together with a method for calculating residual wall interference corrections for an imperfectly set wall. This method was later proposed independently and then developed by Judd [1.40] who found that the underlying analysis needed modification because of wall divergence problems arising from an aerodynamic coupling between the two flexible walls. The methods are in regular use in at least three adaptive wall wind tunnels [1.40 - 1.42], under the computer code name WAS1.

It is unfortunate that Rubbert was not able to proceed to the hardware stage.

William SEARS, Cornell University

Dr. Sears attended the AGARD meeting on high Reynolds number facilities in Göttingen during April 1971 and began to reconsider transonic wall interference. Shortly thereafter, he contacted Calspan (then Cornell Aeronautical Laboratory) with the adaptive-wall concept, which he initially called a "Self-Adjusting Wind Tunnel". Calspan personnel, principally Dr. Alfred Ritter, Dr. John C. Erickson, Jr., and the late Robert J. Vidal, with Dr. Sears as a consultant, proposed a theoretical feasibility study to the Office of Naval Research (ONR). The ONR contract was awarded to Calspan in November 1971.

The aim of the concept in the Sears/Calspan approach was to improve upon existing ventilated-wall capabilities so that reliable, interference-free data could be obtained at higher transonic Mach numbers than was possible at that time. From the beginning the Sears/Calspan implementation was planned using perforated walls, basically like those of the Calspan Eight-Foot Transonic Tunnel, but with adjustable wall porosity and/or plenum pressure. The plans were to demonstrate the fundamental validity and feasibility of the concept experimentally, as

quickly as possible, in two dimensions. Then attention could be turned to three-dimensional test sections for testing typical flight vehicles

The fundamental principle of the Sears adaptive-wall concept is that interference-free flow can be verified by obtaining agreement at the interface (control surface) in the distributions of two independent flow disturbance quantities as measured and as calculated by the exterior flow functional relationships between the two quantities.

From late 1971 to spring 1972 many discussions were held with U.S. Navy (ONR), Air Force (AFOSR, AEDC, Flight Dynamics Laboratory) and NASA (Langley Research Center) personnel concerning the concept and its implementation. These led to a proposal for an experimental demonstration in two dimensions using the Calspan One-Foot Transonic Tunnel. This included the design and fabrication of a new adaptive-wall test section with the associated equipment. During this period (in January 1972 at the AIAA 10th Aerospace Sciences Meeting) Sears gave an outline of his proposed principles [1.30, p21]; he also proposed his original ideas on application of the adaptive-wall concept to the high lift and large flow deflections that are typical of V/STOL testing, later brought to fruition at the University of Arizona.

In June 1972 a contract addition was awarded to Calspan for test section design and fabrication so that an experimental demonstration could be performed. Funding was provided jointly by the ONR and the Air Force Office of Scientific Research. Work proceeded during the following year on test section design, an instrumentation investigation and the development of exterior flow calculation procedures for both linearized subcritical and nonlinear transonic small disturbance representations of the flow. Numerical demonstrations of the adaptive-wall iterative procedure in subcritical [1.43] and supercritical [1.44, 1.45] flow were performed

The following two years saw the appearance of hardware. Tests on a NACA 0012 airfoil model were carried out in the Calspan Eight-Foot Transonic Tunnel to acquire reference two-dimensional data that are considered to be free of wall interference [1.46]. Fabrication of the adaptive wall test section, its checkout and empty-tunnel calibration, instrumentation development, operational investigations and hardware modifications were performed. During this time several meetings were held with personnel from ONR, AFOSR, AEDC, Air Force Flight Dynamics Laboratory, NASA (Ames and Langley Research Centers), and Advanced Technology Laboratories. The adaptive-wall concept and implementation were discussed extensively in a Workshop Meeting on Transonic Tunnel Wall Interference Effects at NASA Langley Research Center in May 1974. In April 1975 additional funding to complete the initial demonstration experiments was received from NASA Langley Research Center

A separate contract was awarded by NASA Ames Research Center in May for a preliminary low-speed, three-dimensional adaptive-wall investigation with V/STOL testing as the ultimate application [reported later in 1.47].

Robert J. Vidal presented the paper, "Experiments with a Self-Correcting Wind Tunnel", at the October 1975 AGARD Symposium on Wind Tunnel Design and Testing Techniques in London [1.45]. This paper included results of initial demonstration experiments.

1.4 References

1.1 Gough, H.J. The Development of a Rectangular High Speed Induced Wind Tunnel. ARC 2721. November 1936.

1.2 Bailey, A. and Wood, S.A. The Development of a High Speed Induced Wind Tunnel of Rectangular Cross Section. British ARC R&M 1791. February 1937. In Technical Report of the Aeronautical Research Committee, 1937. Vol 2, pp. 1304-1318

1.3 Aerodynamics Division, N.P.L. Further Development of a Rectangular High Speed Induced Wind Tunnel. ARC 3260. November 1937

1.4 Bailey, A. and Wood, S.A. Further Development of a High Speed Wind Tunnel of Rectangular Cross-Section. British ARC R&M 1853, Sept 1938. In: Technical Report of the Aeronautical Research Committee, 1938, Vol. II, pp. 753-768

1.5 Cobb, S.M. The Interference due to the Walls of a Two-Dimensional Wind Tunnel with some Attempts to Reduce it. M.Sc. Thesis, Aeronautical Engineering Department, University of Southampton, England. March 1953.

1.6 Holder, D.W. The High-Speed Laboratory of the Aerodynamics Division, N.P.L - Part I, II and III. British ARC R&M 2560. December 1946. Later issued as a British ARC Monograph R&M 2560, 1954.

1.7 Beavan, J.A., and Hyde, G.A.M. Interim Report on the Rectangular High-Speed Tunnel including Some Pitot Traverse Measurements of Drag of the Aerofoil EC 1250. British ARC R&M no. 2067. February 4 1942

1.8 Pruden, F.W. Tailplane observations on a model of F9/40 at high speeds. ARC 6662, April 1945

1.9 Preston, J.H., Sweeting, N.E. and Cox, D.K. The Experimental Determination of the Two Dimensional Interference on a Large Chord Piercy 12/40 Aerofoil in a Closed Tunnel Fitted with a Flexible Roof and Floor. British ARC R & M 2007. September 1944.

1.10 Holder, D.W., North, R.J. and Chinneck, A. Experiments with Slotted and Perforated Walls in a Two-Dimensional High Speed Tunnel. British ARC R&M 2955. November 1951.

1.11 Beavan, J.A. and Hyde, G.A.M. Compressibility Increase of Lift and Moment on EC 1250 for Low Speed C_L 0.17. British ARC R&M 2055. September 1942.

1.12 Lock, C.N.H. and Beavan, J.A. Tunnel Interference at Compressibility Speeds Using the Flexible Walls of the Rectangular High-speed Tunnel. British ARC R&M 2005. September 1944

1.13 Hilton, W.F. and Fowler, R.G. Use of the 20 in. x 8 in. High Speed Tunnel (Fitted with Flexible Walls) at Supersonic Speeds. National Physical Laboratory report NPL/Aero/138, 28 March 1946

1.14 Beavan, J.A. Limiting Mach Number for Aerofoil Tests in the 20 in. by 8 in. Rectangular High Speed Tunnel. British ARC 8720, May 1945

1.15 Hartshorn, A.S. and Squire, H.B. Notes on a Visit to Southern Germany, Aug 10-22 to Investigate German Aerodynamic Research on Cooling Ducts. RAE TN Aero 1694, May 1946.

1.16 Smelt, R. A Critical Review of German Research on High-Speed Airflow. The 696th Royal Aeronautical Society Lecture. October 1946. In: RAeS Journal, vol. 50, December 1946, pp 899-934.

1.17 Goethert, B.H. Transonic Wind Tunnel Testing. AGARDograph 49. Pergamon Press, 1961.

1.18 Martinot-Lagarde, A., Gontier, G. and Nguyen Van Quy. Sur la realisation dans une veine de soufflerie transsonique des contitions de milieu illimité. C.R.Ac.Sc. Paris 9 Mai 1960

1.19 Lock, C.N.H. and Fowler, R.G. Yaw and Sweep-back at High Mach Numbers. British ARC 8718. May 1945

1.20 Beavan, J.A. and Bumstead, N. Test on Yawed Aerofoils in the 20 x 8 in. High-Speed Tunnel. British ARC R&M 2458. July 1947

1.21 Goodyer, M.J. The Self Streamlining Wind Tunnel. NASA TM-X-72699. August 1975.

1.22 Schueler, C.J. Experimental studies in a Ludwieg Tube Transonic Tunnel. In VKI Lecture Series 52, Belgium. January 1973.

1.23 Murman, E.M. and Cole, J.D. Calculation of plane steady transonic flows. BSRL D182 0943. January 1970.

1.24 Krupp, J.A. The numerical calculation of plane steady transonic flows past thin lifting airfoils. BSRL D180 129581. June 1970.

1.25 Chattot, J.J. Petites perturbations transsoniques. Recherche Aerospatiale. No. 1975-5.

1.26 Chevallier, J.P. Calcul des corrections de parois en soufflerie transsonique. 9eme Colloque AAAF. Paris 9 November 1972.

1.27 Chevallier, J.P. Corrections de parois en transsonique. N.T. 4/1865 AN. Juillet 1972.

1.28 Chevallier, J.P. Soufflerie transsonique a parois auto-adaptables. AGARD CP 174, 1976.

1.29 Chevallier, J.P. Soufflerie transsonique auto-correctrice. AGARD Mini-Laws group meeting ONERA-France. 5-6 September 1974.

1.30 Lucasiewicz, J. (Ed.) Aerodynamic Test Simulation: Lessons from the Past and Future Prospects. Agard Report 603. December 1972.

1.31 Ferri, A. and Baronti, P. A Method for Transonic Wind Tunnel Corrections. AIAA Journal, vol. 11 no. 1. January 1973. pp. 63-66.

1.32 Baronti, P., Ferri, A. and Weeks, T. Analysis of Wall Modification in a Transonic Wind Tunnel. ATL-TR-181. AFOSR-73-1900. TR February 1973.

1.33 Weeks, T.M. Reduction of transonic slotted wall interference by means of slat contouring. AF FDL-TR-74-139, March 1975.

1.34 Goodyer, M.J. and Wolf, S.W.D. Development of a Self Streamlining Flexible Walled Transonic Test Section. AIAA Journal, vol. 20 no. 2. February 1982. pp. 227-234.

1.35 Baals, D.D. and Corliss, W.R. Wind Tunnels of NASA. NASA SP-440, 1981, page 139.

1.36 Wolf, S.W.D. Turbine Blade Cascade Testing in a Flexible-Walled Wind Tunnel. Project for B.Sc. Honours Degree in Aeronautical Engineering, University of Southampton, Apr. 1975.

1.37 Goodyer, M.J. A Low Speed Self Streamlining Wind Tunnel. Presented at the Symposium on 'Wind Tunnel Design and Testing Techniques,' London, England. October 6-8, 1975. In. AGARD-CP-174, March 1976, paper no 13.

1.38 Lissaman, P.B.S. Feasibility study of interference free wind tunnel. NCL 70-52P. Northrop Corporate Laboratories, 1970.

1.39 Kroeger, Richard A. and Martin, Walter A. The Streamline Matching Technique for V/STOL Wind Tunnel Wall Corrections. AIAA Paper No.67-183, January 1967.

1.40 Wolf, S.W.D. and Goodyer, M.J. Self Streamlining Wind Tunnel. Low Speed Testing and Transonic Test Section Design-Semiannual Progress Report, April 1976 - December 1976. NASA CR-145257, October 1977.

1.41 Goodyer, M.J. and Wolf, S.W.D. The Development of a Self-Streamlining Flexible Walled Transonic Test Section. Presented at the AIAA 11th Aerodynamic Testing Conference, Colorado Springs, March 18-20, 1980. In: Technical Papers, CP801 (A80-26929). pp. 325-335. Also AIAA Journal, vol. 20, no. 2 February 1982, pp. 227-234.

1.42 Wolf, S.W.D. and Goodyer, M.J. Predictive wall adjustment strategy for two-dimensional flexible walled adaptive wind tunnel - a detailed description of the first one-step method. NASA CR-181635, January 1988.

1.43 Erickson, J.C. Jr. and Nenni, J.P. A Numerical Demonstration of the Establishment of Unconfined-Flow Conditions in a Self Correcting Wind Tunnel. CALSPAN-RK-5070-A01. November 1973.

1.44 Vidal, R.J., Erickson, J.C. Jr. and Catlin, P.A. Experiments With a Self-Correcting Wind Tunnel. Presented at Symposium on 'Wind Tunnel Design and Testing Techniques' London, England. October 6-8 1975. In: AGARD-CP-174 (N76-25213#). March 1976, paper no. 11.

1.45 Sears, W.R., Vidal, R.J., Erickson, J.C. Jr. and Catlin, P.A. Self-Correcting Wind Tunnels: Concept and Demonstration (two reprints). CALSPAN-RK-5070-A-4. October 1975.

1.46 Vidal, R.J., Catlin, P.A. and Chudyk, D.W. Two-Dimensional Subsonic Experiments With a NACA 0012 Airfoil. CALSPAN-RK-5070-A-3. December 1973.

1.47 Erickson, J.C. Jr. Application of the Adaptive Wall Concept to Three-Dimensional Low-Speed Wind Tunnels. NASA CR-137917. CALSPAN-RK-5717-A-1. September 1976.

2.0 FACILITIES

Editor: C. L. Ladson

2.1 Introduction

During the first meeting of the Working Group, it was apparent that the assessment and interpretation of the current level of the technology could be achieved most easily if the investigators themselves provided the information in a common format. This would also minimize any danger of misinterpretation by third parties of existing published information. As a result, the Group developed a questionnaire and distributed it to all involved in adaptive wall research.

The questionnaire solicited information on the mechanical details of the facilities as well as details of the adaptation strategy itself. The scope of testing accomplished and future plans were included. The information contained in the responses is summarized in this and subsequent chapters. This information was the source for much of the data in this report. Because some of the data contained in these questionnaires is not discussed elsewhere, they are reproduced in their entirety as an Appendix to this report. The questionnaire is also presented to serve as a guide to the written responses.

2.2 List of facilities included:

This section of the chapter presents a list of all facilities for which data has been received.

Belgium	VKI	TWT S1
France	ONERA	S4 L Ch
	ONERA	S5 Ch
	ONERA/CERT	T2
Germany	DFVLR	DAM
	DFVLR	HKG
	DFVLR	TWG
	Technical University of Berlin	TUB (2D)
	Technical University of Berlin	TUB (3D)
Italy	University of Naples	AWWT
Peoples Republic of China	Northwestern Polytechnical University	NPU AWWT
United Kingdom	National Physical Laboratory	5 x 2 in.
	National Physical Laboratory	20 x 8 in.
	University of Southampton	Cascade Blade Tunnel
	University of Southampton	SSWT
	University of Southampton	TSWT
United States	AEDC	1T
	AFWAL/FDL	9 in. Pilot
	Calspan/ATC	1 ft.
	NASA/Ames Research Center	25 x 13 cm
	NASA/Ames Research Center	2 x 2 ft
	NASA/Langley Research Center	0.3-m TCT
	Sverdrup Technology	AWAT
	University of Arizona	HLAT

2.3 Description of facilities:

This section of the chapter presents a brief description of each facility along with a sketch or photograph. The current status of the facility is also given.

It is appropriate to mention at this time that many of the facilities listed herein are no longer operational or are operated only on a limited basis. This is a result of the technology development status of these facilities. They were constructed to demonstrate the validity of a concept or operational technique. When this was successfully demonstrated, the facility had fulfilled the design purpose and was delegated to other research areas. Several of the facilities are in the graduate departments of universities and used only when needed to meet the testing needs of the students. The few facilities which were designed for routine testing and are completely automated still are only pilot models for the large production tunnels of the future.

Facility Designation: Transonic Windtunnel S1
Organization: von Karman Institute for Fluid Dynamics
Country: Belgium

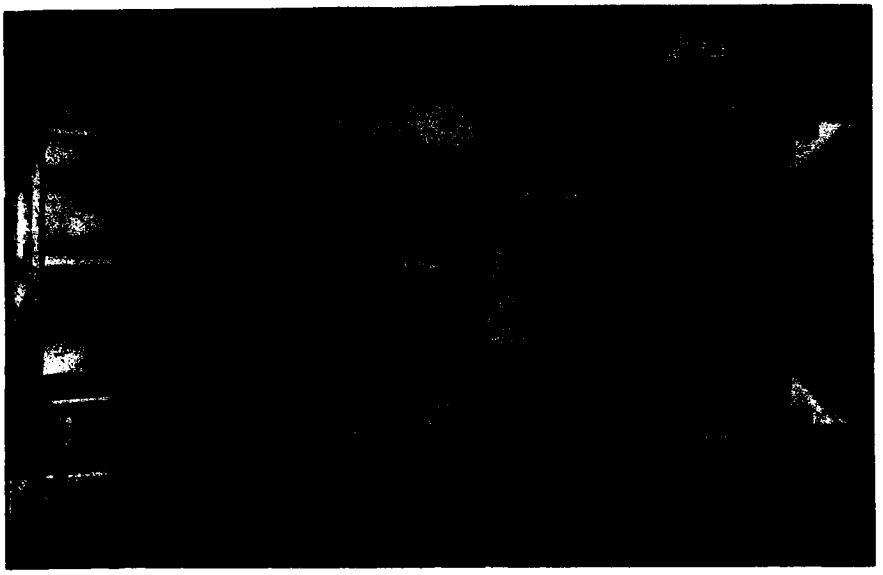

The test section of the VKI S1 transonic wind tunnel is 0.4 m square. In 1981, this facility was equipped with both straight and contoured wall blocks. Two bodies of revolution were tested to verify the method developed for using two dimensional adaptation for three dimensional tests. This was the first experimental demonstration of three-dimensional testing with two adaptive walls. These were the only adaptive wall tests conducted in this facility.

Facility Designation: S4 L Ch
Organization: ONERA
Country: France

The ONERA S4 L Ch Wind Tunnel is a continuous flow closed return tunnel which operates at ambient temperature. This facility was used for adaptive wall test section development from about 1973 to 1977. The adaptive wall test section is 22.5 cm square and 70 cm long. Both the top and bottom walls are flexible. Each flexible wall is driven by ten jacks, unequally spaced, which are manually actuated.
Two airfoil models underwent limited tests for the purpose of evaluating the testing techniques and adaptation algorithms. For three dimensional testing, a wing body model underwent very limited tests. The purpose of these tests was to evaluate the level of model pertubations measured at the walls. Although the facility is still operational, no adaptive wall work has been accomplished since 1977.

Facility Designation: S5 Ch
Organization: ONERA
Country: France

The ONERA S5 Ch wind tunnel is a continuous flow closed return supersonic tunnel which operates at ambient temperature and a Mach number of 1.2. The adaptive wall test section for this facility is 22.0 cm wide, 18.0 cm high, and 95 cm long. It has solid side walls and adaptable top and bottom walls. These adaptable walls are formed of 150 transverse sliding plates which are 2.0 mm thick. They are preset to a given contour prior to a given test program. The time to compute and set the walls to a given shape and install the test section is about one week.
This facility with the adaptive wall test section has been used to test both two- and three-dimensional models with strong shock waves which reach the top and bottom walls. Two cylinder models and a delta wing at high angle of attack have been tested to date. The adaptive wall test section for this facility is still active.

Facility Designation: T2
Organization: ONERA/CERT
Country: France

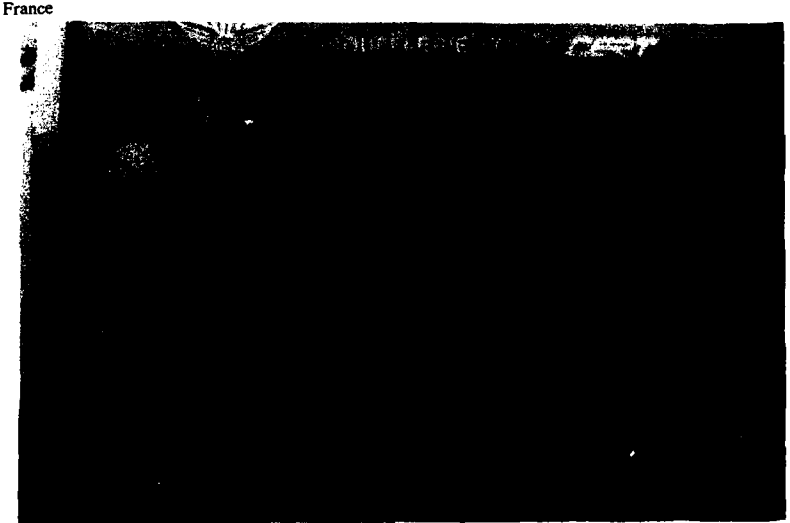

The ONERA T2 adaptive wall wind tunnel is one of the most active facilities in the development of test techniques in use at this time. The tunnel is an injector driven closed circuit transonic cryogenic facility. The adaptive wall test section is 39.0 cm wide, 37.0 cm high, and 1.4 m in length. All four walls are solid with the top and bottom being flexible. These flexible walls are each driven by 16 jacks. The adaptive walls were placed in operation in 1978 and first operated at cryogenic conditions in 1981. The facility is in active use at the present time.
The T2 facility has been extensively used to produce both two- and three-dimensional aerodynamic data. Four airfoil shapes as well as semi-span and sting mounted models are included in the test programs. Both basic research and industrial support programs are supported in this facility.

Facility Designation: DAM
Organization: DFVLR - Göttingen
Country: Germany

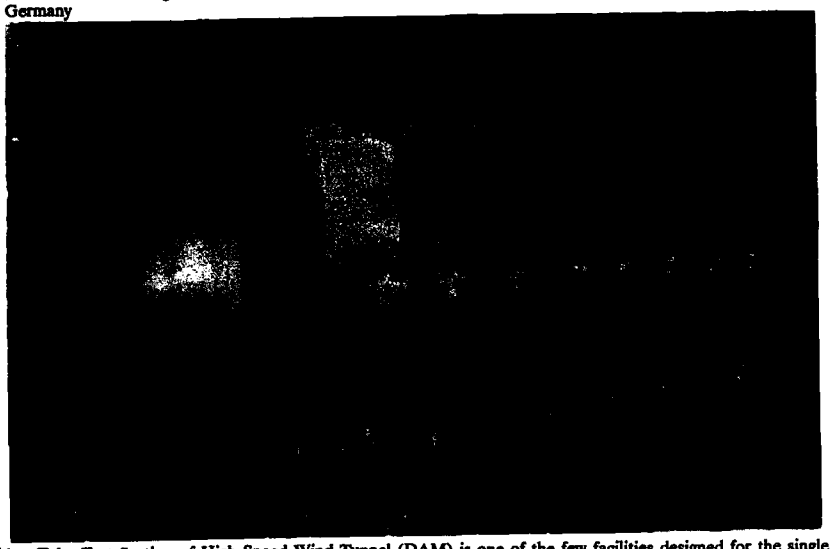

The Rubber Tube Test Section of High Speed Wind Tunnel (DAM) is one of the few facilities designed for the single purpose of three-dimensional testing. The test section is 80.0 cm in diameter and 2.4 m in length. It is constructed of rubber 6 cm in thickness. There are 8 longitudinal rows of jacks equally spaced around the circumference. Each row consists of 8 equally spaced jacks. The Mach number capability is from 0.2 to 0.93.
From 1984 to 1987 this facility has been used to provide three-dimensional data on many configurations including bodies of revolution and winged lifting configurations. One of the objectives of this type of facility is to provide a data base of fully adapted three-dimensional data with which other less complex approaches can be compared.

Facility Designation: HKG
Organization: DFVLR - Göttingen
Country: Germany

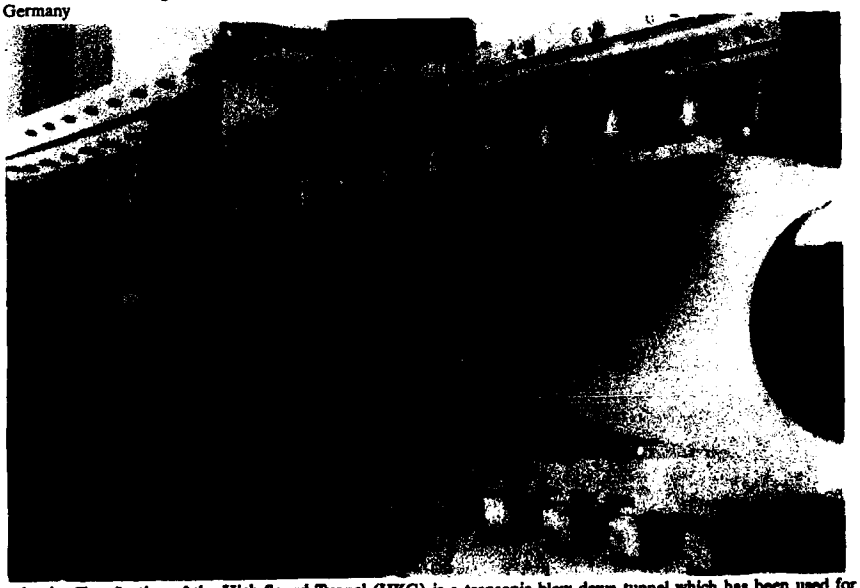

The 2-D adaptive Test Section of the High Speed Tunnel (HKG) is a transonic blow down tunnel which has been used for limited three-dimensional testing. The test section is 67 cm wide, 72 cm high, and 2.2 m in length. The side walls are rigid and the top and bottom walls flexible. Each flexible wall is driven by 9 pairs of jacks. The Mach number capability is from 0.5 to 0.90. The facility is used to obtain data on three-dimensional sting-supported models. Two bodies of revolution and a swept wing pressure distribution model have been tested to date. (In the above photo, the test section is shown in the supersonic configuration.)

Facility Designation: TWG
Organization: DFVLR - Göttingen
Country: Germany

The Transonic Wind Tunnel Göttingen (TWG) is a transonic slotted wall tunnel which has been used for adaptive wall research. The test section is 1.0 m square and 3.1 m in length. The side walls are solid and there are 4 slots in each of the slotted walls. The slot width (or porosity) is independently adjustable. The Mach number capability of the facility is from 0.5 to 2.0.
Although the facility is capable of two- and three-dimensional testing, only two-dimensional airfoil tests have been made with the wall adaptation process. The Mach number range of these airfoil tests was from 0.6 to 0.85.

Facility Designation: TUB (2D)
Organization: Technical University of Berlin
Country: Germany

The Technical University of Berlin adaptive wall facility is a continuous flow open tunnel which operates at atmospheric stagnation pressure. The 2D test section is 15 cm square and 69 cm long. The top and bottom walls are flexible and the sidewalls are solid. Each flexible wall is driven by 13 jacks. The Mach number range of the facility is from 0.3 to 0.95.
This facility has been used to test both two- and three-dimensional models. This is one of the first facilities in which three-dimensional tests were made in a facility with only two adaptive walls.

Facility Designation: TUB (3D)
Organization: University of Berlin
Country: Germany

The 3D test section of the Technical University of Berlin was the first adaptive wall test section designed for three-dimensional testing. It has 8 flexible walls with the top and bottom walls driven by 9 jacks and all other walls by 10 jacks. The test section is 18 cm wide, 15 cm high, and 83 cm long. The joints between adjacent walls are sealed by a number of overlapping strips of spring steel. One end of each strip is attached to one wall and the other end is free to slide on the adjacent wall. The Mach number capability is from 0.3 to 1.3. A series of bodies of revolution and wing body models have been tested in the facility. The test section was placed in operation in 1980 and has been in use up to 1987.

Facility Designation: Adaptive Walls Wind Tunnel (AWWT)
Organization: Istituto di Aerodinamica "Umberto Nobile"
Country: Italy

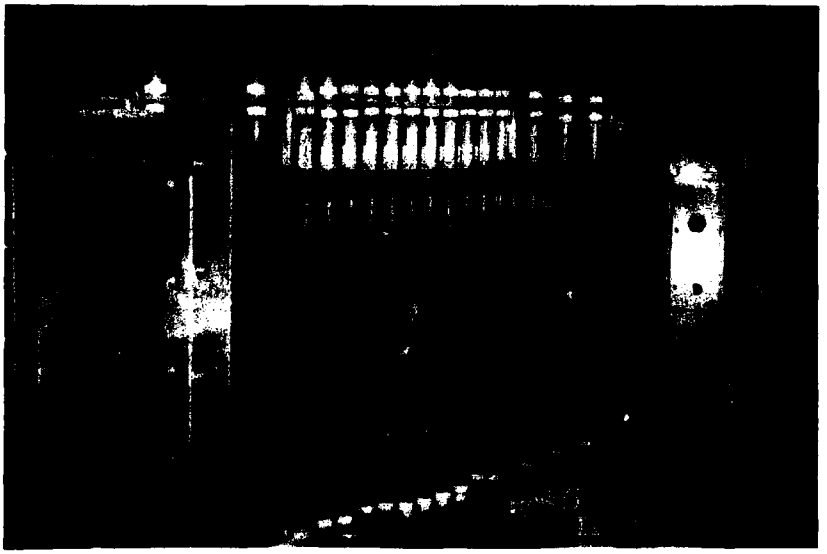

The Istituto di Aerodinamica "Umberto Nobile" has under construction an adaptive wall continuous flow open return facility. The test section is 20 cm square and 1 m in length. The Mach number capability will be up to 0.55. The top and bottom walls are flexible and the side walls are solid. Each flexible wall will be driven by 16 jacks. The facility is designed for two-dimensional testing capability. Initial operation is scheduled for late 1988.

Facility Designation: NPU AWWT
Organization: Northwestern Polytechnical University
Country: Peoples Republic of China

The Northwestern Polytechnical University Adaptive Wall Wind Tunnel is a continuous flow low speed tunnel which operates at ambient conditions. The test section is 23.8 cm wide, 25.6 cm in height and 1.3 m long. Both top and bottom walls are flexible. There are 21 screwjacks and 21 pressure taps located on each wall with the spacing varying along the tunnel length.
Both two- and three-dimensional tests are performed in the facility with a two-dimensional adaptation method. A circular cylinder model and an airfoil model have undergone tests as well as a three-dimensional wing body model. The tunnel is currently operational.

Facility Designation: 5 x 2 inch
Organization: National Physical Laboratory (NPL)
Country: United Kingdom

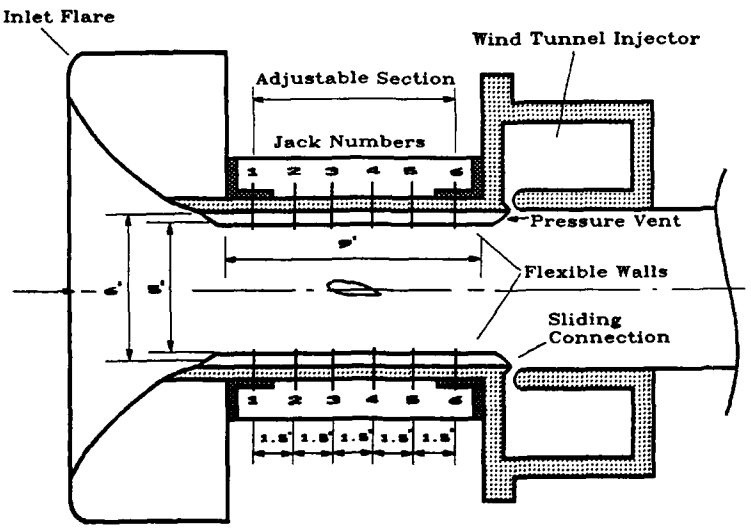

By all accounts, the National Physics Laboratory 5 by 2 in. tunnel was the first adaptive wall tunnel. Placed in operation in the 1937-1938 time period, the facility had a test section 12.7 cm high and 5.1 cm wide. The two 5.1 cm walls were flexible and manually driven by 6 equally spaced jacks on each wall. The facility was used to produce airfoil data and provide design information for a larger test section. It was in use until about 1955.

Facility Designation: 20 x 8 inch
Organization: National Physical Laboratory (NPL)
Country: United Kingdom

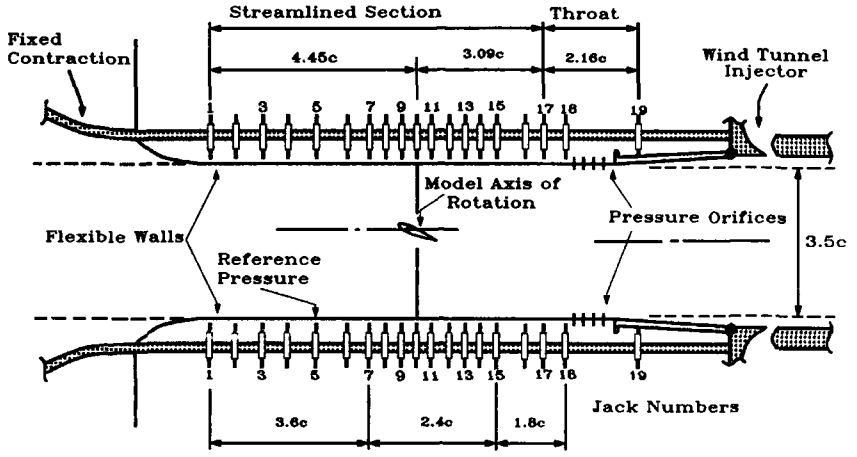

c= Aerofoil chord (= 5.0 inches) Scale 1:10 approx.

The National Physics Laboratory (NPL) 20 by 8 in. adaptive wall tunnel was based on the design of the smaller 5 by 2 in. facility which was built earlier. The test section was 20.3 cm wide and 50.8 cm high. The tunnel was induction driven and operated at transonic speeds up to a Mach number of about 1.0.
This facility first operated in early 1941 and was operational until about 1955. Although the wall adaptation was a manual process, a very large number of both two- and three-dimensional tests were conducted in this tunnel.

Facility Designation: Cascade Blade Tunnel
Organization: University of Southampton
Country: United Kingdom

The Prototype Cascade-blade Flexible-walled Wind Tunnel of the University of Southampton was a very specialized type of facility. Constructed in 1974/75, it was used to test single untwisted highly cambered turbine blade between solid sidewalls, representing cascade flow. The top and bottom walls were flexible and driven by 14 and 12 manually operated jacks respectively. The test section was 7.6 cm wide and 5.6 cm high. The tunnel was a continuous fan-driven open return type and operated at a Mach number of about 0.1. The facility is no longer operational.

Facility Designation: Low Speed Self-Streamlining Tunnel
Organization: University of Southampton
Country: United Kingdom

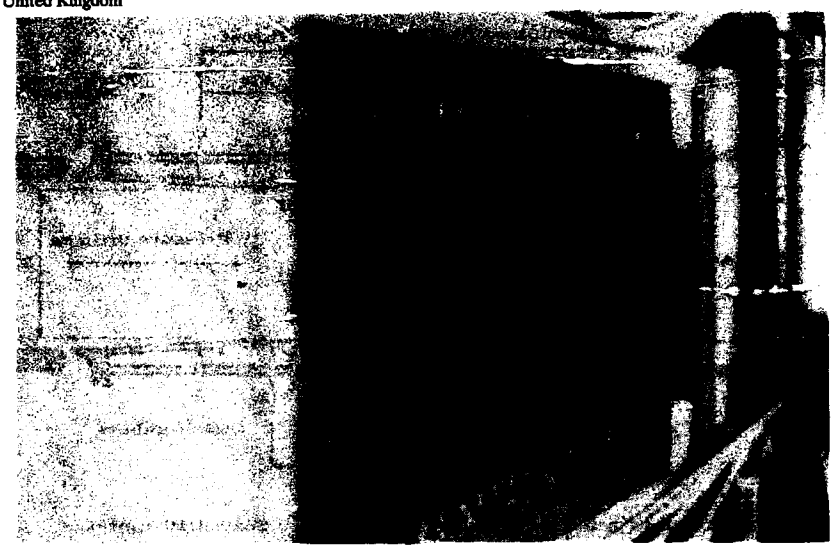

The Low Speed Self-streamlining Tunnel (SSWT) of the University of Southampton has been in operation since 1973. This facility is a continuous flow fan driven open return tunnel which operates at a Mach number of about 0.10. The test section is 30.5 cm wide and 15.2 cm high. The top and bottom walls are flexible and the sidewalls rigid. Each flexible wall is driven by up to 18 jacks, depending upon the stage of development of the test technique. The length of the controlled walls is 127.3 cm. The control of the jacks is manual. Four models have been tested in this facility. Two-dimensional tests included two symmetric airfoils and a circular cylinder. A swept wing which completely spans the test section has also undergone tests to assess this testing capability. This tunnel is still operational.

Facility Designation: Transonic Self Streamlining Tunnel
Organization: University of Southampton
Country: United Kingdom

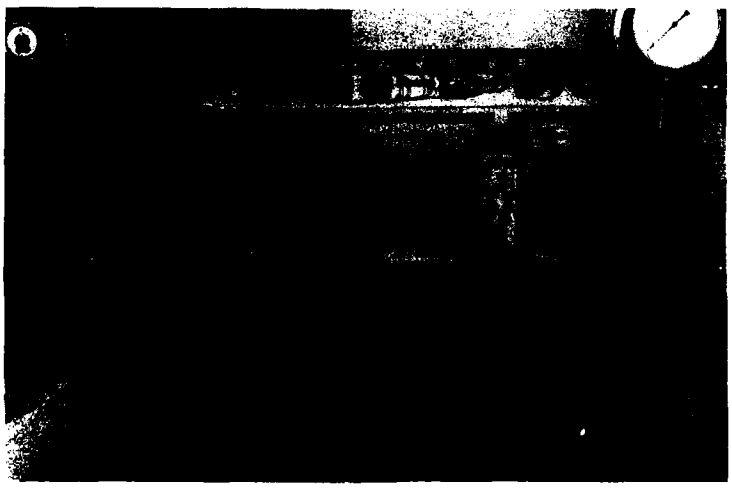

The University of Southampton Transonic Self-streamlining Wind Tunnel (TSWT) is an intermittent, closed return, induced flow tunnel which operates at atmospheric stagnation conditions. The test section is 15.24 cm square and the controlled walls are 111.8 cm long. There are 20 positioning jacks on each wall but only 19 are used in the adaptation process. The flexible walls as well as the sidewalls are solid. Control of the flexible walls is completely automated and under computer control. The maximum Mach number capability of the facility is quoted to be about 1.8.
This facility has been extensively used for both two- and three-dimensional tests. Models tested include three 2D airfoils, two sidewall mounted wings, and a sting mounted wing-body model. Most of the models tested were also tested in other facilities to provide for a comparison of the results. This tunnel is still operational and is being used primarily to develop three-dimensional testing algorithms, and techniques for two-dimensional testing through Mach 1.

Facility Designation: 1T
Organization: AEDC
Country: United States

The Arnold Engineering Development Center One-Foot Aerodynamic Wind Tunnel (1T) has been used to develop the 3D Adaptive-Wall Test Section. The facility is a continuous flow nonreturn tunnel with a 2D flexible nozzle. The adaptive wall test section is 30.5 cm square and 95.3 cm long. The Mach number capability is from 0.5 to 1.0. The walls of the test section are perforated with 60 deg. inclined holes and the porosity is variable from 0 to 10%. The top and bottom walls are each divided into 24 segments and the sidewalls each into 8 segments. The adaptation process is accomplished by independent control of the porosity of each segment and by global plenum pressure control.
The facility has been used to develop algorithms for three-dimensional testing capability. One wing body model has been tested which was also tested in a 4 foot tunnel. Comparisons of the resulting data were used to establish validity of testing technique. This facility was designed to develop the test techniques only and has not been operational since June 1985.

Facility Designation: 9 in. Pilot
Organization: AFWAL/FDL
Country: United States

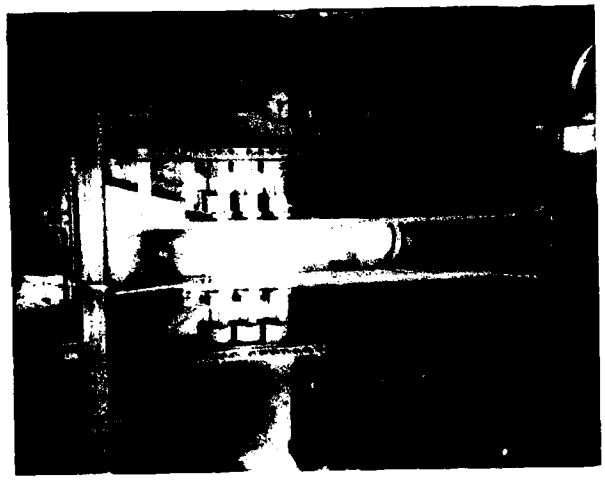

The Air Force Wright Aeronautical Laboratory 9-inch Pilot Self-Adaptive Wall (SAW) Wind Tunnel was one of the first three-dimensional adaptive wall facilities to be constructed. The tunnel is a blowdown to atmosphere type and the maximum Mach number capability is about 1.0. The test section is 22.9 cm square. It has solid sidewalls and flexible top and bottom walls. These flexible walls each consist of 9 parallel longitudinal cylindrical rods. These rods are controlled by three manual jacks at the upstream end followed by 10 motorized jacks. Each rod may be individually controlled to provide three-dimensional streamlining. They may also be set to the same position to simulate two-dimensional streamlining.
Two three-dimensional tests were conducted in this facility. They included a body of revolution and a wing body model. Both three- and two-dimensional contouring of the walls were used in the test programs. This facility was one of the first to demonstrate the capability of using two-dimensional adaptation for three-dimensional testing. Most of the research in this facility was conducted between April 1981 and December 1982. The tunnel is no longer operational.

Facility Designation: 1 ft.
Organization: Calspan/ATC
Country: United States

The Calspan Corp. Advanced Technology Center One-Foot Tunnel was a continuous flow, closed return, variable density tunnel. The adaptive wall test section was 30.5 cm high, 25.4 cm wide, and 1.68 m long. The Mach number capability with this test section was from 0.55 to 1.0. This facility was a two-dimensional tunnel with rigid sidewalls and perforated top and bottom walls. The nominal wall porosity was 22.5%. The plenum above the top wall was divided into 10 independent segments and below the bottom wall into 8 segments. The pressure in each of these plenum segments could be independently varied.
This facility was one of the first adaptive wall facilities and was fabricated, calibrated, and operational from 1973 to 1980. Two airfoil models were tested in the facility to demonstrate the proof of the concept. The tunnel has been inactive since 1980.

Facility Designation: 25 x 13 cm.
Organization: NASA/ARC
Country: United States

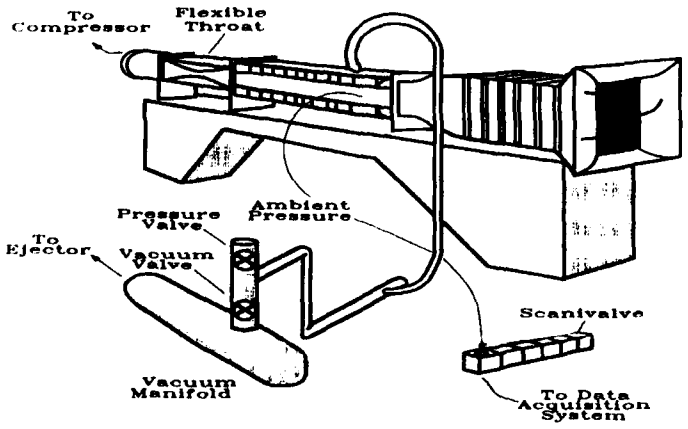

The NASA Ames Research Center 25 by 13 cm tunnel is a continuous flow indraft type tunnel with a flexible downstream throat for Mach number control. The maximum Mach number capability is about 0.8. The adaptive wall test section is 13 cm high, 25 cm wide, and 74 cm long. The sidewalls are solid and the top and bottom walls each have 10 longitudinal slots. The open area ratio is 12%. The top and bottom plenums are separate and are each divided into 10 separate segments for two-dimensional testing and 18 segments for three-dimensional tests. By means of suction and blowing, the pressure in each segment is independently varied. The operation of the control valves for the adaptation process is manual.
One airfoil and one semi-span wing have been tested in this facility. It has been inactive since 1981.

Facility Designation: 2 x 2 ft.
Organization: NASA/ARC
Country: United States

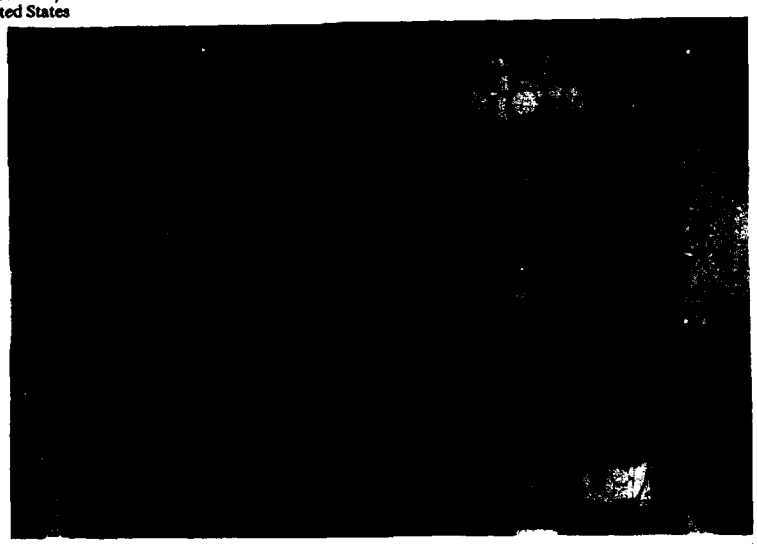

The NASA Ames Research Center 2- by 2-Foot Transonic Wind Tunnel is a continuous flow, closed return facility dedicated to research and industrial operation. The adaptive wall test section is 61 cm square and 1.52 m long. It has slotted top and bottom walls and solid sidewalls. These sidewalls are constructed of schlieren quality glass for complete optical access to the flow field. The plenum chambers for both the top and bottom walls are each divided into 32 segments. A slide valve controls the pressure in each of these segments independently. The valve position and chamber pressure are computer controlled. The tunnel is capable of both two- and three-dimensional tests. The original operational date for this facility was late 1988. In early 1989, a decision was made to terminate further development of this facility.

Facility Designation: 0.3 m TCT
Organization: NASA/LaRC
Country: United States

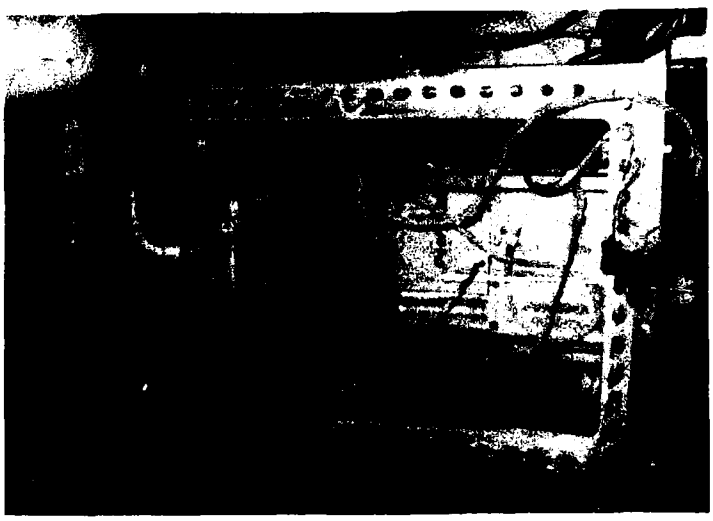

The NASA Langley Research Center 0.3-m Transonic Cryogenic Tunnel is a continuous flow fan driven pressure tunnel which uses nitrogen gas as the test medium. The adaptive wall test section is 33 cm square and 1.42 m long. The top and bottom walls are flexible and the sidewalls are solid. The flexible walls are driven by 18 jacks each. The electric stepper motors which drive the jacks are computer controlled. The adaptive wall test section for this facility was placed in operation in March 1986.
This test section has been used to test both two-dimensional airfoils and three-dimensional semi-span models. A test of a sting mounted wing body model is being planned. The facility is presently operational and supports both basic research and industrial test programs.

Facility Designation: Adaptive Wall Automotive Tunnel
Organization: Sverdrup Technology
Country: United States

The Sverdrup Technology Corporation Adaptive Wall Automotive Tunnel (AWAT) is a special purpose low-speed wind tunnel. Developed as a pilot tunnel to evaluate the capabilities of testing high blockage automotive models, it is strictly a three-dimensional facility. The adaptive wall test section is 30.5 cm high, 61 cm wide, and 2.44 m long. The top wall consists of 6 independent longitudinal slats, each sidewall 3 independent slats, and the bottom wall is solid. Each slat is contoured by 17 manually set screw jacks. The Mach number capability of the facility is from about 0.05 to 0.20.
Three automotive models of different blockage ratios have been tested to date. First operated in the late 1970's, the tunnel has been inactive since March 1987.

Facility Designation: Arizona Adaptable-Wall Wind Tunnel
Organization: University of Arizona
Country: United States

The University of Arizona Adaptable-Wall Tunnel is another of the special purpose adaptive wall facilities. A low speed (M = 0.1) open return tunnel, it is designed for high lift V/STOL type three-dimensional model testing. The test section is 50.8 cm square and 1.15 m long. The adaptive walls are constructed of venetian blind type louvered vanes and the control is by segmented rotation of these vanes. One generic V/STOL transport model has been tested to date. The last use of the facility was December 1987.

3. STREAMLINING ALGORITHMS FOR COMPLETE ADAPTATION

Editor: J. C. Erickson, Jr.
Other Contributors: J. P. Chevallier, M. J. Goodyer, H. G. Hornung, A. Mignosi, W. R. Sears (University of Arizona), J. Smith and E. Wedemeyer

3.1 Introduction

Chapter 1 of this report gives a history of adaptive-wall development up to about 1975. That material will not be repeated here, although the period called the beginnings of the modern era (1970-1975) will be discussed from the point of view of algorithm and facility development. For purposes of the adaptive-wall algorithms to be described here, the modern era is considered to have begun with the simultaneous, independent recognition of the concept of matching an experimental inner flow across an interface to a computed outer flow by Chevallier, Ferri, Goodyer, Lissaman, Rubbert, and Sears, as detailed in Section 1.3. An historical survey at this point in the chapter makes possible presentation of material later in the chapter in a more general and coherent fashion without concern for the chronology. Other surveys of modern adaptive-wall development have been given by Davis [3.1], Ganzer [3.2], [3.3], Wedemeyer [3.4], and Sears and Erickson [3.5].

Fundamental investigations of the adaptive-wall matching concept by means of numerical simulations and theoretical considerations are described in Section 3.1.1. An overview of the development and operation of 2D adaptive-wall facilities from about 1970 until the present is given in Section 3.1.2, followed in Section 3.1.3 by similar material for 3D adaptive-wall facilities from approximately 1978 until the present. A general formulation of adaptation strategy is presented in Section 3.2, with a theoretical basis for adaptation described in Section 3.2.1 followed by 2D flexible, impermeable-wall applications; 2D ventilated-wall applications; 3D flexible, impermeable-wall applications; and 3D ventilated-wall applications in Sections 3.2.2 to 3.2.5, respectively. Representative experimental results are given in Section 3.3, with 2D in Section 3.3.1 and 3D in Section 3.3.2, followed by a discussion of limitations and open questions in Section 3.4. The references for Chapter 3 are in Section 3.5.

3.1.1 Adaptive-Wall Interface Matching Concept

The basic concept of an adaptive-wall wind tunnel is to match two independent flow-disturbance quantities measured at an interface in the tunnel experiment to the same quantities computed from an interference-free outer flow beyond the interface. The configuration is shown schematically in Fig. 3.1 for a 3D, perforated-wall test section where the interface, S, separates the inner, experimental flow region, I, from the outer, computed flow region, II. Note that the shaded zone in Fig. 3.1 denotes the domain beyond the ventilated wall, but not the entire outer region II. Any adjustment of the flow by means of wall control affects the entire flow field, so that both the inner, experimental flow and the outer, computational flow will change. Therefore, adaptation was recognized immediately as being an iterative process. A principal feature of the concept is that there is no requirement for a theoretical representation of the flow about the test article.

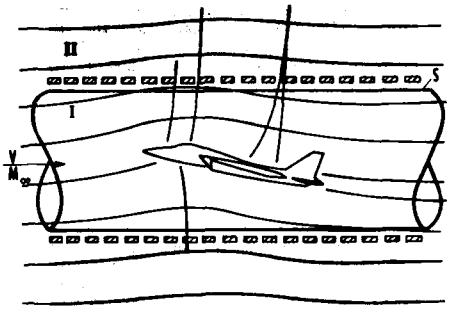

Fig. 3.1 Schematic of transonic flow about a test article in an adaptive-wall test section with interface surface S separating inner (I) and outer (II) regions (from [3.34]).

It was important initially to investigate the nature of the iterative procedure before attempting hardware development. Consequently, numerical simulations were performed with the measurements in the experimental inner flow over the test article replaced by a computational representation. These simulations not only led to practical and efficient iteration procedures, but also facilitated design and operational studies of such important questions as the effects of test-section length truncation and errors in wall settings and interface measurements.

Although many of these simulations probably were not published, several were. Calspan ATC demonstrated the concept numerically in 2D incompressible flow [3.6] and in 2D supercritical flow using a nonlinear representation based upon numerical solutions of the transonic small disturbance equations (TSDE) [3.7]. Later simulations [3.8] modeled the Calspan ATC One-Foot 2D adaptive-wall test section. ONERA also used 2D linearized subsonic and nonlinear TSDE representations for development purposes [3.9], [3.10]. Southampton University performed 2D incompressible simulations [3.11] to examine many aspects of the operational procedures. Numerical simulations were carried out by Technical University - Berlin for 2D incompressible flow [3.12], [3.13] and supersonic flow [3.14], and in 3D for subsonic, subcritical flow [3.15]. AEDC investigated 2D simulations for linearized subcritical and nonlinear supercritical flows based on numerical solutions of the TSDE [3.16]-[3.18]. Everhart at NASA/Langley Research Center [3.19], [3.20] developed a 2D Cauchy-integral formulation of the outer-flow calculation for a closed contour surrounding the model in linearized compressible flow. Everhart simulated iterative adaptations in low-speed flows about a circular cylinder and an airfoil, and one experiment was performed. Much of this work was carried out in 1977, but was not published until 1983. Recently, Schairer at NASA/Ames Research Center [3.21] has performed numerous 2D simulations with both linearized com-

*The research reported herein was performed in part by the Arnold Engineering Development Center (AEDC), Air Force Systems Command. Some of the work and analysis was done by personnel of Calspan Corporation/AEDC Operations, operating contractor of the AEDC aerospace flight dynamics facilities. Further reproduction is authorized to satisfy needs of the U. S. Government.

pressible and nonlinear TSDE representations of the flow within an adaptive-wall test section. For 3D adaptive-wall tunnels, numerical simulations have been reported by Sears at the University of Arizona [3.22], [3.23] for a test section designed for powered lift and large flow deflection with ventilated top and bottom walls and solid sidewalls; by Wang at the Chinese Aeronautical Establishment, Harbin [3.24] using numerical solutions of the TSDE; and by Mendoza at NASA/ARC [3.25] for linear compressible flow in a ventilated test section with solid sidewalls. The results of all of these 2D and 3D simulations were used to guide the experimental design and implementation of adaptive walls. The basic adaptation strategies that evolved are discussed in Section 3.2.

An alternative way of investigating the iterative procedures was by more general theoretical simulations of the iterative adaptive-wall process within the framework of linearized compressible flow represented by the Prandtl-Glauert equation. These investigations began in about 1975. Lo and Kraft [3.16] used separation of variables and Fourier superposition techniques initiated by Weeks [3.26] to prove the convergence of the adaptive-wall iterative scheme in the 2D nonlifting case of a symmetrical airfoil. An important result of the Lo and Kraft analysis was the determination that a single scalar iterative relaxation factor would not lead to immediate convergence although significant improvements in convergence rate could be made by a suitable choice. However, general equations were derived that consisted of certain definite integrals of both measured disturbance quantities over both the top and bottom interfaces to achieve convergence to unconfined free-air flow *in "one step"*. This procedure assumes that the viscous, transonic and vortical effects neglected in the Prandtl-Glauert equation are essentially the same before and after the one-step adaptation. Lo and Sickles extended the Fourier superposition approach to generate one-step formulae for axisymmetric flow [3.18], and 2D lifting flow [3.17], [3.18] with the assumption that the lift is unchanged before and after the one-step adaptation. Kraft and Dahm [3.27] later used the Cauchy-integral formula for 2D flow to remove the necessity for assuming the lift to be unchanged during the one-step adaptation. In related work, Sears [3.28] examined relaxation factors for infinitely-long sinusoidal shapes in 2D nonlifting and lifting flow, axisymmetric flow, and a 3D low-aspect-ratio flow. Sears also examined the implications of imperfect control on the iterative relaxation process [3.29]. Many mathematical aspects of the iterative procedure and one-step methods for linear flows are addressed in the discussion of residual-interference corrections in Section 6.2.1 of this report. Mokry [3.30] also has discussed the mathematical aspects of 2D adaptive-wall procedures.

In 3D flow, one-step methods also have been derived for linearized compressible flow represented by the Prandtl-Glauert equation. Wedemeyer, et al. at DFVLR/Göttingen [3.31] developed a one-step procedure using separation of variables and Fourier analysis in the azimuthal and axial directions for tunnels with a circular cross section. Rebstock at TU-Berlin [3.3],[3.15] developed a one-step procedure for an octagonal cross section using discretization of the governing equations by means of a panel method. Both of these methods assume that the lift remains constant before and after adaptation. Ashill and Weeks [3.32] derived a Green's theorem approach for wall interference assessment and correction. Wedemeyer [3.4] then pointed out that the 2D Cauchy-integral one-step formulation can be generalized to 3D by further development of the Green's theorem approach of [3.32]. Subsequently, Ashill and Keating generalized the analysis of [3.32] to an adaptive-wall one-step method [3.33]. Further discussion of the concept and techniques of "one-step" methods is given in Section 3.2.1.

When the flow is supercritical at the interface, nonlinear equations of motion, e.g., the TSDE, must be used. In the supercritical cases, the linear one-step methods are no longer strictly valid. The lack of linear superposition renders the mathematical problem associated with derivation of one-step methods much more complicated, if not impossible. A discussion of many of the implications of the nonlinear aspects of the calculation procedures are touched upon in the discussion of residual-interference corrections for nonlinear flow in Section 6.2.2 of this report.

For completeness, it must be mentioned that the interference-free environment represented by the outer-flow boundary conditions does not necessarily have to be for flight in free air. Sears [3.34] and Goodyer [3.35] have considered flow over test articles in ground effect, Goodyer [3.35] has described the simulation of steady-state pitching in free-air flight, and Davis [3.36] has discussed the possibility of adaptive-wall experimental simulation of other types of tunnel boundary conditions for which residual interference can be corrected more easily.

3.1.2 2D Adaptive-Wall Test Section Development

Once decisions were made to commence hardware development to implement the adaptive-wall concept, two fundamentally different approaches emerged for providing control of the flow in a 2D test section. The first is the use of flexible, impermeable top and bottom walls of the general type used in the pioneering work of the National Physical Laboratory (NPL) in the UK. The second is the use of ventilated top and bottom walls of the general type used in conventional perforated and slotted test sections, but with the addition of further control distributed along the length of the tunnel. Distributed porosity and segmented, individual plenum chamber control adjoining the ventilated walls were selected by various groups. In all ventilated-wall facilities for adaptive-wall investigations, with the exception of limited experiments by Weeks [3.26] in which contoured slots were examined, the ventilated walls are planar and rigid.

Each of these approaches offered advantages to the organizations that selected them and although there were common problems, there also were problems unique to each. For example, both approaches had to deal with the finiteness of control, not only the truncation of the controlled part of the test section upstream and downstream, but also the finite spacing between control jacks or the finite size of individual plenum chambers and regions of controlled ventilation. The outer-flow computational requirements are essentially the same for both approaches. The interface measurement requirements are distinctly different in the two approaches, however. The flexible, impermeable wall lends itself readily to measurement of wall static pressure by means of static orifices and measurement of wall displacement from its initial, undeformed position. The deformation of the walls from planar surfaces had to be investigated with respect to the outer-flow computation and the modified growth of the boundary layers on the top and bottom walls due to the presence of the model also had to be

investigated. For ventilated walls, it is necessary to place the interface surface a finite distance within the walls in order to remain outside the transpired wall boundary layer and to avoid the complex three-dimensional flow in the immediate vicinity of the ventilation mechanism (perforations or slots). This led to extensive research into suitable means for accomplishing these measurements as efficiently and nonintrusively as possible. Details of the interface measurement systems are contained in the descriptions of the various ventilated test sections in the Appendix.

The 2D facilities that demonstrated the feasibility of the adaptive-wall concept initially during 1970 to 1975 were the Southampton University Low-Speed Self-Streamlining Tunnel (SSWT), the ONERA S4LCh transonic tunnel at Chalais Meudon, and the Calspan ATC One-Foot transonic tunnel at Buffalo. The Southampton and ONERA tunnels have flexible, impermeable walls and the Calspan tunnel had perforated walls with individual, segmented plenum chambers. Descriptions of these three facilities are given in Chapter 2 and the Appendix. Initial experiments were performed during the period 1973 to 1975 and were published in 1975. The initial Southampton results [3.37], [3.38] were for a circular cylinder of about 30% solid blockage and an NACA 0012-64 airfoil section of 10.8% blockage, both at low speeds. The unconfined outer-flow computations were performed with linear, incompressible-flow methods. The ONERA results [3.9],[3.10] were for the strongly supercritical cases of $M = 0.86$, $\alpha = 0$ deg and $M = 0.85$, $\alpha = 6$ deg with an NACA 64A010 airfoil section of 4.4% solid blockage. The unconfined outer-flow computations were numerical solutions of the TSDE. The Calspan ATC case [3.39] was for mildly supercritical flow at $M = 0.55$, $\alpha = 6$ deg for an NACA 0012 airfoil section of 6% solid blockage. The unconfined outer-flow computations were performed with a linear method [3.6] based on the Prandtl-Glauert equation.

During the time period from 1975 to 1980, several additional 2D test sections were built and used, namely the NASA/ARC 25x13 cm transonic tunnel, the ONERA/CERT T2 cryogenic transonic tunnel, the Southampton University Transonic Self-Streamlining Wind Tunnel (TSWT), and the TU-Berlin TUB(2D) transonic tunnel. The NASA/ARC test section has slotted walls and individual, segmented plenum chambers, while the others have flexible, impermeable walls. All of these facilities are described in Chapter 2. Another transonic facility modified in this time period was the AEDC One-Foot Aerodynamic Wind Tunnel (1T). Tunnel 1T is described in Chapter 2, but only in its 3D adaptive-wall configuration. In 2D, two different sets of perforated walls, both with and without individual sub-plenum chambers, were built and tested [3.40],[3.41].

Five additional 2D test sections have been built or modified in the last few years. All of these are described in Chapter 2 and the Appendix, namely the low-speed University of Naples Istituto di Aerodinamica "Umberto Nobile" Adaptive Walls Wind Tunnel (AWWT), the NASA/ARC 2x2 ft Transonic Wind Tunnel, the NASA/LaRC 0.3-m Transonic Cryogenic Tunnel (TCT), the ONERA/Chalais Meudon S5Ch supersonic tunnel, and the low-speed Adaptive Wall Wind Tunnel at Northwestern Polytechnical University in Xian, China. All have flexible, impermeable walls except the NASA/ARC tunnel which has slotted walls and individual, segmented plenum chambers, and S5Ch which has walls formed of thin transverse sliding plates that can be preset to prescribed 2D contours.

The investigations carried out in all of the 2D test sections from about 1975 to the present fall into three general speed ranges, and the flows will be categorized in this report as belonging to Groups 1 to 3. Group 1 flows involve testing at subsonic free-stream conditions with flow over the model that may be supercritical, but with subcritical flow at the interface and walls. Linear compressible outer-flow calculations have been found to be a satisfactory approximation. Research in Group 1 flows has led to the development of rapid and efficient adaptation procedures and other practical aspects for routine operational testing. For example, modern wall interference assessment and correction methods have been introduced to use the interface measurements to evaluate the residual interference that remains after adaptation, see Chapter 6. Most of the test sections listed above have emphasized Group 1 development. Group 2 flows involve testing at subsonic free-stream conditions but with supercritical flow extending to and beyond the interface and wall locations as well. The principal emphasis here was on the fundamental development of techniques to accomplish adaptation at these test conditions. The test sections used most extensively for Group 2 flow development were the AEDC Tunnel 1T and the Calspan ATC One-Foot Tunnel during 1976 to 1981 and the Southampton TSWT Tunnel more recently. Group 3 flows involve testing at supersonic free-stream Mach numbers. The facility used is the ONERA/Chalais Meudon S5Ch where tests at $M = 1.2$ have been accomplished recently. Details of the various adaptation strategies for all flow groups are given in Sections 3.2.2 and 3.2.3 with selected results in Section 3.3.1.

A final class of 2D adaptive-wall test sections that has not been mentioned previously is cascade tunnels. Southampton University did pioneering research in 1975 [3.35], [3.37], [3.42], and the facility is described in Chapter 2 and the Appendix. Recently, the University of Genoa has developed two transonic-flow cascade facilities, one for blade rows with small flow deflection and the other for blade rows with large flow deflection [3.43]. Cascade tunnels will not be discussed further in this report; interested readers should consult the references cited above.

3.1.3 3D Adaptive-Wall Test Section Development

Adaptive-wall development in 3D flows has followed two distinct paths. The first path, which is described in this section, is the extension to 3D of the basic principle of matching two independent flow-disturbance quantities for an experimental inner flow with those for a computed outer flow over an entire interface surrounding the test article. The second path, which is described in Chapter 4, aims at accomplishing testing of 3D configurations in 2D test sections with flexible, impermeable top and bottom walls. Instead of matching over the entire interface, the interference is reduced, or adjusted to be approximately constant and hence correctable, along a specified line in the inner, experimental flow field.

In this chapter, the complete adaptation procedure is under consideration, so the test sections described are those which embody that concept. Just as in 2D, two fundamentally different approaches to wall control have been implemented. The facilities with flexible, impermeable walls are the Sverdrup Technology Adaptive Wall Automotive Tunnel (AWAT) with independent, longitudinally-controlled slats on the top wall and sidewalls for low-speed, high-blockage, road-

vehicle testing; the TU-Berlin TUB(3D) octagonal-cross-section transonic tunnel; and the DFVLR/Göttingen DAM circular-cross-section, rubber-wall transonic tunnel. The facilities with ventilated walls are the NASA/ARC 25x13 cm transonic test section with slotted top and bottom walls that have individual, segmented plenum chambers arranged longitudinally and laterally plus solid sidewalls; the AEDC Aerodynamic Wind Tunnel (1T) with a 3D transonic test section that has a total of 64 individually-controlled, variable-porosity segments on all four perforated walls plus global plenum pressure control; and the University of Arizona Adaptable-Wall Wind Tunnel for low-speed, powered-lift, large-flow-deflection testing with louvered vanes on the top wall, louvered vanes ventilated to the stilling chamber on the bottom wall, solid sidewalls, an upstream variable-angle nozzle to introduce the free-stream flow into the test section, and a valve at the downstream end of the test section. All of these facilities are described in Chapter 2 and the Appendix.

Another facility, which is not described in Chapter 2, is Aerodynamic Wind Tunnel (4T), a Four-Foot square operational facility at AEDC. In laterally-symmetric 3D adaptive-wall experiments [3.44], there were four control degrees of freedom, namely the uniform, but adjustable, porosity of the top, bottom and sidewalls (which were ganged together to move in unison) plus the globally uniform, but variable, plenum-chamber pressure.

Both the NASA/ARC and University of Arizona test sections have ventilated top and bottom walls, but plane, impermeable, undeformable sidewalls. The flow through the top and bottom walls varies laterally because the velocity component normal to a ventilated wall responds to the pressure at the wall induced by the test article. Moreover, the plenum chambers of the NASA/ARC test section are segmented laterally as well as longitudinally. Both test sections are adapted by matching over the entire interface, which does not coincide with the walls. Adaptation may be possible because at every point on the interface, both independent flow-disturbance quantities will change when the wall controls are adjusted. The key requirements for adaptation are first, that the existing top and bottom wall controls have sufficient control effectiveness to accomplish complete matching over the entire interface, and second, that measurements at an interface surface noncoincident with the walls are practical. Therefore, plane, impermeable sidewalls without provisions for controlling the flow do not necessarily preclude practical 3D adaptation over the entire interface. Further analysis is necessary and should be related to the analysis of Chapter 4 for 3D adaptation by means of flexible, impermeable top and bottom 2D walls.

Adaptive-wall investigations have been performed for the same three groups of flow in the 3D transonic tunnels as in 2D; namely Group 1 flows (TU-Berlin, DFVLR, AEDC and NASA/ARC), Group 2 flows (AEDC), and Group 3 flows (TU-Berlin and DFVLR). Details of the adaptation strategies are given in Sections 3.2.4 and 3.2.5 with selected results in Section 3.3.2.

A final type of 3D adaptive-wall experiment was performed recently in the Southampton SSWT for a swept-wing panel at low speed [3.45],[3.46]. Although use is made of skewed 2D wall deflections, the flow field about a swept wing is three dimensional, particularly in the boundary layer. However, for the Southampton test conditions, the adapted results exhibited the characteristics predicted by inviscid, simple-sweep theory.

3.2 Strategy of Adaptation

The flow about a 3D model in a transonic wind tunnel is shown schematically in Fig. 3.1, as described in Section 3.1.1. The flow can be considered to have an inner region, denoted as I, that is separated from an outer region, denoted as II, by an interface (control surface), S. Note that the shaded zone in Fig. 3.1 denotes the domain beyond the ventilated wall, but not the entire outer region II. The schematic is of a perforated, rigid-wall test section for which the interface lies within the wall a finite distance in order to avoid the details of the locally 3D flow through the wall. However, the same principles apply if the interface S is coincident with a flexible, impermeable wall. In that case S no longer is of uniform cross section, but follows a stream surface of the flow and generally is assumed to coincide with the deformed wall or a suitable mean wall position, with proper adjustment for the displacement thickness of the wall boundary layer.

In principle, it is straightforward - but not obvious - to determine whether a given wind-tunnel experiment is interference free, i.e., whether specified far-field boundary conditions are satisfied. All that is required is to measure the distributions of two independent flow variables, such as two velocity components or the static pressure and flow inclination, at the surface S. If these two measured distributions are consistent with the far-field boundary conditions, the flow is matched at the interface and is interference free. A practical procedure to determine far-field consistency is to employ one of the measured distributions as inner boundary values and carry out a calculation of the flow field exterior to the surface S, satisfying both the appropriate equations of motion in the region exterior to S and the far-field boundary conditions. If the experimental flow field is interference free, measured and computed values of the other distribution at S will match at the interface. If they are not the same, there is wall interference in the wind tunnel, i.e., the simulation is not exact.

In other words, the flow field is considered to consist of an experimental inner region joined to a computed outer region; the former satisfies the correct inner conditions (including viscous effects, effects of power, etc.), and the latter incorporates the desired outer conditions. Thus the question of exact simulation is reduced to the question of matching at S, the interface. It seems clear, moreover, that when the matching is not perfect, the matching error is a measure of the interference.

These conclusions can be expressed symbolically. To do this, the general, nonlinear theoretical framework presented by Sears and Erickson [3.5] will be followed. The questionnaire distributed by WG12 used this framework as its basis and so the responses reported in the Appendix are cast in these terms. However, it should be noted that the equation numbers in the Appendix (for the Terms of Reference and the Questionnaire) differ from those in this section.

Let the two flow-variable distributions, which are measured at field points on the interface, be called P_i ($i=1,\ldots N_P$) and Q_i ($i=1,\ldots,N_Q$), where N_P does not need to be equal to N_Q necessarily. Further, let the symbol $P_i[Q_j]$ denote the result of calculating the outer field using the distribution Q_j as inner boundary values and satisfying the far-field conditions; i.e., $P_i[Q_j]$ is the distribution P_i derived from this computation. Let the superscript m denote

measured values; the condition for interference-free simulation is then

$$P_i[Q_j^m] = P_i^m \tag{3.1}$$

Usually, the two distributions of P_i are not found to be identical; there is a distribution of matching error at the interface. Let this be called DP_i, defined as

$$DP_i = P_i[Q_j^m] - P_i^m \tag{3.2}$$

The complete adaptation process aims at driving this matching error to zero iteratively and is discussed next.

3.2.1 Theoretical Basis of Complete Adaptation

In an adaptive-wall tunnel, the control variables can be denoted by X_j (j=1,...,M). The X_j are not, in general, the same as the P_j although they may be, as discussed later. Generally, adjustment of each individual X_j affects all measured values P_i^m and Q_i^m. This can be expressed in terms of control-effect matrices, which can be measured, or approximated in some manner, as $\partial P_i/\partial X_j$, $\partial Q_i/\partial X_j$, which are N_P x M and N_Q x M, respectively.

Adjustment of the control variables gives

$$P_i + (\partial P_i / \partial X_j)\,\Delta X_j$$

$$Q_i + (\partial Q_i / \partial X_j)\,\Delta X_j$$

where summation over j is implied. The matching error after such an adjustment is given by

$$D^{(2)}P_i = P_i[Q_k^m + (\partial Q_k/\partial X_j)\Delta X_j] - P_i^m - (\partial P_i/\partial X_j)\Delta X_j \tag{3.3}$$

which indicates that suitable adjustments ΔX_j should be able to drive $D^{(2)}P_i$ toward zero.

Local linearization of the outer-flow calculation leads, using the expression for DP_i in Eq. (3.2), to

$$D^{(2)}P_i = DP_i + [P_i(\partial Q_k/\partial X_j) - (\partial P_i/\partial X_j)]\Delta X_j \tag{3.4}$$

Then, if $M = N_P$, $D^{(2)}P_i$ will be zero if

$$\Delta X_j = [(\partial P_i/\partial X_j) - P_i(\partial Q_k/\partial X_j)]^{-1} DP_i \tag{3.5}$$

where $\{\ \}^{-1}$ denotes matrix inversion. In the more likely case of $M < N_P$, the matrix inversion must be generalized in some appropriate sense, say by a least-squares procedure. Eq. (3.5) is equivalent to the formula first given by Dowell [3.47].

The special case where $X_j = P_j$ follows in the same way with the control-effect matrices reduced to the single matrix $\partial Q_i/\partial P_j$, which is N_Q x N_P and the control increment is ΔP_j. The general form corresponding to Eq. (3.3) is

$$D^{(2)}P_i = P_i[Q_k^m + (\partial Q_k/\partial P_j)\Delta P_j] - P_i^m - \Delta P_i \tag{3.6}$$

which becomes, upon local linearization,

$$D^{(2)}P_i = DP_i + [P_i(\partial Q_k/\partial P_j) - \delta_{ij}]\Delta P_j \tag{3.7}$$

where δ_{ij} is the Kronecker delta. Inversion (in the same sense as above) to force $D^{(2)}P_i$ to zero gives

$$\Delta P_j = [\delta_{ij} - P_i(\partial Q_k/\partial P_j)]^{-1} DP_i \tag{3.8}$$

For Group I flows in which the outer-flow calculation is linear, the relationship in Eq.(3.8) is equivalent to the "one-step" formulae which have been derived analytically [3.3], [3.4], [3.15]-[3.18], [3.27], [3.31]-[3.33], see Section 3.1.1.

The concept of "one-step" methods has not always been characterized consistently in the literature. As described in Section 3.1.1 and immediately above, the adaptation procedure is fundamentally iterative. That is, each time a control variable is changed the entire flow field within the test section changes. However, by means of various classical analysis techniques (e.g., separation of variables and Fourier analysis in 2D and 3D [3.16]-[3.18],[3.31], Cauchy's integral formula in 2D [3.27], and Green's theorem in 2D and 3D [3.4], [3.32], [3.33]), equations can be developed to use the distributions of both measured variables over the entire interface for predicting control changes that will accelerate convergence. A related numerical method based upon discretization of the governing linear equations in 3D has been developed by Rebstock [3.3], [3.15]. The "one-step" terminology, as used here, implies that the control adjustments to be made result in changes to the entire flow field, but within constraints so that the changes in important flow quantities are of higher order. For example, Lo, et al. [3.16]-[3.18] assume in their 2D analyses that the flow over the test article due to viscous, transonic and vortical effects neglected in linear compressible flow are essentially the same before and after the one step, including the lift. Heddergott and Wedemeyer [3.31] and Rebstock [3.3], [3.15] make the same assumptions in 3D. In 2D only, Kraft and Dahm [3.27] eliminated the necessity for assuming that the lift remains unchanged and so generalized the Lo, et al. approach. The efficacy of any of these "one-step" methods can be judged only by its practical application to experimental adaptations and will be discussed in the remainder of this chapter.

Many of the adaptive-wall investigations to date have made approximations to either Eqs. (3.5) or (3.8). For example, the matrix $\partial Q_k/\partial P_j$ in Eq. (3.8) is often neglected because it requires both extensive measurements and the evaluation of the matrix of all the outer-flow calculations $P_i[\partial Q_k/\partial P_j]$. Neglect of such terms and the approximations that were made in the local linearization to derive Eqs. (3.5) and (3.8) lead to the necessity for the introduction of relaxation factors into these equations to account for what has been neglected and/or approximated.

Finally, the question arises as to what constitutes adaptation; i.e., in what way Eq. (3.1) is to be satisfied. Some investigators have introduced figures of merit to characterize the nature of the matching error in Eq. (3.2). The choices will be discussed below.

For flexible, impermeable adaptive-wall control, the interface generally coincides with the wall and the appropriate control variable, X_j, is wall displacement which is an integral of the wall slope and is directly related to the velocity component normal to the wall, which then is taken as P_j. Thus Eq. (3.8) or approximations to it apply. Ventilated walls, on the other hand, necessarily have the interface noncoincident with the wall and Eq. (3.5) or approximations to it apply. In the ventilated case, it is somewhat arbitrary as to which measurement variables should be taken as P_i and Q_i. The choices that have been made will be described for the individual facilities.

In the discussions which follow, the highlights of the adaptation-strategy techniques of the different investigators are given. More detail generally is available for each facility

in the questionnaire responses given in the Appendix.

3.2.2 2D Flexible, Impermeable-Wall Applications

It is useful to introduce at the outset the concept of aerodynamically-straight walls in an empty flexible, impermeable-wall test section. Due to boundary-layer growth on all four walls, a test section with parallel walls will exhibit an acceleration of the flow along its length. An aerodynamically-straight wall configuration is generated by divergence of the top and bottom flexible walls to the appropriate shapes that insure that the wall static pressure distribution is constant along the test-section length without a model present. The exact configurations for each facility are a function of Mach number and Reynolds number and can be calibrated once and for all. At free-stream Mach numbers approaching one, problems can be encountered in determining aerodynamically-straight contours [3.48], in part, at least, because of the sensitivity of Mach number to flow cross-section area near M = 1.

Flow charts for the alternative adaptation-strategy logic that can be used for this class of test sections are given in Fig. 3.2, which is taken from Chevallier, et al. at ONERA [3.49]. In terms of the analysis in the previous section, the flow-variable distribution Q_i is the longitudinal disturbance velocity component u deduced from the wall static-pressure orifices and P_i is the normal velocity component v deduced from the slope of the wall. In the special case of linearized compressible Group 1 flows represented by the Prandtl-Glauert equation with a planar interface, the operators G and G^{-1} are given by (see also Eqs. (6.34) in Section 6.2.1 of this report)

$$u(x) = G\{v\} = -\frac{1}{n\beta}\int_{-\infty}^{\infty}\frac{v(\xi)d\xi}{\xi - x} \qquad (3.9)$$

$$v(x) = G^{-1}\{u\} = +\frac{\beta}{n}\int_{-\infty}^{\infty}\frac{u(\xi)d\xi}{\xi - x} \qquad (3.10)$$

However, in Fig. 3.2, G and G^{-1} still are in the form of general nonlinear operators.

In the inverse mode in Fig. 3.2, the outer-flow calculation operator G^{-1} corresponds to $P_i[Q_j^m]$. The mismatch error distribution DP_i in the inverse mode is $v_{pre} - v_I$ and is driven to zero in the iterative scheme. This is a straightforward application of the theoretical formulation of the previous section.

The direct mode in Fig. 3.2 involves two outer-flow calculation operators, namely G, which corresponds to $Q_i[P_j^m]$ and its inverse G^{-1}, which in this instance corresponds to $P_i[\omega Q_j[P_k^m] + (1-\omega)Q_j^m]$ where ω is a relaxation factor. The mismatch error distribution DQ_i in the direct mode is $u_{pre} - u_I$, which is driven to zero iteratively. In transonic flow, $u_{pre} - u_I$ is a much more sensitive indicator of convergence of the iterative process than is $v_{pre} - v_I$. Although the direct mode involves two outer-flow calculations per iterative step, it is the preferred mode of operation and the procedures summarized in this section use it.

Judd, Wolf and Goodyer at Southampton University [3.11], [3.50] recognized a simplification in the direct mode for the linear case. They call this their predictive strategy. They assume that the result of the outer-flow operator G is available in the first iterative step from a calculation based on a given wall shape, y_{pre}, at the appropriate test Mach number and Reynolds number. It then follows that the G operator in subsequent iterative steps can be determined by suitably-relaxed addition of its previous value and the current interface measurement; i.e., without an outer-flow calculation. The simplest outer-flow evaluation of the G operator is for a wall which initially is aerodynamically straight; i.e., one for which $v_I = 0$, and so $u_E = 0$ from the G operator. In this case, the outer-flow calculations for G need not be made at all in the direct mode, but only the outer-flow calculations for G^{-1}. Many of the descriptions in the literature, e.g., by Barg at TU-Berlin [3.13], and by He and Zuo at Northwestern Polytechnical University [3.51], begin the iteration procedure with an aerodynamically-straight wall. However, as can be seen in the responses in the Appendix to Question 3.3, most facilities have a wide latitude in the choice of initial conditions in order to facilitate rapid iterative convergence. Usually, the test is begun with previously-obtained results from a closely-related shape, say from a previous iteration or from a good theoretical estimate, rather than from the aerodynamically-straight configuration.

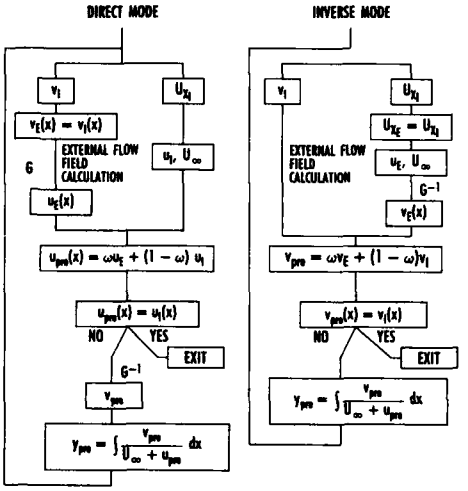

Fig. 3.2 Flow charts for direct and inverse modes of 2D flexible, impermeable-wall-test-section control algorithms (from [3.49]).

Judd, Wolf and Goodyer [3.11],[3.50] further showed from physical arguments that a relaxation factor $\omega = 1/2$ applies if it is assumed that changes in the wall shape adjustment do not affect the model significantly. This is the same value of ω that was conjectured by Ferri and Baronti [3.52] in their first paper. The theoretical analyses mentioned in Section 3.1.1 and subsequent experience by many investigators (including those at Southampton [3.50]) have shown that a scalar relaxation factor of $\omega = 1/2$ is an oversimplification. The resultant modifications will be discussed with regard to the strategies used in specific facilities.

The adaptation strategy at ONERA , both in S4LCh at Chalais Meudon and in T2 at CERT, has

been developed very extensively and is fully automated [3.49], [3.53]. Projections of the measurements of wall position and static pressure onto a mean planar reference surface are made for input to the outer-flow calculations. The calculations are performed by means of singularity distributions in the Prandtl-Glauert approximation for linearized compressible Group 1 flows. The modified growth of the top- and bottom-wall boundary layers from their aerodynamically-straight shapes due to the model influence is taken into account by calculating the displacement thickness from the wall velocity measurements using an integral method [3.49]. The free-stream velocity and angle of attack are determined as part of the iteration procedure by a technique which weights the residual interference by a factor that emphasizes the region of the flow near the airfoil. Procedures used by all of the other investigators (with ventilated and impermeable walls) seem to consist of adjustment of upstream conditions to the values required there by the outer-flow calculations, see the responses in the Appendix to Question 3.4.e. There is extensive discussion of the determination of free-stream velocity and angle of attack in the report of GARTEur Action Group AD(AG-02) [3.54]. Sears [3.22], [3.23] also has discussed this issue extensively, especially with regard to high lift with large flow deflection. ONERA has developed a very sophisticated method of relaxing the iteration. Instead of approximating the matrix inversion in Eq.(3.8) by a single constant, the P_i^m and Q_i^m measurements are decomposed into mode shapes corresponding to a source, a doublet, a vortex and a vortex doublet. Each of these modes has a separate ω that is a good approximation to the nature of the matrix inversion in Eq. (3.8) for that mode. Convergence in at most five steps (and generally less) can be achieved depending on initial conditions and the severity of the case. No figure of merit is used, but the iteration terminates when no further wall adjustment is possible. Finally, residual interference is calculated by the method of Capelier, et al. [3.55].

Southampton University investigators also have developed their adaptation strategy extensively and have automated it for testing in the the transonic TSWT [3.48], [3.56]. Developments of the basic predictive strategy that is discussed above have been used in most of the testing. Subsequently, though, Judd (as reported by Lewis [3.48]) has developed an improved procedure which is called an exact strategy. This exact strategy removes some of the restrictive approximations of the predictive strategy, including limitations due to the use of a mean, planar interface. Lewis, et al. [3.46], [3.48] have discussed results with the various alternative strategies for several configurations. Only the well-tested predictive strategy will be discussed here because of its widespread use in other facilities and the lack of adequate documentation of the exact strategy. The modified boundary-layer growth on the top and bottom walls in the presence of the model can be taken into account, although their experience [3.46], [3.48] has shown that below M=0.85 the effect is unimportant. The outer-flow computations in the predictive strategy are based on singularity distributions in the Prandtl-Glauert approximation with Group 1 flows and on numerical solutions of the TSDE with Group 2 flows [3.46], [3.48]. Southampton University investigators also have refined their method for relaxing the iterative solution. The idealized $\omega = 1/2$ discussed above has been modified empirically to accelerate convergence. That is, top and bottom flexible-wall coupling factors and scaling factors have been determined, which change ω to a value different from 1/2. These factors provide an improved approximation to the matrix-inversion operator in Eq.(3.8) and lead to convergence in only two steps on the average. The figure of merit is the uniformly-weighted average of the modulus of the pressure-coefficient differences across the interface between the measurements and the computed outer flow. Residual perturbations of the flow at the model location are evaluated by the method of [3.32]. Iteration ceases when the residual perturbations are reduced below a fixed level. Additional details of the Southampton residual-interference calculations, with examples, are given in Section 6.2, Tables 6.1 to 6.3, and Fig. 6.1 of this report.

The automated adaptation strategy of TU-Berlin is very similar to what has been discussed for ONERA and Southampton University. A discussion of the effects of the modified boundary-layer growth due to the presence of the model at M = 0.76 is given in [3.57]. The outer-flow computation is based on analytical procedures for the Prandtl-Glauert equation with Group 1 flows and on numerical solutions of the full-potential equations with Group 2 flows. A scalar relaxation factor replacing the matrix-inversion operator of Eq. (3.8) is used in the iterative procedure and has been determined empirically to achieve convergence routinely in two to four steps. Either agreement between the measured and computed longitudinal velocity component at the interface or the limit of no further wall adjustment is the criterion for convergence. Residual interference is computed along the airfoil centerline by a Cauchy-integral method.

The new flexible, impermeable-wall facilities that have been constructed in recent years are building upon the experience that has been achieved elsewhere. The University of Naples AWWT is just beginning operations and has not reported any results. The NASA/LaRC TCT now has accomplished a substantial amount of testing [3.58], [3.59]. The automated adaptation technique used to date in the TCT is based upon the predictive strategy as developed and refined at Southampton University. Northwestern Polytechnical University uses an adaptation strategy very similar to that of Southampton University and TU-Berlin. Besides using a scalar relaxation factor like TU-Berlin, they also have investigated convergence acceleration schemes that use the results of successive iterative steps either in an average scalar sense over the entire interface or locally as a function of distance along the interface [3.51].

3.2.3 2D Ventilated-Wall Applications

Adaptation strategy for the ventilated-wall tunnels has been driven in large measure by the interface-measurement system chosen by each group of investigators. Since the interface is located some distance within the walls of the test section, the wall control variables, X_j, are necessarily different from P_j, so approximations to Eq. (3.5) are in order in the most general formulation. In most applications, however, Eq. (3.8) has been used with a separate relationship established between P_j and X_j.

The Calspan ATC One-Foot Transonic Tunnel and the AEDC Aerodynamic Wind Tunnel (1T), as operated in its 2D adaptive-wall implementation [3.40], [3.41], had different mechanisms for wall control, see Section 3.1.2, and some differences in details of the instrumentation. Both facilities measured static pressure and flow angle at planar interfaces above and below the test article. The NASA/ARC 25x13 cm transonic tunnel uses an entirely different interface-measurement

system, namely laser-velocimeter measurements only of the vertical velocity component; i.e., the component normal to the interface. Each planar interface then actually is comprised of a pair of displaced planar surfaces. Measurement of the one velocity component at the two displaced planes also provides a suitable independent pair of measurements for implementing the adaptive-wall principle. The two displaced planar surfaces are discussed further in Section 6.2.2 with regard to residual-interference calculations. The adaptation strategies of each facility now will be discussed.

In the Calspan ATC investigations [3.39], [3.60], [3.61], experience showed that greater sensitivity and ease of adjusting the individual plenum-pressure control-valve settings, X_j, could be achieved if the disturbance quantity set at the interface, P_i, was u, as determined from static pipes. This followed first because u is much more sensitive than v in transonic flow. Second, the nature of individual plenum-pressure control is such that if the static pressure at an upstream reference point near the test-section entrance is held fixed during valve adjustment, the effect on u is approximately zero upstream of the plenum chamber being adjusted and constant downstream. Thus a sequential adjustment procedure beginning at the upstream end of the test section [3.8] is possible. This procedure was performed manually; no automation was developed for these proof-of-concept experiments. The quantity Q_i was v, measured in Group 1 flows by flow-angle probes and in Group 2 flows by a combination of the probes and the two-component static pipes developed at Calspan ATC [3.62], [3.63]. The outer-flow calculation for Group 1 flows was by a multipole expansion technique based on the Prandtl-Glauert equation [3.6], and for Group 2 flows was by numerical solutions of the TSDE; all calculations were performed off line. Care had to be exercised to avoid an unwanted uniform crossflow induced by imbalance between top and bottom wall plenum-chamber pressure. Initial conditions were either estimates of P_i calculated from theoretical representations of the airfoil or valve settings from a previous result. Although Eq. (3.5) represents the basic iterative procedure for this configuration, the relationship between ΔX_j and ΔP_j was satisfied separately after ΔP_j was found from Eq. (3.8). The actual technique used Eq. (3.8) with the matrix-inversion operator replaced by a scalar relaxation factor between about 0.1 and 0.5, with 0.25 and 0.50 being best in limited experience for subcritical and supercritical cases, respectively. The relationship between the distribution P_j set at the interface and the plenum pressure control valves, X_j, followed the sequential procedure discussed above. No figure of merit was used, but P_i^m and $P_i[Q_j^m]$ were plotted and compared. Iteration terminated when further improvement was no longer possible. Residual corrections were not considered.

The AEDC 2D adaptive-wall experiments [3.40], [3.41] also chose P_i to be u, as measured by one-component static pipes, and Q_i to be v, as measured by traversing flow-angle probes. In this facility, longitudinal wall-porosity distributions and sub-plenum chamber valve settings (in later experiments) were the control variables, X_j. The outer-flow calculation for Group 1 flows was the one-step procedure based on solutions of the Prandtl-Glauert equation [3.16],[3.17] (see also Sections 3.1.1 and 3.2.1), and for Group 2 flows was numerical solution of the TSDE. Initial conditions usually were the uniform-porosity, constant-global-plenum-pressure, empty-tunnel calibration settings for the test condition chosen. Equation (3.5) represents the iterative procedure for this configuration, but separation into Eq. (3.8) and a separate relationship between ΔX_j and ΔP_j was made. The AEDC one-step method is an exact, linear equivalent of the general Eq. (3.8), as already discussed in Section 3.2.1. The TSDE iterations approximated the matrix-inversion operator of Eq. (3.8) with a scalar relaxation factor of 0.5. The relationship between the distribution P_j set at the interface and the control variables X_j was achieved by adjusting ΔP_j to be zero at the upstream and downstream ends of the test section and in the suction-peak region near the model. No figure of merit was used, but P_i^m and $P_i[Q_j^m]$ were plotted and compared. In cases for which the linear one-step method was applicable, no further improvement could be made after the first step. In supercritical cases, iteration terminated when no further improvement could be achieved. Residual corrections were not considered.

The NASA/ARC 2D experiments [3.64], [3.65] in the 25x13 cm adaptive-wall tunnel used non-intrusive, traversing laser-velocimeter measurements of the vertical velocity component, v, which is normal to a pair of displaced planar surfaces, as already mentioned. Therefore, P_i was defined as v at the planar surfaces that are farther from the model, while Q_i was defined as v at the planar surfaces that are nearer. The control-valve settings for the individual plenum chambers adjoining the slotted top and bottom walls were chosen as X_j. The outer-flow calculation was by means of numerical evaluation of analytical expressions based on the linear, Prandtl-Glauert equation [3.66] for Group 1 flows. Although Eq. (3.5) strictly is applicable, Eq. (3.8) was used with the matrix-inversion operator replaced by a scalar relaxation factor of 0.5. NASA/ARC pioneered the measurement of the (square) control-effect matrices $\partial P_i/\partial X_j$ and this was an important contribution. They found that empty-tunnel measurements of these matrices were satisfactory for their operating range of interest. Initial conditions to begin the iteration were "passive walls", i.e., without mass flow through the walls. The figure of merit was the rms difference between the values of P_i at the control points as measured and calculated for the outer flow. The iteration proceeded until no further improvement in the figure of merit was possible. Somewhat after the initial experiments, linear two-variable WIAC methods, see Section 6.2.1, were developed for the displaced-surface configuration [3.67], [3.68] and applied to the data.

The NASA/ARC 25x13 cm adaptive-wall tunnel has been used recently in an experimental program by Celik and Bodapati [3.69]. They built upon the previous NASA/ARC techniques and made an extensive examination of the use of the control-effect matrices $\partial P_i/\partial X_j$. They also investigated sidewall pressure measurements as an alternative to the laser-velocimeter measurements at the displaced surfaces. Finally, they developed a technique in which they carried out the bulk of the iterative procedure for Eq. (3.8) with the control-effect matrices used to simulate the changes in the inner, model-induced flow field during the process. That is, after the first experiment, the next steps were simulations. Upon convergence, the total changes in plenum pressure, ΔX_j, predicted by these simulations were implemented experimentally to verify that the improvements had been achieved.

NASA/ARC also has built a 2D adaptive-wall test section for the 2x2 ft transonic wind tunnel. Details are given in their questionnaire response in the Appendix and in [3.70]. There is a great deal of flexibility available for using

two-component laser velocimetry with alternatives for using u and v at a single planar surface or either component at the displaced planar surfaces. Moreover, the outer-flow calculations can be performed using a variety of linear methods based on the Prandtl-Glauert equation for Group 1 flows or by numerical solution of the TSDE for Group 2 flows. Schairer [3.21] has described these alternatives along with numerical simulations. Preliminary experimental results from this tunnel have been presented in Adaptive Wall Newsletter No. 9, February 1989 and some of them are reproduced in Section 6.2.1 of this report under the Two-Variable Method heading, see Figs. 6.5 to 6.7, especially. The same Newsletter states that development of this test section has been discontinued.

3.2.4 3D Flexible, Impermeable-Wall Applications

There is very little to summarize here that is conceptually new in the streamlining algorithms for complete 3D matching over the entire interface. The principal new features are the 3D one-step methods developed at DFVLR/Göttingen and TU-Berlin. This is not to say that the practical problems of developing and implementing the procedures were not difficult, but rather that the algorithms have been built upon the 2D framework and experience.

There are three facilities with flexible, impermeable walls to be discussed here, namely the rectangular-cross-section, low-speed Sverdrup AWAT, the circular-cross-section, rubber-wall transonic DFVLR DAM, and the octagonal-cross-section, transonic TU-Berlin TUB(3D), see Section 3.1.3 and the Appendix. All three of these tunnels use the inverse mode of Fig. 3.2 and so define P_i as the velocity component normal to the interface (here the mean position of the walls), v_n, as evaluated from the wall slope, and Q_i as the longitudinal velocity component, u, evaluated from static pressure taps on the walls. The iterative procedures in each facility are based upon Eq. (3.8).

The Sverdrup AWAT procedure [3.71] replaced the matrix inversion of Eq. (3.8) with a scalar relaxation factor ω of approximately 0.070. The outer-flow calculations were performed by an incompressible-flow, source-panel method which was satisfactory for their test conditions. Typical iterations converged in three to seven steps beginning either with aerodynamically-straight or suitably-deformed wall shapes. Wall adjustments were performed manually in this proof-of-concept program.

The DFVLR DAM investigation involved both subsonic and supersonic free-stream conditions [3.31], [3.72], [3.73]. For subsonic Group 1 flows, a one-step procedure [3.31], [3.74] was developed to represent the matrix inversion in Eq. (3.8). The procedure is analytical and is based upon separation of variables for a cylindrical coordinate system and makes use of Fourier-series expansions in both the longitudinal and azimuthal coordinates (see also Sections 3.1.1 and 3.2.1). The interface cross section is a uniform circular cylinder. The iterations converged to a maximum error in matched pressure coefficient of 0.005 in one or two steps. For supersonic Group 3 flows, Eq. (3.8) was approximated by a scalar relaxation factor of ω = 0.50. The outer-flow calculations were performed by local application of the linear 2D relationship between flow inclination and pressure coefficient [3.73]. The procedures were totally automated. Residual interference corrections were assumed to be negligible and were not evaluated.

The TU-Berlin TUB(3D) investigations also involved both subsonic and supersonic free-stream conditions [3.3], [3.14], [3.15]. For subsonic free streams, two different approaches to Eq. (3.8) were used. In initial experiments, the matrix inversion was replaced by a scalar relaxation factor, which led to a very slow rate of convergence with an optimum ω of about 0.055 [3.3], [3.15]. Subsequently, a one-step procedure [3.15] was developed in order to represent the matrix inversion better. A separation-of-variables analysis following that developed at DFVLR was not possible for the octagonal cross section. Thus the TU-B one-step method used discretization of the governing equations by means of linear source-panel methods for Group 1 flows. The outer-flow calculations were performed by numerical solutions of the full-potential equations for Group 2 flows. The iterations converged in from one to four steps depending on Mach number and angle of attack, with fewer steps necessary for Group 1 flows. For supersonic Group 3 flows, Eq. (3.8) was approximated by a scalar relaxation factor of ω = 0.50. The outer-flow calculations were performed by numerical evaluation locally of the nonlinear, 2D shock-wave and expansion-wave relationships [3.14]. The procedures were totally automated and residual interference perturbations were evaluated for the subsonic free-stream cases.

3.2.5 3D Ventilated-Wall Applications

Adaptation strategy in 3D ventilated-wall applications has been driven by interface-measurement-system considerations just as in 2D. There is very little generality in the approaches used in the four test sections to be discussed here, see Section 3.1.3, namely the AEDC Tunnels 4T and 1T for Group 2 flows, the NASA/ARC 25x13 cm tunnel for Group 1 flows, and the University of Arizona AWWT for low-speed, powered-lift, large-flow-deflection testing in Group 1 flows.

The AEDC 3D experiments in Tunnel 4T used a straightforward extension to 3D [3.44] of the AEDC 2D procedures that are described in Section 3.2.3. The variable P_i was defined as the longitudinal perturbation velocity component, u, and Q_i was the velocity component normal to the interface, v_n. The control variables, X_j, were the uniform porosity of the top, bottom and sidewalls (which were ganged together to move in unison). The interface was of rectangular cross section and a traversing conical-head pressure probe measured static pressure and flow inclination, from which u and v_n were deduced by means of the TSDE assumptions. The Group 2 outer-flow calculations consisted of numerical solutions of the TSDE. Eq. (3.5) strictly holds, but separation into Eq. (3.8) and a separate relationship between ΔX_j and ΔP_j was made. The iterative procedure approximated the matrix inversion operator of Eq. (3.8) with a scalar relaxation factor of ω = 0.50. The relationship between the ΔX_j and ΔP_j was determined by matching the suction peaks in u at the interface in the vicinity of the model. Initial conditions were the empty-tunnel calibration conditions for the test porosity and Mach number. The procedure was not automated for these exploratory experiments; the iteration terminated when no further improvement could be achieved in matching P_i at the interface. No residual corrections were attempted.

The AEDC 3D experiments in Tunnel 1T utilized a distinctly different iteration procedure from all other adaptive-wall investigations [3.75]-[3.77]. The variable P_i was defined as the static pressure coefficient, c_p, and Q_i was defined as the radial derivative of c_p,

$\partial c_p/\partial r$, which is normal to the circular-cross-section interface. P_i and Q_i were measured by a pair of two-component static pipes that were fixed to a mechanism which rotated to discrete angular positions around the tunnel centerline. The Group 2 outer-flow calculations were numerical solutions of the TSDE, as written in terms of c_p; i.e., a transonic, small-disturbance acceleration potential. The X_j were the ratio of upstream-sidewall-static-pressure to tunnel-stagnation-pressure and the porosity of selected groupings of wall segments. All of this is described and illustrated in greater detail in the Appendix.

The iterative procedure consisted of the definition of a limited figure of merit for the purpose of suggesting the control setting for the next iterative step, namely the rms value of a selected part of the mismatch distribution DP_i. Thus, in each iterative step, DP_i was determined for the whole interface and the limited figure of merit was evaluated; then a search was carried out in control space to reduce it. The control effect was determined by suitably-weighted integration of the $\partial P_i/\partial X_j$ matrix measured at the test conditions in the presence of the test article. It was observed that when the limited figure of merit was reduced, the global matching also improved. Moreover, it was found useful to redefine the limited figure of merit by weighting the rms computation in the region of the model wing and ignoring the region near its tail, and vice versa. There was evidence that the optimal procedure was to use both of these limited weightings in a certain sequence in order to obtain the best global matching [3.77]. Iteration began with initial conditions of the empty-tunnel calibration conditions at the test Mach number and porosity; iteration terminated when no further improvement could be made, usually after two or three steps. Subsequent to the experiments, 3D nonlinear residual-interference calculation procedures have been investigated at AEDC, see Section 6.2.2.

The NASA/ARC 3D experiments in the 25x13 cm tunnel followed an extension [3.78] of the NASA/ARC 2D procedures described in Section 3.2.3. A single flow variable, namely the vertical velocity component, w, was measured at parallel, but displaced surfaces by a traversing one-component laser velocimeter. The displaced surfaces were right rectangular prisms. The variable P_i was defined as w at the surface farther from the model and Q_i was w at the nearer surface. The control variables X_j were defined as the valve settings controlling the plenum pressure in each individual chamber (arranged both longitudinally and laterally) adjoining the slotted top and bottom walls. The sidewalls were rigid, impermeable and planar. The Group 1 outer-flow calculations were numerical finite-difference solutions of the Prandtl-Glauert equation for w [3.66]. Just as in 2D, the iterative procedure of Eq. (3.8) was used with the matrix-inversion operator replaced by a scalar relaxation factor, ω, of between 0.5 and 1.0. Measurement was made of the control-effect matrices $\partial P_i/\partial X_j$ for the empty tunnel to relate ΔX_j to ΔP_j. Initial conditions were "passive walls" without any mass flow through them. The procedure was not automated at this stage of development. The figure of merit was the rms difference between the values of P_i at the control points as measured and calculated for the outer flow. The iteration terminated when no further improvement in matching at the interface was possible, usually after three iterative steps. Residual interference corrections were not considered.

The University of Arizona program was different from all other adaptive-wall investigations because it was directed toward solving the problem of configurations producing very large flow deflections [3.22], [3.23]. Typical of such situations are tests of configurations that produce very large lift, such as V/STOL aircraft, by means of powered high-lift devices. Such tests often involve large wall interference, including difficulty in the accurate establishment of the simulated flight speed and direction. The Arizona project was intended to alleviate these difficulties by use of the adaptive-wall principle; in particular, the simulated flight vector is inclined at large angles to the top and bottom tunnel walls to accommodate the large flow deflection. The flight vector inclination is chosen to insure that the highly-deflected wake flow trails generally down the length of the test section well away from the top and bottom walls.

The goal of the experiments reported by Lee and Sears [3.79], [3.80] was to prove this concept by demonstrating that satisfactory matching could be achieved at the interface in tests of a high-lift aircraft model. The demonstration tunnel used in the experiments had top and bottom walls consisting of panels of louvers whose blade angles were controllable. Tunnel air was supplied through the bottom wall as well as at the upstream end of the test section, and was exhausted through the top wall as well as at the downstream end of the test section. A traversing laser velocimeter was used to measure velocity components at a five-sided rectangular interface (open downstream). A representative test model, namely an airplane model with lower-surface blown wing flaps, was mounted in a nose-down attitude in the test section.

The horizontal velocity component was chosen as Q_i and the vertical component as P_i, except at the sidewalls of the interface, where P_i was a laterally-displaced horizontal component. The iteration procedure was that of Eq. (3.5) with $P_i[\partial Q_k/\partial X_j]$ neglected and a relaxation factor multiplying the remaining terms in the matrix inversion operator. The control-effect matrix $\partial P_i/\partial X_j$ was always measured with the correct model configuration; it was usually found that a given measured matrix could be used successfully throughout an iteration sequence. Relaxation factors varied from 0.10 to 0.25 - usually 0.15. The rms value of the mismatch distribution DP_i was chosen as the figure of merit. Residual interference was calculated using an interface-discontinuity method, see Section 6.2.1 of this report. The mean values of the residual-interference velocity components at the model position were correlated with the interface figure of merit.

3.3 Representative Results

Extensive results have been published by now and there is no intention here to present a great deal of material. Rather, some representative results and citations to the literature will be given. Results for 2D and 3D configurations will be presented separately. All 3D results will be for adaptation by matching over the entire interface, as described in Section 3.1.3.

3.3.1 2D Results

The results in this section are divided into the same three speed-range groups, namely testing at subsonic free-stream conditions, first with subcritical flow at the interface and subcritical or supercritical flow at the model (Group 1

flows) and second with supercritical flow at the interface (Group 2 flows), and finally testing at supersonic free-stream conditions (Group 3 flows). The greatest part of the experimental work to date has been for Group 1 flows. Practical and efficient procedures have been developed to generate high-quality 2D airfoil data. Comprehensive data for Group 1 flows have been obtained only in the flexible, impermeable-wall 2D test sections. The 2D ventilated-wall test sections at AEDC, Calspan ATC and NASA/ARC were used for experimental demonstrations of the concept in Group 1 flows, but without extensive and systematic data gathering. The AEDC and Calspan ATC investigations then concentrated on development of procedures for Group 2 flows before completion in 1980.

At least ten different airfoils have been tested in various adaptive-wall test sections, as can be seen by examination of the responses to Question 3.7 in the Appendix. Moreover, circular cylinders at low speeds and large blockage have been tested successfully by Goodyer [3.37],[3.38] in the 1973-1975 time period, as already described in Section 3.1.2, and by He, et al. [3.51] recently. Group 1 flows for three different airfoils, namely the NACA 0012, the CAST 7 and the CAST 10 sections, have been tested by more than one organization in their adaptive-wall test sections. Adaptive-wall data for these airfoils will be emphasized.

The NACA 0012 section has an extensive literature, and as described by Wolf and Ray [3.59], "So much data exist that almost any data set will agree with something." Fortunately, this very issue has been addressed systematically and comprehensively by McCroskey [3.81], who analyzed the data and categorized it according to its quality. Adaptive-wall data included in the highest-quality category of [3.81] are those acquired in the NASA/LaRC 0.3 m TCT and corrected for residual wall interference by Green and Newman [3.82], see also Section 6.2.2 of this report. Selected results of the TCT data have been reported by Wolf, et al. Interested readers are referred to [3.58], [3.59], [3.81], [3.82] for these TCT NACA 0012 data.

The airfoil section which has the richest adaptive-wall experience is the CAST 7. This came about because the Group for Aeronautical Research and Technology in Europe (GARTEur) set up Action Group AD(AG-02) on "Two-Dimensional Transonic Testing Methods." This action group compared test results obtained with the CAST 7 section in several facilities in the member countries. Both passive- and adaptive-wall test sections were used. The participating adaptive-wall facilities were the TU-Berlin TUB(2D) and the ONERA/CERT T2. The test programs, wall-interference corrections and data analyses were carefully planned, executed, compared and reported [3.54]. Later, the same CAST 7 model tested in TUB(2D) was also tested in the Southampton University TSWT [3.46],[3.83], but too late for inclusion in [3.54]. The GARTEur report is highly recommended to anyone concerned with 2D airfoil testing.

A cooperative program still active is concerned with testing the CAST 10 airfoil. Among the facilities in which this section is being tested are the ONERA/CERT T2 [3.84] and the NASA/LaRC TCT adaptive-wall tunnels [3.59], [3.85]. Some initial comparisons of data are discussed in [3.59]. Also, residual corrections of a TCT data point for the CAST 10 are presented in Figs. 6.3 and 6.4 and discussed in Section 6.2.1 of this report.

An important 2D testing issue that has not been discussed yet is the presence of the test section sidewalls. The interaction of the sidewall boundary layers with the pressure field induced by the 2D model has a profound effect on the two-dimensionality of the flow field. These sidewall effects are intrinsic to all 2D and 3D half-model testing, of course, and are not solely an adaptive-wall difficulty. Sidewall boundary layers are discussed in considerable depth in the GARTEur report [3.54] and were considered carefully by McCroskey [3.81] in his decisions as to the relative quality of the NACA 0012 data sets. Moreover, ONERA/CERT has determined that in T2 the sidewall effects are a major factor in determining Mach-number/angle-of-attack limitations for CAST 7 testing, see their response to Question 3.8.e in the Appendix and [3.49], [3.53]. Also, the TUB(2D) results for the CAST 7 in [3.54],[3.86] encountered undesirable sidewall effects in some regions of the testing envelope. Sidewall interference is discussed further in Section 6.2.3 of this report.

There are a few specific results of general interest that will be presented here for the light that they cast upon various aspects of the adaptive-wall procedures. The first is the effect of testing a 2D airfoil located at and below the centerline of the test section. This provides an important verification of the self-consistency of all aspects of a given adaptive-wall procedure. The results presented are from Archambaud and Mignosi [3.53], but similar results are presented by Chevallier, et al. [3.49]. Figures 3.3a and 3.3b show results for a CAST 7 model located on the centerline (Position A) and 20% of the nominal test-section height below the centerline (Position B). The wall contours and local Mach number distributions on the walls in Fig. 3.3a are much better balanced between the two walls for Position B because the relative effects of thickness and lift are accommodated better. The effect of model location on the local model-upper-surface pressure distribution, p, (normalized by the free-stream pressure, p_0) is shown in Fig. 3.3b for two angles of attack. Most of the T2 data presented in [3.54], [3.87] were obtained for the CAST 7 in Position B.

Another interesting self-consistency check is to rotate the aerodynamic centerline with respect to the geometric centerline. This procedure has been discussed by Goodyer [3.37] and by Chevallier, et al. [3.49]. The results here were obtained by Wolf [3.58] in the NASA/LaRC TCT. In these tests, the aerodynamic centerline was rotated by up to 0.5 deg by suitable modifications of the aerodynamically-straight contours. Then, routine streamlining was performed. The results for normal-force coefficient are shown in Fig. 3.4a and wall deflections in Fig. 3.4b both before and after an upward rotation of 0.5 deg. An angle-of-attack shift of 0.5 deg is observed in c_n up to stall. Similar results have been presented in Fig. 7 of [3.49].

An example of an identical model tested in two different facilities will be presented next. The CAST 7 section was tested in TUB(2D) as part of the GARTEur investigation [3.54] and later in the Southampton University TSWT [3.46], [3.83]. The tests were at identical stagnation conditions so that the Reynolds numbers were identical at identical free-stream Mach numbers. Fig. 3.5, which is from Lewis, et al. [3.46], shows the pressure coefficient distributions, c_p, after streamlining in each facility. The test conditions correspond to the design point of the section. The lift coefficients and Mach numbers are almost equal, leading to reasonable agreement between the c_p distributions. The significant

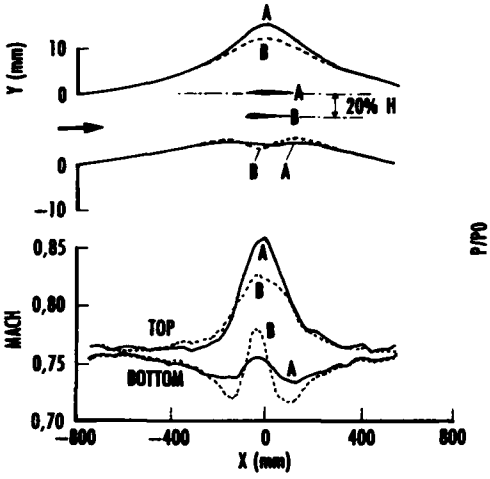

a. Wall contours and local wall Mach numbers for α = 1 deg

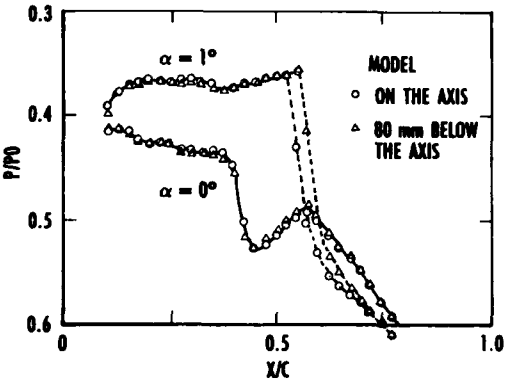

b. Pressure distribution on airfoil upper surface, normalized by freestream pressure, for α = 0 and 1 deg

Fig. 3.3 Effects of airfoil location in ONERA/CERT T2 test section; CAST 7 section at M = 0.76, nominal tunnel height H = 400 mm (from [3.53]).

differences are confined to the regions of the lower-surface suction peak and the upper-surface shocks, the positions of which are displaced by about 4% of the chord.

The final subcritical-interface results to be presented are from a recent systematic study in the Southampton University TSWT. This investigation [3.48],[3.88] compared the Southampton predictive and exact strategies for adaptation (see Section 3.2.2 for a discussion and references) with the pioneering NPL strategy described in Section 1.2 of the Introduction to this report. The results shown in Fig. 3.6 also have been presented by Lewis, et al. [3.46]. The model was a 10.2 cm chord NACA 0012-64 airfoil in the nominally 15.2 cm square TSWT. The tests covered the Mach number range from 0.4 to 0.8 at angles of attack from 0 to 6 deg. The specific form of the NPL streamlining algorithm consisted of testing the model first with aerodynamically-straight walls, then with the walls adjusted to have constant pressure along their length, followed by an adjustment of the walls to a position 0.6 of the way between the aerodynamically-straight and constant-pressure shapes. Fig. 3.6 shows typical model c_p data. The c_p distributions are plotted with the walls streamlined according to the three different algorithms, and all three lead to essentially the same model performance. In particular, the positions of the upper-surface shocks fall within a band of about 2% of the chord. The c_p distributions with the walls set to the aerodynamically-straight and constant-pressure contours are also shown.

The literature for Group 2 flows, subsonic free-stream conditions with supercritical flow at the interface, shows that basically only developmental work defining the problem areas has been accomplished. There are no systematically-acquired data obtained in more than one facility.

The early ONERA S4LCh tests for an NACA 64A010 airfoil section with 4.4% solid blockage [3.9],[3.10] have been mentioned already in

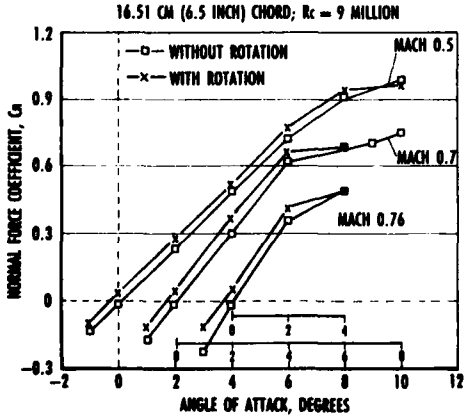

a. Normal force at three Mach numbers

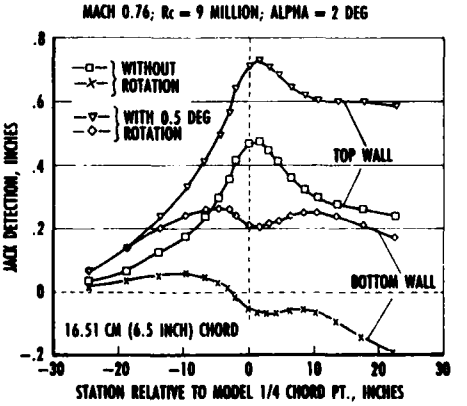

b. Streamlined wall contours at M = 0.76, α = 2 deg

Fig. 3.4 Effects of a test section centerline rotation upward by 0.5 deg; NACA 0012 airfoil in NASA/LaRC TCT (from [3.58]).

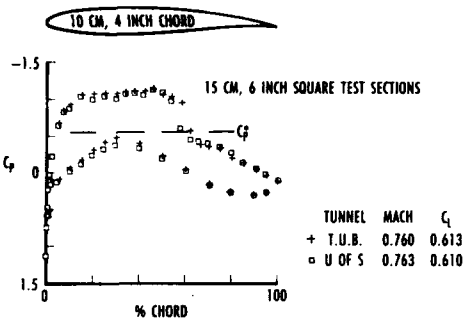

Fig 3.5 Comparison of airfoil surface pressure coefficients for the same airfoil, as streamlined in the Southampton University TSWT and the TU-Berlin TUB(2D) test sections; CAST 7 section at nominal M = 0.76, C_{ℓ} = 0.61 with identical stagnation conditons (from [3.46]).

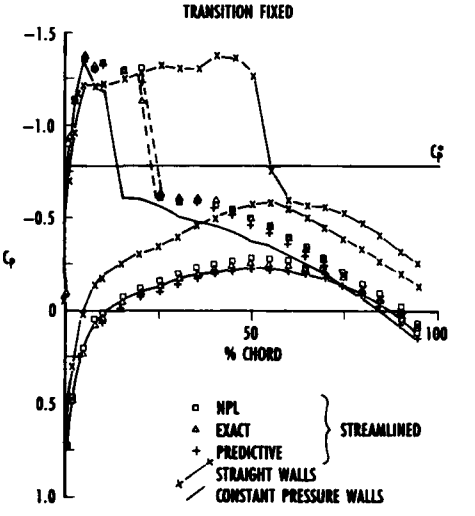

Fig 3.6 Comparison of airfoil surface pressure coefficients in the Southampton University TSWT after aerodynamically-straight and constant-pressure wall adjustments and after streamlining by three adaptation strategies (original NPL, SU predictive and SU exact strategies); NACA 0012-64 section at M = 0.7, α = 4 deg (from [3.46]).

Section 3.1.2. There does not seem to have been a published sequel to these initial Group 2 adaptive-wall demonstration results.

In the 1976 to 1981 time period, the Calspan ATC One-Foot Transonic Tunnel and the AEDC Tunnel 1T (in 2D adaptive-wall configurations) were used to attack the problems of supercritical flow at the interface and walls of perforated-wall test sections. The principal emphasis was on exploration of the flow and facility phenomena involved. This information was necessary for planning 3D implementation. At that stage of the development process, neither facility had been automated. Therefore no systematic data acquisition was attempted.

The Calspan ATC investigation had its best Group 2 success [3.61] for an NACA 0012 section of 4% blockage at M = 0.9, α = 1 deg, 2 deg and 3 deg (nominally). Behavior of the NACA 0012 is very interesting at this Mach number because the lift-curve slope at angles of attack between 0 deg and about 1.5 deg has a significantly smaller value than it does above 1.5 deg. Moreover, the flow tends to be unsteady, even at fixed flow conditions and model attitude, near α = 0 deg. The techniques employed during the experiments are described in the Appendix and in [3.61]. The results after adaptation were improved significantly, although many questions remained unanswered.

The AEDC investigation [3.40], [3.41] also used an NACA 0012 section, but of 6% blockage, and achieved significantly improved results over those obtained with the 1T calibration conditions at M = 0.80, α = 0 deg, 1 deg, 2 deg and 4 deg, as well as limited improvement at M = 0.90, α = 0 deg. It should be noted that for the Group 1 flow at M = 0.65, α = 0 deg with the 1T calibration conditions set, there was no appreciable interference and the functional relationships of Eq. (3.1) were satisfied without iteration [3.40].

Recently, Lewis [3.46], [3.48], [3.89] has performed two series of Group 2 flow experiments in the Southampton TSWT for an NACA 0012-64 section of 8% blockage. Very encouraging results at angles of attack up to 4 deg were obtained in the first series [3.89] for Mach numbers from 0.90 to 0.94, but results for 0.95 to 0.97 were less satisfactory, see Section 6.2 and Table 6.3 of this report for additional details. In the second series of tests, the maximum Mach number was reduced to M<0.90 by air-supply limitations unrelated to the adaptive-wall aspects of the facility. Excellent results were obtained in the Mach number interval from 0.85 to 0.89 [3.46], [3.48]. It is hoped that the Southampton experiments for M>0.90 can be continued, since there are many outstanding questions that warrant further research.

The final experiments to be reported are for 2D Group 3 flows with supersonic free-stream conditions. The only investigation known was performed in the ONERA S5Ch facility [3.90] for the flow about circular cylinders. The longitudinal position of the cylinders in the test section was adjusted until the detached bow shock wave impinged on the walls just at the end of the conventional M = 1.2 nozzle. Downstream of the bow shock, the adjustable transverse sliding plates were shaped to accommodate the small perturbation angle of the flow. The subsonic region behind the bow shock did not exhibit reflections, but some residual wall interference may have existed. However, the flow over the cylinder was observed to be surprisingly insensitive to wall shape during the adaptation process. Some exploratory Group 3 high-lift experiments for a 3D configuration with 2D adaptation are described in Section 4.3.6 and Fig. 4.24 of this report.

3.3.2 3D Results

The results in this section also are divided into Groups 1 to 3 flows. Moreover there is an additional subdivision into axisymmetric test articles at zero angle of attack and more general lifting configurations.

The axisymmetric configuration that has received the greatest attention is the ONERA C5 calibration model which has been tested in the fully 3D impermeable-wall tunnels TUB(3D) [3.3],

[3.15], [3.91], [3.92] and DFVLR DAM [3.72] for Group 1 flows. The results of these investigations have been summarized in the review by Ganzer [3.3] and a selected result is presented in Fig. 4.20 in Chapter 4 of this report along with additional results from testing in Tunnel T2, which has 2D wall-adaptation capability only. Also, the FFA axisymmetric spindle configuration has been tested extensively in the DFVLR DAM facility [3.3], [3.31], [3.72] up to M = 0.85.

Probably the most interesting results to date for axisymmetric configurations are in Group 3 flows, i.e., experiments for a 10 deg half-angle cone-cylinder tested in TUB(3D) [3.14] and in DFVLR DAM [3.73] at M = 1.2. The model surface-pressure distributions measured before and after adaptation in TUB(3D) are shown in Fig. 3.7a in comparison with results from a full-potential numerical solution. The corresponding wall deflection from the aerodynamically-straight position is shown in Fig. 3.7b after adaptation along with the wall Mach number distributions before and after adaptation. The blockage in TUB(3D) was 1.13%. Similar results from DFVLR DAM are shown in Fig. 3.8a before adaptation where η is the aerodynamically-straight contour necessary to achieve M = 1.2 free-stream conditions. Fig. 3.8b presents the results after adaptation with Δr = 3.5 mm as the deflection at the sixth jack station. The blockage was 2.00%. In both Figs 3.8a and 3.8b, the results are compared with reference data for the same model in the passive, perforated-wall AEDC Aerodynamic Wind Tunnel (16T) at 0.008% blockage.

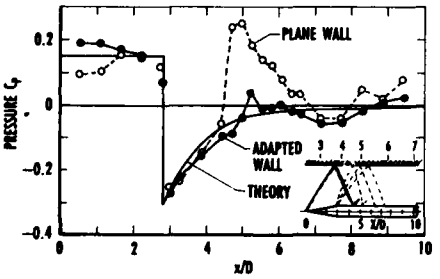

a. Model surface pressure coefficients

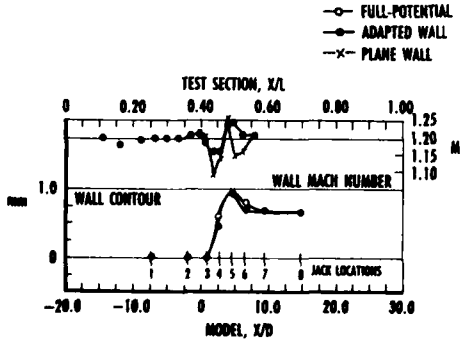

b. Wall contours and local wall Mach number

Fig 3.7 Comparison of full-potential-theory predictions with experimental data before and after adaptation of an axisymmetric body in TU-Berlin TUB(3D) test section; ten-degree-half-angle cone-cylinder at M=1.2, α = 0 deg (from [3.14]).

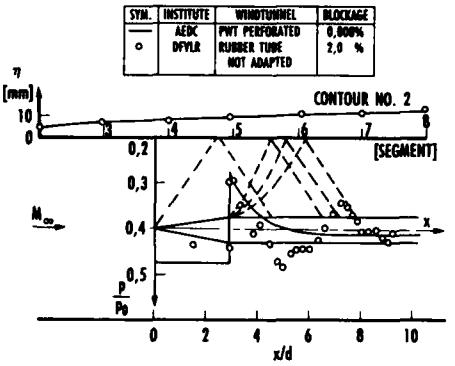

a. Before adaptation

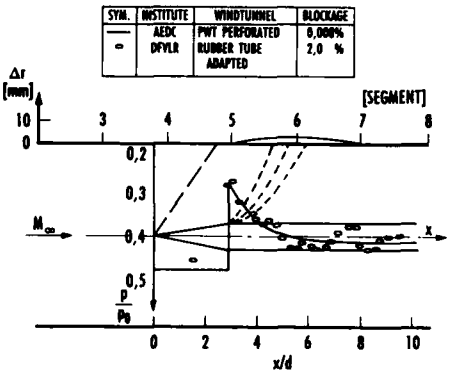

b. After adaptation

Fig 3.8 Comparison of measured model surface pressures and wall contours with reference data for an axisymmetric body in DFVLR DAM test section; ten-degree-half-angle cone-cylinder at M = 1.2, α = 0 deg (from [3.73]).

There has been a much broader selection of lifting configurations investigated in the various 3D facilities. None of them appears to have been tested in more than one fully-3D adaptive-wall tunnel. However, at least one configuration has been tested successfully in two different sizes in the same tunnel. Tests in TUB(3D) have been performed for the Airbus-like full-span wing/body (no tail) F4 configuration [3.3], [3.91], [3.92] and a full-span canard configuration [3.15]. The AGARD B full-span delta wing/fuselage calibration configuration has been tested in DFVLR DAM [3.3], [3.31] in two sizes with solid blockages of 3.5% and 1.0%. Results for the two sizes compared favorably with each other and with reference data. Tests in DFVLR DAM also have been carried out for a full-span wing/fuselage configuration with 30 deg of wing sweepback [3.73], and for the ONERA M3 full-span wing/ fuselage/tail model. Complete M3 lift, drag and pitching-moment data over an extensive range of angles of attack for M = 0.70, 0.75, and 0.80 are given in [3.73]. NASA/ARC tested an unswept, tapered, sidewall-mounted semispan wing in the 3D configuration of the 25x13 cm segmented-plenum, slotted top and bottom walls, solid-sidewall test section. Limited experiments at M = 0.60 and angles of attack from 0 to 6 deg led to significant reductions in interference from the "passive-wall" baseline, but interference could not be

eliminated completely [3.65], [3.78]. All of the above-mentioned tests were for Group 1 flows.

A final Group 1 lifting configuration was a fighter-type full-span wing/fuselage/tail model, Fig. 3.9a, tested in DFVLR DAM [3.72]. Results for lift and drag coefficients before and after adaptation are presented in Figs. 3.9b and 3.9c, respectively, for M = 0.80 and 1.8% blockage. Comparable results with lower blockage in the passive DFVLR TWG perforated-wall and the NLR HST slotted-wall tunnels are shown as well.

Group 2 flows have been investigated principally at AEDC, although some preliminary experiments were performed in TUB(3D) [3.15]. Initial experiments at AEDC were carried out in Tunnel 4T as described in Section 3.2.5 for a generic wing/fuselage/tail configuration similar, but not identical, to that in Figs. 2 and 3 of the AEDC response in the Appendix of this report. Interference at M = 0.90 and 0.95 and α = 4 deg on the wing pressure distributions and model lift and drag was reduced significantly by adaptation, but interference on tail pressures and model pitching moment could not be reduced simultaneously [3.44].

The 3D adaptive-wall test section of AEDC Tunnel 1T was designed to overcome the deficiencies observed in 4T. Of the limited number of cases adapted in 1T, results for M = 0.90, α = 4 deg and an initially-uniform porosity of 3% are most significant [3.77]. The generic wing/fuselage/tail model is shown in the Appendix, along with details of the instrumentation and the steps in the adaptation procedure. Interface pressure matching before and after adaptation are shown in Figs. 3.10a and 3.10b for a pipe position rotated 65 deg from a downward vertical. The trends in the pressure distributions on the wing and tail of the model are shown in Figs. 3.10c and 3.10d, respectively, as the iteration proceeded. Significant reduction in interference on the wing and tail was achieved simultaneously. Model blockage was 2.5% in 1T and 0.16% for the 4T reference data.

The Sverdrup AWAT facility tested large-blockage automotive-type models at both zero and ten degrees of yaw [3.71]. Experimental results for three geometrically-similar models of 10%, 20%, and 30% solid blockage at zero yaw, Fig. 3.11, showed that after adaptation, model centerline pressures were essentially identical for all three model sizes.

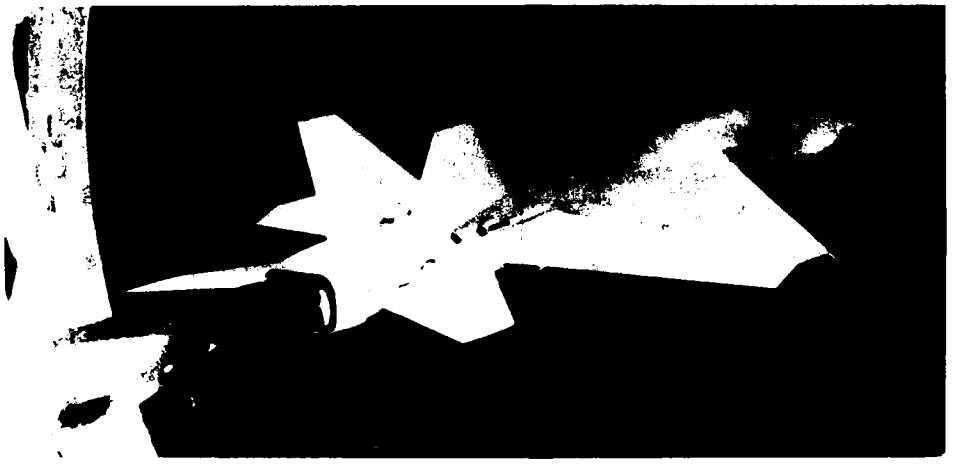

a. Test article configuration

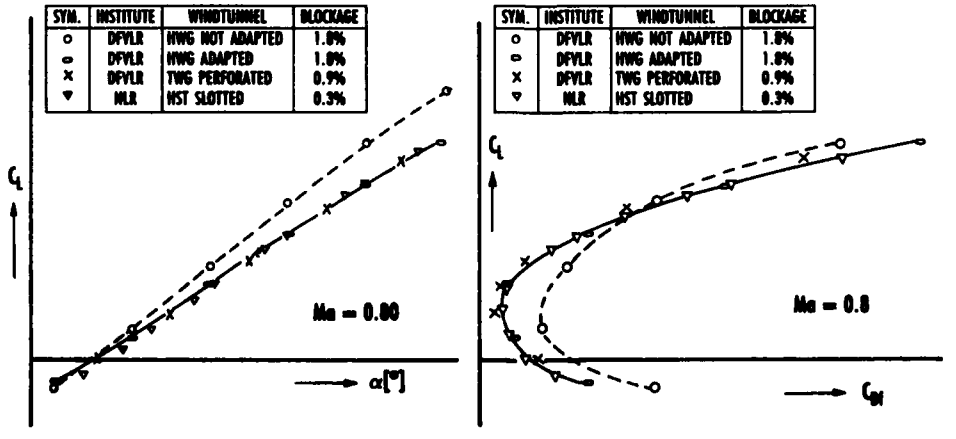

b. Lift coefficient vs angle-of-attack

c. Lift coefficient vs drag coefficient

Fig 3.9 Comparison of measured force data before and after adaptation with reference data for a fighter configuration in the DFVLR DAM test section; M = 0.8 (from [3.72]).

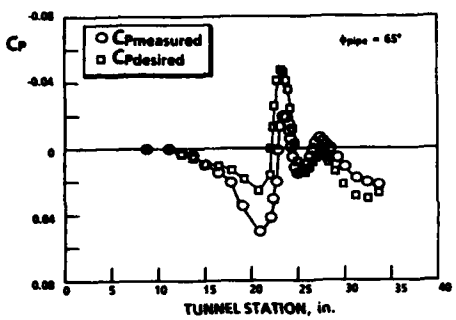

a. Interface before adaptation

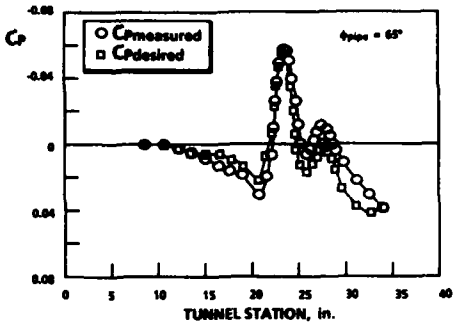

b. Interface after tail-then-wing-region adaptation

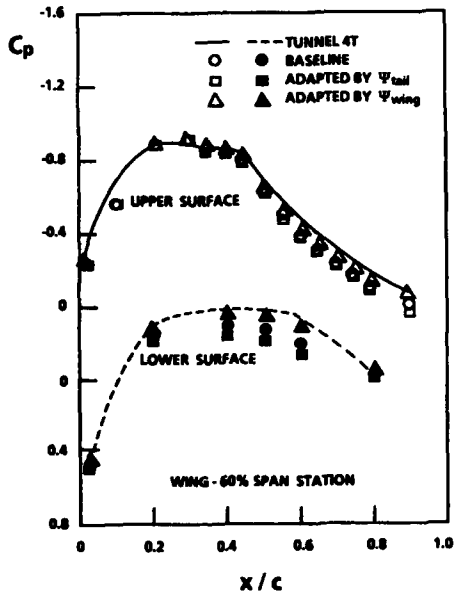

c. Wing 60% semispan before, during and after adaptation

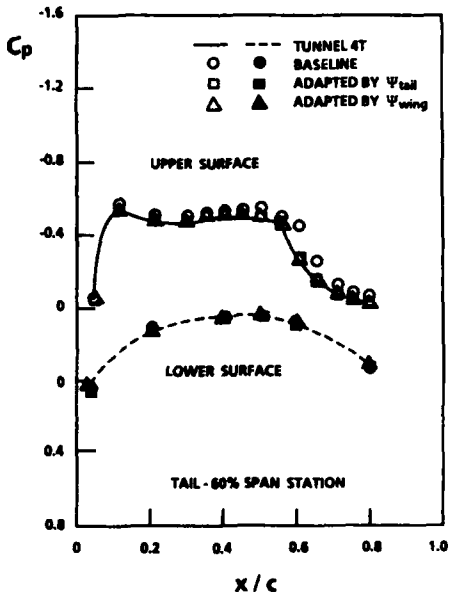

d. Tail 60% semispan before, during and after adaptation

Fig 3.10 Comparison of representative interface, wing, and tail pressure coefficient distributions from measurements and exterior-flow calculations in the AEDC 1T test section; wing/fuselage/tail configuration (Figs. 2 & 3 of AEDC response in Appendix), M = 0.9, α = 4 deg (from [3.77]).

Powered-lift, large-flow-deflection experiments [3.79], [3.80] in the University of Arizona Adaptable-Wall Wind Tunnel will be described briefly. Combinations of low flight speed and lower-surface blowing with large momentum coefficients onto flaps deflected up to 60 deg were set. These conditions provided a free-stream vector that was inclined at up to 45 deg with respect to the tunnel floor and resulted in angles of attack of up to 15 deg. Under such conditions, the adaptive-wall procedure reduced the rms figure of merit at the interface to 3-4% of flight speed. It was determined by residual-interference calculations that the interference velocity components introduced at the model position by the interface-mismatch distributions after adaptation were typically about 1% of flight speed.

3.4 Limitations and Open Questions

The preceding sections give evidence of the large amount of research and development on the adaptive-wall concept since its modern rebirth in about 1970. In particular, for 2D testing of airfoil sections in Group 1 flows for which the flow over the airfoil may be supercritical, but the flow at the interface and walls is subcritical, systematic data of very high quality have been obtained in several facilities, all of which are of the flexible, impermeable-wall type. The evidence presented in the GARTEur investigation of the CAST 7 section [3.54], McCroskey's examination of the NACA 0012 section [3.81], and the ongoing investigation of the CAST 10 section indicates that these adaptive-wall facilities provide data of superior quality for Group 1 flows.

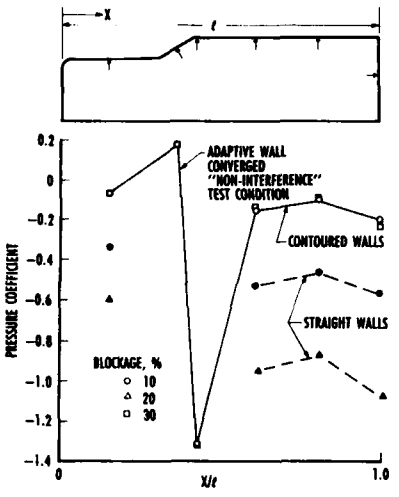

Fig. 3.11 Comparison of model centerline pressure coefficients before and after adaptation for three similar generic automotive-type models with different blockages in the AWAT tunnel; zero yaw angle (from [3.71]).

There has been only a limited amount of research into 2D Group 2 flows with supercritical interface and walls. There is interest in these flows by the helicopter rotor blade designer, for example, who requires knowledge of blade section data over a very wide range of Mach number and angle of attack. Moreover, researchers engaged in CFD code development and validation must rely on very high quality data for Group 2 flows in order to examine turbulence models in flows with strong shock-wave/boundary-layer interaction and separation. Thus, a requirement exists for systematic investigation of the same airfoil configuration in more than one test section for 2D Group 2 flows, just as has been performed for Group 1 flows. It would also seem desirable to acquire systematic data for a representative multi-element airfoil in Groups 1 and 2 flows.

Many adaptive-wall and WIAC researchers now are comparing their 2D experimental results with state-of-the-art CFD viscous-flow numerical solutions for Group 1 flows. In this regard, attention must be drawn to the compendium of results from the Viscous Transonic Airfoil Workshop sponsored by the AIAA Fluid Dynamics Technical Committee [3.93]. On the basis of computed results using many different CFD methods, it is argued [3.93] that satisfactory practical design information can be obtained computationally for many transonic, attached airfoil flows (which correspond to many Group 1 flows). The situation is not nearly as favorable with respect to transonic, separated flows (which correspond more closely to Group 2 flows). In these flows, present turbulence modeling capabilities are inadequate in the regions of separated flows, which can occur as a result of strong shock waves as well as from the flow behavior near the trailing edge. It seems clear that the future of both CFD and adaptive-wall development should be coordinated closely.

The practical limitations in 2D flows as Mach number and angle of attack are increased from Group 1 into Group 2 flows still are not clearly evident. Each facility that has obtained systematic data for a given airfoil section should prepare realistic boundaries, such as those given for a CAST 7 section of one specific size in the ONERA/CERT T2 response in the Appendix. The greatest surprise in that example, perhaps, is that the 3D effects due to the sidewall boundary layers are a more severe limitation to testing in Group 2 flows than the failure of linear theory for the outer-flow computations. The linear theory limitation probably can be overcome more easily than that of the sidewall boundary layers. The sidewall-boundary-layer issue is not unique to adaptive-wall test sections, of course, but its significance seems to have become more apparent as adaptive-wall development has progressed and wall interference has been reduced. The T2 limit for the CAST 7 at lower Mach numbers, but high angle of attack, is due to constraints on allowable wall-control jack movement. This limit can be overcome by designing a test section for larger allowable model chord lengths [3.49]. An alternative point of view for avoiding large jack movements, however, is to eliminate gradients of interference rather than the level of the interference, as discussed in Section 5.2.2 of this report. This approach also holds promise for alleviating difficulties encountered in matching the flexible, impermeable walls with the fixed walls at the diffuser entry downstream of the test section. Another aspect in the definition of realistic boundaries should be the establishment of the capability of each facility to fulfill the flow quality and data accuracy requirements that were recommended by Steinle and Stanewsky [3.94] in 1982 on behalf of the AGARD FDP.

All of the experience indicates that a test section dedicated to 2D Group 1 flows should be of the flexible, impermeable-wall type. The advantages over passive, ventilated-wall tunnels include the means for making efficient engineering tradeoffs among larger model size, lower power requirements and higher Reynolds number capability. A major advantage of flexible, impermeable-wall tunnels is the ease and rapidity of obtaining wall deformation and wall static pressure data, not only for adaptation but also for evaluation of residual wall interference after complete or partial adaptation, as described in Chapter 6. Also, flow quality is improved by reduced tunnel noise and turbulence level. Given the present lack of satisfactory systematic results for any adaptive-wall test section for Group 2 flows, however, it is not entirely clear that flexible, impermeable-wall test sections are superior to those with ventilated walls and adequate wall-control effectiveness. Most of the 2D ventilated-wall work was performed before 1980 with its principal objective being exploratory research into the nature of wall control in this flow regime for 3D applications. Group 3 flows in 2D have received very little attention by adaptive-wall investigators and require a great deal of development if passive, ventilated-wall test sections are to be supplanted.

In 3D testing, significant progress has been made in fully 3D adaptive-wall test sections for Group 1 flows. Although many satisfactory comparisons have been made with existing reference data from passive-wall facilities, there has not been any truly systematic investigation of the same model in several different facilities as has been done in 2D for the CAST 7, CAST 10 and NACA 0012 airfoil sections. Nevertheless, there are some favorable comparisons among specific test points for the same model in different adaptive-wall test sections, as well as testing of the same configuration in two different model sizes in the same test section. Cooperative, systematic, comparative experimental investigations are

strongly recommended. These projects should include testing in 3D test sections with sufficient control effectiveness for complete adaptation, in 2D adaptive-wall test sections as described in Chapter 4, and in existing passive-wall test sections. Preparation of limitation boundaries for given sizes and types of 3D configurations should be given priority throughout these investigations along with estimates on the degree to which flow quality and data accuracy requirements are fulfilled. It would be fruitful in 3D, too, to bring the CFD community into such projects to aid in resolving the roles of experiment, analysis and computations.

Very little investigation has been made for 3D Group 2 flows for which the interface and walls are supercritical. It is claimed by Kraft, et al. at AEDC [3.77] that it is in Group 2 flows and at very high free-stream Mach numbers in Group 1 flows that ventilated, passive-wall tunnels lose their effectiveness for minimizing wall interference. That is, wall interference does not become serious, or uncorrectable, until these flow regimes are reached. It is recommended that existing passive-wall 3D facilities participate in cooperative, systematic investigations of the same model using their latest experimental techniques and WIAC procedures.

Testing in 3D poses greater problems than in 2D since there often are significant gradients of interference over the entire model surface in the longitudinal, lateral and vertical directions. The ideas discussed in Section 5.2.2 for eliminating gradients of interference thus are very important in 3D as well. For 3D Group 1 flows that are supercritical over the model, linear theory is adequate for the outer-flow calculation and linear residual-interference methods can be used to estimate the interference velocities at the model location due to the walls. However, the interpretation of the interference velocities, including their gradients, on the flow over the model is not always straightforward, especially when nonlinear effects are present near the model surface. A related question is that the relationships between local and global matching errors at the interface and the corresponding local and global errors over the entire model are not clear in 3D. Further research is necessary on adaptive walls for 3D flows.

The more specialized 3D applications of large-blockage, low-speed automotive-vehicle testing and powered-lift, large-flow-deflection, V/STOL aircraft testing have received only a small amount of effort to date. The adaptive-wall concept remains attractive in these difficult testing regimes.

As applications of adaptive-wall ideas and their WIAC offshoots (see Chapter 6) have developed, it appears that many questions which previously were masked by wall interference have become more obvious. Certainly, the interrelationships among wall-interference and Reynolds-number effects have been illuminated during this development [3.77]. Proper identification and separation of these effects aid in addressing the ultimate testing questions related to the extrapolation of tunnel test data to flight conditions. The final report of AGARD FDP WG09 on "Boundary Layer Simulation and Control in Wind Tunnels" [3.95] is recommended for discussion of these issues. Also, as wall-interference effects have been reduced, or understood better and corrected, other flow-quality issues that previously were of secondary importance have become of greater significance. An important example is sidewall-boundary-layer effects that have been discussed already for 2D and also are of concern for 3D half-model testing. Other examples are the effects of free-stream turbulence, secondary flows in the corners of the test section, and the whole range of strut/support interference problems in 3D.

The modern adaptive-wall concept, as initially proposed in about 1970, brought together wind-tunnel instrumentation, wall-control mechanisms, control technology, and CFD capabilities into a unified concept. In the elapsed time since 1970, the most remarkable change in these technologies probably has been in the development of both computer hardware and CFD algorithms for solving complex flow fields. Concerning wall interference technology in general, however, the most remarkable effect of the modern adaptive-wall concept has been the recognition of the wealth of information that is available in the interface measurements. The availability of this information implies a variety of tradeoffs between adaptation and residual-interference corrections, and so provides the wind-tunnel engineer with many alternatives that can enhance the acquisition and interpretation of data of very high quality. Vigorous pursuit of all of these technologies and their interactions will benefit both testing and computational capabilities and so will improve flight vehicle design capability.

3.5 References

[3.1] Davis, S. S., "The Evolution of Adaptive-Wall Wind Tunnels," *Recent Advances in Aerodynamics and Aeroacoustics*, Springer-Verlag, Berlin, 1984, pp. 547-566.

[3.2] Ganzer, U., "Advances in Adaptive Wall Wind Tunnel Techniques," *Recent Advances in Aerodynamics and Aeroacoustics*, Springer-Verlag, Berlin, 1984, pp. 567-601.

[3.3] Ganzer, U., "A Review of Adaptive Wall Wind Tunnels," Progress in Aerospace Sciences, Vol. 22, Pergamon Press, 1985, pp. 81-111.

[3.4] Wedemeyer, E., "Use of Computers in Adaptive Wall Wind Tunnels," VKI Lecture Series 1985-06, May 1985.

[3.5] Sears, W. R. and Erickson, J. C., Jr., "Adaptive Wind Tunnels," Ann. Rev. Fluid Mech., Vol. 20, 1988, pp. 17-34.

[3.6] Erickson, J. C., Jr. and Nenni, J. P., "A Numerical Demonstration of the Establishment of Unconfined-Flow Conditions in a Self-Correcting Wind Tunnel," Calspan-RK-5070-A-1, November 1973.

[3.7] Sears, W. R., "Some Experiences with the Exploitation of Measurements of the Perturbation Field in a Wind Tunnel to Improve Simulation," AGARD-CP-210, October 1976.

[3.8] Erickson, J. C., Jr. and Homicz, G. F., "Numerical Simulations of a Segmented-Plenum, Perforated, Adaptive-Wall Wind Tunnel," AIAA Journal, Vol. 20, No. 5, May 1982, pp. 612-623.

[3.9] Chevallier, J. P., "Soufflerie transsonique à parois auto-adaptables," AGARD-CP-174, March 1976; translated as ESA-TT-326, October 1976.

[3.10] Chevallier, J. P., "Parois auto-correctrices pour soufflerie trans-sonique," 12eme Colloque d'Aérodynamique Appliquée, ENSMA/CEAT, Poitiers, November 1975; translated as NASA TT F-17254, October 1976.

[3.11] Judd, M., Wolf, S.W.D., and Goodyer, M. J., "Analytical Work in Support of the Design and Operation of Two-Dimensional Self-Streamlining Test Sections," NASA CR-145019, July 1976.

[3.12] Ganzer, U., "Windkanäle mit adaptiven Wänden zur Beseitigung von Wandinterferenzen," Zeitschrift für Flugwissenschaften and Weltraumforschung, Vol. 3, No. 2, March-April 1979, pp. 129-133; translated as NASA TM-75501, August 1979.

[3.13] Barg, J., "Entwicklung einer Proze-Brechnergesteuerten Regeleinrichtung für die Adaptation von Flexiblen Windkanal-wänden," ILR. Mitt. 70, TU-Berlin, July 1980; translated as NASA TM-76979, September 1982.

[3.14] Rill, S. L. and Ganzer, U., "Adaptation of Flexible Wind Tunnel Walls for Supersonic Flows," AIAA 88-2039CP, May 1988.

[3.15] Rebstock, R., "Verfahren zur Berechnung Transsonischer Strömungen fur die Regelung Adaptiver Windkanäle," Dissertation, TU-Berlin, March 1986; translated as NASA TM-88530, January 1987.

[3.16] Lo, C. F. and Kraft, E. M., "Convergence of the Adaptive-Wall Wind Tunnel," AIAA *Journal*, Vol. 16, No. 1, January 1978, pp. 67-72.

[3.17] Lo, C. F. and Sickles, W. L., "A Hybrid Method of Transonic Computation with Application to the Adaptive Wind Tunnel," Proceedings of the Eighth U. S. National Congress of Applied Mechanics, Los Angeles, California, June 26-30, 1978.

[3.18] Lo, C. F. and Sickles, W. L., "Analytic and Numerical Investigation of the Convergence for the Adaptive-Wall Concept," AEDC-TR-79-55, November 1979.

[3.19] Everhart, J. L., "A Method for Modifying Two-Dimensional Adaptive Wind-Tunnel Walls Including Analytical and Experimental Verification," NASA TP-2081, February 1983.

[3.20] Everhart, J. L., "FLEXWAL: A Computer Program for Predicting the Wall Modification for Two-Dimensional, Solid Adaptive-Wall Wind Tunnels," NASA TM-84648, November 1983.

[3.21] Schairer, E. T., "Methods for Assessing Wall Interference in the 2- by 2-Foot Adaptive-Wall Wind Tunnel," NASA TM-88252, June 1986.

[3.22] Sears, W. R., "On the Definition of Free-Stream Conditions in Wind-Tunnel Testing," Proceedings of the Symposium on Numerical and Physical Aspects of Aerodynamic Flows, California State University, 1981.

[3.23] Sears, W. R., "Adaptable Wind Tunnel for Testing V/STOL Configurations at High Lift," Journal of Aircraft, Vol. 20, No. 11, November 1983, pp. 968-974.

[3.24] Wang, S. C., "Convergence to Unconfined Flow of the Three-Dimensional Transonic Self-Correcting Wind Tunnel," Computer Methods in Applied Mechanics and Engineering, Vol. 28, September 1981, pp. 191-205.

[3.25] Mendoza, J. P., "A Numerical Simulation of Three-Dimensional Flow in an Adaptive Wall Wind Tunnel," NASA TP-2351, August 1984.

[3.26] Weeks, T. M., "Reduction of Transonic Slotted Wall Interference by Means of Slat Contouring," AFFDL-TR-74-139, March 1975.

[3.27] Kraft, E. M. and Dahm, W.J.A., "Direct Assessment of Wall Interference in a Two-Dimensional Subsonic Wind Tunnel," AIAA 82-0187, January 1982.

[3.28] Sears, W. R., "A Note on Adaptive Wall Wind Tunnels," Zeitschrift für Angewandte Mathematik und Physik, Vol. 28, September 25, 1977, pp. 915-927.

[3.29] Sears, W. R., "Adaptive Wind Tunnels with Imperfect Control," Journal of Aircraft, Vol. 16, No. 5, May 1979, pp. 344-348.

[3.30] Mokry, M., "Wind Tunnels with Adaptive Walls," AGARD-AG-281, November 1983.

[3.31] Wedemeyer, E., Heddergott, A., and Kuczka, D., "Deformable Adaptive Wall Test Section for Three-Dimensional Wind Tunnel Testing," Journal of Aircraft, Vol. 22, No. 12, December 1985, pp. 1085-1091.

[3.32] Ashill, P. R. and Weeks, D. J., "A Method for Determining Wall-Interference Corrections in Solid-Wall Tunnels from Measurements of Static Pressure at the Walls," AGARD-CP-335, May 1982.

[3.33] Ashill, P. R. and Keating, R.F.A., "Calculation of Tunnel Wall Interference from Wall-Pressure Measurements," Journal of the Royal Aeronautical Society, Vol. 92, No. 911, January 1988, pp. 36-53.

[3.34] Sears, W. R., "Self Correcting Wind Tunnels," Aeronautical Journal, Vol. 78, February/March 1974, pp. 80-89.

[3.35] Goodyer, M. J., "Developments in Airfoil Testing Techniques at University of Southampton," NASA CP-2045, Vol. 1, Part 1, March 1979, pp. 415-423.

[3.36] Davis, S. S., "Applications of Adaptive-Wall Wind Tunnels," Journal of Aircraft, Vol. 23, February 1986, pp. 158-160.

[3.37] Goodyer, M. J., "The Self Streamlining Wind Tunnel," NASA TM-X-72699, August 1975.

[3.38] Goodyer, M. J., "A Low Speed Self Streamlining Wind Tunnel," AGARD-CP-174, March 1976.

[3.39] Vidal, R. J., Erickson, J. C., Jr., and Catlin, P. A., "Experiments with a Self-Correcting Wind Tunnel," AGARD-CP-174, March 1976.

[3.40] Kraft, E. M. and Parker, R. L., Jr., "Experiments for the Reduction of Wind Tunnel Wall Interference by Adaptive-Wall Technology," AEDC-TR-79-51, October 1979.

[3.41] Parker, R. L., Jr. and Sickles, W. L., "Two-Dimensional Adaptive-Wall Experiments," AEDC-TR-80-63, February 1981.

[3.42] Wolf, S.W.D., "Turbine Blade Cascade Testing in a Flexible-Walled Wind Tunnel," Project for B.Sc. Honours Degree in Aeronautical Engineering, University of Southampton, April 1975.

[3.43] Pittaluga, F. and Benvenuto, G., "The Adaptive Wall Transonic Wind Tunnels of the University of Genova," presented at the 187th Euromech Colloquium on "Adaptive Wall Wind Tunnels and Wall Interference Correction Methods," Göttingen, West Germany, October 15-17, 1984.

[3.44] Parker, R. L., Jr. and Sickles, W. L., "Application of the Adaptive Wall Concept in Three Dimensions," Journal of Aircraft, Vol. 18, No. 3, March 1981, pp. 176-183.

[3.45] Goodyer, M. J., "A Swept Wing Panel in a Low Speed Flexible Walled Test Section," NASA CR-4106, December 1987.

[3.46] Lewis, M. C., Neal, G., and Goodyer, M. J., "Adaptive Wall Research with Two- and Three-Dimensional Models in Low Speed and Transonic Tunnels," AIAA 88-2037CP, May 1988.

[3.47] Dowell, E. H., "Control Laws for Adaptive Wind Tunnels," AIAA Journal, Vol. 19, No. 11, November 1981, pp. 1486-1488.

[3.48] Lewis, M.C., "Aerofoil Testing in a Self-Streamlining Flexible Walled Wind Tunnel," NASA CR-4128, May 1988.

[3.49] Chevallier, J. P., Mignosi, A., Archambaud, J. P., and Seraudie, A., "T2 Wind Tunnel Adaptive Walls - Design, Construction, and Some Typical Results," La Recherche Aérospatiale, No. 4, July/August 1983, pp. 1-19.

[3.50] Wolf, S.W.D. and Goodyer, M. J., "Predictive Wall Adjustment Strategy for Two-Dimensional Flexible Walled Adaptive Wind Tunnel - A Detailed Description of the First One-Step Method," NASA CR-181635, January 1988.

[3.51] He, J. J. and Zuo, P. C., "The Research on Adaptive Wall Wind Tunnel in Northwestern Polytechnical University of China," AIAA 88-2040CP, May 1988.

[3.52] Ferri, A. and Baronti, P., "A Method for Transonic Wind Tunnel Corrections," AIAA Journal, Vol. 11, No. 1, January 1973, pp. 63-66.

[3.53] Archambaud, J. P. and Mignosi, A., "Two-Dimensional and Three-Dimensional Adaptation at the T2 Transonic Wind Tunnel of ONERA/CERT," AIAA 88-2038CP, May 1988.

[3.54] Elsenaar, A., editor, "Two-Dimensional Transonic Testing Methods; Final Report by the GARTEur Action Group AD(AG-02)," NLR TR 83086 U, 1983.

[3.55] Capelier, C., Chevallier, J. P., and Bouniol, F., "Nouvelle méthode de correction des effets de parois en courant plan," La Recherche Aérospatiale, January-February 1978, pp. 1-11; translated as ESA-TT-491, August 1978.

[3.56] Wolf, S.W.D., "The Design and Operational Development of Self-Streamlining Two-Dimensional Flexible Walled Test Sections," NASA CR-172328, March 1984.

[3.57] Ganzer, U., "Adaptable Wind Tunnel Walls for 2D and 3D Model Tests," ICAS Proceedings 1980, pp. 808-816.

[3.58] Wolf, S.W.D., "Evaluation of Flexible Wall Testing Technique to Minimize Wall Interferences in the NASA Langley 0.3-M Transonic Cryogenic Tunnel," AIAA 88-0140, January 1988.

[3.59] Wolf, S.W.D. and Ray, E. J., "Highlights of Experience with a Flexible Walled Test Section in the NASA Langley 0.3-Meter Transonic Cryogenic Tunnel," AIAA 88-2036CP, May 1988.

[3.60] Sears, W. R., Vidal, R. J., Erickson, J. C., Jr., and Ritter, A., "Interference-Free Wind Tunnel Flows by Adaptive-Wall Technology," Journal of Aircraft, Vol. 14, No. 11, November 1977, pp. 1042-1050.

[3.61] Erickson, J. C., Jr., Wittliff, C. E., Padova, C., and Homicz, G. F., "Adaptive-Wall Wind Tunnel Investigations," Calspan-RK-6040-A-2, February 1981.

[3.62] Erickson, J. C., Jr., Wittliff, C. E., and Daughtry, D. C., "Further Investigations of Adaptive-Wall Wind Tunnels," AEDC-TR-80-34, October 1980.

[3.63] Menni, J. P., Erickson, J. C., Jr., and Wittliff, C. E., "Measurement of Small Normal Velocity Components in Subsonic Flows by Use of a Static Pipe," AIAA Journal, Vol. 20, No. 8, August 1982, pp. 1077-1083.

[3.64] Bodapati, S., Schairer, E., and Davis, S., "Adaptive-Wall Wind Tunnel Development for Transonic Testing," Journal of Aircraft, Vol. 18, No. 4, April 1981, pp. 273-279.

[3.65] Schairer, E. T. and Mendoza, J. P., "Adaptive Wall Wind Tunnel Research at Ames Research Center," AGARD-CP-335, May 1982; also NASA TM-84236, May 1982.

[3.66] Davis, S. S., "A Compatibility Assessment Method for Adaptive-Wall Wind Tunnels," AIAA Journal, Vol. 19, No. 9, September 1981, pp. 1169-1173.

[3.67] Schairer, E. T., "Two-Dimensional Wind-Tunnel Interference from Measurements on Two Contours," Journal of Aircraft, Vol. 21, No. 6, June 1984, pp. 414-419.

[3.68] Lo, C. F., "Direct Assessment of Two-Dimensional Wind-Tunnel Interference from Measurements on Two Interfaces," AIAA 88-2539CP, June 1988.

[3.69] Celik, Z. Z. and Bodapati, S., "Convergence Schemes for an Adaptive-Wall Wind Tunnel," Journal of Aircraft, Vol. 25, No. 8, August 1988, pp. 733-739.

[3.70] Morgan, D. G. and Lee, G., "Construction of a 2- by 2-Foot Transonic Adaptive Wall Test Section at the NASA Ames Research Center," AIAA 86-1089, May 1986.

[3.71] Whitfield, J. D., Jacocks, J. L., Dietz, W. E., and Pate, S. R., "Demonstration of the Adaptive Wall Concept Applied to an Automotive Wind Tunnel," SAE Paper 820373, February 1982; also AIAA 82-0584, March 1982.

[3.72] Heddergott, A., Kuczka, D., and Wedemeyer, E., "The Adaptive Rubber Tube Test Section of the DFVLR Göttingen," Paper presented at the 11th International Congress on Instrumentation in Aerospace Simulation Facilities, Stanford, CA, In: ICIASF '85 RECORD, IEEE publ. 85CH2210-3, 1985, pp. 154-164.

[3.73] Heddergott, A. and Wedemeyer, E., "Some New Test Results in the Adaptive Rubber Tube Test Section of the DFVLR Göttingen," ICAS Proceedings, 1988, Vol. 2, pp. 1172-1180.

[3.74] Müller-Wichards, D. and Gülzow, V., "Two Potential Theoretical Methods to Calculate the Contour of an Adaptive Test Section," Paper presented at the 11th International Congress on Instrumentation in Aerospace Simulation Facilities, Stanford, CA, In: ICIASF '85 RECORD, IEEE publ. 85CH2210-3, 1985, pp. 140-145.

[3.75] Parker, R. L., Jr. and Erickson, J. C., Jr., "Development of a Three-Dimensional Adaptive Wall Test Section with Perforated Walls," AGARD-CP-335, May 1982.

[3.76] Parker, R. L., Jr. and Erickson, J. C., Jr., "Status of Three-Dimensional Adaptive-Wall Test Section Development at AEDC," AIAA Paper 84-0624, March 1984.

[3.77] Kraft, E. M., Ritter, A., and Laster, M. L., "Advances at AEDC in Treating Wind Tunnel Wall Interference," ICAS Proceedings, 1986, pp. 748-769.

[3.78] Schairer, E. T., "Experiments in a Three-Dimensional Adaptive-Wall Wind Tunnel," NASA TP-2210, September 1983.

[3.79] Lee, D.C.L. and Sears, W. R., "Experiments with an Adaptable-Wall Wind Tunnel for Large Lift," Journal of Aircraft, Vol. 24, No. 6, June 1987, pp. 371-376.

[3.80] Sears, W. R. and Lee, D.C.L., "Experiments in an Adaptable-Wall Wind Tunnel for V/STOL Testing," AFOSR-86-2088TR, September 1986.

[3.81] McCroskey, W. J., "A Critical Assessment of Wind Tunnel Results for the NACA 0012 Airfoil," AGARD-CP-429, July 1988; also NASA TM 100019, October 1987.

[3.82] Green, L. L. and Newman, P. A., "Transonic Wall Interference Assessment and Corrections for Airfoil Data from the 0.3-Meter TCT Adaptive Wall Test Section," AIAA 87-1431, June 1987.

[3.83] Goodyer, M. J., "Tests on a CAST 7 Two-Dimensional Airfoil in a Self-Streamlining Test Section," NASA CR-172291, January 1984.

[3.84] Seraudie, A., Blanchard, A., and Breil, J. F., "Test Report of the CAST 10 with Fixed Transition, Obtained in the Cryogenic Transonic Wind Tunnel T2 Equipped with Adaptive Walls," ONERA R.T. OA No. 63/1685, August 1985.

[3.85] Mineck, R. E., "Wall Interference Tests of a CAST 10-2/DOA 2 Airfoil in an Adaptive-Wall Test Section," NASA TM-4015, December 1987.

[3.86] Ganzer, U., "On the Use of Adaptive Walls for Transonic Wind Tunnel Testing," AGARD-CP-335, May 1982.

[3.87] Archambaud, J. P., Mignosi, A., and Seraudie, A., "Rapport d'essais sur profil CAST 7 effectués à la soufflerie T2 en présence de parois auto-adaptables en liaison avec le groupe GARTEur AD(AG02)," Report 24/3075, July 1982.

[3.88] Lewis, M. C., "An Evaluation in a Modern Wind Tunnel of the Transonic Adaptive Wall Adjustment Strategy Developed by NPL in the 1940's," NASA CR-181623, February 1988.

[3.89] Lewis, M. C., "The Status of Two-Dimensional Testing at High Transonic Speeds in the University of Southampton Transonic Self-Streamlining Wind Tunnel," NASA CR-3919, October 1985.

[3.90] LeSant, Y., "Adaptation de parois à Mach 1.2," ONERA R.T.S. 26/3075 AY-402, February 1984.

[3.91] Ganzer, U., "A Short Note on Recent Advances in the Adaptive Wall Technique for 3D-Model Tests at the TU-Berlin," AGARD-CP-348, February 1984.

[3.92] Ganzer, U., Igeta, Y., and Ziemann, J., "Design and Operation of TU-Berlin Wind Tunnel with Adaptive Walls," ICAS Proceedings 1984, pp. 52-65.

[3.93] Holst, T. L., "Viscous Airfoil Workshop Compendium of Results," Journal of Aircraft, Vol. 25, No. 12, December 1988, pp. 1073-1087.

[3.94] Steinle, F. and Stanewsky, E., "Wind Tunnel Flow Quality and Data Accuracy Requirements," AGARD-AR-184, November 1982.

[3.95] Laster, M. L., editor, "Boundary Layer Simulation and Control in Wind Tunnels; Report of the Fluid Dynamics Panel Working Group 09," AGARD-AR-224, April 1988.

4. Testing of 3-D models in 2-D adaptive wall test sections.

Editor: E. Wedemeyer
Other contributors: C.L. Ladson, J. Smith, M.J. Goodyer, A. Mignosi, H. Hornung

4.1 Background

As already seen, researchers from many institutions have devoted considerable effort to the development of two-dimensional adaptive wall test sections. Many successful examples of this type of facility are operational. The development of fully three-dimensional test sections, however, has not had this same level of effort expended. Only about three fully three-dimensional facilities exist. The limitations on three-dimensional research are the result of the complexity of both the mechanical design and operational aspects. Typical of the mechanical complexities are lack of readily available model and flow visualization access, and problems of sealing between adjacent walls for multi-wall types of test sections. The operational aspects are complicated by the necessity for many measurements of the boundary conditions which can be very time consuming. This is especially true for the ventilated type test sections which use an array of either fixed or rotating static pipes.

Most researchers agree that, in three-dimensional testing, it is impossible to remove all of the boundary interference. It will be necessary, therefore, to apply residual corrections to the data. The more complex the test section shape, the more complex the calculation of the residual corrections becomes. From both the viewpoint of test section complexity and of ease of residual corrections, a simplified test section geometry is desirable.

To aid in the design of simplified test sections, several researchers investigated the capability of using two-dimensional adaptive wall test sections to perform three-dimensional testing. By use of this type of design, the inherent complications and limitations of the fully three-dimensional design are avoided. The following sections of this chapter will describe strategies of adaptation used for this application as well as sample results and a discussion of some limitations of the technique.

4.2 Strategy of wall adaptation

The term "wall adaptation" has been used, so far, to denote streamlining of the wind tunnel walls, i.e. an adjustment of the walls to the streamlines of the unconfined flow. In practice, the wall adaptation is only approximate since the wall shape can be adjusted only at a finite number of points over a finite length. Nevertheless, the concept of wall adaptation, as it was conceived originally, provides for a shaping of the walls so that they conform, more or less, to unconfined flow conditions.

Obviously, when 2-D adaptive walls are to be used for the testing of three-dimensional models, the concept of streamlining the walls can no longer be applied since the walls can be shaped only in two-dimensional ways and the resulting streamlines are in general not an approximation to those of the unconfined flow.

In spite of the fact that 2-D walls cannot be streamlined to three-dimensional flows it could be shown that the blockage and upwash interferences can be relieved significantly by 2-D wall contouring, see Refs. [4.1, 4.2, 4.3].

A strategy for the adaptation of 2-D walls for three-dimensional flows was first developed at the VKI [4.2, 4.4]. The idea is, to eliminate the wall interferences near the model or, in practice, along the centreline of the test section. In order to compute the wall interferences, wall pressure distributions are measured along the centrelines of the top and bottom walls. The method was tested in the S1 wind tunnel at the VKI and subsequently used in adaptive wall wind tunnels at the TU Berlin [4.5], at ONERA/CERT [4.6], and at the DFVLR Göttingen [4.7].
Extensions of the VKI-method have been proposed or used at NLR [4.8], at Southampton University [4.9], and at NASA Langley [4.10]. The various methods are discussed in the following sections.

4.2.1 The VKI method

The VKI-method was described in two reports [4.2, 4.4], which also contain a detailed description of the adaptation algorithm for linearized flows. A method for non-linear flows, developed at the VKI, is described in [4.11]. A summary of the linear and non-linear method including wind tunnel test experience is found in [4.7]. In the following, an outline of the linear and non-linear method is given.

It is assumed that the flow is, at least approximately, symmetric with respect to the vertical plane of symmetry of the test section, i.e. a symmetric model at zero or small yaw is considered.
It is also assumed that the lateral extension of the model is not a large fraction of the lateral dimension of the test section. Under these conditions the model is exposed only to the flow near the centreline, and it is sufficient that wall interferences are being extinguished near the centreline. That this can always be achieved is seen in the following way: For a symmetrical model at zero yaw angle the interference velocities along the centreline of the test section have only longitudinal (u) and vertical (w) components. By deflecting the walls, equal velocity distributions but of opposite sign can be generated along the centreline. The resulting interferences due to the wall constraints and the wall deflections can therefore be made to vanish along the centreline of the test section. For example, by deflecting the upper and lower walls in a symmetrical way (Fig. 4.1), a disturbance velocity distribution having only a longitudinal component $u(x)$ is generated along the centreline, while an antisymmetrical wall deflection (Fig. 4.2) produces a velocity distribution with only a vertical component $w(x)$. Combining symmetrical and antisymmetrical wall deflections any wall interferences can be extinguished along the centreline.
The wall interferences at the tunnel centreline can be calculated e.g. by the method of Ashill & Weeks [4.12] which requires a detailed wall pressure measurement on all four test section walls. The walls of 2-D adaptive wind tunnels are not generally equipped with a sufficient number of pressure orifices for this purpose but it was shown in [4.2] that the pressure distributions along the centrelines of the top and bottom wall suffice to compute the wall interferences on the tunnel centreline within a reasonable approximation.

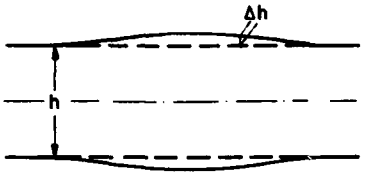

Fig. 4.1: Symmetrical wall displacement.

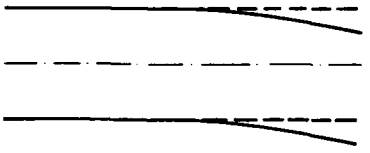

Fig. 4.2: Antisymmetrical wall displacement.

Actually, the pressure distributions at the centrelines of top and bottom wall do not contain sufficient information in order to compute wall interferences for general three-dimensional flows. Therefore, additional assumptions must be made. The VKI-method assumes, in addition to symmetrical flow, that the model can be represented by singularity distributions at the tunnel centreline, an approximation that may be satisfactory for the far-field generated by the model images. Under these assumptions it is possible to relate the wall interferences to the measured pressure distributions in an unambiguous way.

The adaptation procedure is as usual, i.e. in a preliminary test with not adapted or not fully adapted walls the wall pressures are measured on the top and bottom wall. From the wall pressures the interference velocities at the tunnel centreline are inferred and finally the special wall setting is computed that eliminates the interferences along the centreline of the test section.

The adaptation procedure outlined so far is based on the assumption that the flow past the model can be described, at least approximately, by the linearized flow equations. For linear flow the influences of the wall constraints and the wall displacement can be superimposed. Also, a linear relation can be assumed between the pressure distribution measured at the walls and the required wall displacement. Conveniently the symmetrical and antisymmetrical parts of the wall deflection are considered separately (Figs. 4.1 and 4.2). Defining the symmetrical part $c_{ps}(x)$ and the antisymmetrical part $c_{pa}(x)$ of the wall pressure distribution by:

$$\begin{aligned} c_{ps} &= (c_{pt} + c_{pb})/2\,, \\ c_{pa} &= (c_{pt} - c_{pb})/2\,, \end{aligned} \qquad (4.1)$$

where c_{pt} and c_{pb} are the pressure coefficients at the top and bottom wall respectively, the symmetrical and antisymmetrical part of the wall displacement

$$\begin{aligned} \Delta h_s &= (\Delta h_t + \Delta h_b)/2\,, \\ \Delta h_a &= (\Delta h_t - \Delta h_b)/2\,, \end{aligned} \qquad (4.2)$$

are obtained simply by integrations:

$$\Delta h_s(x) = -\frac{\beta}{2}\int c_{ps}(\xi)\,\chi(x-\xi)\,d\xi\,, \qquad (4.3a)$$

$$\Delta h_a(x) = -\frac{\beta}{2}\int c_{pa}(\xi)\,\Lambda(x-\xi)\,d\xi\,, \qquad (4.3b)$$

where x and ξ are coordinates in axial direction.

For a fixed width/height ratio of the test section the influence functions χ and Λ depend only on the normalized variable $\bar{x} = (x-\xi)/\beta h$, where β is the Prandtl factor and h the test section height. For a square test section the functions $\chi(\bar{x})$ and $\Lambda(\bar{x})$ are shown graphically in Figs. 4.3 and 4.4.

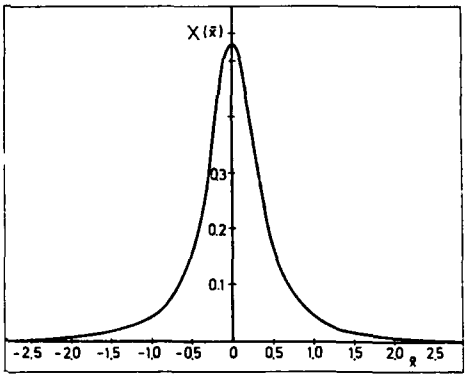

Fig. 4.3: Influence function $\chi(\bar{x})$ of eq. (4.3a).

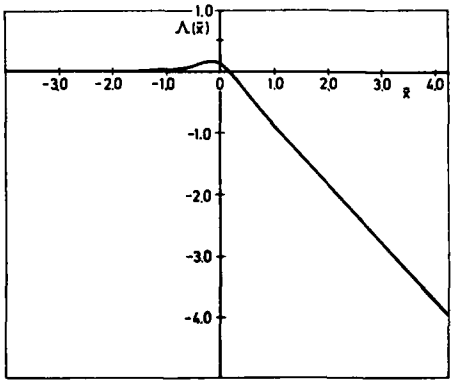

Fig. 4.4: Influence function $\Lambda(\bar{x})$ of eq. (4.3b).

In practice it is useful to start the adaptation procedure with the wall contour of the previous test i.e. to make only small adjustments to the wall contour according to small changes of the test parameters. In order to apply Eq. (4.3) for the case of pre-adapted walls, the wall pressure distribution must be reduced to straight wall conditions by subtracting the contribution of the wall deflection on the measured c_p-values. To compute this contribution, approximate formulas are used, derived from a power series expansion of the disturbance potential, that results from the wall deflection, see Ref. [4.4].

In a number of wind tunnel tests (see section 4.3) Eqs. (4.3) were used for the wall adaptation. Usually, one iteration was sufficient to adapt the walls. In extreme cases, especially at high Mach numbers, more than one iteration was needed when starting from straight walls.
At high subsonic Mach numbers, choking of the tunnel may occur with straight walls. After a preliminary wall adaptation choking may be removed and the flow may become subsonic in the major part of the test section so that the linear adaptation procedure can be used. At still higher Mach numbers, when supersonic regions extend up to the walls for the adapted wall condition, the linear adaptation scheme becomes inadequate. A non-linear scheme was developed at the VKI [4.11] that is briefly outlined in the following.

Wall adaptation for non-linear flow

In the case of full wall adaptation the strategy of streamlining the walls can easily be extended to non-linear flows. In fact, the strategy remains the same and only the computation of the "fictitious external flow" becomes more laborious. An extension of the linear VKI-method to non-linear flows is not as straightforward. The reason is, that the linear method rests on the assumption that the effects of wall constraints and wall deflections can be superimposed, a principle that becomes meaningless for non-linear flows.

To alleviate the blockage effect of a non-lifting body it appears reasonable to shape the walls so that the cross sectional area distribution of the streamtube formed by the walls equals that of the free flight condition.
The prescription to match the area distribution of the streamtube is, of course, not equivalent to the previous prescription viz. to extinguish the u-interferences along the tunnel centreline, but it was shown numerically [4.11] that the two prescriptions give essentially the same result if applied to linearized flow. It is, therefore, reasonable to apply the "area rule" also in the case of non-linear flows. It is convenient again to separate the symmetrical and antisymmetrical parts of the wall pressure distribution and the wall displacement.
The symmetrical part of the pressure distribution $c_{ps}(x)$ is essentially due to blockage, but in non-linear flows the lift component gives an additional small symmetrical component which is proportional to the square of the lift.
The wall pressure signature $c_{ps}(x)$ is now interpreted as if it were generated by an equivalent body of revolution. The shape of the equivalent body is calculated by an inverse method using the transonic small perturbation equation (TSPE). Similar procedures were proposed by Murman [4.13] for 2-D flows and by Rizk & Murman [4.14] for 3-D flows in the context of wall interference assessment.
Next, the free air flow past the equivalent body of revolution is computed, which in turn gives the cross sectional area distribution of the streamtube. Finally, the symmetrical part of the wall displacement is chosen so as to duplicate the correct area distribution.
It should be emphasized that the method outlined does not require any model representation although the known model shape may be used as an initial starting point for the computation of the equivalent body of revolution.
For the antisymmetrical part of the wall pressure distribution, which is related to lift, it was shown that the linear algorithm is still valid. The non-linear terms associated with lift are contained in the symmetrical part of the wall adaptation.

4.2.2 The NASA Langley method

The VKI-method was extended by Rebstock [4.10] in two regards:

1. A more accurate assessment of wall interferences is accomplished by flow measurements at the entire test section boundary (two variable method). The main merit of this more elaborate procedure is, that the residual interferences can be assessed readily. It requires, however, a sufficient number of pressure orifices on the test section walls (three rows on the top and bottom walls and one row at one sidewall are typically used).
2. Wall interferences are eliminated at a straight line which is not necessarily the test section centreline but can arbitrarily be defined by the user.

Initial wind tunnel tests were performed in the NASA Langley TCT tunnel to validate the method [4.10]. The model tested was an unswept semi-span wing which was mounted on one sidewall. The ratio semi-span/tunnel-width was 0.51. The vertical position of the wing in the test section was moved up in order to increase the wall interferences. The "target line" on which the wall interferences were eliminated was along the root chord of the wing, extended in upstream and downstream directions. The tests have shown that wall interferences could substantially be reduced even when the model was mounted near the upper wall. Assessment of the residual interferences has shown, however, that the wall-induced upwash varies significantly across the wing span (see section 4.3). The 2-D adaptation can only eliminate the chordwise variation of the upwash angle at a given spanwise position but not its spanwise variation. A discussion of the resulting residual interferences and a possible alleviation by the use of rectangular rather than square test sections is given in section 4.4. Presently it should be mentioned that the test conditions for the wing, mounted near the upper wall, are extremely unfavorable, since the proximity of the wall has the effect that the wall interferences are not only larger but also less uniform across the wing span compared with a wing mounted in the centre of the test section. Nevertheless, it was shown that the elimination of the wall interferences on a line in the wing plane rather than along the tunnel centreline allows a considerable improvement if the model is mounted off the centreline.

4.2.3 The NLR method

The NLR adaptation strategy aims at fast algorithms for high-productivity testing, preventing the need of iteration as much as possible. To these purposes, the eventual algorithm is formulated in terms of a simple matrix . vector operation, implicitly accounting for the distribution of jacks as well as for end effects associated with finite test section length. In addition, only axial upwash gradients and blockage interferences are eliminated, leaving the model's effective incidence (which is assumed to be correctable) unaltered.

In common with the NASA Langley method, the more accurate assessment of both, "initial" and "residual", wall interference by means of boundary measurements is used [4.15]. Also, the wall interferences are essentially eliminated along a straight target line running in axial direction. The position of the target line can be chosen arbitrarily.

The wall shape is assumed to be composed of elementary wall shapes corresponding with, mutually independent, jack actions (unit load, unit displacement, or other equivalent quantity) according to linear theory of elasticity and accounting for the wall supports at the test section entrance and exit. For convenience, ideal-

ized jack loads P_j are used as working variables. The perturbation flow velocities (w_c) associated with these elementary wall shapes are, assuming linearized flow, proportional to P_j and can be expressed in terms of influence coefficients. Adopting a generalized matrix notation:

$$w_d = A \cdot P = -w_i \,, \tag{4.4}$$

where w_i denotes both velocity components (in axial and "upwash" direction), A the influence coefficient matrix and P the load vector. Obviously, w_d must counteract the initial interference w_i.

The principle stated in Eq. (4.4), however, requires further treatment. First of all, the matrix A will generally not be square. Secondly, the wall interference cannot be eliminated along a target line of infinite length because of finite test section length. Thirdly, a wavy wall still tends to produce a rather smooth perturbation flow at some distance away from it, indicating that a slight waviness in w_i may turn out to "require" an extremely wavy wall for its cancellation (cf. [4.2]). The first problem is easily solved by seeking a least-squares solution; the second by introducing weighting factors G applied to $w_d + w_i$ and decreasing in value with increasing distance from the model or, more conveniently, from the test section centre. Wall waviness is suppressed by the additional requirement that the jack loads P_j, possibly multiplied by weighting (or rather: scaling) factors W_j are a minimum in a least squares sense.

Taking these considerations into account, the actually applied matrix equation takes the following form:

$$C \cdot P + D \cdot w_i = 0 \tag{4.5}$$

with

$$C = A^T \cdot G \cdot A + W$$
$$D = A^T \cdot G$$
$$A^T = \text{transpose of A}$$

The matrices C and D are square, the weighting matrices G and W diagonal. The idealized jack loads follow from inversion of eq.(4.5):

$$P = -C^{-1} \cdot D \cdot w_i \,. \tag{4.6}$$

For an incidence sweep at constant Mach number, the matrix $C^{-1} \cdot D$ can be computed prior to the sweep (e.g. during Mach number setting), thus allowing fast computation of P (and, therefrom, jack displacement for wall control, wall shape, etc.) from w_i by a simple matrix · vector multiplication, during the sweep.

4.2.4 The Southampton method

The strategy developed for the TSWT tunnel at the University of Southampton calculates interference velocity components (u, v, w) existing everywhere in the test section. Interference is computed from the wall loading. Inputs to this section of the code are the reference flow conditions and the internal pressure distributions all over, and the contours of, the test section walls. The streamtube formed by the curved test section walls, which should be viewed as immersed in an infinite flow field, has sharp edges usually not aligned with the free stream. Singularities in the external flow field associated with these corners were expected to introduce computational complexity and therefore have been avoided by means of notional infinite spanwise extensions of the two flexible walls of the test section, the extensions having the same camber as the walls. The complete flow field thus partitioned is shown in Fig. 4.5. As well as avoiding the singularities which

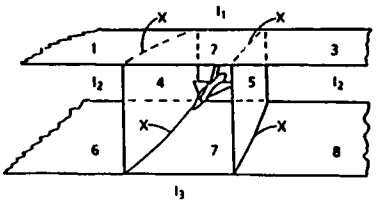

Fig. 4.5: Partitions used in the Southampton 3-D wall adjustment strategy.

would have existed along corners X, the partitions render the imaginary flow field entirely two-dimensional and relatively easy to compute compared with their three-dimensional counterpart. There are four portions of exterior two-dimensional flow fields identified as I_1 to I_3. Portions I_2 are identical.

In the analysis the partitions are replaced by vorticity distributions. Generally all partitions are loaded and account must be taken of the vorticity existing everywhere in determining interference. Partitions 1 and 3, separating the two-dimensional fields I_1 and I_2, carry identical distributions of vorticity, functions only of streamwise position. Likewise partitions 6 and 8. The contributions to interference at the model of the loading on all four panels, analytic in the spanwise direction, are simply determined. The real three-dimensional flow field about the model combined with the nature of the flow components I_2 renders the loadings on partitions 2, 4, 5 and 7 more complex because of the streamwise and cross-stream variations of loading. One step in the analysis is to derive the velocity vectors at the walls from measurements of wall pressures. Partitions 2, 4, 5 and 7 carry two components of vorticity, each functions of both directions. The effects of these are integrated piecewise and summed with the two velocity components arising from partitions 1, 3, 6 and 8 to yield three components of wall interference in the test section.

The aim in streamlining the walls is to eliminate two of the interference velocity components along lines passing in the streamwise direction in the general region of the model. The two components are streamwise u and vertical w, and each may be eliminated along one line. The interferences are modified by differential and collective movements of the walls respectively. The third component of inteference, v, is not controlled although it is quantified. The selection of wall contours is based upon the use of jack movement influence coefficients. The coefficients allow the interference velocity distributions along the lines to be converted into demands for wall movement. The streamlining process is iterative because the behaviour of the model is affected by wall movement, and because the values of the influence coefficients are known only approximately.

4.2.5 Concluding remarks

The linear methods discussed in the preceding sections all use as an adaptation strategy the elimination of the wall interferences on a given target line that runs in axial direction.
Further generalizations could include still more general target lines, e.g. a line along the span of a swept wing. (The direction of the target line must have a component in axial direction i.e. it cannot run along the span of an unswept wing.)
An important feature of the above linear methods is, that the computation of the wall shape can be reduced

to simple integrations as in Eqs. (4.3a,b) or, in discretized form, matrix operations as in Eq. (4.6), thus providing fast algorithms for the computation of the wall shape.
An extension of the present adaptation strategy to non-linear flows encounters extreme difficulties. It appears that other strategies must be used for non-linear flows, like the non-linear VKI-method.

4.3 Facilities and results

4.3.1 Facilities

A large number of facilities have provided interesting results concerning the ability to minimize wall interference on 3-D models by acting only on two walls. These facilities are mainly used to verify different strategies of wall adaptation and for aerodynamic research.
The adaptation qualities can be tested by a comparison with interference free data and by correction methods giving the residual errors during the adaptation process. Experiments are always strongly connected with theoretical analysis.
An alphabetic list of the facilities presented in this chapter is shown in Table 1 with their main features. A discussion of the major points for each wind tunnel is given in the following.

4.3.2 AFWAL 3-D and 2-D adaptive wall wind tunnel

To improve wind tunnel capability at the Flight Dynamics Laboratory of the Air Force Wright Aeronautical Laboratories, a pilot wind tunnel of 9×9 inches was constructed for subsonic and transonic researches by Harney [4.3].
The test section Fig. 4.6 was equipped with solid sidewalls and flexible upper and lower walls each composed of nine cylindrical rods which are 7/8 inch in diameter. Flexible followers back up the rods and act as seals for non-ventilated walls.
A parabolic arc-body of revolution (blockage 2.5%) as well as a lifting model Fig. 4.7 (blockage 2.5%, width 6.3 inches) were tested.
The nine rods on the upper and lower wall were deflected according to a mathematical model that accounts for the blockage effect of the sidewalls by additional displacements of the rods on the upper and lower wall. Fig. 4.8 shows typical rod contours for the lifting model.
The good results obtained by the partial adaptation led Harney to study the performance of 2-D as compared to 3-D wall contouring. The 2-D contouring was accomplished by setting all nine rods of the upper and lower wall to an intermediate wall contour, thus simulating the configuration of a flexible-plate wall.
These tests have shown that the results obtained by 2-D wall contouring completely match the results of 3-D contouring when the walls were set to a calculated mid-semispan streamline (Fig. 4.9).

4.3.3 Experimental results from the HKG at DFVLR Göttingen

Experimental tests to verify the method developed by Wedemeyer and Lamarche using 2-D wall adaptation for 3-D flows have been performed at DFVLR Göttingen.

An axisymmetrical model (FFA parabolic spindle, blockage 3.1%) has confirmed that interference free data can be achieved by a comparison with interference free data obtained in the 3-D adaptive rubber tube test section (DAM) of the DFVLR [4.16].
As outlined in section 4.2 residual interferences at the model are expected, if at all, for models with a large lateral extension.

In order to explore experimentally the range of applicability of 2-D wall adaptation, tests were performed with a large span airplane model [4.7, 4.16].
The model shown in Figs. 4.10 and 4.11 has pressure orifices at four wing sections. The outboard section at 92.5% of the semispan could accomodate only three pressure holes because of its limited thickness. The ratio of wing span to tunnel width was as large as 75% so that it should be possible to detect residual interferences.
From a number of test cases, interference free data were obtained in the rubber tube wind tunnel (DAM).
Fig. 4.12 shows typical adapted wall contours. The difference of upper and lower wall displacements is due to the blockage by the fuselage, the wing and the sting support.
The thickening of the support sting from 60 to 90 mm is clearly reflected by the wall contours at x = 2 m. The mean value of upper and lower wall displacements reflects the downwash.

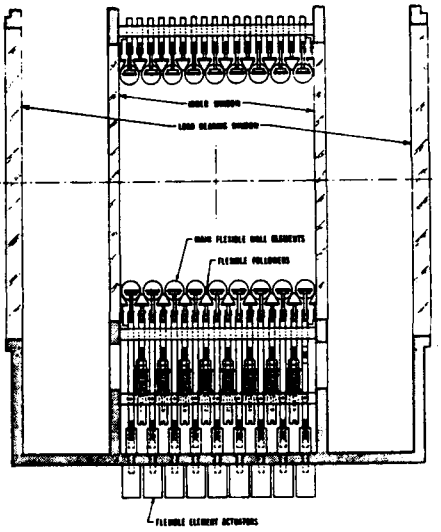

Fig. 4.6: Cross section through the adaptive wall test section at Wright Aeronautical Laboratories.

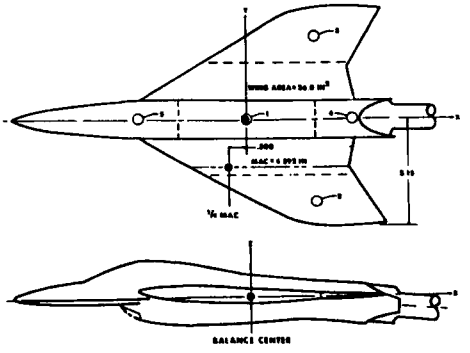

Fig. 4.7: Lifting model tested at Wright Aeronautical Laboratories.

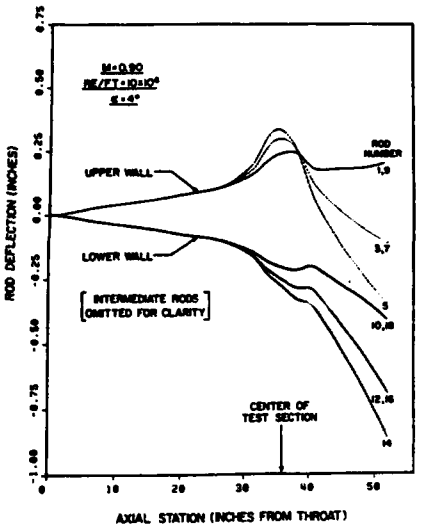

Fig. 4.8: Typical three-dimensional rod contouring for the lifting model.

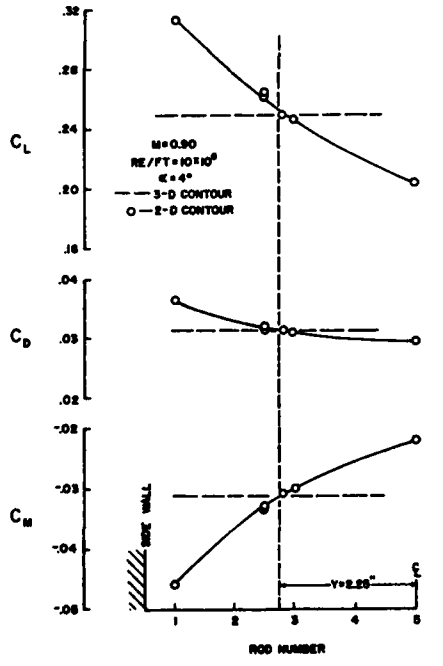

Fig. 4.9: Effect of varying 2-D wall contours in relation to a 3-D contour.

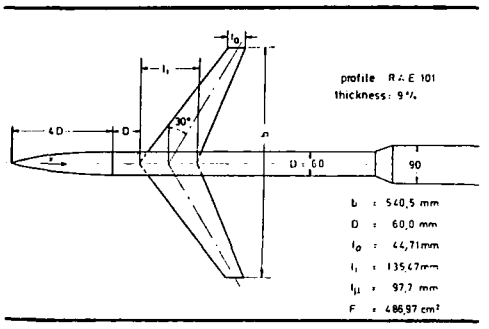

Fig. 4.10: Plan view of lift model with tunnel wall.

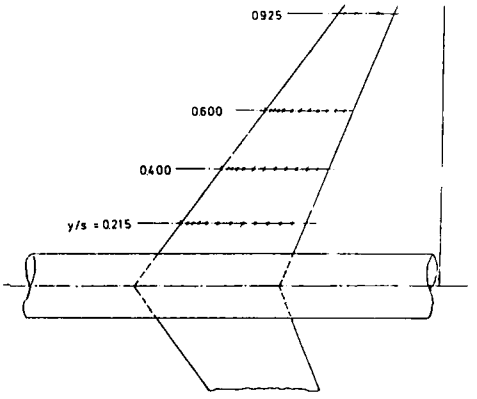

Fig. 4.11: Location of pressure orifices for lift model.

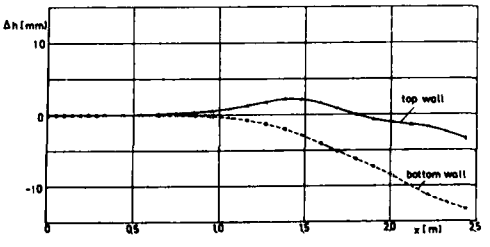

Fig. 4.12: Typical wall displacement for lift model.

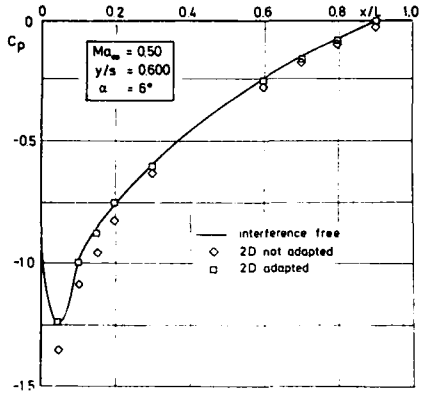

Fig. 4.13: Pressure distribution for wing section y/s = 0.6.

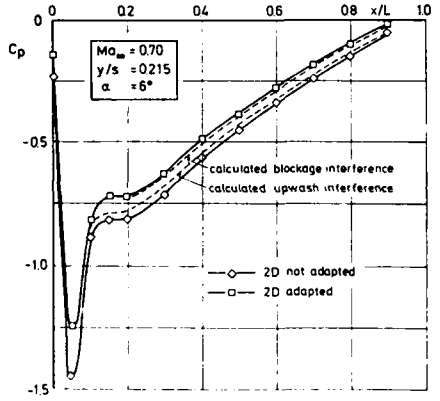

Fig. 4.14: Pressure distribution for wing section y/s = 0.215.

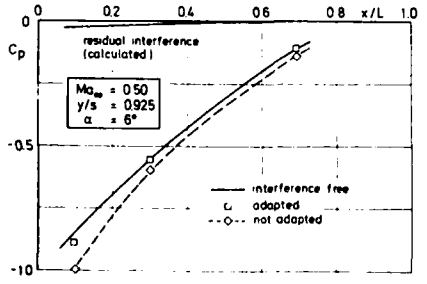

Fig. 4.15: Pressure distribution for wing section y/s = 0.925.

Fig. 4.13 shows pressure distributions at the wing section y/s = 0.6. The effect of adaptation is clearly seen. After wall adaptation the agreement with interference free data is very good.

Fig. 4.14 shows similar results for the inner wing section y/s = 0.215. This figure also shows calculated wall corrections for *blockage and upwash interferences*. (The calculation of wall corrections was based on conventional methods, representing the model by simple singularities). The total calculated interference correction nearly matches the correction by wall adaptation.

The most relevant results are for the outboard wing section y/s = 0.925 shown in Fig. 4.15. The data for not adapted walls and interference free reference data are plotted for comparison. Also plotted are calculated residual interferences.

There is a small difference between the curves for 2-D adapted and interference free reference data which may be interpreted as the expected residual interference. The difference has the correct sign and magnitude but is very small so that it hardly rises above the level of experimental scatter.

In summary, the tests have shown that wind tunnel wall interferences can substantially be reduced by the use of two-dimensional adaptive walls The method seems to be applicable over a wider range than might have been anticipated.

Residual upwash and blockage interferences remain negligibly small over extended parts of the test flow, they increase toward the tunnel walls and produce maximum disturbances at the wing tips.

Even more favorable conditions are attained in rectangular test sections. In an optimum test section, having a width to height ratio of about 1.4, residual interferences remain negligibly small over the entire wing span (see section 4.4).

The wall adaptation procedure is simple and requires little computational effort so long as the flow equations can be linearized. A non-linear code was developed that may be used in severe cases, see [4.11]. The non-linear code was also used to estimate the range of validity of the linear approach.

4.3.4 Initial 3-D model test in the 0.3 m TCT adaptive wall test section at NASA Langley

An initial wind tunnel test was conducted to validate the method of Rebstock [4.10] outlined in section 4.2.2. The model was an unswept semi-span wing mounted on the right sidewall of the TCT: aspect ratio 4, airfoil section NACA 65A006, semi-span/width 0.51, solid blockage 0.79%, reference data LRC 7'×10' tunnel (1951). Tests were performed at Mach numbers between 0.7 and 0.9 and in an angle of attack range between 0° and 7°. Two model locations were tested: wing centred and a high position halfway between the turntable center and the top wall in order to increase the wall interferences. Measurements include model forces, wall pressures and deflections.

Fig. 4.16 shows the calculated lift and blockage interference at the root for a high angle of attack with walls straight and the wing high. The induced Mach number is small and almost constant at the wing planform. However the induced upwash varies considerably in chord direction from 0.35° at the leading edge to 1.7° at the trailing edge of the root section as well as in spanwise direction (see Fig. 4.18).

The aim of the adaptation is to reduce the chordwise and spanwise gradients. Since the wall deflections are constant across the wind tunnel width, wall interference can only be controlled at one target line. Interference is highest at wing root and the target line is positioned accordingly.

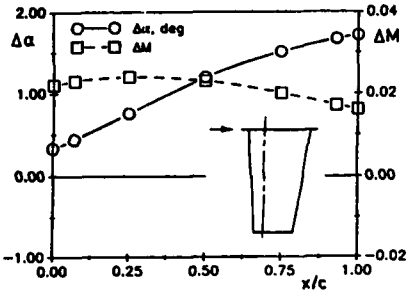

Fig. 4.16: Chordwise variation of wall interference; walls straight, $M_\infty = 0.7$, $\alpha = 7°$, wing high

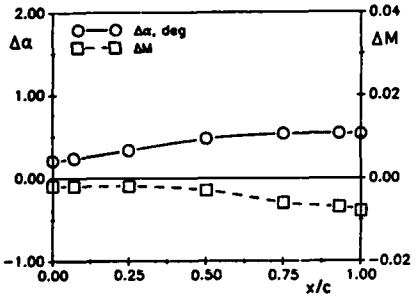

Fig. 4.17: Chordwise variation of wall interference; first iteration, $M_\infty = 0.7$, $\alpha = 7°$, wing high

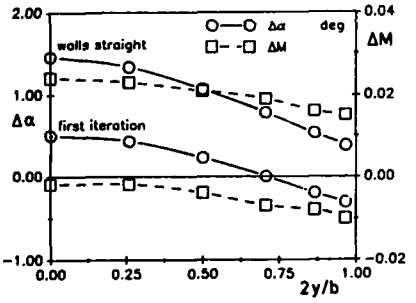

Fig. 4.18: Interference at wing after first iteration; $M_\infty = 0.7$, $\alpha = 7°$, wing high

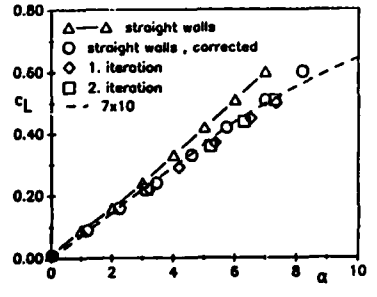

Fig. 4.19: Measured wing lift versus interference-free data; $M_\infty = 0.7$, wing high

Fig. 4.17 shows the residual interference after the first iteration. Blockage velocity and upwash angle are greatly reduced. A second iteration would probably further reduce the chordwise variation of blockage and upwash interferences. However, the upwash angle still varies in spanwise direction (Fig. 4.18). The plots indicate the progress of adaptation and help to position the target line for the wall shape calculation. The calculated Mach number increment ΔM at each spanwise location is simply an average value across the respective chord. The lift interference across the span is represented by the induced angle of attack $\Delta\alpha$. The remaining gradient cannot be eliminated by 2-D wall deflection.

Fig. 4.19 shows the measured model lift for one angle of attack sweep during the wall adaptation process. Interference free values, obtained in NASA Langley's 7×10 foot wind tunnel, are also shown for comparison.

4.3.5 3-D model tests in the T2 wind tunnel at ONERA/CERT

Various wind tunnel tests [4.6] were carried out in the T2 since 1985 to validate and improve the strategy due to Wedemeyer and Lamarche [4.2, 4.4] for 3-D models in test sections with two adaptive walls.

A first application of the 3-D adaptation process was performed with an axisymmetrical model called C5 (blockage 2%). Walls were streamlined to eliminate interference along the model axis. Tests were performed at Mach numbers between 0.6 and 0.95. The top of Fig. 4.20 shows at Mach 0.84 the significant effect of the adaptation from straight walls on the Mach number distribution along the model. The adaptation process in this case requires three iterations, the first giving already a rather good result. Data are in good agreement with TU Berlin results obtained from a real 3-D adaptation [4.5, 4.17].
The bottom of Fig. 4.20 shows a similar comparison for a higher Mach number of 0.9 between NASA Ames 11×11 foot wind tunnel (interference free) and T2 after adaptation.
Residual errors along and around the axis seem to be negligible for axisymmetrical bodies.
Other tests were conducted with full airplane models located on the wind tunnel axis or with half models with a large span.

The results presented in this part are related to a half-wing model mounted on the right sidewall giving a very high interference level. Details of the model and of the test section are included in Fig. 4.21. Fig. 4.22 shows at the top contours of constant wall induced blockage and upwash at the wing planform for straight walls at $M = 0.78$ and $\alpha = 3.25°$. The induced Mach number is not small, due to the fuselage section and the induced upwash varies considerably. Wall adaptation was aimed at eliminating the two components of interference along the "target line" which is the fuselage axis, see the bottom of Fig. 4.22. The blockage interference is nearly eliminated after the wall adaptation however a significant spanwise gradient of the upwash interference remains. The top of Fig. 4.22 illustrates the different behavior of blockage and upwash interferences. The latter is less uniform in spanwise direction and, therefore, less reducible by 2-D wall adaptation (see also Fig. 4.25).

Fig. 4.23 illustrates an interesting comparison between correction and adaptation. Configuration A corresponds to straight walls moved in rotation by 0.5°. The angle of attack of the wing related to the upstream flow is 3.5° and the upstream Mach number 0.78.
From the wall measurements interference terms can be computed along the wing midspan axis. Corrections are very large near the wing: $\Delta M = 0.06$ and $\Delta\alpha = 0.5°$.

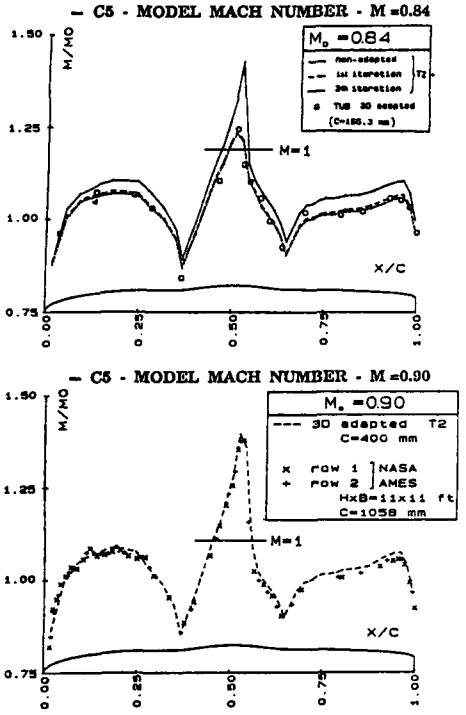

Fig. 4.20: Mach number distribution on C5 axisymmetrical body.

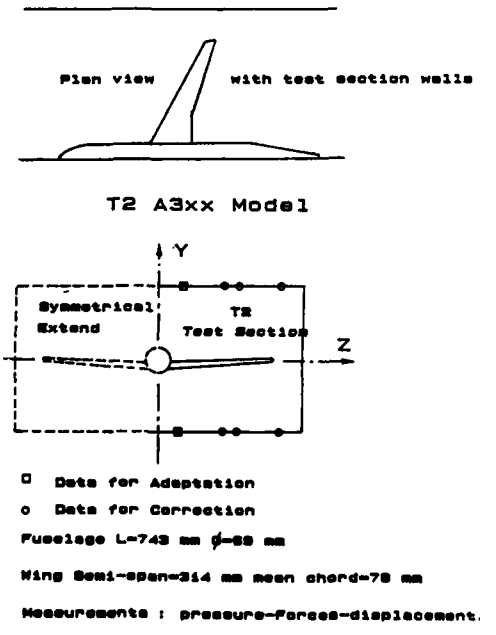

Fig. 4.21: Details of the T2 A3xx half model.

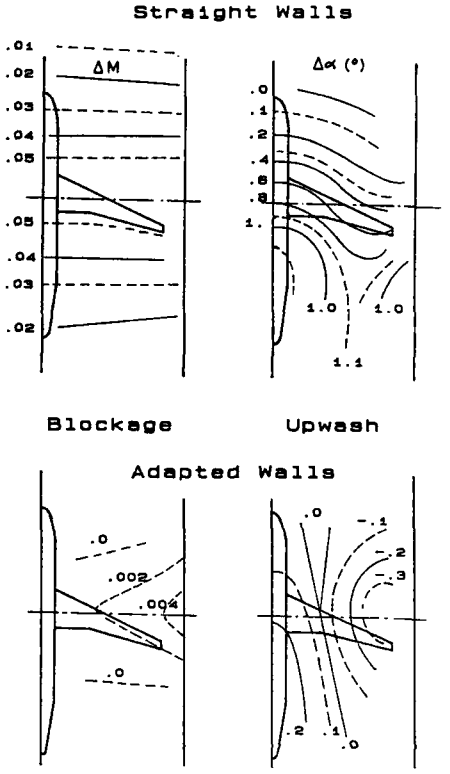

Fig. 4.22: T2 A3xx half model M = 0.78, α = 3.25°. Contour map of wall-induced blockage and upwash in the plane of the model.

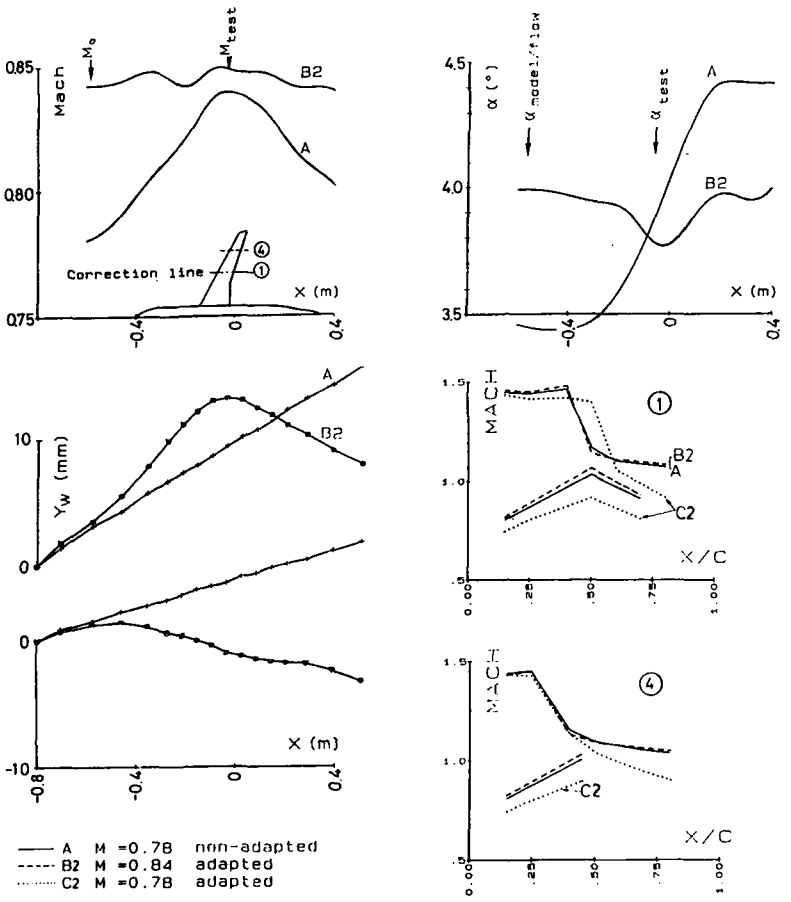

Fig. 4.23: Comparison of results from wall correction and wall adaptation.

This result means that the wing vicinity should be adapted at M = 0.84 and α = 4° to give equal results on the model.

After adaptation of the walls to these flow conditions (case B2) the corrections decrease to $\Delta M < 0.007$ and $\Delta\alpha < 0.2°$ near the midspan. The agreement between the Mach number distributions at the two sections is fairly good.

As expected the adaptation of case A at M = 0.78 and α = 3.5° gives very different results (case C2), see the bottom of Fig. 4.23.

The 3-D adaptation code is operational at T2 since 1985 and it has been extended by a correction method [4.18, 4.19] to improve the efficiency of the process. A Mach number range up to 0.95 for axisymmetrical bodies and up to 0.84 for half models has been sucessfully explored, the adaptation being realized in one or two iterations.

4.3.6 Preliminary supersonic tests in the S5Ch wind tunnel at ONERA Chalais Meudon

Preliminary supersonic tests were carried out in the S5Ch wind tunnel at ONERA Chalais Meudon, see Fig. 4.24. The test section of 0.22 m height, 0.18 m width and 0.95 m length is equipped with two upper and lower adaptive walls consisting of transverse sliding plates of 1.5 mm thickness. The sidewalls are straight. The upstream Mach number is fixed by a nozzle to 1.2. A delta wing at high angle of attack ($30° < \alpha < 60°$) is tested to prove that wall adaptation can be realized even in a difficult case [4.20].

The flow field was measured around the model with a 5-hole probe. Test results are presented in Fig. 4.24 with the associated wall shapes S1, S2 and S3.

Three shapes are compared: S2 is very near to the adapted case, S1 is symmetrical with straight parts and S3 is an extremely asymmetrical shape with a large step at the upper wall.

The Mach number distribution presented at the bottom of Fig. 4.24 shows the tolerance to the wall shape. Only at 60° an upwash of about 3° appears.

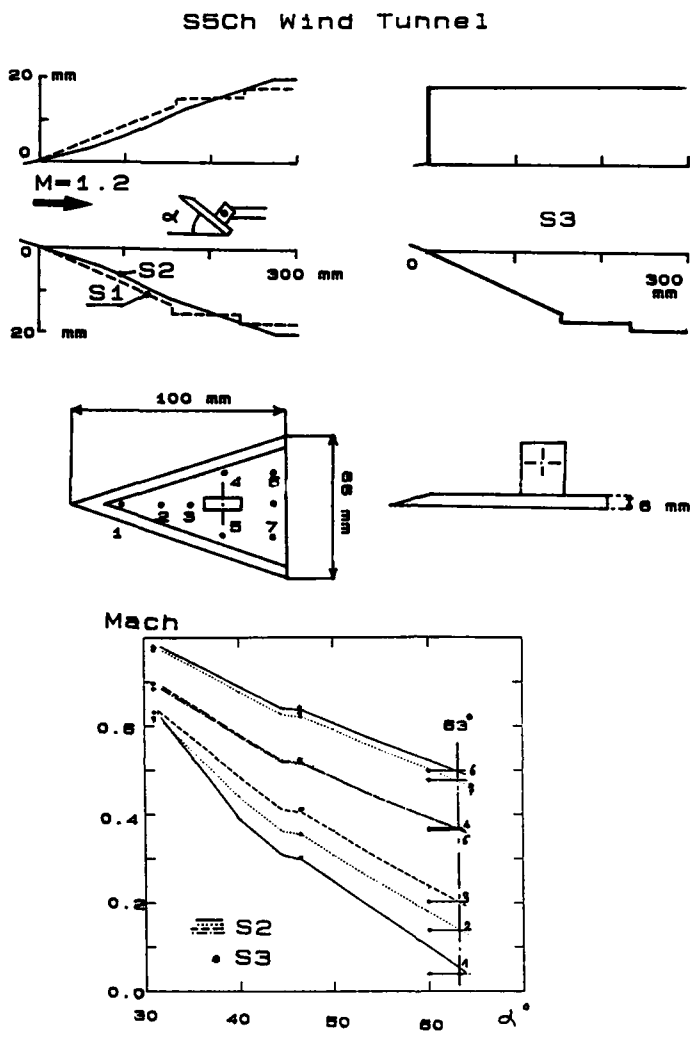

Fig. 4.24: Supersonic tests with different adapted wall contours: S2, S3.

4.3.7 Experimental results from TSWT at the University of Southampton

Experimental tests [4.9] were performed with two side-wall-mounted half-wing models, a cropped delta wing (Fig. 4.25) and a swept wing (Figs. 4.26, 4.27).

The data are in three parts. Fig. 4.25 shows contours of constant wall-induced blockage and wall-induced upwash, each as velocity perturbations referenced to the freestream velocity, for the cropped delta wing. Wall adaptation was aimed at eliminating these two components of interference along the "target line" which, in this example, is the horizontal tunnel centreline. The contours show interference levels on the horizontal plane through the centreline. The model was mounted nominally in this plane. The contours are shown at 0.002 intervals. Blockage is shown to be eliminated within this tolerance by wall adaptation.
Upwash is eliminated along the target line but remains at significant levels near to the root. This fact underlines Wedemeyer's suggestion to use a different tunnel cross section for large span models, if upwash is to be reduced over the full wing span.

Fig. 4.26 shows some adapted wall contours for the swept wing model tested at 8° incidence and Mach number 0.8. The target line in this case was the sidewall, the root of the half-wing model. The wall deflections in the region of the model are 2 mm or less, in sharp contrast with deflections in this region in typical tests on two-dimensional models where deflections of 10 mm are quite commonly experienced in TSWT.

However the removal of wall-induced downwash downstream of the half wing requires quite substantial downward movements, rising to about 9 mm at these test conditions. This could lead to a misalignment of the flexible walls with the remainder of the tunnel, but in the case of TSWT there is an adjustable diffuser between the ends of the flexible walls and the next fixed part of the tunnel which accommodates the misalignment.

Corresponding measures of residual upwash interference for the same model, test condition and target line are shown in the table enclosed in Fig. 4.27. The table includes also the interferences present as the target line is moved across the span. The measures of residual upwash are expressed in terms of root camber, tip camber, and twist from root to tip. As the target line is moved from the root towards the tip (y/b rising from 0 towards 1) the residual induced camber shifts from zero at the root to zero at the tip. The data is rounded to the nearest 0.1 of a degree. It appears from an inspection of the table that a target line should not be chosen at the root, but that any line between about 1/4 to 3/4 semi-span will give the lowest levels of curvature. For example, if the curvature figures for the y/b = 0.27 target line are summed in order to establish a rough figure of merit, the figure is about 0.4 degrees. With straight walls the corresponding figure was 2.2 degrees.

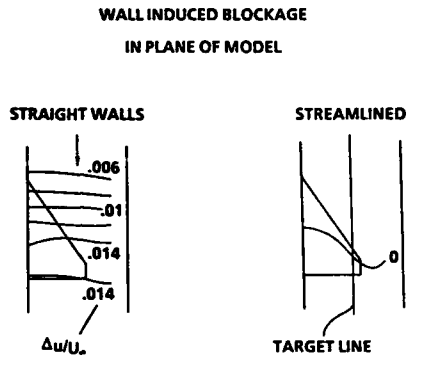

Crossed delta half wing in TSWT at Mach 0.7 and 8°

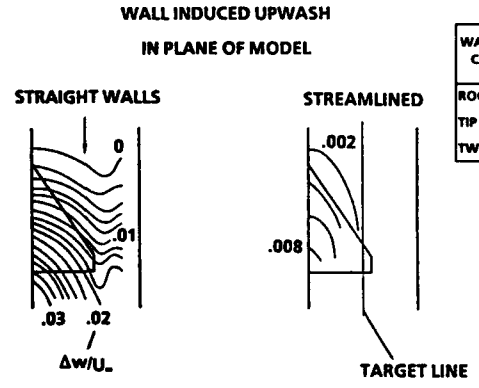

Crossed delta half wing in TSWT at Mach 0.7 and 8°

Fig. 4.25: TSWT half-wing tests ($M_\infty = 0.7$, $\alpha = 8°$). Contour map of wall-induced blockage and upwash in the plane of the model.

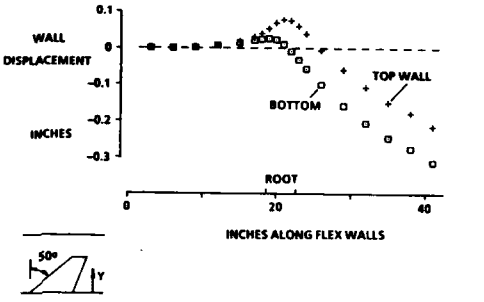

AR=2.7 swept half wing in TSWT at Mach 0.8 and 8°

Wall shapes after streamlining. Target line is the wing root (Y=0).

Fig. 4.26: Wall displacement for sidewall mounted swept wing, AR = 2.7.

WALL-INDUCED CURVATURE	STRAIGHT WALLS	STREAMLINED WALLS			
		y/b = 0	y/b = 0.27	y/b = 0.54	y/b = 0.81
ROOT CAMBER	1.4	-0	+0	0.2	0.3
TIP CAMBER	0.3	-0.1	-0.1	-0	-0
TWIST	-0.5	0.5	0.3	0.3	0.2

DEGREES

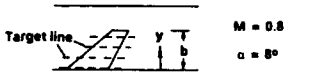

AR=2.7 swept half wing in TSWT

Influence of target line on residual flow curvature

Fig. 4.27: Influence of targetted line.
AR 2.7 swept wing, sidewall mounted.

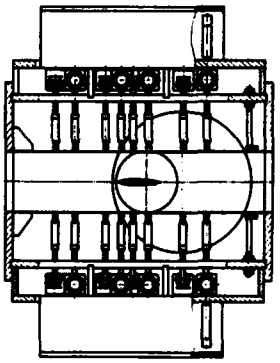

Fig. 4.28: The 2-D adaptive wall test section at TU Berlin.

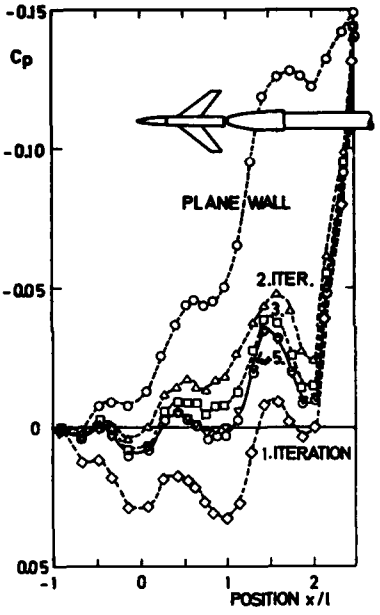

Fig. 4.29: Pressure along centreline of the flexible wall. Model F1, M = 0.80, α = 0°.

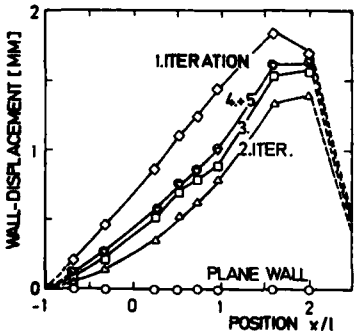

Fig. 4.30: Displacement of the flexible walls. Model F1, M = 0.80, α = 0°.

4.3.8 Experimental results at TU Berlin

Important research was done at the technical University of Berlin by Ganzer [4.5, 4.17]. The main part of the work concerning 3-D flows was performed in an octagonal test section (H = 0.15 m, W = 0.15 m, L = 0.85 m) allowing a complete 3-D adaptation.

Originally, a test section was built and equipped with two flexible fiberglass walls as shown in Fig. 4.28. Eight to thirteen jacks driven by electro-motors were used. This test section, mainly devoted to airfoil tests, was also used for 3-D model tests employing the adaptation method of Wedemeyer and Lamarche.

An example of wall adjustment is shown in Fig. 4.29 and Fig. 4.30 with the model F1 (blockage 1.1%), which is a swept wing fixed to a cylindrical body with an ogive nose. Measurements were made at the wall and with a six-component balance.

Results indicate very small displacements of the jacks corresponding to very small pressure variations along the walls. The blockage effect of the support was also noticed.

Ganzer concluded that adaptation of only two walls can provide a solution to the problem of transonic blockage. Wall interferences become amenable to theoretical correction methods, in particular as the boundary measurements on solid walls are easier to perform than for ventilated walls.

Wall adaptation for supersonic flows ($1 < M < 1.3$) was also studied. Due to the nearly conical shape of the shock waves (and other waves) the adaptation in a 2-D test section with flexible top and bottom walls appears to be not feasible.

4.4 Limitations and open questions

4.4.1 Introduction

Perfect adaptation would generate a wall shape such that, when the model is in the test-section flow, the wall boundary layer displacement surface coincides with a stream surface that would be observed if the test section had infinite size. In a three-dimensional flow this stream surface is, in general, also three-dimensional. Furthermore, the free-stream Mach number and model orientation relative to the free stream, in the ideal infinite flow, would have to be the same as their effective values in the real, adapted-wall tunnel. Many of the problems arising in attempts to achieve perfect adaptation occur even when the wall is capable of three-dimensional deformation, such as in the rubber-wall test section at Göttingen, the octagonal test section at Berlin or the variable porosity test section at Tullahoma, see e.g. Ref. [4.5]. Some, however, are peculiar to the situation that arises in two-dimensional adaptation for three-dimensional flows. As has been shown in the previous sections of this chapter, this technique has very important advantages, and it is possibly the only arrangement that is feasible for high-productivity tests, see next chapter.

Two-dimensional wall adaptation is necessarily imperfect. The residual interferences that occur must therefore be determined. To keep them small, the model and flow are subject to certain restrictions. For example, the strategy of Wedemeyer and Lamarche [4.2, 4.4], in which wall interferences are eliminated along the centreline of the test section, is subject to the following assumptions:

1. The lateral extent of the model is not a large fraction of the test section width.
2. The asymmetry of the flow with respect to the vertical centre plane of the test section is small.

In this section we first address the limitations imposed by these assumptions and then discuss other limitations.

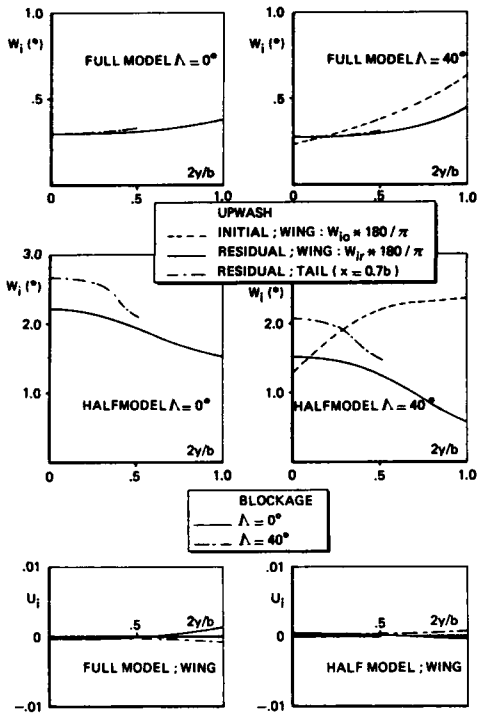

Fig. 4.31: Residual interference distributions for a *full* model at $M = 0.80$ and $C_L = 1.0$ and a half model at $M = 0.20$ and $C_L = 5.0$.

4.4.2 Limitations due to model size

An important feature of the residual interferences is that they are zero at the test section centreline *and* have a minimum there. Hence they remain small to second order with increasing distance from the centreline. A consequence is that the limitations of 2-D adaptation for 3-D flows are far less restrictive than might otherwise be anticipated. This has been demonstrated by numerical studies. An example of the results of the computation by Smith [4.8] for a model of a typical transport aircraft with span equal to 65% of the width of a square test section are presented in Fig. 4.31, taken from [4.8]. The figure shows at the top the upwash distribution W_i across the span for a full model at $C_L \approx 1$ and $M_\infty = 0.80$, with zero and 40° sweep. As may be seen, the wall-induced upwash increases slightly towards the wing tips [1]), but amounts only to less than 0.1° for $\Lambda = 0$ and less than 0.2° for $\Lambda = 40°$ for the wings and much less for the tail. The residual blockage interference is smaller than 0.1%, see bottom left of Fig. 4.31. These numbers are in the same range as the accuracy achievable in modern wind tunnels, so that they do not represent a serious limitation.

The residual interferences can actually be further reduced by using a rectangular rather than a square test section. This may be understood by considering the images of the model in the sidewalls and in the top and bottom walls. The sidewall and horizontal walls have opposite effects on the spanwise variation of the upwash. Changing the aspect ratio of the test section changes the relative importance of the sidewall and horizontal wall images, so that a more favourable upwash distribution may be achieved.

This was examined numerically by Wedemeyer and Lamarche [4.7]. An example of their results is presented in Fig. 4.32. A typical transport aircraft model with span 2s was considered at $M_\infty = 0.7$ and $C_L = 0.5$ in a test section of height h and width b. The ratio $2s/\sqrt{bh}$ was taken to be 0.7 corresponding to $2s/b = 0.7$ in the square test section. As may be seen, the residual upwash and blockage interferences are approximately minimized by choosing $b/h = 1.4$. At this value, the residual upwash and the residual blockage are nearly zero. The effect of test-section aspect ratio is even more favourable if the model span is larger. This is shown in Fig. 4.33, giving results for the residual upwash for the same conditions as in Fig. 4.32 but for $2s/\sqrt{bh} = 0.7$, 0.8 and 0.9. The maximum residual upwash at $2s/\sqrt{bh} = 0.9$ in the test section with $b/h = 1.4$ is only 0.06°, i.e. significantly below the value at $2s/\sqrt{bh} = 0.7$ in the square test section, which is about 0.33°.

Clearly, the residual interferences are not an important limitation in full-model testing. The situation is significantly different for half-model testing, as may be seen from Fig. 4.31 center, where the residual upwash wall interferences are seen to be negative if cancellation is achieved by adaptation along the centreline in the symmetry plane of the model. This is in keeping with Fig. 4.32, bottom left, because the effective aspect ratio of the square test section with a half-model is $b/h = 2$.

Further numerical studies of residual interferences for various aspect ratios of the test section are reported by Lewis [4.24] and presented here in Fig. 4.34. The parameter on this figure is the variation of wall-induced upwash velocity along the span referenced to the free stream $\Delta w/U$ and expressed as a percentage. The calculations were for low speed flow around a simple horse-shoe vortex of unit strength. Elliptical spanwise loading was assumed.

4.4.3 Limitations in asymmetric flow

In section 4.4.2 we have only considered flows with a symmetry plane passing through the model axis. Clearly, the 2-D adaptation cannot cancel sidewash interferences. This is therefore a serious limitation of the technique whenever the sidewash interference is significant. Such situations are very rare, however, as may be seen by the following argument. Objects tested in wind tunnels are, with few exceptions, designed to produce only small side force per unit yaw angle, while the opposite is true of the normal force. Upwash and sidewash interferences $\Delta\alpha$ and $\Delta\beta$ are proportional to the forces experienced by the model in the respective directions.

Hence

$$\frac{\text{side force}}{\beta} \ll \frac{\text{normal force}}{\alpha},$$

or

$$\frac{\Delta\beta}{\beta} \ll \frac{\Delta\alpha}{\alpha}.$$

Therefore, sidewash interferences are usually very much smaller than upwash interferences and need not be considered.

[1]) Similar results were obtained by Rosenhead [4.21] and Prandtl [4.22] for wings in circular test section, see also Glauert [4.23].

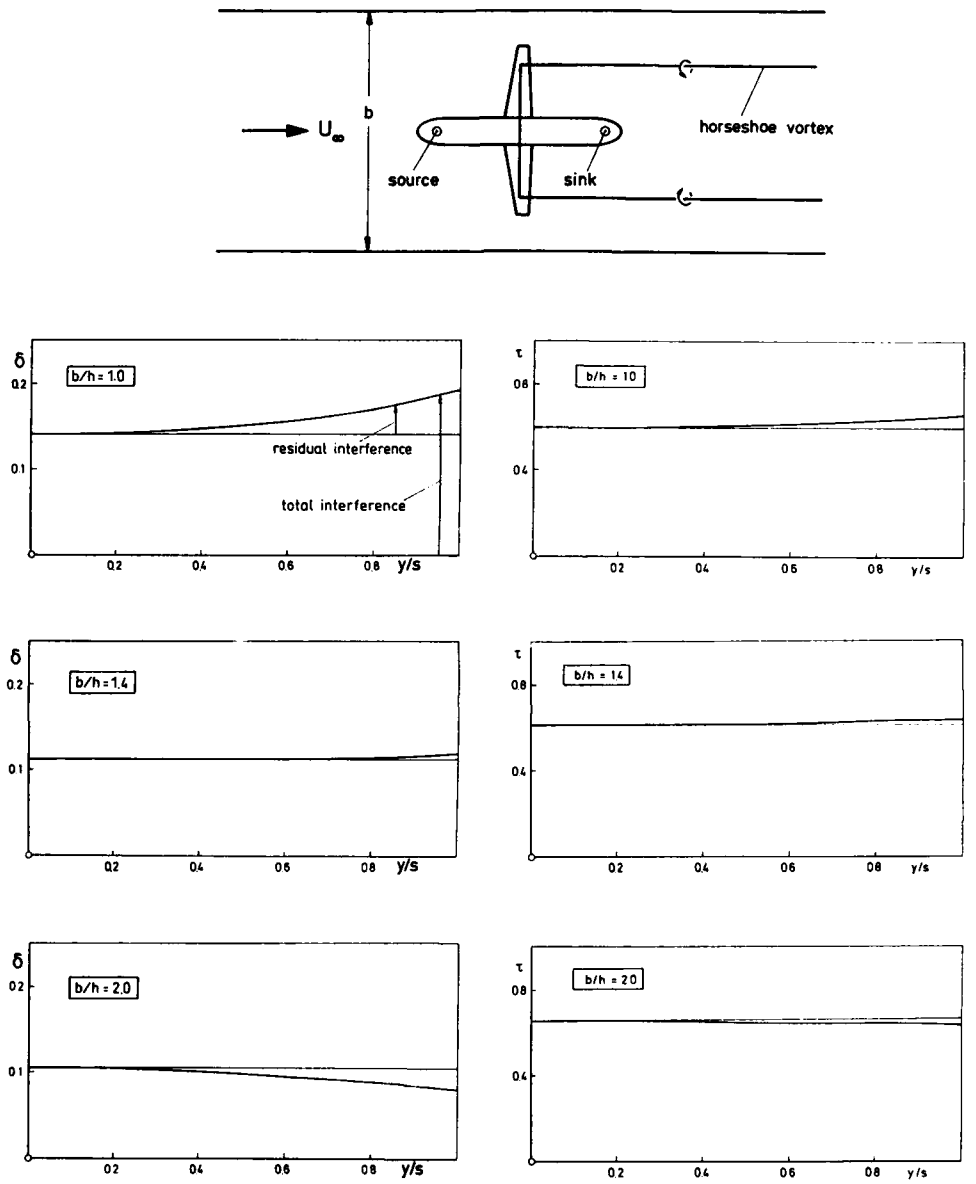

Fig. 4.32: Effect of test-section aspect ratio on upwash and blockage interference.
$\Delta\alpha = (A_{wing}/A_{tunnel}) \cdot C_L \cdot \delta$; $\beta^2 \Delta u / U_\infty = (A_{body}/A_{tunnel}) \cdot \tau$; y = spanwise position, s = semispan.

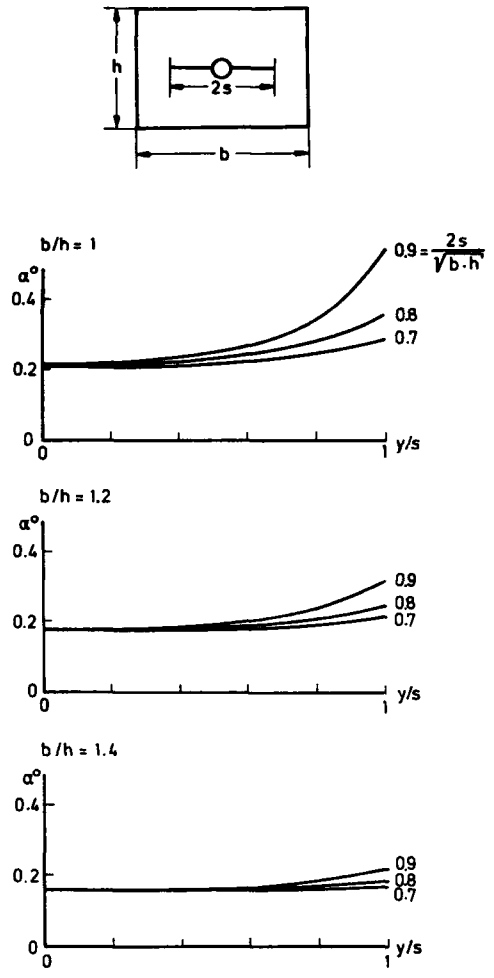

Fig. 4.33: Upwash angle α versus spanwise position y for various test-section aspect ratios b/h and wing span ratios $2s/\sqrt{b \cdot h}$. Wing with elliptical load distribution, $C_L = 0.5$.

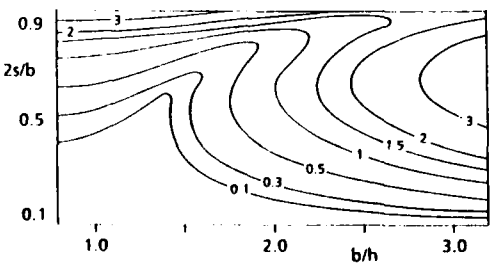

Fig. 4.34: Upwash variations along the span of a wing in a straight test section.

4.4.4 Other limitations

Requirements of adaptive wall techniques such as minimum test section length, density of adjustment jacks, performance as $M_\infty \rightarrow 1$, ability to return the flow direction to the upstream direction etc. apply equally to other techniques as to 2-D adaptation for 3-D flows.

One of the important advantages of 2-D adaptation for 3-D flows is that the full test section is optically accessible at least in one direction. This is not achievable in 3-D adaptation. Some modern diagnostic techniques such as laser induced fluorescence show promise of providing significantly more information about flows than has been possible to date, and do so at a very high rate. They require limited optical access in one direction and full optical access at right angles to it, however. This seems difficult because a window needs to be made on the flexible wall. Since it needs only to be small, however, it is probably possible.

4.4.5 Conclusions

Results of calculations made for transport aircraft models show that the residual interferences can be reduced to such small values that they are in the same order of magnitude as the uniformity of the test section flow achievable today or less. Adjusting the test section aspect ratio improves the situation significantly. Residual interferences are not so small in half-model tests but can be reduced significantly if a special aspect ratio test section is used.

It is advisable in any event to measure the residual interferences by instrumenting all four walls with a sufficiently large number of pressure tappings.

The advantages of the 2-D adaptation seem to outweigh the limitations in view of the more general limitations on flow uniformity achievable in transonic wind tunnels.

4.5 References

[4.1] Wolf, S.W.D., Cook, I.D. and Goodyer, M.J.: The Status of Two- and Three-Dimensional Testing in the University of Southampton Transonic Self-Streamlining Wind Tunnel. AGARD-CP-335, paper no.15, May 1982, 14pp.

[4.2] Wedemeyer, E.: Wind Tunnel Testing of Three-Dimensional Models in Wind Tunnels with Two Adaptive Walls. VKI-TN-147, Oct. 1982, 30pp.

[4.3] Harney, D.J.:Three-Dimensional Test Experience with a Transonic Adaptive-Wall Wind Tunnel - Final Report, Apr.1981 - Dec.1982. AFWAL-TR-83-3028, Mar.1983, 86pp.

[4.4] Lamarche, L. and Wedemeyer, E.: Minimization of Wall Interference for Three-Dimensional Models with Two-Dimensional Wall Adaptation. VKI-TN-149, Mar.1984, 56pp.

[4.5] Ganzer, U.: A Review of Adaptive Wall Wind Tunnels. Progress in Aerospace Sciences, vol.22, Pergamon Press, 1985, pp.81-111.

[4.6] Archambaud, J.P. and Mignosi, A.: Two-Dimensional and Three-Dimensional Adaptation at the T2 Transonic Wind Tunnel of ONERA/CERT. AIAA 15th Aerodynamic Testing Conference, San Diego, Cal., May 18-20, 1988, pp.342-350, paper no.88-2038.

[4.7] Wedemeyer, E. and Lamarche, L.: The Use of 2-D Adaptive Wall Test Sections for 3-D Flows. AIAA 15th Aerodynamic Testing Conference, San Diego, Cal., May 18-20, 1988, pp.363-371, paper no.88-2041.

[4.8] Smith, J.: A Theoretical Exploration of the Capabilities of 2-D Flexible Wall Test Sections for 3-D Testing. NLR MP 84018 U (1984).

[4.9] Lewis, M.C., Neal, G. and Goodyer, M.J.: Adaptive Wall Research with Two- and Three-Dimensional Models in Low Speed and Transonic Tunnels. AIAA 15th Aerodynamic Testing Conference, San Diego, Cal., May 18-20, 1988, pp.331-340, paper no.88-2037.

[4.10] Rebstock, R. and Lee, E.E.jr.: Capabilities of Wind Tunnels with Two Adaptive Walls to Minimize Boundary Interference in 3-D Model Testing. NASA CP-3020, Vol. 1, Part 2 (1989), pp. 891-910.

[4.11] Lamarche, L.: Reduction of Wall Interference for Three-Dimensional Models with Two-Dimensional Wall Adaptation. Dissertation, Universite Libre de Bruxelles, 1986.

[4.12] Ashill, P.R., Weeks, D.J.: A Method for Determining Wall-Interference Corrections in Solid-Wall Tunnels from Measurements of Static Pressure at the Walls. AGARD Conference Proceedings No.335 (1982).

[4.13] Murman, E.M.: A Correction Method for Transonic Wind Tunnel Wall Interference. AIAA paper no.79-1533, 1979.

[4.14] Rizk, M.H. and Murman, E.M.: Wind Tunnel Wall Interference Corrections for Aircraft Models in the Transonic Regime. Journal of Aircraft, Vol.21, No.1, pp.54-61, 1984.

[4.15] Maarsingh, R.A., Labrujère, Th.E. and Smith, J.: Accuracy of Various Wall Correction Methods for 3D Subsonic Wind Tunnel Testing. AGARD-CP-429, paper 17 (1987), 13pp.

[4.16] Holst, H., Raman, K.S.: 2-D Adaptation for 3-D Testing. DFVLR-IB 29112-88 A 03, Göttingen (1988).

[4.17] Ganzer, U.: Adaptable Wind Tunnel Walls for 2-D and 3-D Model Tests. TU Berlin, Germany ICAS Paper 23.3, Oct. 1980.

[4.18] Capelier, C., Chevalier, J.P., Bouniol, F.: Nouvelle Méthode de Correction des Effets de Parois en Courant Plan. La recherche aérospatiale, Jan.-Feb. 1978, pp.1-11. Also translated into English as ESA-TT-491, Aug. 1978, pp. 1-30.

[4.19] Le Sant, Y.: Corrections 3D des Effets de Paroi dans un Domaine Rectangulaire à 2 Parois Verticales. ONERA RT 37/3075 AN 203 A.

[4.20] Le Sant, Y.: Adaptation de Parois à M = 1.2 Essais. ONERA RTS 39/3075 AY.

[4.21] Rosenhead, L.: The Effect of Wind Tunnel Interference on the Characteristics of an Aerofoil. Proc. Roy. Soc., A 129, p.135 (1930).

[4.22] Prandtl, L.: Experimentelle Prüfung der Berichtigungsformel für Flügel von großer Spannweite im Luftstrom der Versuchsanstalt. Ergebnisse der AVA zu Göttingen, Vol.2, p.17 (1923).

[4.23] Glauert, H.: Wind Tunnel Interference on Wings, Bodies and Airscrews. British A.R.C. R.&M. 1566 (1933).

[4.24] Lewis, M.C.: Influence of Test Section Proportions on Residual Wall Interference in Two-dimensional Adaptive Walled Tunnels. University of Southampton, Department of Aeronautics and Astronautics Memo AASU 88/8, September 1988.

Organization	Tunnel	HxWxL [m]	Testing Envelope	Walls : jacks Pressure	Tunnel Equipment
AFWAL	FLD9 SAW	0.22×0.22×1.3	M < 1 Pt < 4.2b Ambient	10×(9 rods)/w. Aut.	
DFVLR	HKG	0.67×0.725×2.2	M < 1.2 Pt = 1b Ambient	17(8 fixed)/w. Man. 228(12 rows U + L + S)	PDP 11/21 + P.S.I.
NASA Langley	TCT	0.33×0.33×1.42	M < 1 Pt = 6b Cryo	18/wall Automated 64(2 rows U + L) + 28S	Micro Vax 2
ONERA/ CERT	T2	0.37×0.39×1.32	M < 1 Pt < 3b Cryo	16/wall Automated 214(6 rows U + L)	HP 1000 P.S.I.
ONERA	S5Ch	0.22×0.18×0.3	M = 1.2 Pt = 1b Ambient	Multiplate Man. 5 Hole Probe	
Southampton University	TSWT	0.15×0.15×1.12	M < 1 Pt = 1b Ambient	19/wall Automated 300(U + L + S)	PDP 11/84
Tech. Univ. Berlin	1/2	0.15×0.15×0.99	M < 1 Pt = 1b Ambient	13/wall Automated	HP 1000 P.S.I.

Table 1. 2-D adaptation for 3-D flow facilities

5. HIGH PRODUCTIVITY TESTING

Editor: J. Smith
Other contributors: E. Wedemeyer, A. Mignosi

5.1. General considerations

Important parameters of a production windtunnel are its efficiency and versatility. Efficiency can be expressed in terms of "cost per data point", accounting for both the investment and running cost. Versatility refers to the variety of tests the windtunnel can accept and is suited for. Both aspects can be affected by the introduction of an adaptive wall test section.

The additional investment required for fully automated adaptive walls, relative to passive walls, is estimated to be of the order of 8 - 20% of the "turn-key" cost of a transonic windtunnel depending on e.g. the number of adaptive walls. Maintenance cost will also slightly increase. The running cost may be much more sensitive and is dominated by energy consumption and production rate.

For 3D testing, the power requirement does not strongly depend on the adaptive or passive nature of the walls. However, the energy losses in a solid wall test section may be 20 - 50% smaller than those in a similar ventilated one; roughly half of this reduction may still remain when considering a complete closed-circuit windtunnel. Therefore, an interesting reduction of power requirement can be obtained by applying adaptive solid walls instead of ventilated walls.

The production rate depends strongly on tunnel control, data acquisition and data processing, and test procedures. There is no apparent reason why tunnel control should differ much for either passive or adaptive walls, apart from the additional adaptive wall control as such. Adaptive walls, however, require fast data acquisition, not only of model data but also of wall boundary data. Moreover, data processing should be very fast in order to allow feed-back of measured data to wall control. For high-productivity testing, traversing systems (e.g. traversing probes, LDV) and mechanical scanning devices do not seem acceptable as methods for determining the flow near the walls.

In general, the test procedures applied in present day adaptive wall research facilities reflect that relatively little attention has been paid to production rate (for obvious reasons). The proven strategies require the measurement of an "initial test condition" and one or more subsequent measurements of nominally the same test condition in order to arrive at the optimum wall setting at which the effective data point is taken (Sections 3.2 and 4.2). Such strategies are limited to measurements in a "step/-pause" fashion and require, per data point, at least twice the amount of time used for conventional step/pause testing. However, the "true" conditions can be defined a priori instead of after correction. This may considerably reduce the required amount of data points (and testing time) by eliminating the need to interpolate between (closely spaced) data points in order to arrive at the desired test conditions.

For "continuous" testing, i.e. performing measurements while the test conditions are gradually changing with time, different and probably less rigorous strategies will be required. Since "continuous testing" provides the higher production rate and is more demanding with respect to both hardware and software, it will be discussed in more detail in Section 5.2.

The operational versatility of an adaptive wall test section will generally be less than that of a conventional one. For instance, possibilities for optical access and auxiliary mounting provisions are more limited since they may interfere with the active walls. Moreover, in the particular case of 2D flexible solid walls, testing at near-sonic free-stream conditions is not (yet?) possible. On the other hand, the better flow quality that can be achieved with solid walls may be of importance for e.g. Natural Laminar Flow development and transport aircraft drag optimization while, in addition, the associated reduced power requirement may be re-invested in order to obtain higher Reynolds number.

5.2. Towards high production rates

In the past decade, the operation of production windtunnels has shown an appreciable shift from "step/pause" to "continuous" testing. Continuous force measurement procedures are well-established, while developments are still directed to ever increasing rates of change of, especially, the angle of attack, exploring the possible limits. Similar advances have been made for pressure measurements since the advent of electronic pressure scanning systems. Therefore, it is to be expected that adaptive wall windtunnels will have to be able to operate in a "continuous testing" mode in order to be competitive. Unfortunately, "continuous testing" adaptation strategies are not yet well-established, so the following discussions are, for an important part, bound to be rather speculative in nature.

Considering power requirement, flow quality and relative ease of wall boundary measurement, flexible solid walls seem to have definite advantages as compared with adaptive ventilation, except for the near-sonic flow domain in which perforated walls (passive or adaptive) are still unrivalled. Regarding operational versatility, it seems undesirable to aim at full 3D streamlining of the walls. Besides, full streamlining (i.e. wall interference elimination) tends to increase the need of iteration as opposed to adaptation aimed at obtaining correctable conditions, to be discussed later. For these reasons, but also because of the simpler presentation involved, the following discussions will mainly be phrased in terms of 2D adaptation (for both 2D and 3D testing; see also Chapter 4) by means of flexible solid top and bottom walls and plane solid side walls. They will also be limited to test conditions with subsonic flow near the adaptive walls. Within these limitations, however, the general philosophy should also globally apply to adaptive ventilated walls.

5.2.1. Data acquisition and wall control

In order to meet the "continuous testing" requirement, both model quantities and wall boundary conditions must be measured almost instantaneously and simultaneously. This seems feasible with respect to force balance, electronically scanned pressure and wall displacement measurements. (Wall boundary condition measurements in a ventilated test section are still much more problematic).

A possible approach to fast wall control is the concept of a "live wall", where all control units (e.g. jacks) move simultaneously and proportionally from a previous setting to the next to arrive there (quasi-) simultaneously. Such a "live wall" also seems feasible, although safeguarding the process seems a major, but solvable, problem. In fact, ONERA T2 already applies proportional, but not simultaneous, jack control.

5.2.2. Adaptation algorithms and strategies

Wall adaptation calculations must be performed extremely rapidly in order to keep the walls "live". Moreover, it is not sufficient to calculate the optimum wall shape for the data point taken at a specific moment. On the contrary, at that moment the walls should be instructed where to go to for the NEXT data point. In other words: the adaptation algorithms should to some extent be predictive, probably by some kind of extrapolation of data from preceding data points. It may be expected that such an approach has inherent imperfections. However, considering the data point density that can easily be obtained in continuous testing, it may be expected that the imperfections can be satisfactorily eliminated by applying residual interference corrections. Obviously, iterative techniques can never cope with continuous testing. Only so-called "One-Step Methods" ([5.1] - [5.5]) could be combined with a data prediction scheme.

It has been argued (e.g. [5.1]) that One-Step Methods can not exist: "because the pressure and velocity fields of the model will change after the wall adjustment and resultant interference reduction". This will undoubtedly be the case if the adaptation process is aimed at the elimination of interference. If, however, wall adaptation is limited to the elimination of interference gradients only [5.5], then the associated changes of the model flow may generally be expected to be sufficiently small to be ignored. Of course there are exceptions, for instance in case these gradients happen to induce or suppress flow separations or shock wave displacements. In continuous testing with a "live" adaptive wall, however, such effects are relatively small because the gradients are relatively small due to the gradually changing, always partly adapted for, test conditions, provided that the starting point of each "sweep" is properly adapted for. These starting points could be treated by means of iterative techniques (including One-Step Methods), without seriously increasing the running time.

Although present day One-Step Methods are restricted to linear flows, the following must be stressed [5.6]: All modern linearized flow theories for wall adaptation and wall interference assessment (not: corrections!) are fundamentally related (See also Subchapter 6.2); those considering the "interior flow domain" are compatible with and complementary to those considering the "imaginary exterior flow domain" and will, therefore, have very similar limits of validity. It is generally assumed that these limits are encountered when supersonic pockets extend to the test section walls.

The linearized flow assumption creates the possibility to reduce the necessary on-line calculations, with respect to both "One-Step" wall adaptation and residual interference assessment, to mere matrix * vector multiplications. The vector represents the measured wall boundary conditions; the matrices represent the corresponding influence coefficients. It would be most profitable if the test procedure were such that the matrix coefficients could be calculated during the time in between successive "sweeps" and would remain constant during the sweeps.

5.2.3. Test procedure

In the early days, NPL adopted the policy of using the Mach number sweep (i.e. varying Ma at a fixed angle of attack setting α) in preference to the α-sweep (i.e. varying α at fixed Ma) in order to minimise the time required to set walls by minimising the distance travelled between test conditions (Chapter 1). For continuous testing in a flexible wall test section, however, there are distinct advantages of applying the α-sweep instead.

First of all, the matrix coefficients mentioned in the previous section depend on a variety of geometrical quantities (e.g.: test section geometry, distribution of wall boundary data, location of the "target line", see also Section 4.2) and the reference Mach number. The geometrical quantities can be fixed during a test, so the matrix coefficients will then only depend on Mach number and, therefore, do not need to be recalculated during an α-sweep. The time between successive sweeps, already required to change the Mach number setting, can be used to calculate the coefficients for the successive Ma-sweep without delaying the test.

Secondly, buoyancy is generally very small in a solid wall test section (except for, maybe, wings with massive flow separation, isolated propellers, etc.) and blockage is, therefore, correctable. Consequently, the reduction of streamline curvature, which is roughly proportional to lift, seems to be the main issue. Lift is a major driving factor in terms of wall interference and, even at fixed angle of attack, varies considerably at higher Mach numbers (around the "lift divergence" conditions).

Thirdly, the speed required for wall adjustment during α-sweeps does not seem to present a major problem for test sections of the usual sizes. For instance, [5.7] suggests a maximum displacement of about 1.50 mm/deg. or roughly $0.002 * \sqrt{B * H}$ per degree change of angle of attack at Ma = 0.70 (See also Fig. 1). Tripling that value in order to, generously, account for half models, higher Mach numbers, etc. and assuming $\sqrt{B * H} = 2$ m would,

for example, lead to a speed requirement of 12 mm/deg. This seems quite feasible for the currently common rates of change of up to 1 deg./sec. Of course, the requirement may cause serious problems should the rate of change be much larger.

Finally, varying α at constant Ma can generally be performed at much higher rates (in terms of useful data points per second) than its opposite, because of inertia.

5.3. Conceivable high-productivity strategy

From the previous sections, a possible high-productivity strategy can be conceived. For convenience, the strategy will be phrased in terms of an aircraft model with its pitch axis coinciding with the centre of a 2D adaptive flexible wall test section and tests consisting of (continuous) α-sweeps.

a) Test preparation

Perform numerical simulations of the model in the test section, for various Mach numbers and at least two, sufficiently different, values of lift. Also numerically simulate the associated optimum wall shapes in the best possible way. Separate lift and blockage effects.

From these, derive first estimates of wall displacements as functions of lift. Considering the linearity of the problem, wall displacement may be expected to vary linearly with lift, so the functions will essentially be constants $k_j = d\sigma/dC_L$ for each jack location and Mach number (section 5.4.1).

b) Before the first and in between successive α-sweeps

Set the Mach number and simultaneously calculate the influence coefficient matrices with respect to a One-Step adaptation method and wall interference assessment (Section 5.2.2). Estimate the initial $dC_L/d\alpha$.

c) First data point of each sweep

Take data and perform wall adaptation as well as possible, starting with an initial wall shape derived from step a) and, if necessary, using an iterative technique. The eventual adapted wall should eliminate blockage, buoyancy and streamline curvature, but not necessarily the upwash level, in the vicinity of the test article along e.g. "a target line" (Section 4.2.).

Predict C_L and wall setting for the next data point, using the known next value of α and the first estimates of $dC_L/d\alpha$ and k_j by adding the associated increments to the present values.

d) Start or continue the actual α-sweep

Change α and wall setting simultaneously and linearly with time towards the predicted next setting. When the next setting is reached, perform the next step (e) without changing the ongoing movements.

e) Data points

Take data, calculate (and possibly apply) residual corrections and "optimum wall setting" (One-Step Method), which may differ slightly from the predicted one, for this data point and improve the estimates of $dC_L/d\alpha$ and k_j using the present and previous data points. Predict C_L and wall setting for the next data point, using the improved estimates of $dC_L/d\alpha$ and k_j as well as the presently calculated "optimum wall setting".

f) Completing the α-sweep

Repeat steps d) and e) until the sweep is completed. Then proceed with step b) if additional sweeps are required.

It may be useful to recall here that the strategy is mainly based on minimisation of streamline curvature effects. After the first data point of each sweep, however, also blockage and buoyancy may vary per data point and certainly the upwash level will. Upwash and blockage are assumed to be correctable (they surely are if no gradients occur) and buoyancy is assumed to be small (Section 5.2.3.).

5.4. Some experimental and numerical support for proposed strategy

5.4.1. Experiment

Some typical examples of wall displacements associated with 2D wall adaptation for an aircraft model, taken from [5.7], are shown in Fig. 5.1. Because forces have not been measured during this test, wall displacement is shown as a function of incidence. The stations A-D have been chosen arbitrarily and are identified in the top of the figure. The actual wall displacements have been divided into a part representing the "camber" of the test section (σ) and a part associated with the local increase in test section height (δ). The "camber" σ is associated with model lift and δ reflects the compensation of blockage.

As expected, σ turns out to vary linearly with lift, enabling its prediction (with confidence) for a subsequent data point from preceding ones. The local height variation δ varies non-linearly with lift, but omitting such a variation mainly affects the (correctable) blockage level, unless massive flow separation occurs.

A similar example, taken from a half model test in ONERA T2, is shown in Fig. 5.2. At the higher lift coefficients, some non-linearity appears in the σ-curves which might be associated with large supersonic pockets on the wing's upper surface. Besides, it is indicated that δ may be well-predicted by area ruling, i.e. by creating a constant cross-section stream tube.

Very similar results, not shown here, have been obtained for tests on 2D aerofoils.

5.4.2. Numerical simulation

Although the experimental results do suggest the feasibility of a predictive adaptation strategy, such a strategy has never been applied. Therefore, a numerical simulation has been performed [5.8].

A panel method was used to simulate a typical aircraft model in a 2D flexible wall test section (Fig. 5.3). Since the Mach number merely represents a scaling factor (in linearized subsonic flow), Ma = 0 was adopted, for convenience. For comparison, unbounded flow, one-step adaptation (as would be used in a step/pause mode) and conventional plane solid walls have also been considered.

The strategy applied for predictive adaptation corresponds with the NLR strategy (see Chapter 4), with one exception:
The initial estimates of k_1 (= $d\alpha/dC_l$) were obtained in an approximate way, simulating the plane wall "experiment" by means of a method of images with a very conventional model representation (swept horseshoe vortex). In addition, the values of k_1 have not been updated during the sweep. This omission allowed faster calculations, because intermediate applications of a One-Step Method then are no longer necessary! In order to update $dC_l/d\alpha$ before reaching the second effective data point, an intermediate point was taken at $\alpha = -4°$, not shown here.

The small differences between the results of the One-Step (OS) and Predictive Adaptation (PA) for the first data point $\alpha = -5°$ are due to the fact that the Predictive Adaptation, in this case, applied the NLR One-Step Method twice (i.e. iteratively).

The OS and PA "measured" data also agree very well for the remaining data points, again supporting the predictive strategy. As was to be expected, the data "measured" with Plane Solid walls (PS) are less satisfactory. After the application of (residual) corrections, all date agree very well, including the Unbounded Flow (UF) reference data. These results confirm the effectiveness and similarity of the two different adaptation procedures.

On the other hand, the results hardly demonstrate the necessity of adaptive walls. Apparently, the low Mach number suppresses the mutual differences considerably (scaling factor). For more conclusive results, higher Mach numbers (and preferably local supersonic flow on the model) ought to be considered. For such studies, however, experiments seem more appropriate.

5.5. Concluding remarks

Considering investment cost, running cost, operational versatility and flow quality, the present feeling is that a so-called "two-dimensional flexible wall test section" is a near-optimum solution for production windtunnels, up to high subsonic Mach numbers. For near-sonic test conditions, ventilated walls are still unrivalled.

High productivity implies the requirement of "continuous testing", i.e. performing measurements while the test conditions are gradually, but continuously, varying in a controlled way. "One Step Methods" are not by themselves suited for continuous testing. In order to anticipate the ever varying test conditions, the necessary wall adaptation strategy must also to some extent be predictive.
Such strategies are presently not well established. Therefore a possible high productivity strategy has been discussed in a somewhat speculative fashion, although supported by a little experimental and numerical evidence.

5.6. References

[5.1] Judd, M. Goodyer, M.J. and Wolf, S.W.D.: Application of the computer for on-site definition and control of windtunnel shape for minimum boundary interference. AGARD-CP-210, paper no. 6, 12 pp., 1976.

[5.2] Wolf, S.W.D. and Goodyer, M.J.: Predictive wall adjustment strategy for two-dimensional flexible walled adaptive windtunnel - A detailed description of the first one-step method. NASA CR-181635, January 1988.

[5.3] Wedemeyer, E.: Wind Tunnel Testing of Three-Dimensional Models in Wind Tunnels with Two Adaptive Walls. VKI-TN-147. Oct.1982, 30pp.

[5.4] Lamarche, L. and Wedemeyer, E.: Minimization of Wall Interference for Three-Dimensional Models with Two-Dimensional Wall Adaptation. VKI-TN-149, Mar.1984, 56pp.

[5.5] Smith, J.: A Theoretical Exploration of the Capabilities of 2-D Flexible Wall Test Sections for 3-D Testing. NLR MP 84018 U (1984).

[5.6] Garteur Action Group AD (AG-02): Two-dimensional *transonic* testing methods; final report. Garteur/TP-011. (Also: NLR TR 83086 U), 1981.

[5.7] Holst, H. and Raman, K.S.: 2D Windtunnel wall adaptation for testing 3D models. DFVLR Goettingen IB 29112 88A04, Feb. 1988.

[5.8] Smith, J. and Labrujère, Th.E.: To be published (NLR)

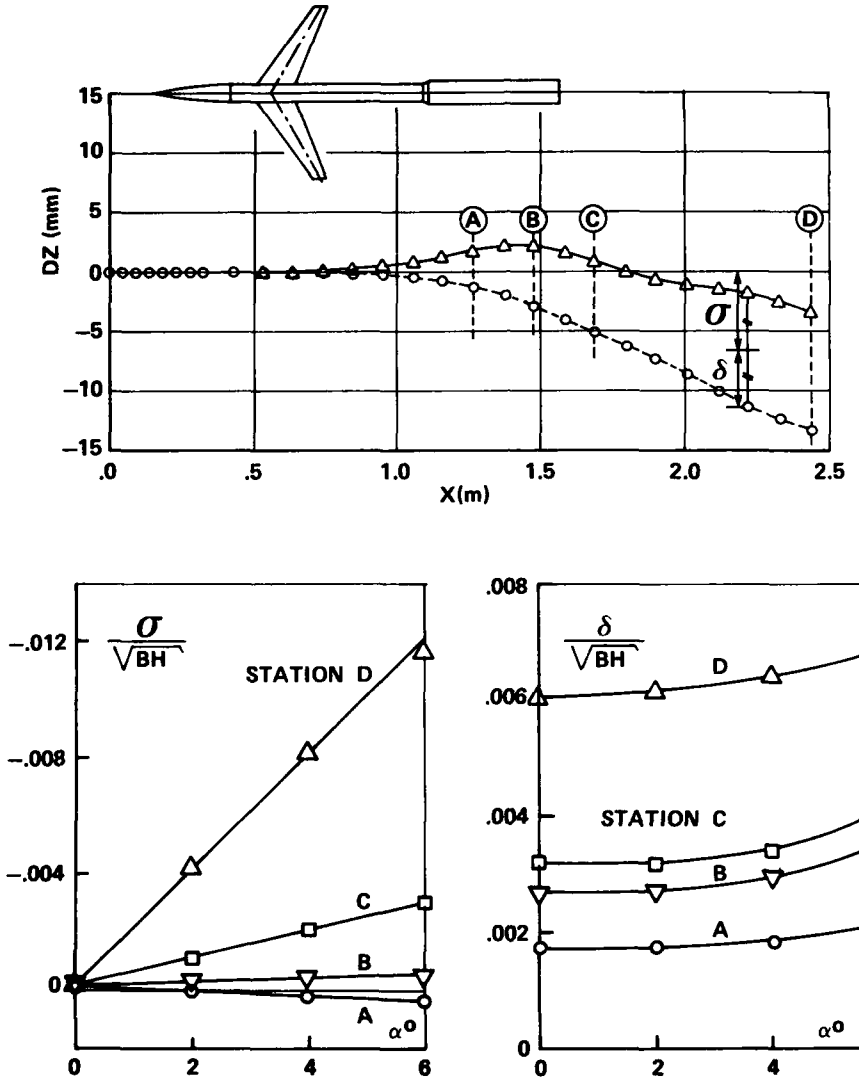

Fig. 5.1 Typical wall displacements for 2D adaption. (DFVLR HKG; Ma = 0.70; 2s/B = 0.75; From Ref. 7)

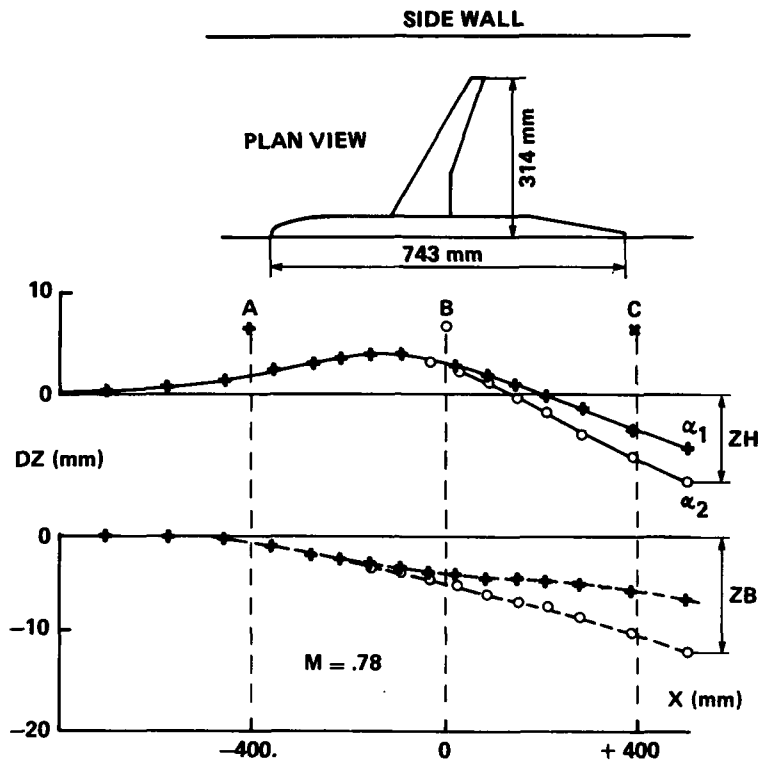

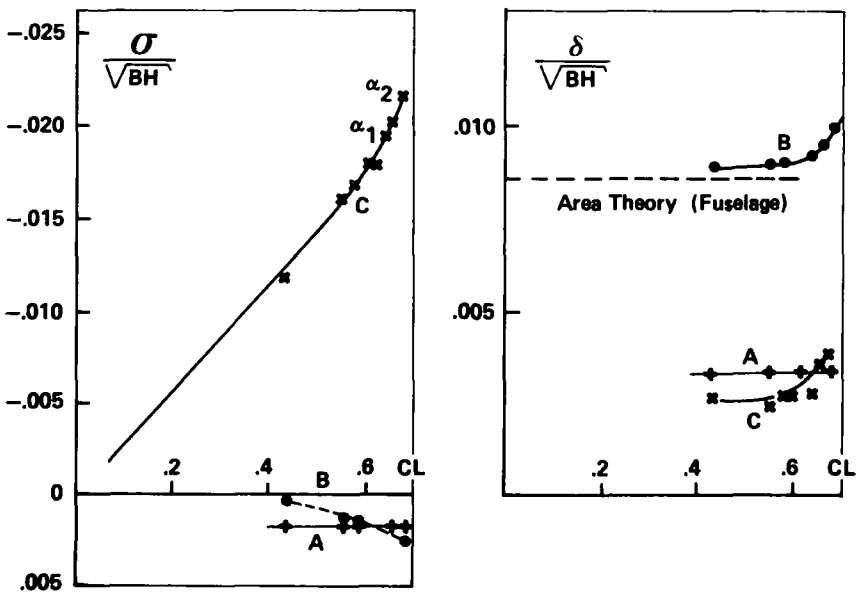

Fig. 5.2 Typical wall displacements for 2D adaptation (From: ONERA T2; 2s/B = 0.80)

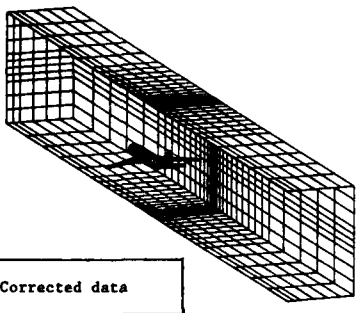

BLOCKAGE RATIO = .017
H*B*L = 2.0 * 1.6 * 5.0 m
2s/B = 0.69
SWEEP = 20 deg.
MACH = 0

	"Measured" data			Principal (residual) corr.			Corrected data		
Type*)	$\alpha°$	C_L	C_M	$\Delta u/U$	$\Delta\alpha°$	$\Delta\alpha°_H$	$\alpha°_c$	C_{L_c}	C_{M_c}
UF	-5.009	.0500	-.3206	--	--	--	-5.009	.0500	-.3206
OS	-5.000	.0500	-.3206	.0005	-.009	-.007	-5.009	.0499	-.3201
PA	-5.000	.0499	-.3203	.0003	-.009	-.009	-5.009	.0499	-.3200
PS	-5.000	.0511	-.3247	.0026	-.009	+.012	-5.009	.0502	-.3213
UF	.195	.5841	-.6154	--	--	--	.195	.5841	-.6154
OS	.000	.5869	-.6169	.0005	.196	.206	.196	.5861	-.6155
PA	.000	.5851	-.6161	.0001	.183	.194	.183	.5846	-.6150
PS	.000	.5963	-.6361	.0024	.204	.389	.204	.5875	-.6178
UF	5.400	1.1049	-.8604	--	--	--	5.400	1.1049	-.8604
OS	5.000	1.1097	-.8646	.0004	.401	.419	5.401	1.1083	-.8625
PA	5.000	1.1061	-.8633	.0001	.374	.396	5.374	1.1056	-.8616
PS	5.000	1.1265	-.8971	.0024	.415	.759	5.415	1.1100	-.8644

*) UF = unbounded flow
PA = predictive adaptation (continuous testing)
OS = one-step adaptation (step/pause)
PS = plane solid walls

Fig. 5.3 Numerical simulation of different procedures

6. Limits of adaptation, residual interferences

Editor: M. Mokry
Other contributors: J.C. Erickson, Jr., M.J. Goodyer, A. Mignosi, G.P. Russo,
J. Smith, E. Wedemeyer, and P.A. Newman (NASA/LaRC)

6.1 Adaptation vs. passive walls

The need to perform wind tunnel tests at high subsonic and transonic Mach numbers has led to an early recognition of the fact that conventional solid wall wind tunnels become choked and that wall interference corrections based on linearized theory diverge as the test speed approaches Mach number one. To overcome these difficulties new test section designs were investigated avoiding the detrimental influence of rigid walls. An obvious solution was the contouring of the test section walls which led to the early development of adaptive wall wind tunnels at the National Physical Laboratory in the late 1930's. Another solution, that also goes back to the late 1930's, was the development of test section walls with longitudinal slots.

The technical and operational simplicity of the slotted wall wind tunnel may have led to the decision to abandon the adaptive wall approach in the 1950's. Twenty years later, in the early 1970's, a renewed interest in adaptive walls arose. Test experience had uncovered certain deficiencies of ventilated wall test sections that will be discussed below. Most important for the revival of the adaptive wall wind tunnel was, however, that adaptation strategies could be used to determine the exact, interference free wall contour with the aid of high speed computers.

6.1.1 Ventilated walls

It has been known that the combined effect of solid and open wall elements can largely reduce wall interference, Ref.[6.1], and calculations of Wieselsberger in 1939, Ref.[6.2], had shown how wall interferences could be minimized, theoretically, by a suitable arrangement of longitudinal slots in the test section walls. Moreover, the configuration of slots was independent of the test section Mach number so that the same slotted wall test section could be used throughout the whole range of subsonic, transonic, and even low supersonic speeds. It was found later that at supersonic speeds perforated walls are better suited to cancel wave reflections, Ref.[6.3].

Under certain simplifying assumptions it can be shown that the flow over slotted walls is subject to the following boundary condition for the velocity potential ϕ:

$$\phi + K\frac{\partial\phi}{\partial n} = 0, \qquad (6.1)$$

where n is the coordinate along the outward normal of the wall surface. The *slot parameter* K depends on the number of slots and the open area ratio. The free jet boundary is represented by $K = 0$ and a solid wall by $K = \infty$. Since the wall interferences have opposite signs for free jet and solid wall test sections, it is obvious that they can be minimized for an intermediate value of K. Precisely, the wall induced upwash (v_w) or the blockage induced velocity (u_w) at the model station can be eliminated by a proper choice of K. Fortunately, for the K-value that eliminates the upwash interference the blockage interference becomes very small. Nevertheless, since only one parameter (K) can be adjusted, the elimination of wall interference is limited to only one component at only one station within the test section. For large models residual interferences must, therefore, be taken into account. Moreover, an estimate of the residual interferences is not simple. In principle, the conventional method of calculating wall interferences, representing the model by singularities, can be extended to wind tunnel walls that obey the boundary condition (6.1). It should be noted, however, that Eq.(6.1) is a simplified boundary condition, related to "ideal slotted wall" while the boundary condition for real walls is more complicated and probably nonlinear. Thus, using Eq.(6.1) introduces some uncertainty into the calculations.

The boundary condition for "ideal perforated wall" is

$$P\frac{\partial\phi}{\partial x} + \frac{\partial\phi}{\partial n} = 0, \qquad (6.2)$$

where x is the coordinate in the streamwise direction. The *porosity parameter* P depends on the geometry of the wall, notably the open area ratio, and on the local flow condition at the wall, Ref.[6.4]. The free jet boundary is represented by $P = \infty$ and a solid wall by $P = 0$. Again, since only one parameter (P) can be adjusted, the elimination of wall interferences is only partial. Evaluation of wall interferences based on Eq.(6.2) is unreliable; a true, universal boundary condition for perforated walls is not known.

More rigorous methods to calculate wall interference, which are discussed in Section 6.2, require the measurement of two variables over a control surface (two-variable method) or the measurement of of one flow variable and additional model data (one-variable method). Either method can be used to assess the residual wall interferences. However, in performing the required measurements, the operational simplicity - a great advantage of the passive wall wind tunnels - is lost. It should be remembered that, due to the inhomogeneity of the flow near a slotted or perforated wall, the required flow variables cannot be measured on the walls, which renders the assessment of residual interferences extremely cumbersome.

Other disadvantages of slotted and perforated test section walls are:

- the generation of aerodynamic noise and
- the drive power is increased by about 50% compared with a solid wall wind tunnel.

6.1.2 Adaptive walls

In contrast to passive (slotted or perforated) walls, adaptive walls allow, in principle, a complete elimination of wall interferences - at the expense of a more or less complicated and time consuming adaptation procedure.

For the case where the wall adaptation is achieved by a deformation of solid walls, the procedure is still relatively simple as the required flow variables on a control surface can be gained readily by measuring the wall pressure distribution and the wall displacement.

For two-dimensional flows the use of flexible plates as top and bottom walls offers itself as a simple solution. Three-dimensional adaptation of solid walls is not easy to

Table. 6.1 Summary of 'streamlined' data; NACA 0012-64 airfoil in the TSWT

Reference Number	Model Incidence (Deg)	Reference Mach Number (M_∞)	Model Performance			Residual Interferences(1)			Wall Loadings	
			C_L	C_D	C_M	α Error (Deg)	Camber Error (Deg)	C_p Error	E_T	E_B
1	0.5	0.4024	0.0326	-0.0126	-0.0083	0.0034	-0.0081	-0.0026	0.0040	0.0045
2	0.5	0.4985	0.0330	-0.0127	-0.0068	0.0135	0.0001	0.0022	0.0052	0.0055
3	0.5	0.6006	0.0344	-0.0124	-0.0071	0.0089	-0.0092	-0.0035	0.0096	0.0085
4	0.5	0.7035	0.0363	-0.0117	-0.0066	0.0104	0.0047	-0.0019	0.0034	0.0040
5	0.5	0.8052	0.0444	-0.0098	-0.0073	0.0014	0.0071	0.0026	0.0038	0.0034
6	2.0	0.4040	0.1577	-0.0121	-0.0359	0.0059	0.0049	-0.0042	0.0083	0.0091
7	2.0	0.5041	0.1655	-0.0122	-0.0362	0.0069	0.0035	-0.0066	0.0088	0.0082
8	2.0	0.6047	0.1688	-0.0120	-0.0352	0.0094	0.0124	-0.0041	0.0066	0.0068
9	2.0	0.7011	0.1802	-0.0112	-0.0336	0.0020	-0.0053	-0.0018	0.0047	0.0044
10	2.0	0.8040	0.2128	-0.0048	-0.0394	-0.0041	0.0093	-0.0066	0.0085	0.0077
11	4.0	0.4010	0.3392	-0.0080	-0.0766	0.0078	0.0083	-0.0012	0.0043	0.0053
12	4.0	0.5026	0.3534	-0.0088	-0.0778	0.0003	0.0189	-0.0034	0.0076	0.0076
13	4.0	0.6022	0.3719	-0.0100	-0.0778	-0.0059	0.0031	-0.0035	0.0068	0.0078
14	4.0	0.7019	0.4333	-0.0074	-0.0829	0.0026	0.0022	-0.0026	0.0072	0.0067
15	4.0	0.8022	0.3417	0.0127	-0.0613	-0.0115	-0.0227	-0.0003	0.0077	0.0059
16	6.0	0.4049	0.5120	0.0009	-0.1138	-0.0032	0.0110	-0.0049	0.0066	0.0049
17	6.0	0.5054	0.5323	-0.0034	-0.1140	0.0064	0.0230	-0.0027	0.0053	0.0061
18	6.0	0.6052	0.5697	-0.0003	-0.1132	-0.0003	0.0209	-0.0031	0.0058	0.0063
19	6.0	0.6998	0.6521	0.0153	-0.1309	0.0112	0.0307	0.0027	0.0042	0.0061
20	6.0	0.7981	0.3851	0.0379	-0.0720	-0.0047	-0.0018	-0.0044	0.0047	0.0050

Note: (1) Residual Interferences

α Error:- Wall-induced angle of incidence at the aerofoil leading edge.

Camber Error:- Wall-induced camber over the aerofoil chord

C_p Error:- Streamwise velocity error at the quarter chord point of the aerofoil expressed as an error in pressure coefficient.

Table. 6.2 Summary of 'straight wall' data; NACA 0012-64 airfoil in the TSWT

Reference Number	Model Incidence (Deg)	Reference Mach Number (M_∞)	Model Performance			Residual Interferences			Wall Loadings	
			C_L	C_D	C_M	α Error (Deg)	Camber Error (Deg)	C_p Error	E_T	E_B
1	0.5	0.4079	0.0372	-0.0131	-0.0093	-0.0096	-0.0533	-0.0458	0.0342	0.0368
2	0.5	0.5040	0.0391	-0.0130	-0.0076	-0.0080	-0.0371	-0.0493	0.0372	0.0371
3	0.5	0.6001	0.0387	-0.0118	-0.0072	-0.0124	-0.0378	-0.0548	0.0437	0.0430
4	2.0	0.4067	0.1851	-0.0122	-0.0442	-0.1103	-0.4125	-0.0494	0.0509	0.0273
5	2.0	0.5019	0.1959	-0.0117	-0.0450	-0.1150	-0.4158	-0.0480	0.0522	0.0282
6	2.0	0.6064	0.2070	-0.0117	-0.0454	-0.1179	-0.4384	-0.0581	0.0569	0.0320
7	4.0	0.4050	0.4050	-0.0076	-0.0958	-0.2692	-0.9404	-0.0555	0.0760	0.1710
8	4.0	0.4986	0.4334	-0.0082	-0.1030	-0.2766	-0.9849	-0.0578	0.0768	0.0237
9	4.0	0.6002	0.4656	-0.0086	-0.1000	-0.2981	-1.0388	-0.0681	0.0856	0.0264
10	4.0	0.7046	0.4541	0.0202	-0.0896	-0.4360	-1.0966	-0.1219	0.1251	0.0676
11	6.0	0.4044	0.6046	0.0022	-0.1395	-0.4028	-1.4520	-0.0640	0.1008	0.0226
12	6.0	0.5088	0.6580	-0.0031	-0.1470	-0.4385	-1.5397	-0.0692	0.1066	0.0249
13	6.0	0.6121	0.8327	0.0177	-0.1803	-0.6008	-1.9180	-0.1070	0.1482	0.0374
14	6.0	0.7092	0.6725	0.1334	-0.2015	-1.0695	-1.7473	-0.2929	0.3038	0.2105

achieve as it requires highly elastic material, like rubber, for the test section walls or a complicated construction as for the octagonal test section of the TU Berlin.

Finally, the use of test sections with two flexible walls for three-dimensional flows is a compromise, offering a very simple operation and "clean" solid walls at the expense of a somewhat imperfect wall adaptation. Compared with passive wall test sections, the two-dimensional wall adaptation is by far superior from the point of view of reduction of wall interferences, since both the downwash and blockage interferences are eliminated on a line rather than at a point. The residual interferences are, therefore, less severe. Moreover, they can be assessed easier and more accurately.

Performance of the solid wall test sections near sonic and supersonic speeds is somewhat less satisfactory, because of high sensitivity of flow to small changes of geometry of impermeable boundaries. Minor imperfections (waviness) of the walls produce large disturbances if the flow velocity is close to or above sonic. In spite of the fact that the near-sonic regions are not as extensive in the presence of a (large) model as they could possibly be in an empty test section, the adaptation is still adversely affected. If supersonic pockets extend to the wall, the linear adaptation procedure may fail. Also, in supersonic flow the absorption of shock waves would require a large curvature of the walls at the shock position. So far, very little experience has been accumulated with wall adaptation in supersonic flows.

For adaptive test sections utilising suction or blowing through ventilated walls, the wall adaptation is possible throughout the range of subsonic, transonic, and supersonic speeds. The ventilated adaptive walls share, of course, the disadvantage of partially open walls. The inhomogeneity of the flow near the wall necessitates the cumbersome measurement of the flow variables on a control surface inside the flow.

6.1.3 Concluding remarks

A more detailed comparison of the performance of adaptive walls and passive walls is possible when the flow quality and data accuracy requirements are specified. In many cases a conventional (slotted or perforated) wall test section may fulfil the requirements. However, in order to produce interference free data, a passive wall test section would have to be much larger and, therefore, much costlier to run than an adaptive one. The testing time of adaptive wall tunnels can be reduced - by using rational adaptation procedures - to nearly the testing times of conventional tunnels (see Chapter 5). If this is indeed the case, then the adaptive wall tunnel has definite advantages: high flow quality, low drive power, and low residual interferences, which can easily be assessed.

Although the adaptive wall wind tunnel was intended, originally, for transonic testing, it has found important applications in the low speed range. For testing of automobiles in adaptive wall test sections blockage ratios of 30% are acceptable whereas in conventional test sections the blockage ratio is limited to about 3%, see Section 3.3.2 and Fig.3.11 of this report for details.

Neither solid walls nor slotted walls are suitable for a complete absorption of shock waves. For the present, there is no simple substitute for the perforated wall test sections at supersonic speeds.

6.2 Residual interferences

Because of a finite number of wall control devices (jacks, plenum compartments), limited number of instrument readings and the approximation character of adaptation algorithms, the unconfined flow conditions are not expected to be precisely attained even in the 'fully' adapted stage, Refs.[6.5]-[6.7]. The quality of wall adaptation can be judged by:

i) global criteria, such as the mean modulus of wall loading for flexible walls, or
ii) residual interferences at representative model locations.

The discrete values of wall loading at the pressure orifice locations are estimated as the difference of the interior (measured) and exterior (computed) pressure coefficients at the pressure orifice locations. Residual interference can be calculated from wall loading or alternate flow variables along control surfaces (interfaces) at or near test section boundaries.

Table 6.1 contains typical examples of the above measures obtained from 20 tests on section NACA 0012-64 of 4-inch chord in the Transonic Self-streamlining Wind Tunnel (TSWT) in Southampton. The angles of attack vary up to 6 degrees and the Mach numbers up to 0.8; the flexible walls are subcritical (Group 1 flow). The mean moduli of top and bottom wall loadings are denoted by the symbols E_T and E_B respectively. Residual interferences are calculated from the loadings in terms of:

a) angle of attack error at the wing leading edge,
b) induced camber, which is assumed to be the difference between the flow angles at the leading and trailing edges, and
c) disturbance to free stream velocity at the wing quarter-chord, converted to C_p.

The E-values, all below 0.01, may be compared with those in Table 6.2, which refer to the same model and tunnel but straight walls, and range between about 0.02 and 0.3. In some straight-wall cases one of the walls was supercritical, but not both, as without streamlining the Mach number could not be increased any further (explanation of missing data in higher Mach number range).

Table 6.3 shows data taken on the same model under conditions where, even with the walls streamlined, both flexible walls are supercritical (Group 2 flow) and the supercritical zones, at some test conditions, extend substantial distances into the imaginary flowfields. The sample of the results in Table 6.3 is one of the first ones reported for this flow regime [6.8]; the quality of streamlining is nevertheless good up to about $M = 0.95$.

A more detailed assessment of wall adaptation can be based on the spatial distribution of residual interference in the vicinity of the model. Figure 6.1 refers to a 2D airfoil test in the TSWT facility with straight and streamlined walls, and shows wall-induced velocity perturbations several chords up- and down-stream, evaluated by the two-variable method, Ref.[6.9]. The reduction of wall effects achieved by streamlining is impressive. In this context the term *residual interference* is certainly appropriate.

Similar reduction of wall interference on half-model tests, achieved by 2D wall adaptation in the T2 and TSWT facilities, is shown in Figs.4.22 and 4.25 respectively.

Table. 6.3 Summary of 'streamlined' data; mixed flow in imaginary flowfields

ORIGINAL FLEXIBLE WALLS (SEPT. 1984)

Reference Number	Nominal Mach Number	Model Incidence (Deg)	Reference Mach Number (M_∞)	Model Performance			Wall Loadings		
				C_N	C_C	C_M	E_T	E_B	E_{av}
1	0.87	4.0	0.8658	0.1159	0.0379	0.0461	0.0083	0.0155	0.0119
2	0.90	4.0	0.8997	0.1761	0.0535	0.0185	0.0155	0.0117	0.0136
3(1)	0.90	4.0	0.9062	0.1953	0.0549	0.0052	0.0139	0.0082	0.0110
4	0.92	4.0	0.9257	0.3987	0.0785	-0.1635	0.0161	0.0069	0.0115
5(1)	0.92	4.0	0.9228	0.3788	0.0759	-0.1420	0.0120	0.0055	0.0087
6	0.94	4.0	0.9434	0.3617	0.0752	-0.1388	0.0190	0.0172	0.0181
7(1)	0.94	4.0	0.9417	0.3815	0.0759	-0.1511	0.0136	0.0123	0.0129
8(1)	0.95	4.0	0.9543	0.3882	0.0777	-0.1640	0.0152	0.0129	0.0140
9(1)	0.96	4.0	0.9638	0.3617	0.0740	-0.1387	0.0170	0.0170	0.0170
10(1)	0.97	4.0	0.9721	0.3828	0.0761	-0.1630	0.0166	0.0153	0.0159

Note: (1) The effective aerodynamic contour used in the imaginary flowfield computations includes an allowance for the variations of δ^* caused by the presence of the model.

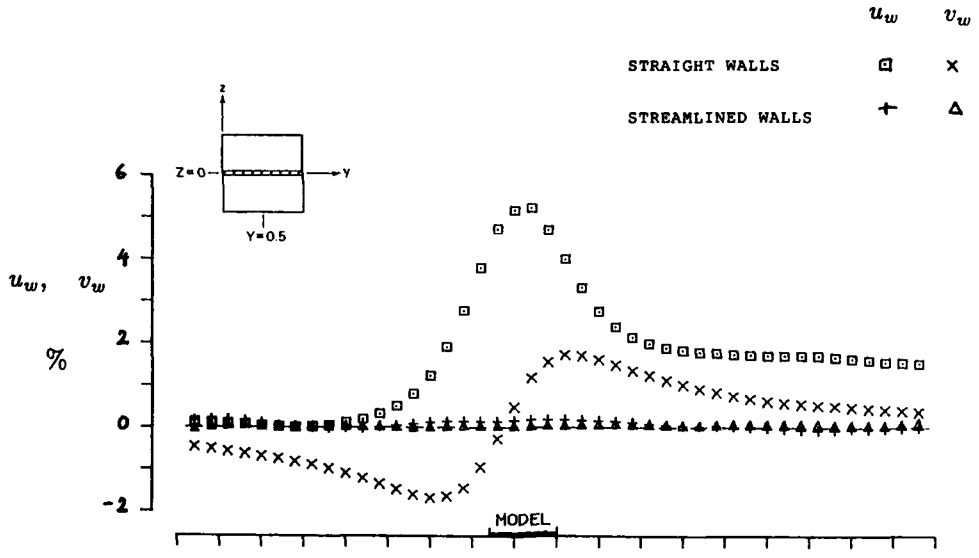

Fig. 6.1 Wall-induced velocity perturbations at tunnel centreline, evaluated by two-variable method for NACA 0012-64 airfoil in the TSWT, $M = 0.60$, $\alpha = 4.0°$.

6.2.1 Linear flow

The procedures for the evaluation of residual wall interference in Group 1 flows are essentially the same as those used for assessing the corrections in conventional, non-adaptive wind tunnels [6.10]. The present review is a shorter version of that given in Ref.[6.11].

Depending upon the number of flow variables utilised, we speak of *one-* or *two-variable* methods [6.12]; in two dimensions also of *Schwarz-* or *Cauchy-type* methods [6.13].

The one-variable methods use the measured static pressure distribution at the test section boundary and supplement it with the far field representation of the model, estimated from its geometry and measured forces.

The two-variable methods use measurements of static pressure and normal velocity at the test section boundary, but do not require any model representation. This is clearly of an advantage for adaptive wall test sections, which are often relatively small with respect to the test model, and for the variety of complex flows commonly encountered in

wind tunnel testing. For test sections with flexible walls the normal component of velocity is given by the shape of the wall, adjusted for the boundary-layer displacement thickness. For ventilated test section walls the flow direction can be measured by the Calspan Pipes, Laser Doppler Velocimetry, or other appropriate techniques.

The *interface discontinuity method*, also described, is a 'genuine' residual interference assessment technique. It is specific to adaptive wall wind tunnels, where the computation results for the fictitious flow in the exterior of the test section are provided.

Since the adaptive walls introduce only minor disturbances to the unconfined far field of the test model, the linearisation of the potential equation near the walls is applicable as long as the flow remains subcritical there.

The governing equation for the disturbance velocity potential is

$$\beta^2 \frac{\partial^2 \phi}{\partial x^2} + \frac{\partial^2 \phi}{\partial y^2} + \frac{\partial^2 \phi}{\partial z^2} = 0, \qquad (6.3)$$

where $\beta = \sqrt{1 - M^2}$ and $M < 1$ is the stream Mach number. For simplicity, the disturbance velocity potential ϕ is normalised by stream velocity.

The scaling of the streamwise coordinate,

$$x' = \frac{x}{\beta}, \qquad (6.4)$$

reduces Eq.(6.3) to Laplace's equation, $\nabla^2 \phi = 0$.

The linear flow region where ϕ satisfies Eq.(6.3) is shown schematically in Fig.6.2a. It excludes the volume occupied by the test model, its viscous and transonic flow regions, and the wind tunnel exterior, where no real flow exists. The outer bounding surface, enclosing the test model, is expected to lie entirely within the linear flow region, off the viscous or nonisentropic flow at the walls.

Using the principle of linear superposition, the disturbance velocity potential is split as [6.14]

$$\phi = \phi_m + \phi_w, \qquad (6.5)$$

where ϕ_m is that due to the model in free air and ϕ_w is that due to wall interference.

The model potential, ϕ_m, satisfies Eq.(6.3) in the infinite space outside the model and the adjacent nonlinear flow regions, Fig.6.2b.

The wall interference potential, ϕ_w, is assumed to satisfy Eq.(6.3) in the entire test section interior, including the model and its nonlinear flow regions, as indicated in Fig.6.2c.

This assignment of the singular and nonsingular parts as the effects of the model and the walls respectively is consistent with the concept of Green's function for the Laplace operator. Accordingly, it is rigorous for an infinitesimal model, but only approximate for a finite-size model. The consideration of the coupled nature of interference between the walls and the finite-size model indicates that the wall interference potential may also have singularities inside the model.

The derivatives of ϕ_w are interpreted as disturbances to stream velocity components. They are usually evaluated at the model reference station or as averages over the model and interpreted as *global corrections* to stream Mach number [6.15]

$$\Delta M = (1 + \frac{\gamma - 1}{2} M^2) M \frac{\partial \phi_w}{\partial x}, \qquad (6.6)$$

and to flow angles (in radians)

$$\Delta \alpha_y = \frac{\partial \phi_w}{\partial y} \quad \text{and} \quad \Delta \alpha_z = \frac{\partial \phi_w}{\partial z}. \qquad (6.7)$$

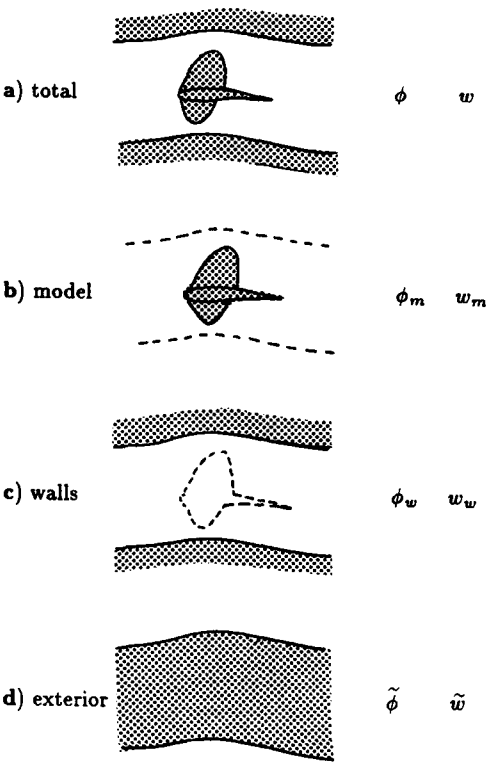

Fig. 6.2 Linear regions for Group 1 flows (from [6.11]).

From the spatial variations of these corrections over the model additional streamline curvature and buoyancy effects on model force data can be determined.

The evaluation of the *local corrections* to model surface pressure coefficient or Mach number is an approach more rigorous, but of course less practical from the point of view of the interpretation of the wind tunnel data in terms of free flight conditions. Unlike the conventional, passive walls, the adaptive walls can in principle be adjusted to minimize the wall induced velocity gradients to render the test data *correctable* in terms of the global corrections to stream parameters even in very extreme conditions (large models with respect to the test section size, high-angle-of-attack tests, etc.).

In connection with adaptive wall wind tunnels, another type of the disturbance velocity potential is of importance: that corresponding to the 'fictitious' flow outside the wind tunnel. The potential, denoted here by the symbol $\tilde{\phi}$, satisfies Eq.(6.3) in the exterior of the outer bounding surface, Fig.6.2d. The surface, separating the real wind tunnel flow and the computed exterior flow is often termed the *interface*. The aim of adaptation is to adjust the walls in such a way that ϕ and $\tilde{\phi}$ constitute a single potential ϕ_m, continuous at the interface. For an imperfect adaptation, there is a direct relationship between ϕ_w and the difference $\phi - \tilde{\phi}$ at the interface.

One-variable method

The method, due to Capelier, Chevallier and Bouniol [6.16], is the most popular technique for post-test assessment of subsonic wall interference in wind tunnels with perforated walls. It retains the essential features of the classical wall interference approach [6.14], but replaces the idealised wind tunnel boundary conditions (6.1) and (6.2) by the linearized "pressure" boundary condition

$$\frac{\partial \phi}{\partial x} = -\frac{1}{2} C_p. \tag{6.8}$$

where C_p is the measured boundary pressure coefficient. The control surface along which the pressure is measured is required to be some distance away from the walls, where the disturbances from the individual holes (perforations) are sufficiently smeared out.

The axial component of wall interference velocity,

$$u_w = \frac{\partial \phi_w}{\partial x}, \tag{6.9}$$

satisfying inside the test section

$$\beta^2 \frac{\partial^2 u_w}{\partial x^2} + \frac{\partial^2 u_w}{\partial y^2} + \frac{\partial^2 u_w}{\partial z^2} = 0, \tag{6.10}$$

is obtained from the corresponding boundary values

$$u_w = -\frac{1}{2} C_p - \frac{\partial \phi_m}{\partial x} \tag{6.11}$$

as a solution of the interior *Dirichlet problem*. The transverse velocity components,

$$v_w = \frac{\partial \phi_w}{\partial y} \quad \text{and} \quad w_w = \frac{\partial \phi_w}{\partial z}, \tag{6.12}$$

can be obtained from u_w by integrating the irrotational-flow conditions

$$\frac{\partial v_w}{\partial x} = \frac{\partial u_w}{\partial y} \quad \text{and} \quad \frac{\partial w_w}{\partial x} = \frac{\partial u_w}{\partial z} \tag{6.13}$$

along a path from the upstream end of the test section.

The Dirichlet problem for Laplace's equation is one of the best explored problems in mathematical physics and there are a large number of methods available to solve it numerically. A natural approach is to solve the problem in terms of the double layer potential [6.17], leading to a doublet panel method [6.18]. For simpler geometries, closed form solutions are obtainable using integral transforms [6.16] or the Fourier method [6.19]-[6.21].

The complex-variable treatment [6.16] of the 2D problem leads, as pointed out in Ref.[6.13], to the *Schwarz problem*, consisting of determining an analytic function inside a domain from its defined real part on the boundary. Theory [6.22] shows that the integration of Cauchy-Riemann equations (irrotational-flow conditions) introduces an unknown imaginary constant that needs to be specified in order to make the solution unique (specification of the upstream flow angle).

The accuracy of the one-variable method depends greatly on the accuracy with which the free air potential ϕ_m can be predicted on the control surfaces [6.23],[6.24]. Details of a transonic model representation for 2D tests are described in Refs.[6.25]-[6.28]. Since the far field of ϕ_m is normally evaluated using the measured model data subject to wall interference, the prediction tends to be more exact near a fully adapted stage. However, when compared to the size of the model, the adaptive wind tunnels have typically a smaller cross-section than the conventional ones, so that the representation of flow near the walls as a model far field may still be inaccurate.

Another source of inaccuracy, which is common to all residual interference methods based on boundary measurements, is the finite length of the test section and sparseness of the experimental pressure data. The boundary values of u_w have to be interpolated or extrapolated over a complete boundary (closed or infinite), in order to make the Dirichlet problem soluble. The adaptive test sections, which are typically longer than the conventional ones, will have a slight advantage in this regard.

The method can be used to monitor the reduction of wall interference corrections in the course of adaptation, but can also be incorporated into the adaptation algorithm [6.29]. The necessary condition for flow to be interference-free (unconfined) is that the boundary values of u_w vanish:

$$u_w \equiv 0 \quad \text{on} \quad S. \tag{6.14}$$

Compensation for errors of the reference velocity or pressure [6.16], also called the *autocorrective property* [6.24] or *autoconvergence* [6.30], is an important feature of the method. It applies within the limits of linearization and may be stated as follows: if the error of the (upstream) reference velocity U is δU, then the perturbation velocities measured on the boundary will be offset by $-\delta U$. Since $-\delta U/U$ = constant is also a solution of Eq.(6.10), the incremental correction, being of equal magnitude but opposite sign to the reference velocity error, restores U as the reference velocity.

Besides compensating for genuine reference velocity errors, the autocorrective principle also establishes the correspondence between U based on plenum pressure and actual stream velocity in ventilated test sections.

Two-variable method

Measurement of the static pressure and normal velocity distributions along the control surface, which is prerequisite for wall adaptation, opens the possibility of evaluating subsonic wall interference without model representation. Incidentally, this feature also allows to account for the presence of the strut/support system, but only as far as the indirect, wall induced effect on the model is concerned. The direct strut/support effect on the model cannot be extracted from the far field measurements only.

The two-variable method is most easily applied to solid wall test sections where the walls or, more accurately, their boundary-layer displaced stream surfaces can serve as control surfaces. The first successful evaluation of the 2-D interference flow field from two flow variables measured at the control surface was reported by Lo [6.31]. Both numerical demonstration and experimental verification are given in the same paper. The method uses the Fourier transform solution [6.32] for linearized subsonic flow past a nonlifting airfoil. A more straightforward Cauchy's integral approach to the two-variable method was subsequently described by Kraft and Dahm [6.33], Smith [6.13], and Amecke [6.34]. An extension to 3-D flows, based on Green's theorem, is due to Ashill and Weeks [6.9].

To describe the method, we introduce the position vectors of an interior point and a boundary point,

$$\mathbf{r}_0 = (x_0', y_0, z_0) \quad \text{and} \quad \mathbf{r} = (x', y, z). \tag{6.15}$$

Further, denote by

$$G(\mathbf{r}_0, \mathbf{r}) = -\frac{1}{4\pi |\mathbf{r}_0 - \mathbf{r}|} \tag{6.16}$$

the fundamental solution (unit-strength source), satisfying

$$\nabla^2 G(\mathbf{r}_0,\mathbf{r}) = \delta(\mathbf{r}_0 - \mathbf{r}), \tag{6.17}$$

where δ is the 3D Dirac delta function.

Green's second identity gives for a function ϕ_w harmonic in the test section interior

$$\phi_w(\mathbf{r}_0) = \iint_S [\phi_w(\mathbf{r}) \frac{\partial G(\mathbf{r}_0,\mathbf{r})}{\partial n} - G(\mathbf{r}_0,\mathbf{r}) \frac{\partial \phi_w(\mathbf{r})}{\partial n}] dS$$

and for a function ϕ_m harmonic in the test section exterior

$$0 = \iint_S [\phi_m(\mathbf{r}) \frac{\partial G(\mathbf{r}_0,\mathbf{r})}{\partial n} - G(\mathbf{r}_0,\mathbf{r}) \frac{\partial \phi_m(\mathbf{r})}{\partial n}] dS.$$

The differential and integral operations are taken with respect to the unsubscripted coordinates; S is the control surface (interface) enclosing the test section interior, and $\partial/\partial n$ is the derivative along the outward normal with respect to the test section interior. As indicated in Fig.6.2, ϕ_m and ϕ_w are identified as the velocity disturbance potentials due to the model and walls respectively.

Adding the above formulae and eliminating ϕ_m from Eq.(6.5), we obtain the correction formula of Ashill and Weeks [6.9]:

$$\phi_w(\mathbf{r}_0) = \iint_S [\phi(\mathbf{r}) \frac{\partial G(\mathbf{r}_0,\mathbf{r})}{\partial n} - G(\mathbf{r}_0,\mathbf{r}) \frac{\partial \phi(\mathbf{r})}{\partial n}] dS. \tag{6.18}$$

It expresses the interior value of the wall interference potential in terms of the boundary values of the (total) disturbance velocity potential.

Physically, integral (6.18) can be interpreted as a surface distribution of doublets

$$\frac{\partial G(\mathbf{r}_0,\mathbf{r})}{\partial n} \qquad \text{with the density} \qquad \phi(\mathbf{r})$$

and a surface distribution of sources

$$G(\mathbf{r}_0,\mathbf{r}) \qquad \text{with the density} \qquad -\frac{\partial \phi(\mathbf{r})}{\partial n}.$$

The normal component of disturbance velocity $\partial\phi/\partial n$ can be measured directly. The potential ϕ, on the other hand, is evaluated by the streamwise integration of the measured pressure coefficient, Eq.(6.8).

As indicated in Ref.[6.35], for a cylindrical test section (walls parallel to the x-axis), an integration by parts in Eq.(6.18) converts the surface distribution of doublets into a surface distribution of horseshoe vortices

$$\Omega(\mathbf{r}_0,\mathbf{r}) = \int_{x'}^{\infty} \frac{\partial G(\mathbf{r}_0,\mathbf{r})}{\partial n} dx' \tag{6.19}$$

with the density

$$\frac{\partial \phi(\mathbf{r})}{\partial x'} = -\frac{\beta}{2} C_p(\mathbf{r})$$

that can be measured directly. The isolated integration terms vanish by the virtue of

$$\Omega(\mathbf{r}_0,\mathbf{r}) \to 0 \quad \text{as} \quad x' \to \infty$$

and assuming

$$\phi(\mathbf{r}) \to 0 \quad \text{as} \quad x' \to -\infty.$$

The *autocorrective property* applies [6.24] and is easy to verify. Denoting once again by δU the error of the reference velocity, the boundary values of the disturbance velocity potential ϕ will be subject to the (systematic) error

$$\delta\phi(\mathbf{r}) = -\frac{\delta U}{U} x.$$

The corresponding increment $\delta\phi_w$ of the wall interference potential is obtained by substitution $\delta\phi \to \phi$ in Eq.(6.18). Transforming the surface integral into the volume integral by Green's second identity, using Eq.(6.17) and the fact that $\delta\phi$ satisfies Laplace's equation in the entire test section volume V, it follows

$$\begin{aligned}\delta\phi_w(\mathbf{r}_0) &= \iiint_V [\delta\phi(\mathbf{r}) \nabla^2 G(\mathbf{r}_0,\mathbf{r}) - G(\mathbf{r}_0,\mathbf{r}) \nabla^2 \delta\phi(\mathbf{r})] dV \\ &= \delta\phi(\mathbf{r}_0),\end{aligned}$$

which was to be proved.

Taking in Eq.(6.18) the limit as $\mathbf{r}_0$ becomes a point of a smooth surface element, we obtain

$$\begin{aligned}\phi_w(\mathbf{r}_0) &= \frac{1}{2}\phi(\mathbf{r}_0) \\ &\quad + \iint_S [\phi(\mathbf{r}) \frac{\partial G(\mathbf{r}_0,\mathbf{r})}{\partial n} - G(\mathbf{r}_0,\mathbf{r}) \frac{\partial \phi(\mathbf{r})}{\partial n}] dS, \ \mathbf{r}_0 \in S.\end{aligned} \tag{6.20}$$

The integral is to be interpreted as a principal value in the sense that a small circular neighbourhood of the (singular) point $\mathbf{r}_0$ is removed from the surface S for the doublet integral; its contribution has already been accounted for by the isolated term $\frac{1}{2}\phi(\mathbf{r}_0)$. There is no ambiguity concerning the source integral, as the contribution of a small circular element around the point $\mathbf{r}_0$ is zero.

The 3D *single-step convergence formula* [6.36] is obtained by substituting of Eq.(6.20) in Eq.(6.5):

$$\begin{aligned}\phi_m(\mathbf{r}_0) &= \frac{1}{2}\phi(\mathbf{r}_0) \\ &\quad - \iint_S [\phi(\mathbf{r}) \frac{\partial G(\mathbf{r}_0,\mathbf{r})}{\partial n} - G(\mathbf{r}_0,\mathbf{r}) \frac{\partial \phi(\mathbf{r})}{\partial n}] dS, \ \mathbf{r}_0 \in S.\end{aligned} \tag{6.21}$$

This formula determines the boundary value of the free air potential, ϕ_m, from the measured boundary values of ϕ and $\partial\phi/\partial n$. Provided that the differences between the boundary values of ϕ and ϕ_m are small, it may be possible to achieve $\phi = \phi_m$ in a single adjustment of the walls.

Alternative formulations of the correction method based on Green's theorem are given in Refs.[6.37] and [6.38], comparisons and accuracy aspects are discussed in Ref.[6.39]. Model representation, as shown above, is no longer required, but the sparseness of boundary data and incomplete test section boundary remain as a major source of inaccuracy.

The specification of *interference-free conditions* in the two-variable method is straightforward. Setting $\phi_w = 0$ in Eq.(6.20) or $\phi_m = \phi$ in Eq.(6.21), we obtain

$$\begin{aligned}\frac{1}{2}\phi(\mathbf{r}_0) = -\iint_S [\phi(\mathbf{r}) \frac{\partial G(\mathbf{r}_0,\mathbf{r})}{\partial n} - G(\mathbf{r}_0,\mathbf{r}) \frac{\partial \phi(\mathbf{r})}{\partial n}] dS, \\ \mathbf{r}_0 \in S.\end{aligned} \tag{6.22}$$

which interrelates the values of ϕ and $\partial\phi/\partial n$ on the bounding surface of an adapted test section.

The 2D versions of the above formulae are obtained by substituting

$$\mathbf{r}_0 = (x_0', y_0), \quad \mathbf{r} = (x', y), \quad G(\mathbf{r}_0,\mathbf{r}) = \frac{1}{2\pi} \ln|\mathbf{r}_0 - \mathbf{r}|,$$

and replacing the surface integrals by contour integrals.

More readily applicable results are obtained using Cauchy's integral formula but, of course, both Green and Cauchy formulations are equivalent. To illustrate the latter approach, we introduce the complex coordinate

$$z = x' + iy = \frac{x}{\beta} + iy \tag{6.23}$$

and the complex disturbance velocity

$$w(z) = \beta u(x,y) - iv(x,y) = \beta\frac{\partial\phi}{\partial x}(x,y) - i\frac{\partial\phi}{\partial y}(x,y). \tag{6.24}$$

In accordance with Eq.(6.5), the complex disturbance velocity is decomposed as

$$w(z) = w_m(z) + w_w(z), \tag{6.25}$$

where w_w is analytic in the test section interior and w_m is analytic in the test section exterior. Applying the Cauchy integral formula to a counterclockwise oriented contour C, we obtain for an interior point z_0

$$w_w(z_0) = \frac{1}{2\pi i}\int_C \frac{w_w(z)}{z - z_0}dz$$

and

$$0 = \frac{1}{2\pi i}\int_C \frac{w_m(z)}{z - z_0}dz.$$

Adding the integrals and eliminating w_m from Eq.(6.25), we obtain the correction formula of Smith [6.13]:

$$w_w(z_0) = \frac{1}{2\pi i}\int_C \frac{w(z)}{z - z_0}dz, \tag{6.26}$$

expressing the wall interference velocity in terms of boundary values of the (total) disturbance velocity.

Using Eq.(6.24), the components of the wall interference velocity are obtained as:

$$\begin{aligned} u_w(x_0,y_0) &= \frac{1}{\beta}\mathrm{Re}\{w_w(z_0)\}, \\ v_w(x_0,y_0) &= -\mathrm{Im}\{w_w(z_0)\}. \end{aligned} \tag{6.27}$$

An example of wall pressures and deflections from the tests [6.40] of the 9-in chord CAST 10-2/DOA 2 airfoil in the 13-in by 13-in flexible-wall test section of the of the Langley Transonic Cryogenic Wind Tunnel (TCT) is shown in Fig.6.3. The wall pressure distribution at the stream Mach number of 0.700 is well below the critical value ($Cp^* = -0.779$). The downstream end of the integration contour was placed so as to eliminate the three most downstream pressure points which, because of diffuser influence, diverge from the undisturbed flow level. The distribution of residual corrections along the wind tunnel axis, evaluated by the two-variable method, is shown by solid lines in Fig.6.4. The flow in the test section is not interference free, but considering the size of the model with respect to the test section, the corrections are certainly small.

The broken lines in Fig.6.4 are the corrections corresponding to the stream Mach number arbitrarily decreased from 0.700 to 0.695. The input pressure coefficients in Fig.6.3 were adjusted accordingly. We note that the resultant Mach number correction curve, corresponding to $M = 0.695$ is displaced approximately by 0.005 in the positive direction, confirming the validity of the autocorrective principle. The angle of attack correction, as expected, is not greatly affected by the change of the reference Mach number.

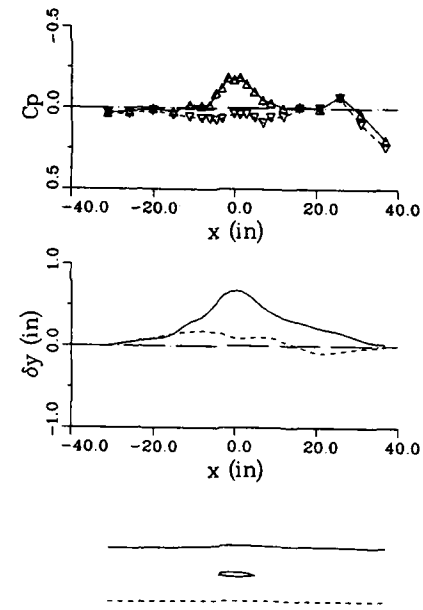

Fig. 6.3 Wall pressure coefficients and deflections; 9-in chord CAST 10 airfoil in the 13-in × 13-in test section of NASA TCT, $M = 0.70$, $\alpha = 1.20°$, $C_N = 0.50$, $Re_c = 30 \times 10^6$.

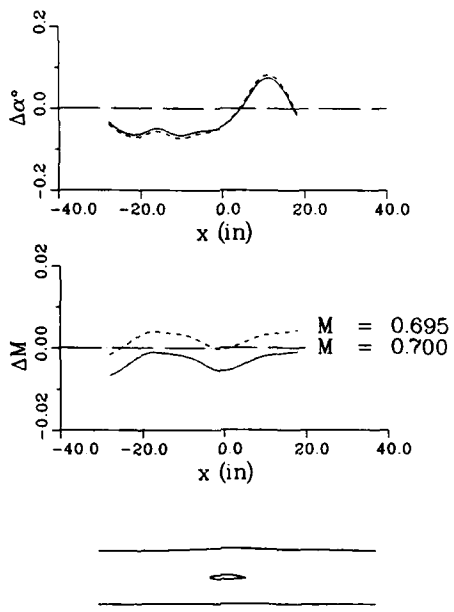

Fig. 6.4 Residual corrections along test section axis, evaluated by two-variable method from data of Fig.6.3.

The two-variable correction method is also applicable to test data from adaptive test sections with ventilated walls, provided that the two components of velocity on a control surface are known. For example, in the NASA/Ames Research Center 2 × 2 ft wind tunnel a fast-scanning laser velocimeter is used to measure two components of flow velocity along a rectangular contour surrounding the model. Wall adjustments are determined from an influence matrix that describes the effect of pressure changes in plenum compartments on the velocities along the contour.

Again, the wall adaptation procedure was found to reduce wall interference significantly, but not below the levels that could be ignored [6.41]. Data for the test case of a NACA 0012 airfoil at $M = 0.7$, $\alpha = 2°$ are presented in Figs.6.5-6.7. Figure 6.5 compares the measured and theoretical streamwise velocity distributions along the control contour 1.5 chords above and below the tunnel centerline, before and after the walls were adjusted. The wall adjustments dramatically reduce differences between theory and experiment. Figure 6.6 is a similar comparison of normal velocities. The residual corrections along the tunnel centerline, evaluated using a linear two-variable method, are shown in Fig.6.7. Although the wall adjustment essentially eliminated blockage interference, the residual angle of attack correction remained large.

More detailed two-variable correction formulae for 2D testing, together with evaluated residual interferences for the adaptive wall facilities T2 of ONERA/CERT and TU Berlin can be found in Ref.[6.34].

The Cauchy-type integral (6.26) can be written as

$$w_w(z_0) = \int_C \left[\frac{i\gamma(z)}{2\pi(z_0 - z)} + \frac{\sigma(z)}{2\pi(z_0 - z)}\right] ds, \qquad (6.28)$$

where $ds = |dz|$ is the counterclockwise oriented contour length element. In this form it represents a line distribution of vortices with the density

$$\gamma(z) = \mathrm{Re}\left\{ w(z)\frac{dz}{|dz|} \right\} = q_t(z) \qquad (6.29)$$

and a line distribution of sources with the density

$$\sigma(z) = -\mathrm{Im}\left\{ w(z)\frac{dz}{|dz|} \right\} = -q_n(z), \qquad (6.30)$$

where q_t is the tangential component of disturbance velocity (positive in the counterclockwise direction) and q_n is the normal component of disturbance velocity (positive in the direction of the outward normal).

Correction formula (6.26) is closely related to wall adaptation criteria for 2D testing. In the limiting process as z_0 becomes a point on a smooth segment of the contour C, we obtain

$$w_w(z_0) = \frac{1}{2}w(z_0) + \frac{1}{2\pi i}\int_C \frac{w(z)}{z - z_0}dz, \quad z_0 \in C, \quad (6.31)$$

where the (singular) integral is to be interpreted as Cauchy's principal value.

Substituting Eq.(6.31) in (6.25), we find the 2D *single-step convergence formula*

$$w_m(z_0) = \frac{1}{2}w(z_0) - \frac{1}{2\pi i}\int_C \frac{w(z)}{z - z_0}dz, \quad z_0 \in C, \quad (6.32)$$

which determines the boundary value w_m of the complex disturbance velocity due to the model in free air, in terms of the measured values w. The special case of straight line boundaries can be found in Refs.[6.32] and [6.33].

Setting $w_w = 0$ in Eq.(6.31) or $w_m = w$ in Eq.(6.32), we obtain the *interference-free condition*

$$\frac{1}{2}w(z_0) = -\frac{1}{2\pi i}\int_C \frac{w(z)}{z - z_0}dz, \quad z_0 \in C \qquad (6.33)$$

in terms of the complex disturbance velocity on the boundary. The factor $\frac{1}{2}$ was left uncancelled, to emphasize the connection with the 3D condition, Eq.(6.22).

Considering straight line boundaries at $y = \pm\frac{h}{2}$, we obtain in terms of disturbance velocity components

$$u(x_0, \pm\frac{h}{2}) = \mp\frac{1}{\beta\pi}\int_{-\infty}^{\infty} \frac{v(x, \pm\frac{h}{2})}{x - x_0}dx, \qquad (6.34a)$$

$$v(x_0, \pm\frac{h}{2}) = \pm\frac{\beta}{\pi}\int_{-\infty}^{\infty} \frac{u(x, \pm\frac{h}{2})}{x - x_0}dx. \qquad (6.34b)$$

These 'compressible-flow' versions of Hilbert's transforms, introduced by Sears [6.5] as *functional relationships* between two velocity components, define unconfined flow in a 2D test section. We may note that in this particular case the upper and lower boundary values are independent of one another (decoupling of infinite exterior regions). It is also important to remember that Eqs.(6.34) constitute a transform pair, so that the enforcement of either one ensures interference-free flow.

Interface discontinuity method

This residual interference method, utilizing computations of the fictitious flow in the test section exterior, is a version of the two-variable method,

The general idea, as proposed by Sears and Erickson [6.42] is essentially this: the flow field is considered to consist of an experimental inner region joined at an interface to a computed outer region. If the computed outer flow satisfies the unconfined flow conditions and matches along the interface the inner flow, then the combined flow field is continuous, representing unconfined flow around the model. The matching error, or discontinuity, provides a measure of the residual interference. It can be quantified by removing the discontinuity by a surface distribution of singularities. These singularities do not influence the far field in the outer region, but do introduce velocity perturbations at the position of the test model, which then can be interpreted as the usual wall interference corrections.

As for the two-component method, Green's theorem will give us a guidance to the appropriate singularities and their densities.

Considering the disturbance velocity potential $\tilde{\phi}$ of the fictitious flow in the exterior region, satisfying the far field boundary condition

$$\nabla\tilde{\phi}(\mathbf{r}) \to 0 \quad \text{as} \quad |\mathbf{r}| \to \infty,$$

then for an interior point $\mathbf{r}_0$ it follows

$$0 = \iint_S [\tilde{\phi}(\mathbf{r})\frac{\partial G(\mathbf{r}_0, \mathbf{r})}{\partial n} - G(\mathbf{r}_0, \mathbf{r})\frac{\partial\tilde{\phi}(\mathbf{r})}{\partial n}]dS.$$

Subtracting it from Eq.(6.18), we obtain the interior value of the wall interference potential in terms of the differences of the interior and exterior flow potentials and their normal derivatives along the interface:

$$\begin{aligned}\phi_w(\mathbf{r}_0) = \iint_S \Big\{ &[\phi(\mathbf{r}) - \tilde{\phi}(\mathbf{r})]\frac{\partial G(\mathbf{r}_0, \mathbf{r})}{\partial n} \\ &- [\frac{\partial\phi(\mathbf{r})}{\partial n} - \frac{\partial\tilde{\phi}(\mathbf{r})}{\partial n}]G(\mathbf{r}_0, \mathbf{r}) \Big\} dS.\end{aligned} \qquad (6.35)$$

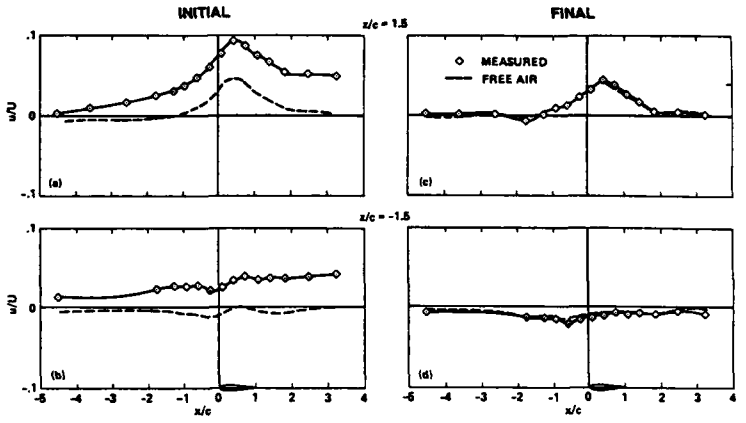

Fig. 6.5 Measured and theoretical streamwise velocity distributions, NACA 0012 airfoil in the NASA/ARC 2 x 2 ft wind tunnel, $M = 0.70$, $\alpha = 2°$, $Re_c = 2 \times 10^6$ (from [6.41]).

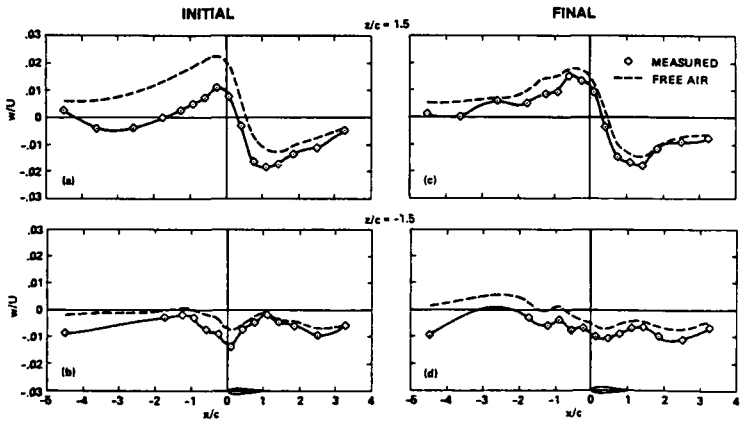

Fig. 6.6 Measured and theoretical normal velocity distributions, NACA 0012 airfoil in the NASA/ARC 2 x 2 ft wind tunnel, $M = 0.70$, $\alpha = 2°$, $Re_c = 2 \times 10^6$ (from [6.41]).

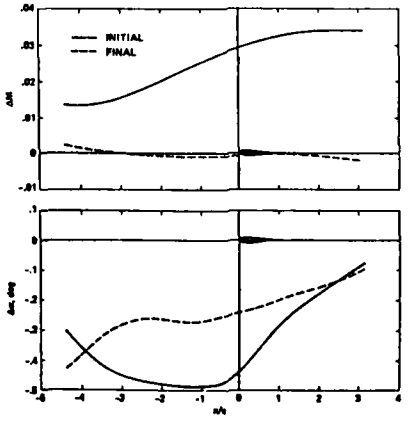

Fig. 6.7 Residual corrections along test section axis, evaluated by two-variable method from data of Figs. 6.5 and 6.6 (from [6.41]).

Physically, integral (6.35) can be interpreted as a surface distribution of doublets

$$\frac{\partial G(\mathbf{r}_0,\mathbf{r})}{\partial n} \qquad \text{with the density} \qquad [\phi(\mathbf{r}) - \tilde{\phi}(\mathbf{r})]$$

and a surface distribution of sources

$$G(\mathbf{r}_0,\mathbf{r}) \qquad \text{with the density} \qquad -\left[\frac{\partial \phi(\mathbf{r})}{\partial n} - \frac{\partial \tilde{\phi}(\mathbf{r})}{\partial n}\right].$$

The potential $\tilde{\phi}$ is obtained by solving an exterior flow problem (CFD), but ϕ_w is obtained by a simple surface integration, as in the two-variable method. The autocorrective property again applies

The exterior flow can be calculated as a solution of a Neumann problem, satisfying the boundary condition

$$\frac{\partial \tilde{\phi}(\mathbf{r})}{\partial n} = \frac{\partial \phi(\mathbf{r})}{\partial n}, \quad \mathbf{r} \in S, \tag{6.36}$$

where $\partial\phi(\mathbf{r})/\partial n$ is the normal component of disturbance velocity on the interface. For the solid wall boundary, it is equal and opposite to the normal component of the free stream velocity. Integral (6.35) then reduces to the distribution of doublets,

$$\phi_w(\mathbf{r}_0) = \iint_S [\phi(\mathbf{r}) - \tilde{\phi}(\mathbf{r})] \frac{\partial G(\mathbf{r}_0,\mathbf{r})}{\partial n} dS. \tag{6.37}$$

For a cylindrical interface, the integration by parts in the streamwise direction yields

$$\phi_w(\mathbf{r}_0) = -\frac{\beta}{2} \iint_S [C_p(\mathbf{r}) - \tilde{C}_p(\mathbf{r})] \Omega(\mathbf{r}_0,\mathbf{r}) dS, \tag{6.38}$$

where the term in square brackets is the discontinuity of the pressure coefficient across the boundary and Ω is the vortex singularity, Eq.(6.19). Equation (6.38) shows that in this case wall interference is defined by the *loading of the walls* [6.43].

Alternatively, the exterior flow can be calculated as a solution of a Dirichlet problem, satisfying the boundary condition

$$\tilde{\phi}(\mathbf{r}) = \phi(\mathbf{r}), \quad \mathbf{r} \in S, \tag{6.39}$$

so that integral (6.35) reduces to the distribution of sources,

$$\phi_w(\mathbf{r}_0) = -\iint_S \left[\frac{\partial \phi(\mathbf{r})}{\partial n} - \frac{\partial \tilde{\phi}(\mathbf{r})}{\partial n}\right] G(\mathbf{r}_0,\mathbf{r}) dS. \tag{6.40}$$

This approach has recently been described in Ref.[6.44].

Finally, if the walls are adjusted to satisfy the conditions (6.36) and (6.39) simultaneously (a perfect match), then from Eq.(6.35)

$$\phi_w(\mathbf{r}_0) \equiv 0,$$

indicating that the flow inside the test section is interference free. The conditions of flow tangency and equal pressures along the interface imply that the desired interface is a stream tube. This streamlining principle for an adaptive wall test section, introduced by Goodyer [6.6], is of course quite general and not just restricted to linear subsonic flow.

The Cauchy integral approach, applicable to 2D flow, proceeds along similar lines. Considering the complex disturbance velocity $\tilde{w}$ of the fictitious flow, analytic in the exterior region and vanishing at infinity, then for an interior point z_0 it follows

$$0 = \frac{1}{2\pi i} \int_C \frac{\tilde{w}(z)}{z - z_0} dz.$$

Subtracting it from Eq.(6.26), we obtain

$$w_w(z_0) = \frac{1}{2\pi i} \int_C \frac{w(z) - \tilde{w}(z)}{z - z_0} dz. \tag{6.41}$$

If the normal component of disturbance velocity is continuous across the interface,

$$\tilde{q}_n(z) = q_n(z), \quad z \in C, \tag{6.42}$$

then from Eqs.(6.29)-(6.30)

$$w_w(z_0) = \int_C [(q_t(z) - \tilde{q}_t(z)] \frac{i}{2\pi(z_0 - z)} ds. \tag{6.43}$$

The wall interference velocity is represented by a contour distribution vortices, whose density is equal to the discontinuity of the tangential component of velocity.

Conversely, if the tangential component of disturbance velocity is continuous,

$$\tilde{q}_t(z) = q_t(z), \quad z \in C, \tag{6.44}$$

then

$$w_w(z_0) = \int_C -[(q_n(z) - \tilde{q}_n(z)] \frac{1}{2\pi(z_0 - z)} ds. \tag{6.45}$$

The wall interference velocity is represented by a contour distribution of sources, whose density is equal and opposite to the discontinuity of the normal component of velocity.

As indicated earlier, schemes for calculating residual interferences and strategies of wall adaptation are closely interrelated. This can be illustrated [6.45] on the Judd streamlining algorithm [6.46].

This iterative procedure utilizes calculations of the fictitious external flow matching the normal velocity,

$$\tilde{v}_j = v_j,$$

along the interface $y = \pm\frac{h}{2}$, which approximates the upper and lower walls of a 2D test section. Index j indicates the iteration (wall adjustment) step. In order to introduce sufficient damping into the scheme, the aim of the wall slope adjustment $v_{j+1} - v_j$ is to provide the next computed value of the streamwise component, $\tilde{u}_{j+1}$, equal to the average of the measured value, u_j, and the computed value, $\tilde{u}_j$:

$$\tilde{u}_{j+1} = \frac{1}{2}(u_j + \tilde{u}_j).$$

This condition is equivalent to

$$\tilde{u}_{j+1} - \tilde{u}_j = \frac{1}{2}(u_j - \tilde{u}_j). \tag{6.46}$$

The slope adjustment can be obtained explicitly, using the unconfined flow conditions for the velocity pair $\tilde{u}_j$ and v_j. From Eq.(6.34b)

$$v_j(x_0, \pm\frac{h}{2}) = \pm\frac{\beta}{\pi} \int_{-\infty}^{\infty} \frac{\tilde{u}_j(x, \pm\frac{h}{2})}{x - x_0} dx. \tag{6.47}$$

Applying Eq.(6.47) to the difference $v_{j+1} - v_j$ and substituting from Eq.(6.46), Judd's wall adaptation formula is readily obtained:

$$\begin{aligned} &v_{j+1}(x_0, \pm\tfrac{h}{2}) - v_j(x_0, \pm\tfrac{h}{2}) \\ &= \pm\frac{\beta}{2\pi} \int_{-\infty}^{\infty} \frac{u_j(x, \pm\frac{h}{2}) - \tilde{u}_j(x, \pm\frac{h}{2})}{x - x_0} dx. \end{aligned} \tag{6.48}$$

The integral is interpreted as the Cauchy principal value.

Consistency of Eq.(6.48) is easily verified: if

$$\widetilde{u}_j(x, \pm\frac{h}{2}) = u_j(x, \pm\frac{h}{2}), \tag{6.49}$$

then the integrand is zero, and

$$v_{j+1}(x_0, \pm\frac{h}{2}) = v_j(x_0, \pm\frac{h}{2}),$$

indicating that the iterative process has terminated. Substituting Eq.(6.49) in (6.47), we obtain the unconfined flow condition for the measured disturbance velocity components u_j and v_j, implying that the tunnel flow in the j-th iteration is interference free. For linear subsonic flow at the interface, an acceptable accuracy of wall adaptation is usually reached in 2-3 iterative steps.

6.2.2 Nonlinear flow

Discussion of the procedures for the evaluation of nonlinear residual wall interference will follow a basic outline similar to that of the previous section with one-variable and two-variable methods discussed in turn. The emphasis will be on use of measured interface data of the type routinely obtained in adaptive-wall tunnels. These procedures have become known as *wall-interference assessment and correction* (WIAC) methods. Nonlinear wall-interference correction procedures which model the flow through the walls of ventilated test sections are an important aspect of pretest prediction of interference. However, these approaches will not be described here in detail because they are considered to be beyond the scope of the present report. Furthermore, there will not be any discussion of asymptotic analyses of wall interference since these generally use idealized-wall boundary conditions and not measured data.

The particular nonlinearities treated will be those arising from transonic flow effects as the free-stream Mach number approaches unity with significant regions of supercritical flow extending to and beyond the test-section interface or walls (Group 2 flows). Although nonlinearities due to powered lift with large flow deflections may occur at subsonic, subcritical test conditions, there has been little emphasis on this regime in adaptive-wall development, with the exception of the University of Arizona Adaptable-Wall Wind Tunnel, as described in Chapters 2, 3 and the Appendix. Residual wall-interference corrections in this regime will not be considered here. Wall interference for high lift was the subject of an AGARD FDP Symposium in 1980 and the papers given there [6.47] summarize work to that date. More recently, NASA has published a selected, annotated bibliography of wall interference in V/STOL and high-lift testing [6.48].

There have been several investigations in which wall or interface pressures have been measured to provide a complete set of boundary-condition data for validation of computational fluid dynamics (CFD) codes. These studies will not be discussed here except in specific instances where the computed results have contributed directly to the development of residual-interference correction procedures.

A significant source of wall interference in all test sections, not just those with adaptive walls, is the presence of sidewalls when test articles are mounted on them. This will be the case for a 2D model spanning a 2D test section and for a 3D semispan model mounted on an impermeable sidewall. In supercritical flows and high-lift flows, the interaction of the sidewall boundary layers with the flow about a 2D test article can cause serious contamination of the two-dimensionality of the flow field. These phenomena have been mentioned briefly in Section 3.3.1 and will be discussed in Section 6.2.3.

Historically, Kemp [6.49], [6.50] generated much of the impetus for the development of WIAC procedures for treating nonlinear residual wall interference by use of measured wall or interface pressures. Kemp applied a nonlinear transonic CFD approach and discussed the idea of test sections with interference that is *correctable* just by changes in Mach number, M, and angle of attack, α. Murman [6.51] also contributed by developing Kemp's ideas further. These two-variable procedures were developed specifically for 2D applications. Discussion of the subsequent development of the fundamental ideas of [6.49]-[6.51] is presented below in the section on two-variable methods. Nonlinear transonic one-variable methods were developed initially by Stahara and Spreiter [6.52], [6.53] and by Hinson and Burdges [6.54]. The basic ideas of these approaches also have been developed extensively, principally for 3D applications, and are discussed next. Finally, Smith [6.28] has developed an approximate transonic representation in order to extend a linear 2D one-variable method so that it yields results that are comparable to those from a linear two-variable method.

One-variable method

The basic data required are the same in the nonlinear regime as in the linear; i.e., the pressure distribution measured at the interface and a representation of the test article. However, the lack of superposition prohibits breakup into a flow field due to the model in free air and the flow field due to wall interference. Instead, a solution for the entire flow field with the model in the tunnel and a separate solution with the model in free air must be computed and interpreted properly. There are several ways that interpretation can be accomplished and these will be brought out in the ensuing discussion. This method can be regarded as the nonlinear equivalent of that discussed in Section 6.2.1.

One of the first applications of nonlinear assessment of wall interference was carried out by Stahara and Spreiter [6.52], [6.53] for various axisymmetric bodies of revolution in the free-stream Mach number range from 0.975 to 1.10. Numerical solutions of the transonic small-disturbance equation (TSDE) were obtained at the test M in the tunnel and in free air. Differences between the tunnel and free-air solutions were attributed to wall-interference effects and differences between the tunnel solution and the experimental model data were attributed to the effects of viscosity and vorticity that are not represented in the TSDE.

Another application was part of a larger investigation by Hinson and Burdges [6.54] into the accuracy of a variety of CFD methods for semispan wing and wing/fuselage models with three different swept-wing planforms. As part of the experimental program, static pressure was measured near the perforated walls of the Lockheed CFWT test facility, by means of six rails. The specific wall-interference contribution in [6.54] was a set of computations of the wing-alone flow using the rail pressure measurements as boundary conditions. An extended form of the TSDE was solved numerically. With the wing α adjusted in the calculation method to match the experimentally-measured lift in the free-air calculation, both free-air and tunnel solutions were obtained. The results displayed a shift in shock-wave location between tunnel and free air. The free-stream M then was adjusted, in a free-air solution at the same α, to match the pressure distribution that was calculated on the wing surface in the tunnel solution. At a test M of 0.820, a ΔM correction of -0.005 was found to provide a good match for all three wing-alone planforms at their design conditions. It should be emphasized that no use of measured wing pressure was made in the procedure. The comparisons and

matching were accomplished with calculated wing pressure distributions only.

Rizk and Murman [6.55], [6.56] have developed a general 3D code, called TUNCOR, along similar lines. The TSDE are solved numerically and it is assumed that the lift and pitching moment have been measured in the test along with the static pressure distribution on an interface at or within the tunnel walls. The interface can be of rectangular [6.55] or circular [6.56] cross section. The basic TUNCOR scheme consists of two steps. First, the flow about the model in the tunnel is computed by using the measured interface pressures as boundary conditions. In this step, the wing and tail angles of attack are determined separately within the iterative CFD solution procedure to match the measured lift and pitching moment. Second, the flow about the model in free air is computed. In this step, M and the wing and tail angles of attack are determined within the iterative solution method such that the model lift and pitching moment continue to match the experimental values, while simultaneously the difference in local Mach number on the model between the computed tunnel and free-air solutions is minimized.

TUNCOR has been used by Newman, Kemp and Garriz [6.57] to correct M and α at two test points for a swept semispan wing tested [6.58] in the NASA/Ames Research Center High Reynolds Number Channel I at Mach numbers between 0.80 and 0.85. Free-air CFD computations were made using a code [6.59], [6.60] incorporating the thin-layer approximation to the Reynolds-averaged Navier-Stokes equations. Results from this code, which includes the reflection-plane boundary layer as an option, tend to verify the M, α corrections generated by TUNCOR. Corrections for data obtained in the National Transonic Facility (NTF) at NASA/LaRC for the Pathfinder I transport-like configuration also were evaluated in [6.57] and [6.61]. Sickles and Erickson [6.62] also have investigated TUNCOR with an extensive data base obtained for a wing/fuselage/tail model. These results will be discussed in the next paragraphs. First, though, it should be noted that the principles and techniques of TUNCOR have been used in new codes developed by Rizk, et al. [6.63], [6.64] with the TSDE flow solver replaced by an Euler solver. There have not been any published applications of these new codes to experimental data, although examples with numerical simulations are presented in [6.63], [6.64].

TUNCOR was compared in [6.62] with experimental data and with results of a 3D code developed at AEDC. The AEDC code considers an interface of circular cross section an ..lves a different form of the TSDE numerically. There are provisions for calculating global corrections. However, neither lift nor pitching moment is constrained so that besides corrections to M and α there are residual corrections to the lift and pitching moment. The procedure first obtains a tunnel solution with the measured interface pressure distribution specified, but with the test α prescribed as well. The free-air solution allows M and α to vary so that the dimensional static pressure distributions on the model, as calculated in the tunnel and in free air, are matched as closely as possible in a least-squares sense. The assumption is made that the stagnation pressure is the same in both the tunnel and equivalent free-air solutions. An alternative correction procedure in the AEDC code is to perform local corrections to the flow on the model at the test M and α. In this alternative, the free-air solution is obtained at the test M and α. Then the differences in the calculated pressure distributions on the model between the tunnel and free-air solutions are evaluated. The differences can be applied as corrections to measured model pressure distributions, if they are available, and are integrated to give corrections to the lift and pitching moment. The neglected effects of viscosity and vorticity in the tunnel and equivalent free-air solutions are probably represented better in the global correction procedure by matching the calculated pressure distributions. However, the local correction procedure gives a better representation of the significant gradients in interference which exist over typical 3D aircraft configurations and also provide corrections at the actual test conditions. The local correction procedure has been developed further at AEDC by replacing the TSDE flow solver, first with an Euler solver, and second with a solver for the thin-layer approximation to the Reynolds-averaged Navier-Stokes equations (TNS).

Results [6.62] for several examples using both TUNCOR and the AEDC code indicated that the global corrections predicted by the two codes are very similar with no obvious superiority. Moreover, local corrections were found to be of comparable accuracy to the global ones. Therefore, the majority of the results in [6.62] are local corrections based on the AEDC code. It was found that when the flow over the AEDC wall-interference wing/fuselage/tail model, see Figs.2 and 3 of the AEDC response in the Appendix, is subcritical, or mildly supercritical ($M \leq 0.80$), the local corrections are reasonably satisfactory. This is shown in Fig.6.8, for four mildly supercritical cases at $M = 0.80$. These cases are representative of eight examples tested prior to adaptation in the adaptive-wall test section of the AEDC Aerodynamic Wind Tunnel (1T), see Chapters 2, 3 and the Appendix. The uniform porosity in 1T was 2% and 5% in the cases in Fig. 6.8. The corrected lift coefficients are compared to interference-free results for the same model tested in AEDC Aerodynamic Wind Tunnel (4T) at the same conditions. However, when the flow is strongly supercritical, ($M \geq 0.90$), neither local nor global corrections from the AEDC and TUNCOR codes are adequate, see Fig.6.9 which is representative of thirteen examples tested prior to adaptation. Replacing the TSDE flow solver with the Euler solver in two selected examples at $M = 0.90$ did not improve the results significantly [6.62]; i.e., the corrections are still of the incorrect sign. The source of the error appeared to arise from deficiencies of the inviscid approximation. Viscous effects, particularly the shock-wave/boundary-layer interaction, were not modeled so that the shock waves were in the wrong location and did not have the correct strength.

Calculations for the same two selected examples with viscous effects included by means of the TNS solver were very encouraging compared with the Euler results. One of these examples is the 7% porosity case of Fig.6.9 at $\alpha = 4°$. The TNS lift correction was practically zero which is consistent with the measured data in Fig.6.9. The second example is an early step in an AEDC adaptive-wall iteration (see Section 3.2.2 of this report) for $M = 0.90$, $\alpha = 4°$ with a uniform porosity of 3%. The 4T, 1T and corrected 1T lift data are shown in Fig. 6.10 and the erroneous sign of the lift correction has been reversed. Furthermore, the TNS solver results for both examples, using the one-variable method, agree very well with corresponding TNS solver results using a pretest prediction procedure developed at AEDC by Jacocks and reported by Kraft, et al. [6.12]. The AEDC pretest prediction procedure is used in the same sense as the AEDC one-variable procedure. That is, the local corrections are evaluated as the differences between free-air and tunnel computations at the test M and α. In fact, the free-air computation is identical to that in the one-variable method. The pretest tunnel computation does not use measured data, of course, but instead Jacocks

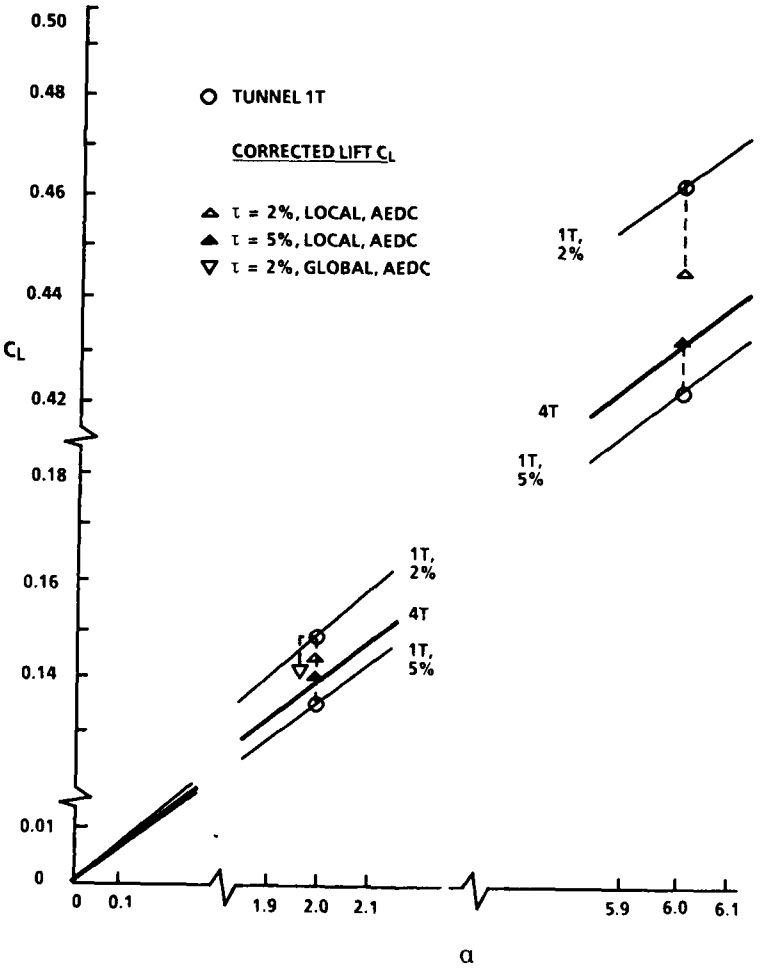

Fig. 6.8 Comparison of Tunnel 4T lift coefficients with Tunnel 1T lift coefficients uncorrected and corrected using the AEDC one-variable-method code, $M = 0.80$ (adapted from [6.62]).

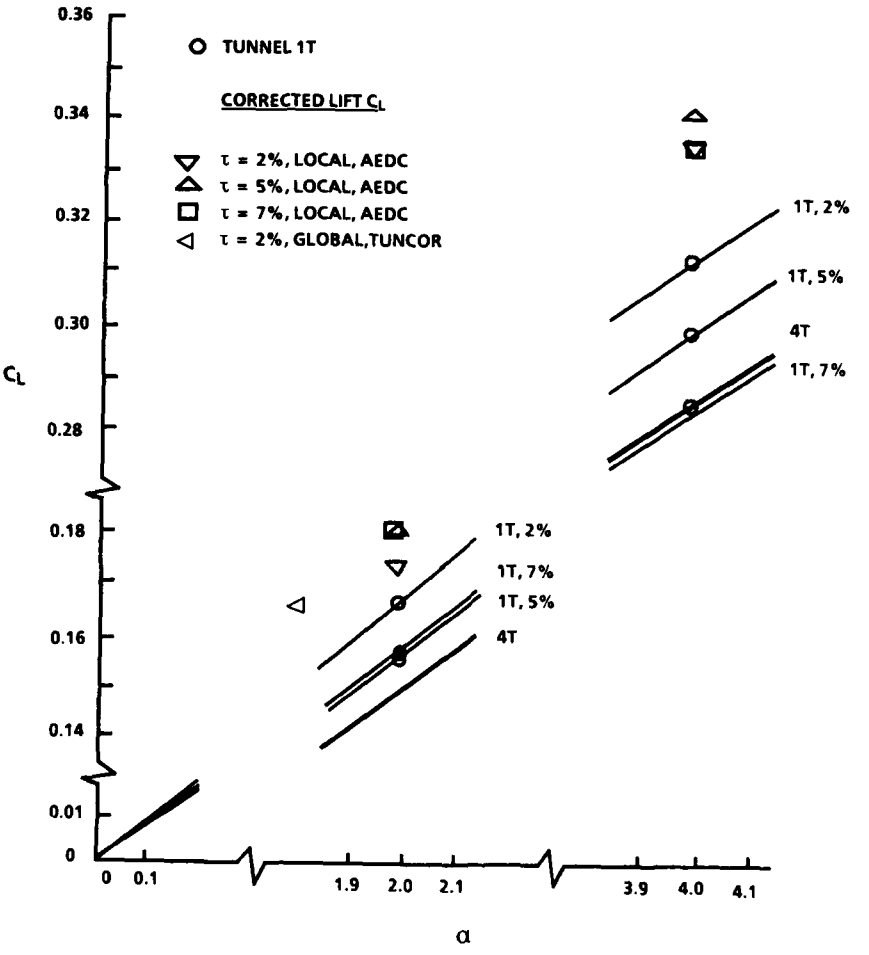

Fig. 6.9 Comparison of Tunnel 4T lift coefficients with Tunnel 1T lift coefficients uncorrected and corrected using the AEDC and TUNCOR one-variable-method codes, $M = 0.90$ (adapted from [6.62]).

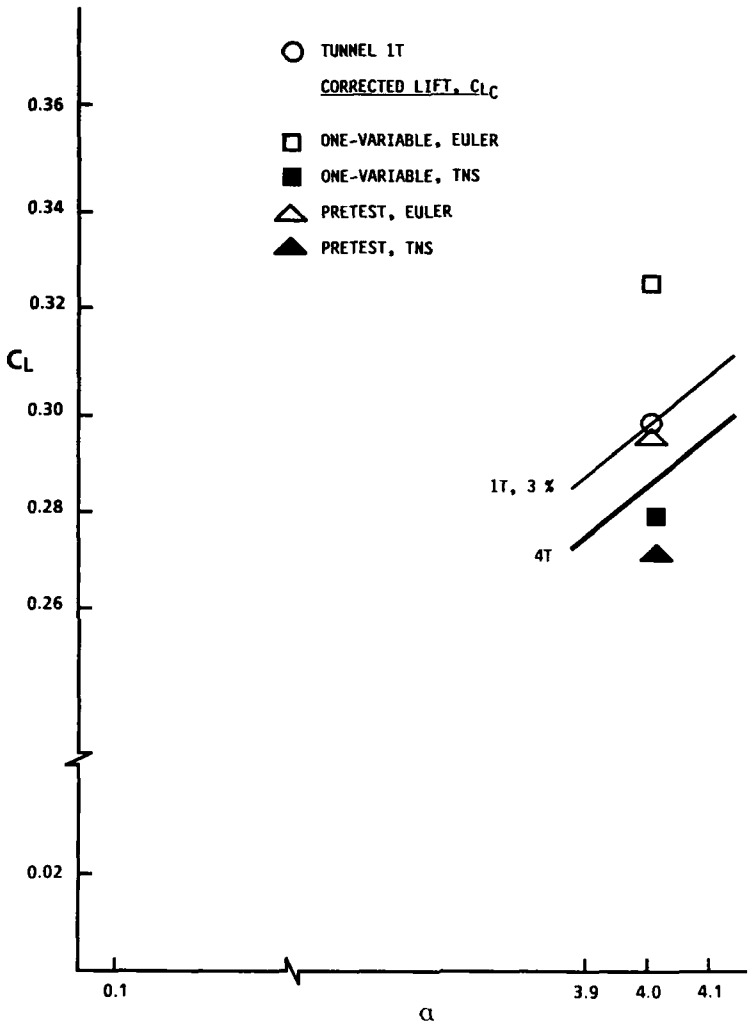

Fig. 6.10 Comparison of Tunnel 4T lift coefficients with Tunnel 1T lift coefficients uncorrected and corrected using the AEDC Euler and thin-layer Navier-Stokes one-variable-method codes and pretest-prediction codes, $M = 0.90$, $Re = 0.9 \times 10^6$ based on wing chord.

models the wall cross-flow characteristics semi-empirically by means of a local representation of the transpired turbulent boundary-layer flow on the perforated walls. The boundary-layer computation is coupled to and calculated simultaneously with the CFD solution for the flow over the test article (see [6.12] for more detail).

The TNS pretest-prediction method has been applied subsequently to a wing/fuselage/tail configuration which has a general geometrical likeness to the model discussed above. This configuration was tested in AEDC Aerodynamic Wind Tunnels (4T and 16T) [6.65]. The 16T, 4T and corrected 4T drag data at a Mach number of 0.95 are shown in Fig.6.11 and are very encouraging. At the 40% and 60% wing semispan locations, the predicted and measured chordwise pressure distributions are in good agreement. However, the most remarkable results are at the 90% wing semispan location for $\alpha = 4°$. The detailed differences between the flows in 4T and 16T are shown in Fig.6.12. At this wing station there are significant differences in the flow separation characteristics between 4T and 16T; these differences are predicted by the pretest procedure with sufficient fidelity to achieve satisfactory corrections. Clearly, additional solutions must be obtained for these and other model configurations and compared with data; efforts are underway to do this. Finally, further investigation is required to examine more thoroughly the relative advantages of the global and local corrections.

Two-variable method

Two-variable methods offer a significant advantage over the one-variable methods in linear flow because explicit test article representation is no longer necessary, as described in Section 6.2.1. In nonlinear flow, there also is promise of a corresponding advantage; however, the lack of linear superposition renders the problem more complicated. There are two fundamentally different approaches to the use of two measured variables in nonlinear wall-interference procedures. The first approach assumes that static pressure distributions are measured at the interface and on the model surface. It would not seem to qualify as a two-variable method, however Schairer [6.66] has shown that the use of a single variable along a double boundary is equivalent to that of two variables along a single boundary, in the sense that the far field perturbations due to the model in free air need not be estimated. The adaptive-wall implications of this are discussed in Section 3.2.3. With the interface and model pressure data at hand, nonlinear wall interference can be assessed by matching the pressure distribution measured on the model with that computed for an effective model in free air. This has been termed the *matching method* by Smith [6.13] and has been used by Kemp [6.49], [6.50], Murman [6.51], and in subsequent developments at NASA/LaRC [6.57], [6.61], [6.67]-[6.71]. Since

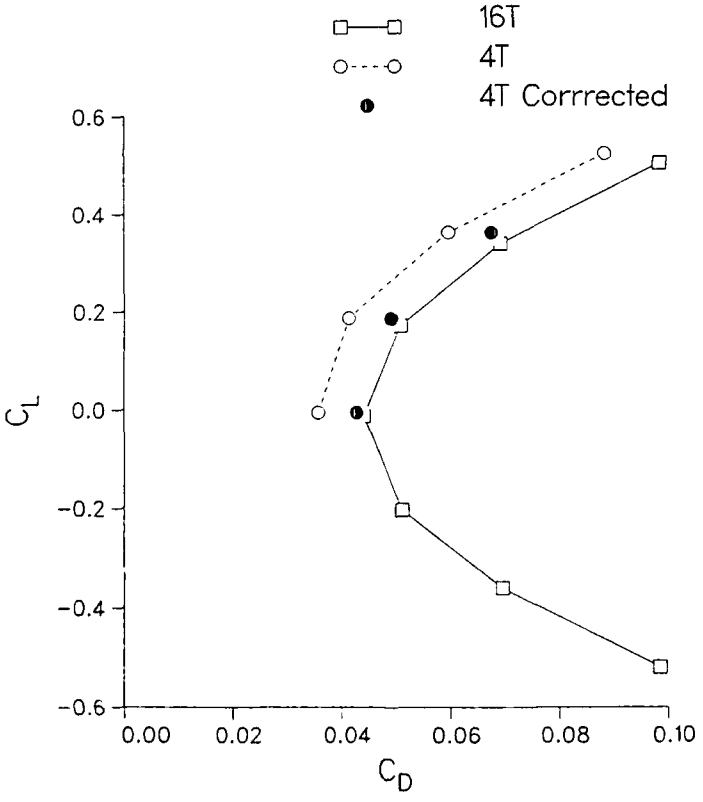

Fig. 6.11 Comparison of Tunnel 16T drag coefficients with Tunnel 4T drag coefficients uncorrected and corrected locally using the AEDC pretest-prediction, thin-layer Navier-Stokes code, wing/fuselage/tail model from [6.65], $M = 0.95$, $Re = 3.0 \times 10^6$ **based on wing chord.**

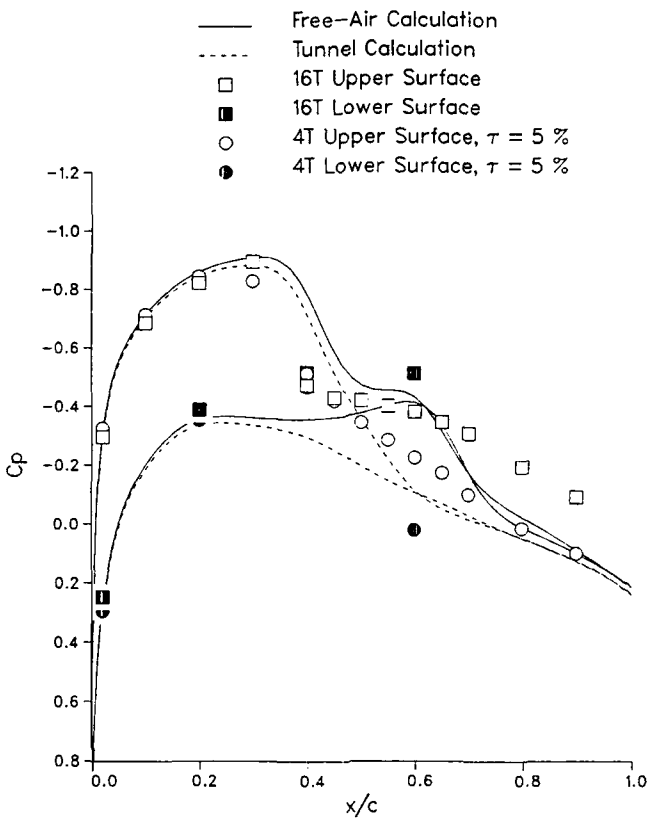

Fig. 6.12 Model pressure coefficients measured and calculated using the AEDC pretest-prediction, thin-layer Navier-Stokes code, wing/fuselage/tail model from [6.65], $M = 0.95$, $\alpha = 4°$, $Re = 3.0 \times 10^6$ based on wing chord, 90-percent wing semispan.

airfoil tests generally include measurements of the model pressure data, this is a very useful approach in 2D. In 3D, however, model pressure data generally are not available, so there has been no development of this approach for nonlinear 3D flow. The second approach assumes that the two variables are measured at the interface, without any pressure measurements on the model surface, so is attractive for 3D flow. This approach corresponds to that discussed in Section 6.2.1. The use of two variables at the interface has been investigated in 3D at AEDC [6.12], [6.62], [6.72].

In both approaches, the effective shape of the test article must be determined explicitly. The effective shape is the original geometric shape plus modifications to account for viscous, vortical and other physical effects that are missing from the equations of motion represented by the CFD flow solver, but are present in the measured data. In linear flow, an effective shape is considered implicitly, but never requires actual computation because the results are independent of its explicit representation. The independence exists as long as the viscous effects in the flow over the model remain approximately the same between the tunnel and free-air solutions, so that the effective shape remains the same.

The early work of Kemp [6.49], [6.50] and Murman [6.51] established the basic ideas of the matching method in 2D nonlinear flow. Kemp, et al. continued the development with 2D codes known as TWINTAN [6.67] and TWINTN4 [6.68]-[6.70], which differ in that the former considers top and bottom wall interference only, while the latter considers sidewall-boundary-layer effects as well. The latest version is TWNTN4A [6.71], which extends TWINTN4 to include flexible top and bottom adaptive walls. The procedures consist of three numerical solutions of the TSDE. The first is the calculation of the flow around the airfoil in the tunnel at the test M using the measured pressure distributions on the airfoil and interface as boundary conditions. The effective shape of the airfoil is one result of this calculation. The second calculation is the free-air flow around the effective shape, and is found by adjusting M and α in the iterative solution procedure in order to match the experimental lift simultaneously with minimization of the least-squares difference between the airfoil surface velocity distributions calculated in the tunnel and in free air. The M and α determined from this solution define the free-air conditions to which the tunnel test most closely corresponds. The residual least-squares difference is a measure of the correctability of the data. This completes calculation of the corrected conditions. However, a third calculation is made to estimate the velocity field induced by the walls. This calculation also is a free-air flow at the corrected M, with the properly-scaled differences in the pressure and normal

velocity across the airfoil specified from the first solution. The scaled differences of the streamwise and normal velocity components along the airfoil centerline between the third and the first solutions are interpreted as being due to wall interference.

The sidewall-boundary-layer interference is calculated in TWNTN4A using Murthy's [6.73] extension of the Barnwell and Sewall [6.74], [6.75] model, see Section 6.2.3 for more detail. The TWNTN4A code offers two options for applying four-wall corrections. The first option is the sequential application of sidewall similarity-rule corrections (see Section 6.2.3) directly to the measured data, followed by an additional correction for the top and bottom wall interference. The second option is the unified application to all four walls simultaneously, with the sidewall-boundary-layer effect represented as an additional term in the TSDE.

Other than cases examined by Kemp and cited above, early applications of TWINTAN and TWINTN4 were reported in [6.76] and [6.77], respectively. Recent results by Green, Newman et al. [6.61], [6.71], [6.78], used TWNTN4A in the unified four-wall approach and found that the Murthy extension [6.73] is preferred for application to adaptive-wall data obtained in the NASA/LaRC TCT. Representative results obtained by the WIAC procedure [6.61], [6.78], are shown in Fig.6.13. In Fig.6.13, data obtained during successive adaptive-wall iterative steps beginning from aerodynamically-straight walls at two different ratios of tunnel half-height to airfoil chord length, h/c, have been corrected by three passes through the TWNTN4A code. Several passes through these partially-adapted data were required in order to adjust the upstream flow-angle distribution iteratively since no measurements of that distribution were made.

The two-variable method with both variables measured at the interface leads to a much more difficult solution procedure. Mathematically, there is a question whether the problem is posed properly [6.72]. Nevertheless, an approximate procedure was developed for 3D flows [6.62] as an extension of the AEDC one-variable method of local corrections using solutions of the TSDE. The method begins with the model geometric shape prescribed along with the measured interface pressure just as in the one-variable procedure. Then the geometric shapes of the wing and tail are adjusted while continuing to impose the interface pressure distribution. The process is accomplished by adding approximate mode shapes, such as a constant, a linear distribution or a square-root distribution, to the geometric shapes to approximate the boundary-layer growth. This entails additional solutions until a least-squares match is obtained on the second measured variable. In the AEDC experiments, the second variable is the streamwise derivative of the velocity component normal to the interface, $\partial v_n/\partial x$, as measured by the two-component static pipes. This procedure was investigated by means of numerical simulations [6.12] of the viscous flow over the AEDC wall-interference model and the results were promising. However, when applied to experimental data for the same model [6.62], major changes to the geometric shape were necessary to improve agreement with the measured $\partial v_n/\partial x$. The resulting changes in the local pressure-distribution corrections on the model were not consistently better. Therefore, further development of the approach was postponed and the one-variable method was emphasized in the AEDC investigation.

6.2.3 Flow quality and sidewall-boundary-layer effects

Flow quality and sidewall-boundary-layer effects are two important issues for all wind tunnels, not only those with adaptive walls. Flow quality and data accuracy requirements have been considered in depth recently by the AGARD FDP. The Wind Tunnel Testing Techniques Subcommittee of the FDP examined these requirements and

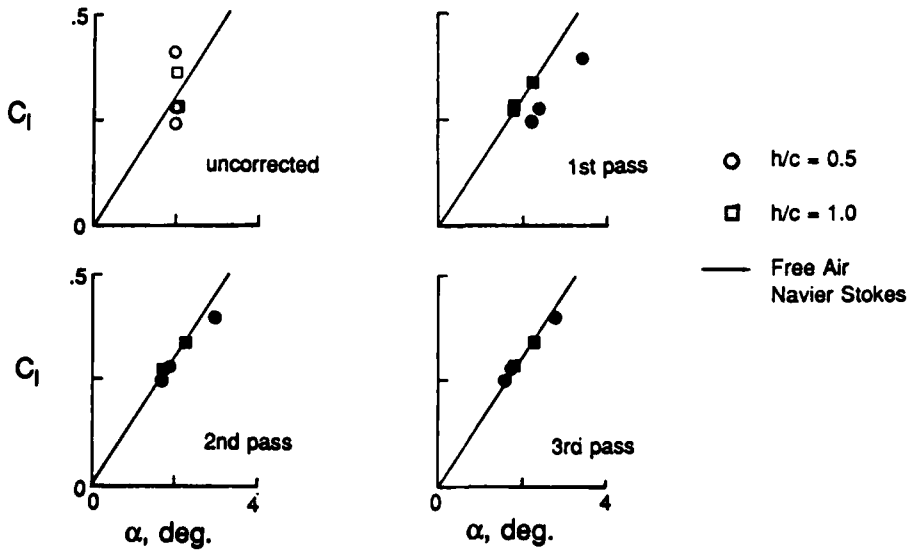

Fig. 6.13 Comparison of free-air, thin-layer Navier-Stokes CFD lift coefficients with 0.3-m TCT partially-adapted lift coefficients uncorrected and corrected using the TWNTN4A two-variable-method code, NACA 0012 airfoil, $M = 0.65$, $\alpha = 2$ deg., $Re_c = 9 \times 10^6$ (from [6.61]).

the results were reported by Steinle and Stanewsky in 1982 [6.79]. Flow quality and data accuracy also were the subject of the AGARD FDP Symposium in Naples in 1987 [6.80]. A further aspect of all wind tunnel testing, namely viscous simulation and control, has received a great deal of attention and is summarized in the final report of AGARD FDP working Group 09 [6.81]. Viscous simulation and control will not be discussed explicitly in this section. However, flow quality and sidewall-boundary-layer effects are discussed here specifically for adaptive-wall applications.

Flow quality

Flow quality in a wind tunnel is very important for proper viscous simulation and control, especially for experiments and tests in laminar flows and flows for which boundary-layer transition location is significant. The use of flexible, impermeable walls in a test section prevents an increase in the usual acoustic noise emitted by the turbulent boundary layers on transonic test-section walls.

An adaptive-wall test section flow-quality investigation was performed at ONERA/CERT in the flexible, impermeable wall tunnel T2 [6.82]. Static-pressure spectra measured at the center of the turntable are presented in Fig.6.14. The measured noise level is plotted using the reduced variables n and $[nF_p(n)]^{1/2}$, where $n = fH/V$ is a Strouhal number, $F_p(n)$ is the reduced power spectral density, f is the frequency, H is the test section height, and V is the free-stream velocity. This noise is very close to the minimum corresponding to turbulent boundary-layer noise. The integration of a pressure spectrum defines the RMS reduced noise $\tilde{p}/q$, i.e., $\int F_p(n)dn = (\tilde{p}/q)^2$, where $\tilde{p}$ is the RMS fluctuating pressure and q is the dynamic pressure. In these experiments the measured frequency range was 1 Hz to 20 KHz. This noise is constant as a function of free-stream Mach number at a level of 3.8×10^{-3}, see Fig.6.15.

Velocity fluctuations also were measured with hot wires and hot films and are presented in Fig.6.16. The turbulence intensity in the stilling chamber probably depends on the wind tunnel design, but the low level measured in the test section is a consequence of the use of flexible, impermeable walls and the large contraction ratio of 23.

Sidewall boundary layers

The presence of sidewalls can provide a significant source of wall interference in all wind tunnels with 2D flows over test articles spanning the tunnel and with 3D flows over semispan test articles mounted on a sidewall.

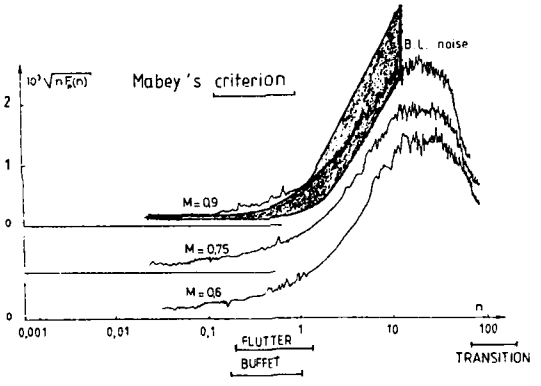

Fig. 6.14 Tunnel-empty static-pressure fluctuation spectra measured on a sidewall of Tunnel T2 at ONERA/CERT (from [6.82]).

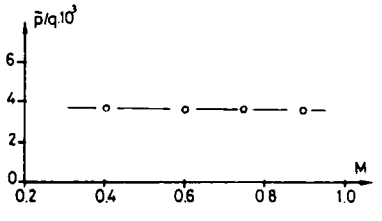

Fig. 6.15 Mach number variation of RMS pressure-fluctuation noise level on a sidewall of Tunnel T2 at ONERA/CERT (from [6.82]).

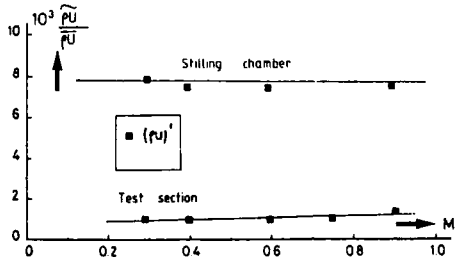

Fig. 6.16 Mach number variation of RMS velocity-fluctuation level on a sidewall of Tunnel T2 at ONERA/CERT (from [6.82]).

The basic, empty-tunnel growth of the boundary layers in adaptive-wall test sections with flexible, impermeable walls has been discussed in Section 3.2.2. This boundary-layer growth is accommodated by diverging the flexible walls in such a way that they are "aerodynamically straight", i.e., provide a uniform static pressure along the test-section length and so account for the boundary-layer growth on all four walls.

Most of the algorithms discussed in Section 3.2.2 for 2D adaptive-wall test sections with flexible, impermeable walls have provisions for computing the displacement effect of the model-induced pressures on the top and bottom walls. The displacement effect is found by calculating the boundary layers with the measured pressure distributions as input. This accounts well for the modulation of the empty-tunnel boundary-layer growth on the top and bottom walls due to the presence of the model. For 2D ventilated adaptive-wall test sections, the transpired boundary layers on the top and bottom walls are beyond the interface surfaces and so are taken care of automatically in the adaptation.

In supercritical and very high-lift flows, the sidewall boundary layers interact in a very complex manner with the flow over the test article for all 2D test sections. Serious contamination of the desired 2D flow can occur as a result of the interaction, particularly for narrow test sections. The variations of the sidewall-boundary-layer growth in the presence of the model were calculated by Newman and Anderson [6.83], [6.84] for early 2D adaptive-wall experiments performed at NASA/LaRC by Everhart [6.85]. More recently, ONERA/CERT has found that these sidewall effects are a major factor in determining Mach-number/angle-of-attack limitations in Tunnel T2 for 2D airfoil testing [6.86]-[6.89]; see also their response in the Appendix to Question 3.8e. The sidewall-boundary-layer displacement thickness in T2 for a CAST 7 airfoil section at $M = 0.76$ and $\alpha = 0°$ is presented in Fig.6.17. The sidewall effects correspond to a change in displacement thickness of 1 to 2 mm, which is not negligible compared to the displacements of 10 to 20 mm needed to adapt the upper and lower walls.

A great deal of consideration was given to sidewall boundary layers in the GARTEur cooperative project on CAST 7 airfoil data [6.24]. Other recognition of the importance of 2D sidewall boundary layers is given in [6.90],[6.91]. Some researchers [6.86],[6.91] attribute the principal effect of sidewall interference to changes in the induced downwash at the model due to the spanwise variation of lift. Other work focuses on blockage as the principal effect.

Major effort has been devoted to the blockage approach by a group associated with NASA/LaRC. Development of procedures to estimate 2D sidewall-boundary-layer blockage corrections is given in a series of reports, which are summarized, chronologically, in papers by Barnwell [6.74], Sewall [6.75] and Murthy [6.73]. The models of [6.74],[6.75] account for three-dimensional blockage effects along the airfoil span based on an average of the perturbations of the sidewall-boundary-layer displacement thickness due to the test article. Subsonic [6.74] and transonic [6.75] similarity rules for interpreting the measured airfoil data also have been derived. The Murthy extension [6.73] accounts approximately for the airfoil aspect ratio and reduces to the equations of [6.74],[6.75] in the limit of vanishing aspect ratio. In Fig.6.18, airfoil drag data from the NASA/LaRC TCT with slotted walls have been corrected [6.61],[6.92] by the Barnwell-Sewall [6.74],[6.75] and Murthy [6.73] methods.

Finally, Obayashi and Kuwahara [6.93] have obtained CFD solutions using the thin-layer approximation to the Reynolds-averaged form of the Navier-Stokes equations. The thin-layer approximation is applied on both the sidewalls and airfoil surfaces in a simulated 2D wind-tunnel test with locally supercritical flow.

Clearly, further investigation of sidewall-boundary-layer effects on 2D testing is necessary. With further understanding, it may be possible to consider 2D tests as the sum of an ideal 2D flow perturbed by 3D effects from the sidewalls. Moreover, if a reliable correction term can be estimated in the central part of the flow, it might be feasible to establish a new adaptation strategy to cancel the sidewall perturbation.

In 3D flows, the boundary layer on the mounting wall for all semispan models presents problems similar to those in 2D, but possibly exacerbated by the presence of a half fuselage. No work in this problem area is known for adaptive-wall tunnels.

For 3D testing in 2D test sections with impermeable walls, the sidewall boundary layer(s) adjacent to the wing tip(s) must be investigated to establish their significance for inclusion in adaptation algorithms. In 3D tests a sidewall boundary layer adjacent to the tip sustains lower pressure gradients than in 2D, but can be highly three dimensional, as shown in Fig.6.19. These 3D experimental data were obtained in T2 by a boundary-layer-probe survey carried out on the sidewall of the test section off the tip of the wing, which was 60 mm from the sidewall. The boundary-

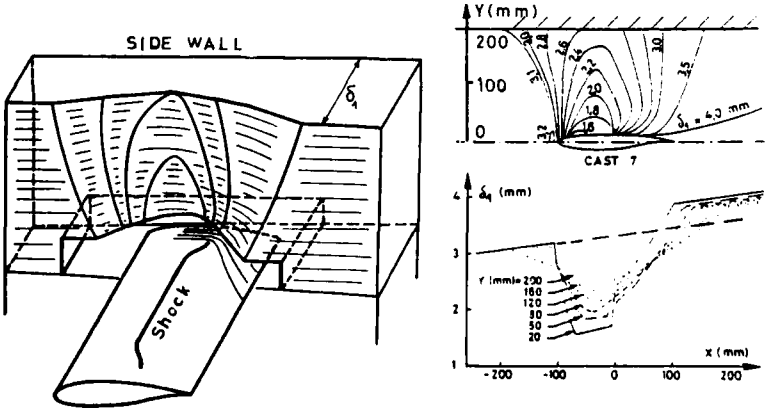

Fig. 6.17 Displacement-thickness contours on the sidewall of Tunnel T2 at ONERA/CERT for a CAST 7 airfoil section at $M = 0.76$, $\alpha = 0°$.

layer thickness is changed principally downstream of the wing where the trailing vortex system induces an upwash near the wall. The pressure gradients are small, but the flow direction changes, so the displacement thickness can vary 1.4 mm in the vertical plane. In 3D flows, too, further investigation of sidewall-boundary-layer effects clearly is necessary.

6.2.4 Concluding remarks

Methods of determining linear residual wall interference appear to be well established theoretically; however they need to be validated, for example by comparative studies of test data on the same model in different adaptive-wall wind tunnels as well as in passive, ventilated-wall tunnels. The GARTEur CAST 7 [6.24] and the CAST 10/DOA 2 [6.94] investigations are excellent examples of such comparative studies.

Results to date in both one-variable and two-variable methods for nonlinear wall interference indicate that a great deal more research and validation are required. The status in 2D flow is advanced over that in 3D flow as is the case generally with adaptive-wall development. Nevertheless, it is now well established that for transonic testing with extensive supercritical flow present, significant wall interference is likely to exist in conventional ventilated test sections. Consequently, residual correction procedures require further development hand-in-hand with further adaptive-wall development.

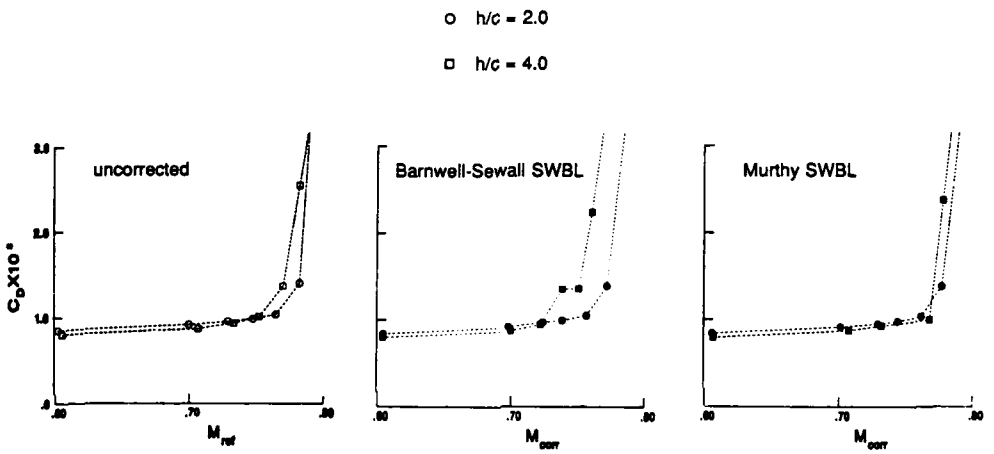

Fig. 6.18 Comparison of 0.3-m TCT, slotted-wall drag coefficients uncorrected and corrected using the Barnwell-Sewall [6.74], [6.75] and Murthy [6.73] sidewall-boundary-layer techniques, CAST 10 airfoil, $C_l = 0.5$, $Re_c = 15 \times 10^6$ (from [6.61]).

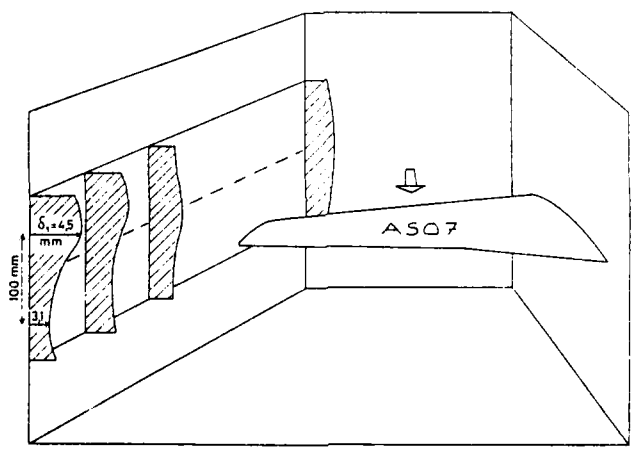

Fig. 6.19 Displacement-thickness profiles on the sidewall adjacent to the tip of an AS07 semispan wing in Tunnel T2 at ONERA/CERT.

6.3 References

[6.1] Theodorsen, T., "The Theory of Wind Tunnel Wall Interference," NACA Rept. 410, 1931.

[6.2] Wieselsberger, C., "Über den Einfluss der Windkanalbegrenzung auf den Widerstand, i: sbesondere im Bereiche der kompressiblen Strömung," Luftfahrtforschung, Vol.19, May 1942, pp.124-128.

[6.3] Goethert, B.H., *Transonic Wind Tunnel Testing*, Pergamon Press, 1961.

[6.4] Jacocks, J.L., "An Investigation of the Aerodynamic Characteristics of Ventilated Test Section Walls for Transonic Wind Tunnels," Doctoral Thesis, The University of Tennessee, 1976.

[6.5] Sears, W.R., "Self Correcting Wind Tunnels," The Aeronautical Journal, Vol.78, March 1974, pp.80-89.

[6.6] Goodyer, M.J., "The Self Streamlining Wind Tunnel," NASA TMX-72699, Aug.1975.

[6.7] Sears, W.R., "Adaptive Wind Tunnels with Imperfect Control," Journal of Aircraft, Vol.16, May 1979, pp.344-348.

[6.8] Lewis, M.C., "Airfoil Testing in a Self-Streamlining Flexible Walled Wind Tunnel," NASA CR-4128, May 1988.

[6.9] Ashill, P.R. and Weeks, D.J., "A Method for Determining Wall-Interference Corrections in Solid-Wall Tunnels from Measurements of Static Pressure at the Walls," AGARD-CP-335, May 1982, pp.1.1 - 1.12.

[6.10] Tuttle, M.H. and Cole, K.L., "Wind Tunnel Wall Interference (January 1980-May 1988)," *A Selected, Annotated Bibliography*, NASA TM 4061, 1988.

[6.11] Mokry, M., "Residual Interference and Wind Tunnel Wall Adaptation," AIAA-89-0147, Jan.1989.

[6.12] Kraft, E.M., Ritter, A., and Laster, M.L., "Advances at AEDC in Treating Transonic Wind Tunnel Wall Interference," ICAS Proceedings 1986, pp.748-769.

[6.13] Smith, J., "Measured Boundary Conditions Methods for 2D Flow," AGARD-CP-335, May 1982, pp.9.1 - 9.15.

[6.14] Baldwin,B.S., Turner, J.B., and Knechtel, E.D., "Wall Interference in Wind Tunnels With Slotted and Porous Boundaries at Subsonic Speeds," NACA TN 3176, 1954.

[6.15] Garner, H.C., Rogers, E.W.E., Acum, W.E.A., and Maskell, E.C.,"Subsonic Wind Tunnel Wall Corrections," AGARDograph 109, Oct.1966.

[6.16] Capelier, C., Chevallier, J.P., and Bouniol, F., "Nouvelle méthode de correction des effets de parois en courant plan," La recherche aérospatiale, Jan.-Feb. 1978, pp.1-11; also translated as ESA-TT-491, Aug. 1978.

[6.17] Stakgold, I., *Boundary Value Problems of Mathematical Physics*, Vol.II, Macmillan, 1968.

[6.18] Mokry, M., Digney, J.R., and Poole, R.J.D., "Doublet-Panel Method for Half-Model Wind-Tunnel Corrections," Journal of Aircraft, Vol.24, May 1987, pp.322-327.

[6.19] Mokry, M. and Ohman, L.H., "Application of the Fast Fourier Transform to Two-Dimensional Wind Tunnel Wall Interference," Journal of Aircraft, Vol.17, June 1980, pp.402-408.

[6.20] Mokry, M., "Subsonic Wall Interference Corrections for Finite-Length Test Sections Using Boundary Pressure Measurements," AGARD-CP-335, May 1982, pp.10.1 - 10.15.

[6.21] Risk, M.H. and Smithmeyer, M.G., "Wind-Tunnel Interference Corrections for Three-Dimensional Flows," Journal of Aircraft, Vol.19, June 1982, pp.465-472.

[6.22] Gakhov, F.D., *Boundary Value Problems*, Pergamon Press, 1966.

[6.23] Chevallier, J.P., "Survey of ONERA Activities on Adaptive-Wall Applications and Computation of Residual Corrections," Wind Tunnel Wall Interference Assessment/Correction 1983, NASA CP 2319, 1984, pp.43-58.

[6.24] GARTEUR Action Group AD(AG-23), "Two-Dimensional Transonic Testing Methods," NLR TR 83086 U, 1983.

[6.25] Smithmeyer, M.G. and Murman, E.M., "Far-Field Boundary conditions for Airfoils in Transonic Wind Tunnels," Rept.78, Flow Research Co., Dec.1976.

[6.26] Chan, Y.Y., "A Singular Perturbation Analysis of Two-Dimensional Wind Tunnel Interferences," Journal of Appl. Math. and Phys., Vol.31, 1980, pp.605-619.

[6.27] Chan, Y.Y., "Lift Effect on Transonic Wind-Tunnel Blockage," Journal of Aircraft, Vol.17, 1980, pp.915-916.

[6.28] Smith, J., "A Transonic Model Representation for Two-Dimensional Wall Interference Assessment," NLR TR 86026 U, Feb.1986.

[6.29] Archambaud, J.P. and Chevallier, J.P., "Utilisation de parois adaptables pour les essais en courant plan," AGARD-CP-335, May 1982, pp.14.1 - 14.14; also translated as NASA TM-77380, Feb.1984.

[6.30] Paquet, J.B., "Perturbations induites par les parois d'une soufflerie - méthodes intégrales," Thèse Ing. Doc., Université de Lille, 1979.

[6.31] Lo, C.F., "Tunnel Interference Assessment by Boundary Measurements," AIAA Journal, Vol.16, No.4, April 1978, pp.411-413.

[6.32] Lo, C.F. and Kraft, E.M., "Convergence of the Adaptive-Wall Wind Tunnel," AIAA Journal, Vol. 16, Jan.1978, pp.67-72.

[6.33] Kraft, E.M. and Dahm, W.J.A., "Direct Assessment of Wall Interference in a Two-Dimensional Subsonic Wind Tunnel," AIAA-82-0187, Jan.1982.

[6.34] Amecke, J., " Direkte Berechnung von Wandinterferenzen und Wandadaptation bei zweidimensionaler Strömung in Windkanälen mit geschlossenen Wänden," DFVLR-FB 85-62, Nov.1985; also translated as NASA TM-88523, Dec.1986.

[6.35] Ashill, P.R. and Keating, R.F.A., "Calculation of Tunnel Wall Interference from Wall-Pressure Measurements," Journal of the Royal Aeronaut. Soc., Jan.1988, pp.36-53.

[6.36] Lamarche, L., "Reduction of Wall Interference for Three Dimensional Models with Two Dimensional Wall Adaptation," Doctoral Thesis, Université Libre de Bruxelles, 1986.

[6.37] Barche, J., "Zur Ermittlung von Wandinterferenzen," Zeitschrift für Flugwiss. und Weltraumforschung, 4, 1980, pp.389-396.

[6.38] Labrujère Th.E., "Correction for Wall-Interference by Means of a Measured-Boundary-Condition Method", NLR TR 84114 U, Nov.1984.

[6.39] Maarsingh, R.A., Labrujére Th.E., and Smith, J., "Accuracy of Various Wall-Correction Methods for 3D Subsonic Wind Tunnel Testing," AGARD-CP-429, Sept.1987, pp.17.1 - 17.13.

[6.40] Mineck, R.E., "Wall Interference Tests of a CAST 10-2/DOA 2 Airfoil in an Adaptive-Wall Test Section," Supplement to NASA TM 4015, Dec.1987.

[6.41] Schairer, E., "Adaptive-Wall Tests in the Ames Two-by Two-Foot Transonic Wind Tunnel," Adaptive Wall Newsletter, NASA Langley Research Center, Feb. 1989.

[6.42] Sears, W.R. and Erickson, J.C.,Jr., "Adaptive Wind Tunnels," Ann.Rev.Fluid Mech., Vol.20, 1988, pp. 17-34.

[6.43] Goodyer, M.J. and Wolf, S.W.D., "The Development of a Self-Streamlining Flexible Walled Transonic Test Section, AIAA Journal, Vol.20, No.2, Feb.1982, pp.227-234.

[6.44] Rebstock, R., and Lee, E.E.,Jr., "Capabilities of Wind Tunnels With Two Adaptive Walls to Minimize Boundary Interference in 3-D Model Testing," NASA CP-3020, Vol.1, Part 2, pp.891-910, 1989.

[6.45] Russo, G.P. and Zuppardi, G., "Numerical Simulation of an Adaptive Wall Wind Tunnel: A Comparison of Two Different Strategies," L'aerotecnica, missili e spazio, n.4, 1987.

[6.46] Judd, M., Wolf, S.W.D., and Goodyer, M.J., "Analytical Work in Support of the Design and Operation of Two Dimensional Self Streamlining Test Sections," NASA CR-145019, 1976.

[6.47] Dietz, R.O. and Laster, M.L., eds., "Wind Tunnel Corrections for High Angle of Attack Models," AGARD-R-692, Feb.1981.

[6.48] Tuttle, M.H., Mineck, R.E., and Cole, K.L., " Wind Tunnel Interference in V/STOL and High Lift Testing," NASA TM-89066, Dec.1986.

[6.49] Kemp, W.B., Jr., "Toward the Correctable-Interference Transonic Wind Tunnel," AIAA-76-1794CP, June 1976.

[6.50] Kemp, W.B., Jr., "Transonic Assessment of Two-Dimensional Wind Tunnel Wall Interference Using Measured Wall Pressures," NASA CP-2045, Vol.1, Part 2, Mar.1978, pp.473-486.

[6.51] Murman, E.M., "A Correction Method for Transonic Wind Tunnel Wall Interference," AIAA-79-1533, July 1979.

[6.52] Stahara, S.S. and Spreiter, J.R., "Transonic Flows Past Non-axisymmetric Slender Shapes - Classical Equivalence Rule Analysis," AIAA Journal, Vol.17, No.3, Mar.1979, pp.245-252.

[6.53] Stahara, S.S. and Spreiter, J.R., "A Transonic Wind Tunnel Interference Assessment - Axisymmetric Flows," AIAA Journal, Vol.18, No.1, Jan.1980, pp.63-71.

[6.54] Hinson, B.L. and Burdges, K.P., "Evaluation of Three-Dimensional Transonic Codes Using New Correlation-Tailored Test Data," Journal of Aircraft, Vol.18, No.10, Oct.1981, pp.855-861.

[6.55] Rizk, M.H. and Murman, E.M., "Wind Tunnel Wall Interference Corrections for Aircraft Models in the Transonic Regime," Journal of Aircraft, Vol.21, No.1, Jan.1984, pp.54-61.

[6.56] Rizk, M.H., "Improvements in Code TUNCOR for Calculating Wall Interference Corrections in the Transonic Regime," AEDC-TR-86-6, Mar.1986.

[6.57] Newman, P.A., Kemp, W.B.,Jr., and Garriz, J.A., "Emerging Technology for Transonic Wind-Tunnel-Wall Interference Assessment and Correction," SAE Technical Paper Series No.881454, October 1988.

[6.58] Lockman, W.K. and Seegmiller, H.L., "An Experimental Investigation of the Subcritical and Supercritical Flow About a Swept Semispan Wing," NASA TM-84367, June 1983.

[6.59] Vatsa, V.N., "Accurate Numerical Solutions for Transonic Viscous Flows Over Finite Wings," Journal of Aircraft, Vol.24, No.6, June 1987, pp.377-385.

[6.60] Vatsa, V.N. and Wedan, B.W., "Navier-Stokes Solutions for Transonic Flow Over a Wing Mounted in a Tunnel," AIAA-88-0102, Jan.1988.

[6.61] Newman, P.A., Kemp, W.B., Jr., and Garriz, J.A., Wall Interference Assessment and Corrections," NASA CP-3020, Vol.1, Part 2, pp.817-851, 1989.

[6.62] Sickles, W.L. and Erickson, J.C., Jr., "Evaluation of Wall Interference Assessment and Correction Techniques," AEDC-TR-87-45, June 1988.

[6.63] Rizk, M.H. and Lovell, D., "Two-Dimensional Transonic Wind-Tunnel Wall Interference Corrections Based on the Euler Equations," AIAA-86-0124, Jan.1986.

[6.64] Rizk, M.H., Lovell, D.R., and Baker, T.J., "Euler Procedure for Correcting Two-Dimensional Transonic Wind-Tunnel Wall Interference," AIAA Journal, Vol.26, No.12, Dec.1988, pp.1457-1466.

[6.65] Parker, R.L., Jr. and Sickles, W.L., "Application of the Adaptive Wall Concept in Three Dimensions," Journal of Aircraft, Vol.18, No.3, March 1981, pp.176-183.

[6.66] Schairer, E.T., "Two-Dimensional Wind-Tunnel Interference from Measurements on Two Contours," Journal of Aircraft, Vol.21, No.6, June 1984, pp.414-419.

[6.67] Kemp, W.B., Jr., "TWINTAN: A Program for Transonic Wall Interference Assessment in Two-Dimensional Wind Tunnels," NASA TM-81819, May 1980.

[6.68] Kemp, W.B., Jr. and Adcock, J.B., "Combined Four-Wall Interference Assessment in Two-Dimensional Airfoil Tests," AIAA Journal, Vol.21, No.10, Oct.1983, pp.1353-1359.

[6.69] Gumbert, C.R., Newman, P.A., Kemp, W.B., and Adcock, J.B., "Adaptation of Four-Wall Interference Assessment/Correction Procedure for Airfoil Tests in the 0.3-m TCT," NASA CP-2319, 1984, pp.393-411.

[6.70] Kemp, W.B., Jr., "TWINTN4: A Program for Transonic Four-Wall Interference Assessment in Two-Dimensional Wind Tunnels," NASA CR-3777, 1984.

[6.71] Green, L.L. and Newman, P.A., "Transonic Wall Interference Assessment and Corrections for Airfoil Data from the 0.3-Meter TCT Adaptive Wall Test Section," AIAA-87-1431, June 1987.

[6.72] Lo, C.F. and Sickles, W.L., "Two-Measured Variable Method for Wall Interference Assessment/Correction," NASA CP-3020, Vol.1, Part 2, pp.853-866, 1989.

[6.73] Murthy, A.V., "Effect of Aspect Ratio and Sidewall Boundary-Layer in Airfoil Testing," Journal of Aircraft, Vol.25, No.3, March 1988, pp.244-249.

[6.74] Barnwell, R.W., "Similarity Rule for Sidewall Boundary-Layer Effect in Two Dimensional Wind Tunnels," AIAA Journal, Vol.18, No.9, Sept.1980, pp. 1149-1151.

[6.75] Sewall, W.G., "The Effect of Sidewall Boundary Layers in Two-Dimensional Subsonic and Transonic Wind Tunnels," AIAA Journal, Vol.20, No.9, Sept.1982, pp.1253-1256.

[6.76] King, L.S. and Johnson, D.A., "Comparison of Supercritical Airfoil Flow Calculations With Wind-Tunnel Results," AIAA Journal, Vol.23, No.9, Sept. 1985, pp.1301-1307.

[6.77] Gumbert, C.R. and Newman, P.A., "Validation of a Wall Interference Assessment/Correction Procedure for Airfoil Tests in the Langley 0.3-m Transonic Cryogenic Tunnel," AIAA-84-2151, Aug.1984.

[6.78] Green, L.L.R., "Wall Interference Assessment and Corrections for Transonic Adaptive Wall Airfoil

Data," M.S. Thesis, George Washington University, April 1988; also [N88-21129].

[6.79] Steinle, F. and Stanewsky, E.,"Wind Tunnel Flow Quality and Data Accuracy Requirements," AGARD-AR-184, Nov.1982.

[6.80] "Aerodynamic Data Accuracy and Quality: Requirements and Capabilities in Wind Tunnel Testing," AGARD-CP-429, 1987.

[6.81] "Boundary Layer Simulation and Control in Wind Tunnels: Report of the Fluid Dynamics Panel Working Group 09," AGARD-AR-224, April 1988.

[6.82] Blanchard, A., Dor, J.B., Seraudie, A., and Breil, J.F., "Flow Quality in the T2 Cryogenic Wind Tunnel - Problems and Solutions," ONERA/CERT Second Cryogenic Technology Review Meeting, DFVLR Köln/Porz, June 1988.

[6.83] Newman, P.A. and Anderson, E.C., "Analytical Design of a Contoured Wind-Tunnel Liner for Supercritical Testing," NASA CP-2045, Vol.1, Part 2, March 1978, pp.499-509.

[6.84] Newman, P.A. and Anderson, E.C., "Numerical Design of Streamlined Tunnel Walls for a Two-Dimensional Transonic Test," NASA TM-78641, April 1978.

[6.85] Everhart, J.L., "A Method for Modifying Two-Dimensional Adaptive Wind-Tunnel Walls Including Analytical and Experimental Verification," NASA TP-2081, Feb.1983.

[6.86] Chevallier, J.P., "Effects tridimensionels sur les profiles," ONERA TP-1981-117, 1981; also translated as NASA TM-77025, Feb.1983.

[6.87] Chevallier, J.P., Mignosi, A., Archambaud, J.P., and Seraudie, A., "T2 Wind Tunnel Adaptive Walls - Design, Construction, and Some Typical Results," La Recherche Aérospatiale (English Edition), No.4, July/Aug. 1983, pp.1-19.

[6.88] Archambaud, J.P. and Seraudie, A., "Etudes de parois adaptables à T2 ONERA/CERT," 20ième Colloque d'aerodynamique appliquée, Toulouse, Nov. 1983; also ONERA TP-1983-150, 1983.

[6.89] Archambaud, J.P. and Mignosi, A., "Two-Dimensional and Three-Dimensional Adaptation at the T2 Transonic Wind Tunnel of ONERA/CERT," AIAA-88-2038 CP, May 1988.

[6.90] Chan, Y.Y., "Wall Boundary-Layer Effects in Transonic Wind Tunnels," AGARD-CP-335, May 1982, pp.7.1-7.15.

[6.91] Ganzer, U., Stanewsky, E., and Ziemann, J., "Sidewall Effects on Airfoil Tests," AIAA Journal, Vol.22, No.2, Feb.1984, pp.297-299.

[6.92] Gumbert, C.R., "Wall Interference Assessment/Correction of Data From Tests of a CAST 10-2/DOA 2 Airfoil in the Langley 0.3-m Transonic Cryogenic Tunnel," M.S. Thesis, George Washington University, May 1988; also [N88-26331].

[6.93] Obayashi, S. and Kuwahara, K., "Navier-Stokes Simulation of Side Wall Effects of Two-Dimensional Transonic Wind Tunnel," AIAA-87-0037, Jan.1987.

[6.94] Ray, E.J., ed., "Proceedings of the CAST 10/DOA 2 Airfoil International Workshop, Langley 1988", to appear as a NASA CP.

Chapter 7

Adaptation for Unsteady Flow

Editor: H. Försching
Contributor: R. Voß (DLR, Göttingen)

7.1 Introduction

Wind tunnel wall interference in unsteady flow has not been as thoroughly investigated as in steady flow. In the case of unsteady flow the wind tunnel wall interference problem is much more complicated by additional parameters describing the time-dependent variation of the unsteady flow field. Moreover, other sources of interference, such as tunnel wall reflections in the form of acoustic waves and, as a consequence, wind tunnel resonance, may play an important role as well.

All investigations on unsteady wind tunnel wall interference known so far have concentrated on (harmonically) oscillating lifting systems and bodies undergoing small amplitudes of motion in closed and ventilated wind tunnel test sections. For the case of such motion-induced unsteady flow, a general outline of the problem from a theoretical point of view is given in Ref.[7.1]. Experimental results from systematic wind tunnel interference measurements are reported in Refs. [7.2] and [7.3].

With the recent development of adaptive wind tunnel walls, by which steady wall effects are eliminated or significantly reduced by actively controlling flow near the walls, new possibilities for correction of wind tunnel wall interference have also emerged for unsteady flow. In the following, prospects and concepts of experimental and analytical techniques for correction of unsteady wind tunnel wall effects, appearing with aerodynamic and aeroelastic measurements of oscillating lifting systems and bodies, are presented. First, some fundamental relations of motion-induced unsteady flow fields, basic to a physical understanding and analytical treatment of unsteady flow phenomena, are explained. Then the principal causes of unsteady wind tunnel interference are described and the practicability of adaptive wind tunnel walls to eliminate unsteady aerodynamic wall interference effects in unsteady aerodynamic and aeroelastic wind tunnel model measurements is discussed. Finally prospective wind tunnel wall corrections for motion-induced unsteady flow, applying steady flow wall adaptation and CFD-techniques, are outlined. Wind tunnel wall effects on other unsteady aerodynamic processes, such as flow separations at high incidences, vortex and boundary layer flows, are beyond the scope of this chapter.

7.2 Basic Physical Relations of Motion-Induced Unsteady Flow Fields

The differential equation that governs the inviscid unsteady flow due to small oscillatory perturbations imposed on a steady, uniform flow field is a wave equation. In reference to rectangular coordinates, see **Fig.7.1**, this equation for two-dimensional unsteady compressible flow, generated by an oscillating airfoil, reads, see Ref.[7.4]:

$$\left(1 - M_\infty^2\right)\phi_{xx} + \phi_{yy} - 2\,\frac{M_\infty^2}{U_\infty}\,\phi_{xt} - \frac{1}{a_\infty^2}\,\phi_{tt} = 0 \quad , \tag{7.1}$$

Here, $\phi = \phi(x, y, t)$ is the time-dependent perturbation velocity potential, U_∞ the velocity of the undisturbed flow, M_∞ the corresponding Mach number and a_∞ the velocity of sound. When the steady free stream Mach number M_∞ is close to unity, the governing equation for 2d transonic flow in its simplest form reads, see Ref.[7.4]:

$$\left(1 - M_\infty^2\right)\phi_{xx} - (\gamma + 1)\,\frac{M_\infty^2}{U_\infty}\,\frac{\partial}{\partial x}\left(\phi_x^0\phi_x\right) + \phi_{yy} - 2\,\frac{M_\infty^2}{U_\infty}\,\phi_{xt} - \frac{1}{a_\infty^2}\,\phi_{tt} = 0 \quad , \tag{7.2}$$

where γ denotes the ratio of specific heats. Eq.(7.2) is the time linearised transonic small perturbation (TSP) equation, where we recognize a non-linear term associated with the steady flow potential ϕ^0 independent of time t.

In the case of harmonic motion of the airfoil,

$$\phi(x, y, t) = \phi(x, y)\, e^{i\omega t} \quad , \tag{7.3}$$

with the coordinate transformations (L = reference length)

$$\bar{x} = x/L \;\; , \;\; \bar{y} = \beta y/L \;\; \text{and}$$

$$T = \frac{t\,U_\infty}{L} \;\; , \;\; \text{with} \;\; \beta = \sqrt{1 - M_\infty^2} \quad , \tag{7.4}$$

and upon introduction of a reduced velocity potential φ,

$$\phi = \varphi e^{ik\bar{x}} \quad , \tag{7.5}$$

Eq.(7.1) can be transformed into the well-known Helmholtz wave equation:

$$\varphi_{\bar{x}\bar{x}} + \varphi_{\bar{y}\bar{y}} + \lambda^2\varphi = 0 \quad . \tag{7.6}$$

A fundamental solution of Eq.(7.6) is

$$\varphi \sim H_0^{(2)}(\lambda r) \quad , \tag{7.7}$$

where

$H_0^{(2)}$ = Hankel function of second kind and order zero, satisfying the Sommerfeld radiation condition,

$k = \dfrac{\omega L}{U_\infty}$ = reduced frequency (ω = circular frequency),

$\lambda = \dfrac{kM_\infty}{\beta^2}$ = reduced wave number,

$\varepsilon = \lambda M_\infty$ and

$r = \sqrt{(\bar{x} - \bar{\xi})^2 + (\bar{y} - \bar{\eta})^2}$ = distance between transmitting ($\bar{\xi}$, $\bar{\eta}$) and receiving field point.

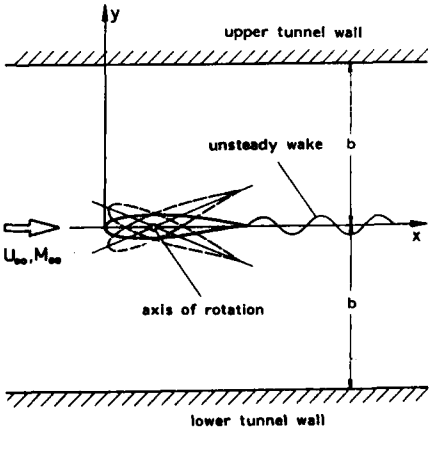

Fig.7.1: Oscillating airfoil in a wind tunnel with coordinate system

Hence, the unsteady part of the flow field of a harmonically oscillating airfoil may be represented by a superposition of perturbation sources which move with the base flow velocity U_∞ and propagate in the form of waves with the velocity of sound a_∞ , thus exhibiting a waviness of the flow field dependent on the parameters λ and/or ε and on the mode of oscillation as well. As a typical example, **Fig.7.2** illustrates the motion-induced unsteady flow field of an oscillating airfoil in 2d compressible flow, where φ' denotes the real part (in phase with the oscillating airfoil) and φ'' the imaginary part (90 degrees out of phase) of the unsteady velocity potential φ . It can be seen in **Fig.7.2** that this unsteady flow field is by far more complicated than the steady flow field of an airfoil at rest.

7.3 Wind Tunnel Interferences in Unsteady Flow

From the practical point of view, the most important types of motion-induced unsteady flow fields in a wind tunnel arise from forced or self-excited (flutter) oscillations of the model. In such wind tunnel investigations the unsteady aerodynamic data of main interest are the magnitude and phase of the motion-induced unsteady aerodynamic pressures. For instance, for an airfoil performing a pitching oscillation of amplitude Θ about a mean incidence α_0 , the wall interference effects on magnitude and phase of the unsteady pressures can be considered under the following headings:

- *steady* effects on the flow for the mean incidence α_0 ,
- *quasi-steady effects in context with the time-dependent* kinematic flow conditions for all changes of incidence within the range $(\alpha_0 - \Theta) < \alpha < (\alpha_0 + \Theta)$,
- *unsteady* effects on the manner in which the magnitude and phase of the motion-induced unsteady pressure vary with frequency in context with the unsteady wake.

Hence, the requirements for avoidance of wind tunnel wall interference effects on unsteady measurements are:

- correct (undisturbed) base flow and correct steady perturbations,
- absence of any additional unsteady effects,

i. e. an unsteady process may be directly affected by steady flow wall interference as well as by the purely unsteady sources of interference, as demonstratively shown in Refs. [7.5 and 7.6].

The principal causes of unsteady tunnel interference - in addition to the well-known steady interference effects, such as wall constraint, shock wave reflection in transonic flow and wall boundary layers - are, see **Fig.7.3** :

- *unsteady effects of wall constraint,*
- reflection by the walls of model-generated acoustic disturbances, and - as a consequence - acoustic wind tunnel resonance,
- distortion of the oscillatory wake of the model by other tunnel deficiencies,
- inherent tunnel flow fluctuations.

Since a clear understanding of these unsteady wind tunnel interference effects is of basic concern for the application of adaptive wall concepts, they will be discussed in more detail in the following.

Corrections for unsteady effects of wall constraint - excluding transonic flow - in tunnels having well-defined wall boundary conditions can readily be obtained from theoretical investigations. The corresponding boundary conditions for open and closed (solid) wind tunnel walls can easily be established, see Ref.[7.1], but it is difficult to obtain quantitative estimates for ventilated wind tunnel walls because of mathematical uncertainties about the boundaries. For two-dimensional airfoils oscillating in sub- and supersonic flow several such analytical unsteady wall correction techniques have already been elaborated, see Refs.[7.7 – 7.12] .

Reflection of acoustic disturbances from wind tunnel walls and their return to the model is a crucial unsteady interference problem. As shown in the previous section, an oscillating model generates unsteady pressure disturbances in the form of travelling acoustic waves which propagate outwards in the tunnel. After being reflected from the walls, these disturbances return to the model causing additional pressure changes there This is in contrast to the Sommerfeld far-field radiation condition which requires a reflection-free propagation of the disturbances to infinity in free atmosphere. **Fig.7.4** shows an airfoil in 2d subsonic flow and the wave fronts from an acoustical disturbance in a uniform flow. It is seen that the velocity of propagation of the pressure disturbance from a point P_0 in the direction normal to the wall is $\sqrt{a_\infty^2 - U_\infty^2}$, and the

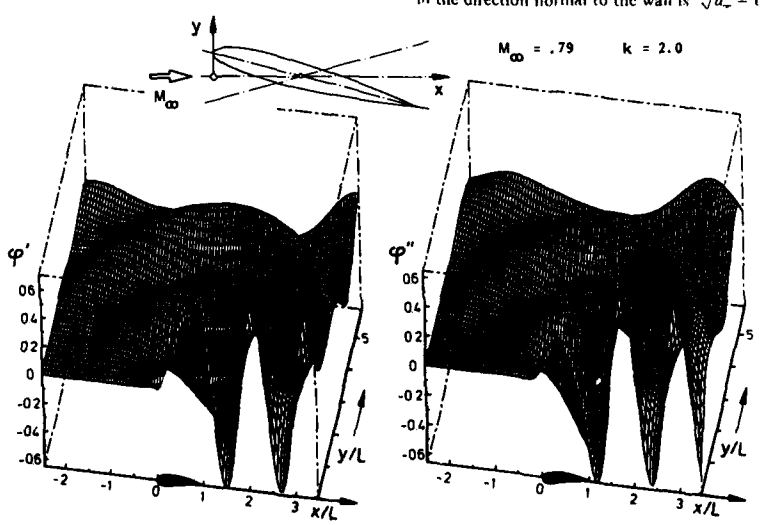

Fig.7.2: Motion-induced unsteady flow field (complex unsteady potential function φ) of an airfoil performing harmonic pitching oscillations about the 0.425-chord axis (φ' = real part, φ'' = imaginary part of φ)

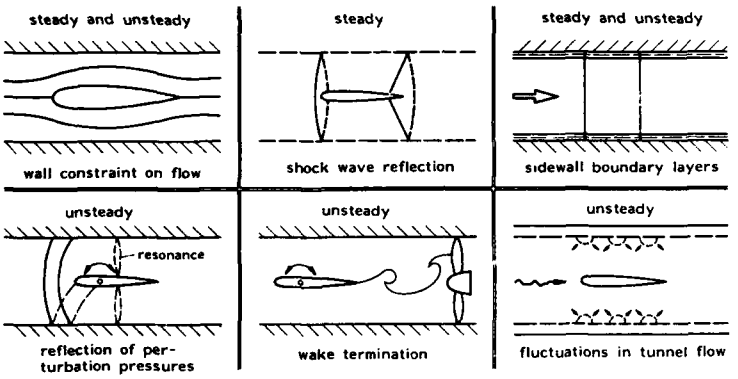

Fig.7.3: Principal causes of wind tunnel interference

time needed for the disturbance to be reflected by the wall and return to P_0 is

$$\Delta t = 2b / \sqrt{a_\infty^2 - U_\infty^2} \approx 2b / \beta a_\infty \quad . \tag{7.8}$$

where b is the distance to the wall. The attenuation of the disturbance by the time it returns to the source will depend on the distance travelled in the moving air which is

$$a_\infty \Delta t = 2b / \beta \quad . \tag{7.9}$$

Thus, the reflected wave when it returns will be weaker (by natural damping), the higher the Mach number. When a disturbance from the oscillating airfoil is reflected from the tunnel wall back to the wing with such a phase relationship that it reinforces, or cancels out, a succeeding disturbance and hence the pressure changes currently occuring on the model, then we have the case of acoustic resonance. This certainly is the most severe unsteady wall interference problem, first described in Ref.[7.13] and experimentally verified in Ref. [7.14] . For solid walls, that do not change the phase of the wave on reflection, the resonance circular frequency is

$$\omega_n = (2n - 1)\, \pi\, U_\infty \frac{\beta}{M_\infty} \frac{1}{2b} \quad , \quad n = 1, 2, \ldots \quad . \tag{7.10}$$

For open jet boundaries the phase change on reflection is π , so that

$$\omega_n = 2n\, \pi\, U_\infty \frac{\beta}{M_\infty} \frac{1}{2b} \quad , \quad n = 1, 2, \ldots \quad . \tag{7.11}$$

For a tunnel with ventilated walls, theoretical expressions for the resonance frequencies depending on wall porosity, depth of plenum chamber and Mach number are given in Ref. [7.15] . In the case of resonance, where the disturbances form a standing wave pattern, the normal velocity has a maximum amplitude and the pressure has a node, i. e. is of zero amplitude at the position of the oscillating airfoil. Accordingly, the unsteady airloads on the oscillating airfoil will vanish at resonance. A typical example is shown in **Fig.7.5** . Whereas for incompressible flow $(M_\infty \to 0)$ there is no tunnel resonance - the resonance frequency decreases with increasing Mach number - and since it tends to zero as $M_\infty \to 1$, the predicted resonance frequency must coincide with a test frequency for some intermediate Mach number causing dramatic changes in the magnitude and phase of the unsteady lift on the oscillating model. Fortunately at the higher Mach numbers there are influences to reduce these effects. Even for strong reflections from solid walls, the effective air distance travelled increases with Mach number and the reflections thus become more attenuated. Also, the reflected disturbances travel more with the flow than across it, see **Fig.7.4** . Furthermore, for transonic conditions, when the resonance frequencies are low enough, the (adapted) walls in typical transonic wind tunnels will be perforated or slotted and the reflections thus more diffuse and attenuated.

In a free atmosphere an oscillating model would leave behind an oscillating wake the vorticity distribution of which is consistent with the unsteady flow at the model. If in a tunnel this wake is affected by a tunnel shock wave, the driving fan or a near tunnel corner, the unsteady aerodynamic loading at the model may be notably influenced. There are reasons to suggest that this source of unsteady interference is of considerable importance in certain special cases of low flow speed and less important in transonic flow.

Finally, various types of flow fluctuations, often described collectively as *tunnel noise*, can have several unwanted effects, particularly in aeroelastic model investigations. One of the principal sources of noise in transonic tunnels is the flow over ventilated walls. It is possible to reduce the noise from this source by covering the perforations with gauze cloth and to apply sound-absorbing material to the tunnel walls, as shown in Ref.[7.16] .

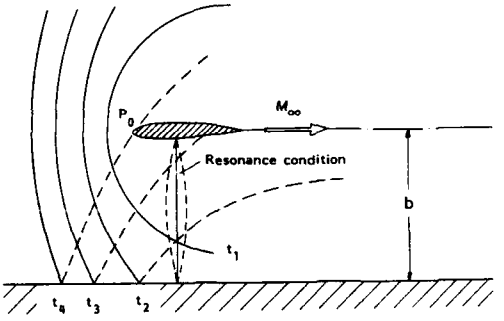

Fig.7.4: Positions of wave front from a disturbance at P_0 and reflection of acoustic waves from a wall

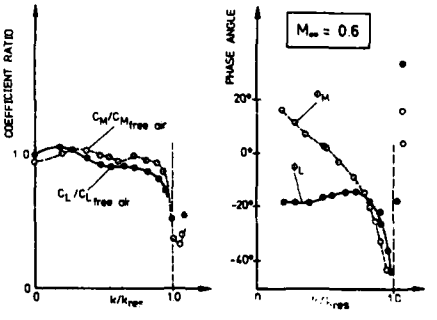

Fig.7.5: Resonance in a solid wall test section (adapted from Ref.[7.14])

7.4 Application of Adaptive Wind Tunnel Walls in Unsteady Flow

From the preceding explanations we have seen that the following wind tunnel interference effects, due to an unsatisfactory test environment, are of main concern in unsteady aerodynamic and aeroelastic experiments with oscillating models:

1. interference of the steady base flow field by steady wall constraints, including shock wave reflections in transonic flow,
2. interference of the (superimposed) motion-induced unsteady flow field by wall constraints,
3. reflection of the model-generated acoustic disturbances by the walls,
4. acoustic tunnel resonance in the test section.

With regard to the application of adaptive wind tunnel wall concepts to eliminate or significantly reduce these wall interference effects in unsteady flow measurements, the following statements can be made.

Ad 1: Practicability and feasibility of wall adaptation for steady flow have already successfully been demonstrated, as shown in the previous chapters.

Ad 2: Unsteady wall adaptation can be realized, at least theoretically, in the same way as for steady flow conditions. However, enormous technical effort is mandatory even for 2d-measurements. Unsteady wall adaptation would require oscillatorily moving flexible walls, where the motion of the walls and the wall contours would depend on the frequency and vibration mode of the model, on the model amplitude of oscillation and on certain phase relationships with respect to the motion of the model. Streamlining algorithms for such a non-stationary wall adaptation, even for the simplest case of non-flexible (rigid body) oscillations of the model, would be very difficult to establish. 3d adaptive walls lie beyond the realm of practicability.

Ad 3: Elimination would demand basically the same techniques and requirements as for nonadaptive walls, i. e. ventilated walls to diminish the reflections and a model-to-tunnel size-ratio as small as possible.

Ad 4: Remains essentially unaffected by adaptive walls and cannot completely be eliminated by any type of tunnel wall.

Summarizing it can be stated that the elimination or at least reduction of unsteady wind tunnel wall interference by means of adaptive walls is extremely difficult to realize, if at all possible. Unsteady wall adaptation, therefore, cannot be considered to be a reasonable means to overcome this problem. However, since unsteady aerodynamic processes may also strongly be affected by steady flow wall interferences, particularly in the transonic flow regime, avoidance of steady flow wall effects by application of steady flow wall adaptation will also significantly improve the results of unsteady wind tunnel measurements, as demonstrated by Kuczka [7.17] and shown in **Fig.7.6.** He obtained some satisfactory agreements between results from a tunnel with steady adapted closed walls and results from tunnels with perforated walls for the in-phase-component of unsteady lift and moment coefficients. However, the corresponding out-of-phase components disagree, even for low reduced frequencies. They are especially affected by reflections of model-generated disturbances from the walls, because they are i.g. smaller than in-phase-components. In addition, the wall reflected disturbances are phase shifted with respect to the model oscillations.

Thus, steady wall adaptation is a necessary prerequisite for obtaining interference-free unsteady results. These, however, still have to be corrected for unsteady tunnel wall effects. Kuczka applied a simple correction method to model the influence of reflections from closed tunnel walls on low frequency unsteady test results [7.17] of low aspect ratio models.

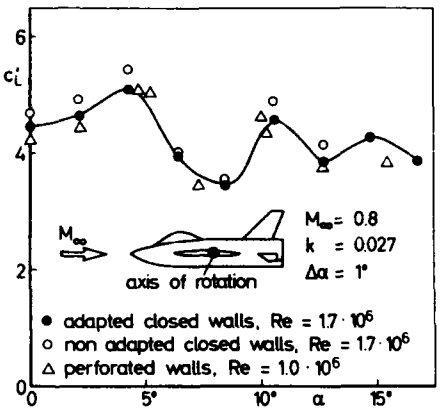

Fig.7.6: In-phase-component c_L' of unsteady lift coefficient of a harmonically oscillating model ("Standard Dynamics Model") with and without steady closed tunnel wall adaptation and with perforated walls (adapted from Ref.[7.17])

In general, more sophisticated correction methods are needed. In order to model unsteady wall boundary conditions in such methods, unsteady pressure data should also be measured at the walls. Indeed, the application of adaptive walls to minimize interference from steady flow wall constraints, together with the application of CFD-techniques which take into account unsteady wall pressure data from experiments to describe precise wall boundary conditions, is most promising in deriving corrections for wind tunnel wall interferences in unsteady flow. Prospects and concepts for such hybrid wind tunnel wall *correction* techniques are outlined in the following.

7.5 Wind Tunnel Wall Corrections for Unsteady Flow Applying Steady Wall Adaptation and CFD-Techniques

7.5.1 Prediction Methods for 2D Unsteady Wall Interference

Analytical predictions of wall effects on unsteady pressures and airloads require exact knowledge of the wall boundary conditions. Only three types of boundary conditions are well-defined, namely those of solid (closed) walls, free jet and of prescribed unsteady wall pressure distributions (known from experiment). Porous or slotted walls can be simulated only approximately by mixed boundary conditions including free parameters. Until now systematic theoretical studies of unsteady wall effects have only been carried out for 2d airfoils oscillating in subsonic and supersonic flow. As wind tunnel tests with oscillating models are performed primarily for aeroelastic purposes, wind tunnel interference effects have to be studied within a wide range of Mach numbers, oscillation modes and reduced frequencies.

For 2d subsonic flow in one of the first systematic analytical investigations on wind tunnel wall effects, based on Eq.(7.1) Bland [7.7] derived an integral equation relating the downwash w (prescribed by the harmonic motion of the airfoil) to the induced unsteady pressure jump δp at the airfoil:

$$w(x) = \int_0^1 K(\bar{x} - \bar{\xi},\ M_\infty,\ k)\ \delta p(\bar{\xi})\ d\bar{\xi} \quad . \qquad (7.12)$$

This is an extension of Possio's integral equation [7.18] , which is valid for free stream conditions. Bland derived the rather complicated kernel K by Fourier transformation, including tunnel wall boundary conditions to be automatically fulfilled on infinitely extended walls in the general form

$$p \pm c_w \frac{\partial p}{\partial y} = 0 \quad , \quad \text{at} \quad y = \pm h \left\{ \begin{matrix} \text{upper} \\ \text{lower} \end{matrix} \right\} \text{walls} \quad , \qquad (7.13)$$

where c_w denotes a specific wall parameter. The limiting cases of solid walls and free jet are included in (7.13), when

$$c_w = 0 \;\rightarrow\; p = 0 \;\rightarrow\; \varphi = 0 \text{ (free jet)}\,, \qquad c_w = \infty \;\rightarrow\; \partial p/\partial \bar{y} = 0 \;\rightarrow\; \partial\varphi/\partial\bar{y} = 0 \text{ (closed wall)}\,. \tag{7.14}$$

(see also Chapter 6).

Thus, the effects of ventilated walls are described by certain values of c_w, but the dependence of c_w upon the kind of walls, their opening ratio and perhaps Mach number and reduced frequency is unclear and would have to be studied systematically by comparison with experiments.

Bland's method was completed by Fromme and Golberg [7.8, 7.9], who improved the numerical performance of the solution method and extended it to general oscillation modes, including flap motions. They obtained results showing clearly the unsteady wall effects, especially the sharp drops in magnitude of the loads and their phase jumps in the case of acoustic resonance, see **Fig.7.7**. Wall effects are significant in the whole frequency regime and wall-influenced loads are bigger/smaller than the corresponding free stream values for closed/open walls, which is well-known for steady or quasi-steady flow. In particular, the strong changes in phase deserve special attention.

This numerical method provides exact reference results, but it is restricted to 2d flows and to the regime of linear compressibility, i. e. constant Mach number in the whole flow field. It hardly appears possible to extend this method to 3d or transonic flow.

The following numerical approach, elaborated recently at DLR/Göttingen and to be published in Ref.[7.19], is more flexible. It is also based on the 2d linear Eq.(7.1), but can be extended to 3d and even transonic flow as shown later. Within the framework of linearised unsteady theory (small amplitudes of oscillation) the position of the airfoil, its wake and the walls may be assumed to be approximately parallel to the x-axis, see **Fig.7.1**. The airfoil is located midway between the tunnel walls, a distance h away from them. Then, as fully described in Ref.[7.19], this 2d boundary value problem can be solved by application of Green's theorem:

$$\varphi(\bar{x},\bar{y}) = \oint_C \left(\psi\,\frac{\partial\varphi}{\partial n} - \varphi\,\frac{\partial\psi}{\partial n}\right) ds = 0 \quad . \tag{7.15}$$

Here,

$$\psi = \frac{1}{4i}\,H_0^{(2)}(\lambda r) \quad , \quad r = \sqrt{(\bar{\xi}-\bar{x})^2 + (\bar{\eta}-\bar{y})^2} \quad , \tag{7.16}$$

is Green's function which satisfies Equation (7.6) and Sommerfeld's far-field radiation condition according to Eq.(7.7). The integration contour C and the integration path s run along the boundaries of the control volume and along those boundaries where φ is discontinuous, see **Fig.7.8**. For free flight conditions, infinite boundaries have no effect. Thus, only the profile contour and the wake line have to be taken into account. For flows in a wind tunnel the integration path also has to run along the tunnel walls. As a final result one obtains an analytical relationship between the downwash w at the airfoil, which is prescribed by the airfoil's oscillatory motion, and the unsteady potential value f and the normal unsteady velocity component g at the walls,

$$\left.\begin{aligned} w &= \partial\varphi\,/\,\partial\bar{y} \quad \text{at the profile}\,, \\ f &= \varphi \qquad\quad \text{on the walls}\,, \\ g &= \partial\varphi\,/\,\partial\bar{y} \quad \text{on the walls}\,, \end{aligned}\right\} \tag{7.17}$$

in terms of the following set of integral equations:

$$\left.\begin{aligned} w &= A\,\delta\varphi + A_1 f + A_2 g \quad , \\ f &= B_0^{-1}\,(B\,\delta\varphi + B_1 g) \quad , \\ g &= C_0^{-1}\,(C\,\delta\varphi + C_1 f) \quad . \end{aligned}\right\} \tag{7.18}$$

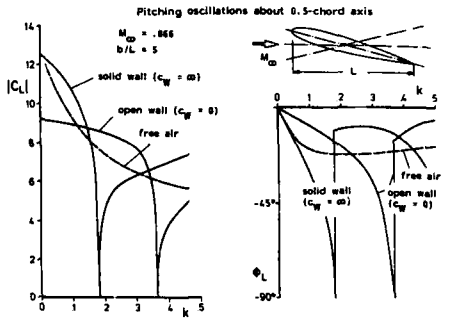

Fig.7.7: Lift coefficient $|c_L|$ and phase angle ϕ_L of an airfoil performing harmonic pitching oscillations about the 0.5-chord axis in the case of acoustic resonance (adapted from Ref.[7.8])

These equations relate the downwash distribution w to an unknown dipole distribution $\delta\varphi$, which provides the unsteady pressure jump at the airfoil by taking the unsteady flow values f and g at the windtunnel walls into account. A, A_1, A_2, B_0, B, B_1 and C_0, C, C_1 are known integral operators (kernel functions).

For the numerical solution of (7.18) the wing profile and the walls are divided into line elements (panels) on which w, $\delta\varphi$, f, g are approximated constant for each discrete step. The dipole strength in the wake in subsonic flow is approximated by the values near the trailing edge and by use of the Kutta condition. Since the unsteady potential function, especially downstream of the airfoil, decreases only slowly, see **Fig.7.2**, the control area of the integral equation should be extended over several chords (at least 10 upstream and 10 downstream, as numerical tests have shown). Applying this panel technique, or any other straight-forward CFD-technique for the numerical solution of Eqs.(7.18), the latter will be transferred to a corresponding system of linear algebraic equations, where A, A_1, A_2, B_0, B, B_1, C_0, C, C_1 are now the known aerodynamic influence coefficient matrices replacing the integral operators, and where w, $\delta\varphi$, f, g are now column vectors of the corresponding values at the airfoil and at the wall control points. For the cases of solid and open walls, Eqs.(7.18) simplify to the closed forms,

$$\left.\begin{aligned} &\text{solid walls}: \quad g = 0 \;\rightarrow\; w = (A + A_1\,B_0^{-1}\,B)\,\delta\varphi\,, \\ &\text{open walls}: \quad f = 0 \;\rightarrow\; w = (A + A_2\,C_0^{-1}\,C)\,\delta\varphi\,. \end{aligned}\right\} \tag{7.19}$$

from which the (wall-affected) potential jumps $\delta\varphi$, and hence the related unsteady pressures, can be calculated for a prescribed downwash w, i. e. oscillatory motion of the airfoil.

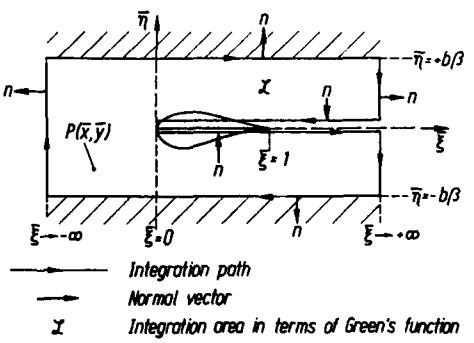

Fig.7.8: Integration path and integration area applying Green's theorem for the solution of Eq.(7.1)

In **Figs.7.9 - 7.11** some typical results obtained from this numerical method are illustrated. **Figs.7.9 and 7.10** show the wall-influenced and free stream pressure jumps in terms of the non-dimensional complex unsteady pressure coefficient $\Delta c_p = (p_{upper} - p_{lower})/(q_\infty \cdot \Delta\alpha)$ (with q_∞ = free stream dynamic pressure and $\Delta\alpha$ = pitching amplitude) on a 2d plate, performing harmonic pitching oscillations about the 0.425-chord axis, and on an oscillating flap for the same Mach number M_∞, reduced frequency k and wall distance h/l. . Again it can be seen that solid walls increase the loads while open walls produce the opposite effect. **Fig.7.11** shows the pressure jump Δc_p for the same conditions as in **Fig.7.9** , except that the reduced frequency has been changed so that it is close to the first solid wall resonance frequency. It can be seen that both the real part $\Delta c_p'$ and the imaginary part $\Delta c_p''$ are nearly zero.

7.5.2 Application of Numerical Methods for Correction of 2D Experimental Results

If it is possible to measure the unsteady wall pressure distributions during the test, they can be used to correct the wall-influenced unsteady pressure data at the model to corresponding freestream values. Such wall pressure measurements are a basic requisite in all steady flow adaptive wall concepts. In this case unsteady wall pressure data (in amplitude and phase) can also readily be measured. Then the afore-mentioned numerical correction technique can be applied in the way described in Ref.[7.19] as follows.

From the experimental unsteady (harmonic) wall pressure distributions c_p^w the corresponding potentials φ^w at the walls can be obtained from

$$c_p^w = -2\left(\varphi_{\bar{x}}^w + i\,\frac{k}{\beta^2}\,\varphi^w\right) e^{ik\bar{t}} \qquad (7.20)$$

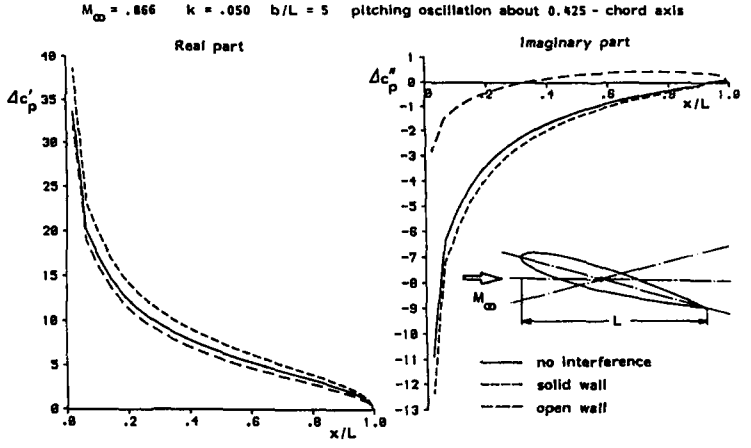

Fig.7.9: Complex unsteady pressure coefficient Δc_p of an airfoil performing harmonic pitching oscillations about the 0.425-chord axis at different wall conditions

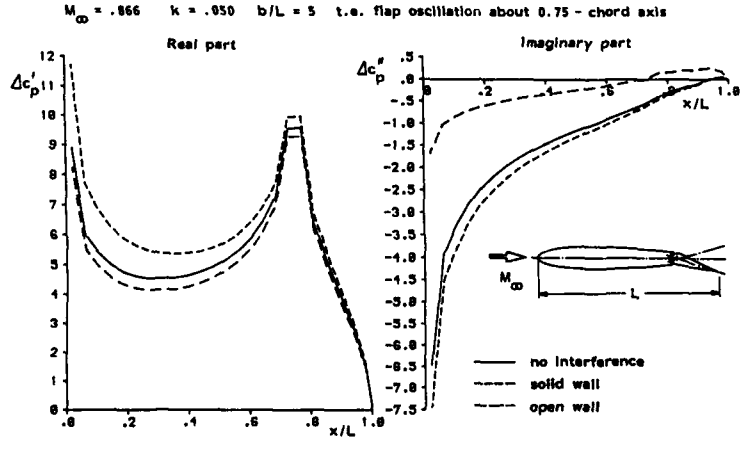

Fig.7.10: Complex unsteady pressure coefficient Δc_p of an airfoil with harmonically oscillating flap at different wall conditions

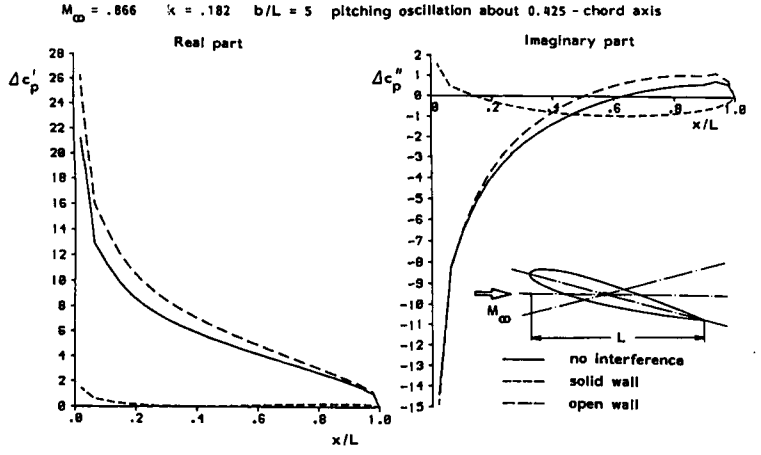

Fig.7.11: Complex unsteady pressure coefficient Δc_p of an airfoil performing harmonic pitching oscillations about the 0.425-chord axis at a reduced frequency k close to the first solid wall resonance condition

and hence

$$\varphi^W = -\frac{1}{2}\int_{-\infty}^{\bar{x}} c_p^W(\bar{\xi})\ \exp\left[i\left(k\bar{\xi} - \frac{k}{\beta^2}\bar{x}\right)\right] d\bar{\xi} \quad . \tag{7.21}$$

The wall pressures have to be measured at enough points upstream and downstream of the model within the area of integration. Then, from Eqs.(7.18), one obtains an integral equation for the wall-affected dipole distribution $\delta\varphi^*$ on the model:

$$(A + A_2 C_0^{-1} C)\,\delta\varphi^* = w - (A_1 + A_2 C_0^{-1} C_1)\,\varphi^W \quad , \tag{7.22}$$

or

$$A_1^*\,\delta\varphi^* = w - A_2^*\,\varphi^W = w - w^W \quad . \tag{7.23}$$

It can be seen that the wall effects change the downwash and the kernel of the integral equation, compared to the corresponding free stream equation

$$A\,\delta\varphi = w \quad . \tag{7.24}$$

Substition of Eq.(7.24) in (7.23), finally, yields the following integral equation:

$$A_1^*\,\delta\varphi^* = A\,\delta\varphi - A_2^*\,\varphi^W \quad , \tag{7.25}$$

in which the kernel functions (influence coefficient matrices) A, A_1^* and A_2^* are known from theory; $\delta\varphi^*$ (and hence Δc_p^*) on the model and φ^W at the wind tunnel walls (see Eq.(7.21)) are known from experiment. Thus, Eq.(7.25) can be used for correction of the measured wall-influenced Δc_p^*-distributions on the model in order to obtain the corresponding free stream values $\delta\varphi$ or Δc_p, respectively. Numerical solution of Eq.(7.25) can again be performed by means of CFD-techniques.

It should be mentioned that Sawada [7.12] arrived in his correction technique, where he also applied Green's theorem, at a formulation similar to Eq.(7.25). The advantage of his approach is, that the pressure distributions at the walls and at the model appear directly in his integral equations. But the kernels of these equations are rather complicated functions. The results he obtained are encouraging for low frequencies but are not as good in the vicinity of the resonance frequencies. Nevertheless, for 2d subsonic flow, this could be a promising unsteady wall correction procedure, but an extension to 3d and transonic flow and to more complicated (elastic) mode shapes of the oscillating model appears to be extremely difficult. Finally, for the sake of completeness, it should be mentioned that Jones in his 2d correction technique, see Ref.[7.20], took the walls into account by an infinite series of image singularity distributions by which he derived a correction technique for wall interference in subsonic flow.

7.5.3 Extension to 2D Transonic Flow

An extension of the correction method described in Ref. [7.19] to 2d transonic flow is possible, if

a) the unsteady flow field may still be treated as a small harmonic disturbance of the steady transonic flow field (i.e. small amplitude of harmonic oscillations),

b) the steady transonic flow field is well adapted (no steady wall interference) and known and the extension of supersonic regions in the wind tunnel test section is significantly smaller than the wall distance from the model.

From a) it follows, that the unsteady flow may be described by a complex velocity potential amplitude function ϕ which is governed by the time linearised TSP-equation (7.2). Then, for harmonic oscillations according to Eq.(7.3) and applying the transformations expressed by Eqs.(7.4) and (7.5), the TSP-equation (7.2) takes the form of an inhomogeneous Helmholtz equation:

$$\begin{aligned}\varphi_{\bar{z}\bar{z}} + \varphi_{\bar{y}\bar{y}} + \lambda^2\varphi &= \\ &= \left(\frac{\partial}{\partial\bar{x}} + i\varepsilon\right)\left((\gamma+1)\,\frac{M_\infty^2}{\beta^2}\,\phi_{\bar{x}}^0\,(\varphi_{\bar{x}} + i\varepsilon\,\varphi)\right) \\ &= S(\varphi) \ .\end{aligned} \tag{7.26}$$

A direct integral equation method for the solution of this equation under free stream conditions is described in Ref. [7.21]. This numerical computation technique can equally be applied to provide corrections for 2d unsteady transonic wall effects, where a wall-interference-free steady transonic flow (by application of adaptive walls) would be a prerequisite. **Fig.7.12** shows the region of integration for this transonic boundary value problem. The additional near-field control area B comprises the local supersonic regions and can be represented by a rather limited number of additional unknowns. Then, an integral equation problem can be formulated for closed walls as well as for the free stream condition, and hence for their difference, which is the potential of the desired correction:

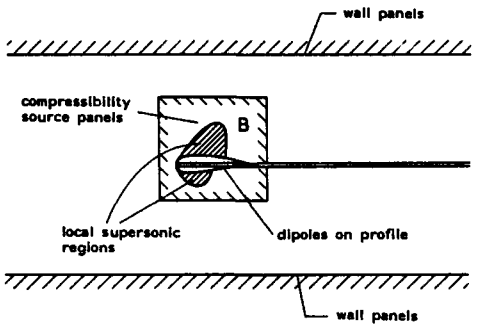

Fig.7.12: Region of integration for the solution of the transonic 2d boundary value problem including the additional near-field control area B

$$\int_0^\infty \delta(\varphi - \varphi')\,\psi_{\bar{n}}\,d\bar{\xi} - \int_B\int S(\varphi - \varphi')\,\psi_{\bar{\eta}}\,df = = -\int_{-\infty}^{\infty} \varphi^w\,\psi_{\bar{n}}\,d\bar{\xi} \tag{7.27}$$

on the profile and

$$\int_0^\infty \delta(\varphi - \varphi')\,\psi_{\bar{n}}\,d\bar{\xi} + (\varphi - \varphi') - \int_B\int S(\varphi - \varphi')\,\psi\,df = = -\int_{-\infty}^{\infty} \varphi^w\,\psi_{\bar{\eta}}\,d\bar{\xi} \tag{7.28}$$

in field control points of B, where φ' denotes the free stream disturbance potential. Eqs.(7.27) and (7.28) can be solved by the numerical method described in Ref.[7.21]. For ventilated walls the integral equation would also contain normal velocity terms at the walls. These terms would have to be eliminated by mixed boundary conditions as formulated in Eq.(7.13) by introducing the unknown wall parameter c_w.

7.5.4 Extension to 3D Problems and Application of Finite Difference Methods

In Ref.[7.22] Garner et alii developed a 3d correction method for ventilated tunnel walls by describing the wall influences through an infinite series of images of the vortex distributions representing the model. This method has been modified in Ref.[7.17] for closed walls, and its applicability was controlled by comparing calculated and experimental pressure data at the walls. Both methods are restricted to low aspect ratio models and to low reduced frequencies (quasi-steady flow).

3d wall correction by application of the integral equation method described in the previous sections for 2d flow will need a great number N of panels for representation of the walls (typically several hundred), thus demanding vast computer storage space ($\sim N^2$) for the calculation of the aerodynamic influence coefficients and long computing time ($\sim N^3$) for inversion of the influence matrices.

A significant simplification, especially for complex wind tunnel models, might be possible by neglecting in Eqs.(7.27) and (7.28) those terms which simulate the model. In Ref.[7.23] Ashill and Keating have shown for steady subsonic wall interference that this simplification is justified if equivalent free stream velocities and model shapes can be defined. An alternative would be the use of finite difference methods. But in this case, the formulation of the unsteady problem in terms of the Helmholtz equation is not adequate because it would introduce severe numerical difficulties. In Ref.[7.24] it has been shown, that for finite difference solution of Eq.(7.6) or Eq.(7.26) a limited upper reduced frequency exists. Relaxation methods converge only below this limit. For the wind tunnel problem its value just equals the lowest tunnel resonance frequency.

This difficulty can be overcome by formulation of the problem in the time domain (such as Eq.(7.1) and Eq.(7.2)) and then application of ADI-solution methods. Assuming again validity of a linearised unsteady potential equation (subsonic or transonic time linearisation), the difference between free stream and wind tunnel flow also satisfies this equation. For example in 2d subsonic flow the potential correction $(\phi' - \phi)$, based on Eq.(7.1), is:

$$\frac{\partial^2}{\partial \bar{x}^2}(\phi' - \phi) + \frac{\partial^2}{\partial \bar{y}^2}(\phi' - \phi) - - 2\frac{M_\infty^2}{\beta^2}\frac{\partial^2}{\partial \bar{x}\,\partial T}(\phi' - \phi) - - \frac{M_\infty^2}{\beta^2}\frac{\partial^2}{\partial T^2}(\phi' - \phi) = 0 \quad . \tag{7.29}$$

While boundary conditions at the model are unchanged by wall effects, thus yielding zero downwash for the potential correction, the other boundary conditions have to be formulated carefully. For the free stream case non-reflecting boundary conditions, as given in Refs.[7.25] and [7.26], have to be used at the walls as well as on upstream and downstream boundaries. For the subsonic problem these boundary conditions read:

$$\frac{\partial \phi'}{\partial \bar{y}} \pm \frac{M_\infty^2}{1 - M_\infty^2}\frac{\partial \phi'}{\partial T} = 0 \quad , \quad for\ \bar{y} \gtrless 0 \quad . \tag{7.30}$$

For closed tunnel walls we have:

$$\frac{\partial \phi}{\partial \bar{y}} = 0 \quad , \quad \phi = \phi^w \text{ (experimental)} \quad .$$

This yields the following boundary conditions for the correction potential $(\phi' - \phi)$:

$$\frac{\partial}{\partial \bar{y}}(\phi' - \phi) \pm \frac{M_\infty^2}{1 - M_\infty^2}\frac{\partial}{\partial T}(\phi' - \phi) = = \pm \frac{M_\infty^2}{1 - M_\infty^2}\frac{\partial \phi^w}{\partial T} \tag{7.31}$$

at walls.

It is clear that such 3d unsteady wall correction techniques based on experimentally determined wall boundary conditions may presently appear rather prospective. However, with the further development of 3d adaptive wall concepts together with further improvements in CFD methods, such hybrid wind tunnel wall correction techniques may soon reach maturity.

7.6 Concluding Remarks

Adaptive wind tunnel walls, already successfully applied to eliminate steady flow wall interference, cannot readily be applied in the same manner to (motion-induced) unsteady flow fields. Even in the case of 2d unsteady flow, wall adaptation would require tremendeous technical effort: 3d adaptive walls for unsteady flow fields lie beyond the realm of practicability. However, as unsteady aerodynamic processes may also strongly be affected by steady flow wall interference, application of steady flow wall adaptation would also considerably improve unsteady aerodynamic wind tunnel test results. Thus, steady flow wall adaptation with the possibility to also measure (after the steady flow adaptation) unsteady wall pressure data, together with the application of advanced CFD-techniques which take the measured unsteady wind tunnel wall data into account in formulating precise tunnel wall boundary conditions, is most promising in the development of new numerical techniques for correction of wall interference in unsteady flow. Elaboration of such hybrid correction techniques, and their experimental verification by corresponding systematic wind tunnel measurements, is a challenging field of future aerodynamic research. It would contribute substantially to a new generation of advanced wind tunnel technology.

7.7 References

[7.1] Mokry,M.; Chan,Y.Y.; Jones,D.J. *Two-Dimensional Wind Tunnel Wall Interference. Chapter 8. Unsteady Wall Interferences.* AGARDograph No.281 (1983), pp.131-158.

[7.2] Lambourne,N.; Destuynder,R.; Kienappel,K.; Roos,R. *Comparative Measurements in Four European Wind Tunnels of the Unsteady Pressures on an Oscillating Model (The NORA Experiments).* AGARD Report No.673 (1980).

[7.3] Moore,A.W.; Wight,K.C. *An Experimental Investigation of Wind-Tunnel Wall Conditions for Interference-Free Dynamic Measurements.* ARC R&M 3715 (1969).

[7.4] Landahl,M.T. *Unsteady Transonic Flow.* Pergamon Press (1961).

[7.5] Lambourne,N. *Wind Tunnel Wall Interference in Unsteady Transonic Testing.* AGARD VKI Lecture Series 1981-4 (1981).

[7.6] Bergh,H.; Zwaan,R. *Present Status of Unsteady Aerodynamics for Lifting Surfaces.* AGARD CP 46 (1970).

[7.7] Bland,S.R. *The Two-Dimensional Oscillating Airfoil in a Wind Tunnel in Subsonic Flow.* SIAM J. Appl. Math., Vol.18 (1970), pp.830-848.

[7.8] Fromme,J.A.; Golberg,M.A. *Unsteady Two-Dimensional Airloads Acting on Oscillating Thin Airfoils in Subsonic Ventilated Wind Tunnels.* NASA CR 2967 (1978).

[7.9] Fromme,J.A.; Golberg,M.A. *Aerodynamic Interference Effects on Oscillating Airfoils with Controls in Ventilated Wind Tunnels.* AIAA J., Vol.18 (1980), pp.417-426.

[7.10] Garner,H.C. *Theoretical Use of Variable Porosity in Slotted Tunnels for Minimizing Wall Interference on Dynamic Measurements.* ARC R&M 3706 (1971).

[7.11] Platzer,M.F. *Wind Tunnel Interference on Oscillating Airfoils in Low Supersonic Flow.* Acta Mechanica, Vol.16 (1973), pp.115-126.

[7.12] Sawada,H. *A New Method of Estimating Wind Tunnel Wall Interference in Unsteady Two-Dimensional Flow.* NRC No.21274 (1983).

[7.13] Runyan,H.L.; Watkins,C.E. *Consideration on the Effect of Wind Tunnel Walls on Oscillating Air Forces for Two-Dimensional Subsonic Compressible Flow.* NACA Report 1150 (1951).

[7.14] Runyan,H.L.; Woolston,D.S.; Rainey,A.G. *Theoretical and Experimental Investigation of the Effect on Tunnel Walls on the Forces on an Oscillating Airfoil in Two-Dimensional Subsonic Compressible Flow.* NACA Report 1262 (1955).

[7.15] Mabey,D.G. *Resonance Frequencies of Ventilated Wind Tunnels.* AIAA J., Vol.18 (1980), pp.7-8.

[7.16] Mabey,D.G. *The Reduction of Dynamic Interference by Sound-Absorbing Walls in the RAE 3 ft Wind Tunnel.* RAE TR 77120 (1977).

[7.17] Kuczka,D. *Hybridverfahren für instationäre Messungen in transsonischen Windkanälen am Beispiel der harmonischen Nickschwingung.* DFVLR-FB 88-19 (1988).

[7.18] Possio,C. *L'azione aerodinamica sul profilo oscillante in un fluido compressibile a velocita ipasonora.* L'Aerotechnica, Vol.18 (1938), pp.441-458.

[7.19] Voß,R. *Prediction and Correction of Unsteady Wind Tunnel Wall Effects on Oscillating Airfoils.* DFVLR-FB to appear (1989).

[7.20] Jones,M.A. *Wind-Tunnel Wall Interference Effects on Oscillating Airfoils in Subsonic Flow.* ARC R&M 2943 (1953).

[7.21] Geißler,W.; Voß,R. *Investigations of the Unsteady Airloads with Oscillating Control in Sub- and Transonic Flows.* in: Proc. 1st Int.Symp.on Aeroelasticity, DGLR Report 82-01 (1982).

[7.22] Garner,H.C. *The Theory of Interference Effects on Dynamic Measurements in Slotted-Wall Tunnels at Subsonic Speeds and Comparisons with Experiment.* ARC R&M 3500 (1968).

[7.23] Ashill,P.R.; Keating,R.F.A. *Calculation of Tunnel Wall Interference from Wall-Pressure Measurements.* RAE TR 85086 (1985).

[7.24] Ehlers,F.E.; Weatherill,W.H. *A Harmonic Analysis Method for Unsteady Transonic Flow and Its Application to the Flutter of Airfoils.* NASA CR 3537 (1982).

[7.25] Engquist,B.; Majda,A. *Radiation Boundary Conditions for Acoustic and Elastic Wave Calculations.* Comm. Pure and Appl. Math., Vol.32 (1979) pp.313-357.

[7.26] Kwak,D. *Non-Reflecting Far-Field Boundary Conditions for Unsteady Transonic Flow Computation.* AIAA J., Vol.19 (1981), pp.1401-1407.

8 Conclusions and recommendations

Editor: H. G. Hornung
Other contributors: All WG12 members

8.1 Summary of the work

A number of recent activities of AGARD's Fluid Dynamics Panel have been related to the assessment or improvement of the accuracy of wind tunnel results [8.1, 8.2, 8.3, 8.4, 8.5, 8.6]. The work documented in this report continues this general effort. The accuracy of wind tunnel simulation in the high subsonic and low supersonic speed range is severely limited by wall interference. It is in this commercially and militarily important speed range that the efforts of adaptive-wall technology have been concentrated. Although adaptive-wall techniques have also been applied to high-blockage and high-lift situations at low speeds, Working Group 12 restricted its attention almost exclusively to the transonic speed range.

The report begins with an historical introduction setting out the aims of adaptive-wall technology and describing the early work and development in the period up to the AGARD meeting in London, October 1975 [8.6]. This marks an important date because the pace of developments increased significantly at about that time.

WG 12 was able to make good use of previous and ongoing activities, such as meetings and reviews of recent years [8.7, 8.8, 8.9, 8.10]. A very important vehicle for the dissemination of new information in the field, the Newsletter "Adaptive Wall," produced by NASA LaRC, provided the opportunity to send out a questionnaire to assess the state of existing facilities as well as adaptation methods and algorithms. This was an essential starting point of the work. The responses to this questionnaire are documented in detail in the Appendix and a description of the facilities is given in chapter 2.

The response to the questionnaire also provided information about the different methods and algorithms for adaptation. These are discussed within the framework of a common theory and notation in chapter 3. The structure of the discussion divides the test section types into four categories according to whether the adaptation is two or three-dimensional and whether the walls are impermeable and flexible or ventilated and rigid. In the case of rigid ventilated walls the interface at which outer and inner flows are matched is necessarily located within the flow field, so that the measurements at the interface (typically static pressure and normal velocity), needed for adaptation, are much more time-consuming and difficult to obtain than in the case of impermeable flexible walls, for which the matching interface is the wall (typically wall static pressure and wall displacement). However, for near-sonic and supersonic free stream flows, perforated walls are still considered to be superior although the position may change as a result of new research.

From the point of view of wall adaptation, it is useful to subdivide the speed range into three groups:

- Group 1: Flows with subsonic free stream, in which locally supersonic regions may occur near the model, but where the walls are in a region well represented by the linearized compressible flow equations.
- Group 2: Flows with subsonic free stream in which the nonlinear regime in unconfined flow would extend beyond the walls.
- Group 3: Flows in which the free stream is supersonic and near sonic.

Most of the algorithm development and most of the experimental work has been in Group 1. Many algorithms exist and it is generally recognized that the wall adaptation may be achieved effectively in one iteration step. This applies equally for two- and three-dimensional flows.

The strategy of wall adaptation for Group 2 flows is an easy extension from the procedure for Group 1 involving only a more laborious computation of the external flow. However, the adaptation may not be achieved in a single step. Much less experimental work has been done in this regime.

Only a small number of investigations have studied the low supersonic flow regime. Typically, experimental work concentrated on the problem of canceling an isolated shock wave that impinges on the wall, by means of wall shaping.

Chapter 3 also presents selected experimental results emphasizing in particular systematic investigations in which experiments were made using the same model in different wind tunnels, or models of different scale in the same wind tunnel. Other critical repeat tests, e.g., with rotation of the test section, or with lateral displacement of the model, are also highlighted. These clearly demonstrate the efficacy of wall adaptation schemes for Group 1 flows and allow the assessment of residual wall interferences or of the quality of adaptation.

Chapter 3 concludes by pointing out that the need for wall adaptation is particularly great in Group 2 flows, because it is these that make conventional techniques (ventilated walls with Wall Interference Assessment and Correction, WIAC) ineffective. Adaptation would render the residual interferences small or at least correctable by WIAC.

Many three-dimensional flows in Groups 1 and 2 produce wall interference distributions that may be canceled almost completely by two-dimensional adaptation. Advantages over three-dimensional adaptation such as better optical accessibility and much-reduced complexity have led to a number of investigations of two-dimensional adaptation for three-dimensional flows. This is the subject of chapter 4. The wall adaptation is used to cancel wall interference along a selected target line within the test section and to determine and correct for the residual wall interference. Only impermeable flexible wall configurations have been used for this type of adaptation.

The various methods and algorithms applied by different research groups are discussed and examples of results presented. Particular attention is given to large aspect ratio wings or wing body configurations. Systematic investigations giving the residual wall interference for high blockage ratio experiments demonstrate the efficacy of this strategy. Typically, the residual wall interference can be reduced to below the minimum non-uniformity achievable in modern wind tunnels. An interesting result is that there are advantages in having a rectangular rather than a square test section.

Chapter 5 discusses the prospects of using adaptive-wall technology in wind tunnels designed for high-productivity industrial testing. The need to acquire data rapidly, e.g., in a continuous angle-of-attack sweep, makes it necessary to use predictive adaptation strategies, as

well as to use extremely fast algorithms and wall control technology to permit live adaptation. The results of this discussion are based on numerical modeling of the situation and some experimental evidence. Chapter 5 concludes that for high-productivity tests up to high subsonic Mach numbers, two-dimensional adaptation of impermeable walls is most desirable. It is essential that a satisfactory *predictive* algorithm be developed. A possible strategy is discussed. For near-sonic free stream conditions ventilated walls remain unrivaled.

Any work on accuracy improvement must compare conventional with new techniques and provide a measure by which to judge the improvement. To this end, Chapter 6 discusses the limits of adaptation in view of residual interferences in comparison with conventional WIAC techniques as well as the development of the latter. Consequently, a large part of chapter 6 is devoted to the discussion of the development of various modern WIAC techniques. It is concluded that in this field there exists a considerable need to validate theoretically well-established techniques for Group 2 flows.

An important limitation of wall adaptation techniques is the effect of the presence of the model on the wall boundary layer. Depending on the flow regime, the effect on the displacement thickness can be quite significant. This is especially true in two-dimensional flows and for wall-mounted half models. In order to correct for this effect, it is necessary to make measurements or at least approximate computations of the side-wall boundary layer. This effect is, of course, not peculiar to adaptive-wall test sections, but, because wall interference effects are dramatically reduced, it plays a more important role among the remaining uncertainties.

Clear advantages of adaptive-wall technology are seen in the much-increased tolerable blockage ratio over that of ventilated walls at the same level of residual interference. This means higher flow quality, much lower drive power, lower residual (and correctable) interference at the same Reynolds number. Perforated walls are still seen to be the best practical method for Group 3 flows.

Chapter 7 considers the possibility of achieving partial adaptation of unsteady flows. After a discussion of theory and experimental results in unsteady transonic flows it is clearly argued that full adaptation is practically impossible. However, initial successes point to a method by which much-improved accuracy can be obtained by adapting for a mean steady flow and measuring the unsteady wall pressure distribution in order to correct for the unsteady component by computational techniques.

8.2 Conclusions and recommendations

The rapid development of the potential of computers and of computational fluid dynamics over the last 25 years has made CFD an equal partner to the traditional wind tunnel simulation in the aerodynamic design and development of aircraft. It has also considerably increased the demand for accuracy of wind tunnel data by the customers of production wind tunnels. The adaptive wall technique represents a significant step towards meeting this demand. It is a prime example of the symbiosis of experiment and computation, a phenomenon of which we are likely to see very many more examples in the future.

From the assessment of the state of the art by WG 12 it has become clear that the adaptive wall technique has been applied successfully in many wind tunnels. The results from these experiments have largely confirmed theoretical expectations, though most of the experiments have been concentrated on Group 1 flows. As regards Group 1 flows, a stage has been reached, at which wall adaptation with impermeable flexible walls can be incorporated with confidence in the design and construction of future wind tunnels both for research and production facilities.

However, a number of open questions remain for future research. These are particularly evident in the areas of adaptation for the upper end of Group 2 flows and in Group 3 flows.

In the flow regimes where the adaptive wall technique has been tested extensively, it provides a number of significant advantages over the conventional approach. In contradistinction to WIAC techniques, it does not require interpretation of the effects of wall-induced disturbances on the nonlinear flow over the model. Residual interferences remain only in the form of linear perturbations on a nonlinear flow. The spatial averages of these can be readily corrected, because the boundary conditions are well-defined by measurements. It is recommended that residual interferences be quantified and expressed in WIAC-like terms. Depending on the constraints of aspect ratio and tunnel width, there is a clear size advantage, blockage ratios of up to 7 times traditional values being tolerable. The power requirements at a given model size are thus dramatically reduced. Furthermore, the power per unit cross sectional area is also reduced with impermeable adaptive walls. Flow quality is increased. Effects due to wall interference may be decoupled from those due to Reynolds number. The productivity of existing automated adaptive-wall wind tunnels compares favorably with that of conventional wind tunnels, because the desired free-stream conditions can be obtained directly, without interpolation, thus minimizing the requirements for test matrix size. While the predictive strategy advocated in chapter 5 requires residual corrections, it does enable testing in continuous sweeps.

8.2.1 Group 1 flows

The technique using impermeable flexible walls is clearly superior to that with rigid ventilated walls, because of the relative speed and accuracy of obtaining measurements on the control surface. Other advantages derive from the smooth wall: Reduced power, increased flow quality.

Incorporation of the flexible adaptive-wall technique is definitely recommended for large-scale wind tunnels designed for two-dimensional testing. The technique using two adaptive walls for three-dimensional flows (see chapter 4) has been tested in several laboratories. It provides a significant improvement over conventional wind tunnels as regards accuracy as well as the advantage of better defined boundary conditions for correction of the residual interferences. The technological difficulties associated with the technique are minor compared with those of three-dimensional adaptation methods. The technology is well proven even in cryogenic conditions in a large number of cycles without maintenance, e.g. T2 (Toulouse), TCT (LaRC).

A new wind tunnel for this category is recommended to incorporate two flexible adaptive walls in its design.

8.2.2 Group 2 flows

Much less experience has been obtained in this area. The work accomplished both with impermeable flexible and with perforated rigid walls indicates that more experience is needed, before it is possible to make definite recommendations committing funds to a production fa-

cility. The perforated rigid wall technique is far from being practicable in this regime, and with impermeable walls the difficulty of reducing reflections of non-planar shocks from the wall, though partially successful in isolated experiments, requires extensive further work. Especially in two-dimensional and half-model testing, the side wall boundary layer becomes very important because of the effects of the shock wave on it (though this is not an effect peculiar to adaptive walls, as pointed out previously).

Based on results so far, it is recommended to test models at a small enough size to make the flow a Group 1 flow if possible. This recommendation is conservative in the sense that current research work may well provide acceptable solutions to the outstanding problems.

8.2.3 Group 3 flows

In this regime, only few initial results are available, indicating that, provided a very high density of wall adjustment jacks is installed, reflections from the walls may be reduced considerably. However, it is not possible to recommend adaptive wall technology for production wind tunnels with Group 3 flows. As for Group 2 flows, it is recommended to test models at a small enough scale so that no waves are reflected onto the model. Otherwise, it is necessary to continue production testing with conventional perforated-wall testing.

8.2.4 Unsteady flows

Adaptation of the unsteady part of the flow is impracticable. The technique of adapting for the steady component of the flow and measuring the unsteady wall pressure distribution so that the remaining interference can be determined and corrected is most promising, as has already been demonstrated in three-dimensional flow [7.17]. This technique is particularly recommended if nonlinear interactions between steady and unsteady components of the flow are to be expected, e.g. in near-sonic flows for which the non-adapted tunnel would be choked. Further development of this approach is recommended. This method may readily be extended to production use.

8.3 Recommended research areas

There are, of course, many directions in which research might proceed in order to try to provide solutions for the many open questions that remain. Rather than be exhaustive in this section, the Working Group singled out a few particularly important areas. These are

- Systematic inter-tunnel experiments of the same model, including tests in conventional tunnels in order to test quantitatively the advantage provided by wall adaptation and the well-definedness of the boundary conditions. It is recommended that two- and three-dimensional flows be tested.
- Development and demonstration of predictive strategies for use in production type wind tunnels (see chapter 5).
- Further experimental development of adaptive-wall and residual-correction methods for Group 2 flows.
- Further experimental development of adaptive-wall and residual-correction methods for Group 3 flows.
- Application of the recommended technique for unsteady flows in two-dimensional adaptive-wall tunnels for three-dimensional flows.
- Continued development of methods for computing or experimentally reducing the effect of the side-wall boundary layer especially for two-dimensional and half-model testing, equally important for conventional and adaptive-wall tunnels.

8.4 References

[8.1] Wall interference in wind tunnels. AGARD-CP-335, London 1982.

[8.2] Steinle, F., Stanewsky, E. "Wind tunnel flow quality and data accuracy requirements." AGARD-AR-184, November 1982.

[8.3] Mokry, M., Chan, Y.Y., and Jones, D. J. "Two-dimensional wind tunnel wall interference." AGAR-Dograph 281, November 1983.

[8.4] Aerodynamic data accuracy and quality: Requirements and capabilities in wind tunnel testing. AGARD-CP-429, Naples, 1987.

[8.5] Boundary layer simulation and control in wind tunnels: Report of the Fluid Dynamics Panel Working Group 09, 1988, AGARD-AR-224.

[8.6] Wind Tunnel Design and Testing Techniques. AGARD CP 174, October 1975.

[8.7] Two-dimensional transonic testing methods, GARTEUR/TP-011, 1981.

[8.8] Wind Tunnel Wall Interference Assessment/Correction 1983. NASA CP-2319, 1984.

[8.9] Euromech Colloquium: Adaptive-wall wind tunnel and wall interference correction methods, Göttingen, October 1984.

[8.10] Mini conference: Adaptive wind tunnel walls, state of the art. Technische Universität Berlin, 1988.

Appendix

Editor : C. Çıray
Other Contributors : C. Ladson

In order to assess the status and design of the adaptive wind tunnels together with the operation and evaluation procedures throughout the world, a questionnare was designed and sent out with the "Adaptive Wall Newsletter" at an early stage in the duration of the W.G 12.

The questions addressing to the characteristic features of the facility, technology and strategy of adaptation, iteration procedures, flow quality, references related to works accomplished form the material of the questionnaire.

The questionnaire and the answers can be found in the sequel. The answers are reproduced in alphabetical order of name of the Nations and the wind tunnels for a given nation are again ordered in the same manner w.r to the name of the facility.

The questionnaire is added at the beginning of the answers in order to help the reader.

The title page of the "Adaptive Wall Newlesletter" which was used to distribute the questionnaire is inserted in its original format in the following page just to express the appreciation of the W.G 12 to NASA Langley Research Center and to the editor for the wonderful idea of creating a Newsletter on Adaptive Wall Wind Tunnels and helping out with the distribution of the questionnaire.

Thanks are also due to those who have very kindly replied to the questionnaire thus providing information about adaptive wall wind tunnels throughout the wold.

It is hoped that this Appendix will be of some help to disseminate the status of the Adaptive Wall Wind Tunnels and contribute to futher advancements on the subject.

Special Edition Published by Experimental Techniques Branch NASA Langley Research Center **December 1987**

This is a special edition of the Adaptive Wall Newsletter published to acquaint you with the activities of the AGARD Fluid Dynamics Panel regarding adaptive wall wind tunnels. At the request of this panel, Working Group 12, "Adaptive Wind Tunnel Walls: Technology and Applications" was formed in May 1987. The purpose of the group is to review the use of adaptive walls for both two- and three-dimensional testing. Guidance criteria will be established to assist the wind tunnel designer and user. The direction for additional research on the optimization of adaptive walls will also be addressed. The group is comprised of members from Canada, France, Germany, Italy, Netherlands, Turkey, UK, and US.

The first meeting of the group was held in Göttingen, Germany during October 1987. During the course of the discussions, the group decided that the assessment and interpretation of the current level of the technology could be achieved most easily if the investigators themselves provided the information in a common format. This would minimize the dangers of misinterpretation by third parties of information contained in published papers and reports. As a result, a questionnaire has been prepared and is attached to this special issue of the Adaptive Wall Newsletter.

The WG 12 would appreciate responses to the questionnaire from all facilities that have been used for adaptive wall investigations, whether they are currently active or not. The members of the group hope you are willing to participate by completing the questionnaire as fully as you can. All North American responses should be sent to:

Mr. John C. Erickson, Jr. Telephone (615) 454-6691
Calspan Corp./AEDC Division
MS 600
Arnold AFS, TN 37389
USA

All other responses should be sent to:

Dr. J. P. Chevallier Telephone 4657-1160
ONERA
BP 72
F-92322 Chatillon
FRANCE

Please feel free to call either of the above if there are questions you have about the form. Responses to the questionnaire are requested to be mailed by January 31, 1988.

QUESTIONNAIRE

1. Generalities About the Facility

   1.1 Organization, location

   1.2 Person to contact for information (name; position; mailing address; telephone; telex; telefax; ...)

   1.3 Name or other designation of the tunnel

   1.4 Purpose (research, pilot, industrial operation, ...)

   1.5 Current operational status; if inactive, date of most recent use

2. Main Features of the Facility

   2.1 Circuit characteristics (continuous; blowdown; closed or open return; cryogenic; ...)

   2.2 Test section shape and size (metric, please)

   2.3 Mach number, speed range; Reynolds number domain

   2.4 Type of control used

      2.4.a Nature of the wall (impermeable; slotted; perforated; ...)

      2.4.b Means of transverse flow control (wall deformation; plenum pressure, global or segmented; wall porosity, global or segmented; ...)

   2.5 General testing capabilities

      2.5.a 2D or 3D test; model configurations and support

      2.5.b Model, flow field and wall measurement capability (forces; pressures; flow angles; wake surveys; ...)

      2.5.c Time required for adaptation; time required for model data acquisition

3. Technology and Strategy of the Adaptation

   3.1 Data used

      3.1.a Definition of the control surfaces (shape; extent, effective or extrapolated; closure; ...)

      3.1.b Nature, number, position, accuracy, independence, redundancy of the measured parameters used for the entire flow control process; please distinguish among the flow control variables, X, and the control surface flow variables P and Q, (see terms of reference)

      3.1.c Pre-processing of the data (filtering recorded data versus time; smoothing the data versus position; interpolation; extrapolation; ...)

   3.2 External Flow Field Computation

      3.2.a Assumptions (2D; axisymmetric; 3D; periodic;...)

      3.2.b Particular choices of variables used for P and Q (see terms of reference)

      3.2.c Methods of evaluation (analytical; numerical; range of application; e.g., $M < 1$ subritical, $M < 1$ supercritical, $M > 1$; ...)

      3.2.d Output and its relation to the control variables, X, used

      3.2.e Type of computer and CPU time

   3.3 Initialization of Control Variables

      3.3.a Previous test; method of extrapolation, if used when performing an α or M sweep

      3.3.b Computation (method; input required from model definition or measurements)

      3.3.c Configuration representative of test section when used in convectional, passive manner (see also 3.9.d)

   3.4 Iteration process

      3.4.a Summary of choices of variables used (P, Q, and X in terms of reference)

      3.4.b Description of approximations made with respect to the derivation of Eqs. (5) and (8) in terms of reference

      3.4.c Determination of influence functions (experiments; computations; ...)

      3.4.d Relaxation factor choice (number; values; ...)

      3.4.e Prescription and/or determination of the free-stream values (M,α) during and at the completion of the adaptation process

      3.4.f Procedure flow chart

      3.4.g Usual number of iterations to convergence

      3.4.h Automation level of process

   3.5 Criteria for end of iteration loop

      3.5.a Control surface figure of merit; if used, give definition, including weighting

      3.5.b Flow control variable adjustment criteria; if used, describe weighting

      3.5.c Residual interference perturbation level; if used, describe where and how calculated

      3.5.d Model measurements; if used, describe

      3.5.e Fixed number of iterations; if used, give number and rationale

   3.6 Residual interference perturbations

      3.6.a Description of methods and range of application ($M < 1$, $M > 1$; 2D adaptation for 2D tests, 3D adaptation for 2D tests accounting for sidewall boundary layers, 3D adaptation for 3D tests, 2D

adaptation for 3D tests)

3.6.b Use of output (M, α; tables, contour plots, ... of entire perturbation field; ...)

3.7 Scope of testing accomplished

3.7.a Total number of articles tested

3.7.b Characteristics of articles tested; 2D: Description (list of airfoil section designations); blockage; ratio of chord length to test section height; M, α range tested; ...)
3D: Description (body, axisymmetric or not; wing; wing/body; wing/body/tail; ...); blockage; ratio of wing span to test section width; ratio of body length to test section lenght; ratio of total planform area to test section cross-section area; M, α range tested; ...)

3.8 Quality assessment

3.8.a Empty tunnel calibration, including approach to M = 1

3.8.b Overall tunnel flow quality, turbulence level

3.8.c Validation tests, use of calibration models

3.8.d Repeatability, including approach to M = 1 (nature of comparisons; examples; ...)

3.8.e Limitations in M, α versus model size

3.9 Miscellaneous topics

3.9.a Nonstationary testing experience

3.9.b Real gas effects in cryogenic tunnels

3.9.c Boundary-layer and corner flow effects

3.9.d Relationship of unadapted and adapted results to previous results in the same or similar facility with passive walls (see also 3.3.c)

3.9.e Pertinent theoretical or numerical simulations of flow control concepts; correlation of simulations with experiment

3.10 References

3.10.a Published papers listed in the selected bibliography (Tuttle and Mineck; NASA-TM-87639) or in the Adaptive Wall Newsletter updates

3.10.b Other published papers

3.10.c Private communications useful for technological details, historical interest, ...

4. Planned Activity

4.1 New facilities

4.2 Refurbishment of old facilities

4.3 Improvement of methods

4.4 Cooperative and calibration tests

4.5 Routine operational testing

BELGIUM

1.1 VKI, BRUSSELS

1.2 Prof.John F. Wendt, Chaussée de Waterloo 72, 1640 Rhode-Saint-Genese, Belgium

1.3 VKI S1 Wind Tunnel

1.4 Research & Industrial

1.5 Most recent use for wall adaptation: 1982

2.1 Continuous, closed return tunnel.

2.2 0.4 m * 0.4 m

2.3 $0.4 < M < 1.05$ and $1.43 < M < 2.25$
$10^6 < Re < 6*10^6$

2.4.a. solid contoured wall blocks

2.4.b. wall shaping

2.5.a. 3D test; sting mounted model

2.5.b. model pressure distribution

2.5.c. automatic model data acquisition

3.1 Model representation by singularity distribution

3.2 2D Adaptation for 3D Flow: Computation and elimination of wall interferences at the tunnel centreline.

3.2.a. 3D axisymmetric

3.2.b. not applicable

3.2.c. numerical, $M < 1$ subcritical

3.2.d. wall displacement

3.2.e. VAX, cpu-time ≈ 1 sec

3.3.a. n.a.

3.3.b. input required from model definition

3.3.c. Slotted walls

3.4.a. Wall interference assessment by one variable method

3.4.b. n.a.

3.4.c. Theoretical influence function

3.4.d. One step method

3.4.e. Prescription of M,

3.4.f. n.a.

3.4.g. one step

3.4.h. no automation

3.5 only one iteration step

3.6.a. 2D adaptation for 3D test

3.6.b. n.a.

3.7.a. one article tested

3.7.b. 90 mm ogive-cylinder body, 4.4% blockage ratio, body length 1m, M = 0.7

3.8.a. empty tunnel calibration

3.8.b. unknown

3.8.c. none

3.8.d. unknown

3.8.e. unknown

3.9.a. none

3.9.b. none

3.9.c. none

3.9.d. Relation to unadapted results and interference free reference data (smaller model in slotted wall test section)

3.9.e. none

3.10.a. Tuttle and Mineck Nr. 147

3.10.b. VKI Project Report 1981-02 (1981)

3.10.c. -

4.1 -

4.2 -

4.3

4.4

4.5

FRANCE

1.1 ONERA CHALAIS MEUDON

1.2 Andre BETREMIEUX, Head of SR wind tunnels, group OAx6 B.P. 72 92322 CHATILLON Cedex FRANCE
Phone (1) 45 34 75 01 ext 42 54
TELEFAX (1) 45 34 75 01 ext 45 25

1.3 S4LCh - Laboratoire de Mécanique des Fluides

1.4 Research and pilot wind tunnel

1.5 Used for research but inactive concerning the adaptation since 1977

2.1 Continuous, closed return, ambient temperature

2.2 0.225 m * 0.225 m; 0.7 m long

2.3 $0.3 < M < 0.90$
ex : $M = 0.85$ $T = 313$ K $p = 1.15$ b
$R = 1.2\ 10^6$ (model chord 80 mm)

2.4.a. Solid side walls, flexible top and bottom wall.

2.4.b. Wall deflection by ten unequally spaced jacks for each wall.

2.5.a. More generally 2 D with just a short attempt with a 3 D sting mounted model.

2.5.b. On the 2 D models mounted between side walls, pressure measurements were obtained (36 pressure holes on small airfoil model), wake probes and schlieren pictures.
Pressure measurements on the walls and model by scanivalve. The time required for adaptation was very long : for each iteration the computed jacks positions were obtained ; the time required for model and wall pressure data acquisition by scanivalves was comparatively short : with time to transfer the data, to use the time sharing computer, to the wake probing about 20 min. Due to recover the results the first step of adaptation may consume one day in 1974.

3.1.a. Rectangular closed contour for the 2 D control surface : 2 segments near the top and bottom wall (parallel) and two normal segments at the entrance and exit plane of the test section (2.3 C upstream and 2.9 C downstream)

3.1.b. The measured parameters are:
- the 2 * 10 . X_j control variables (jacks position)
- the resulting wall shape measured with an electric comparator (numerical output) with continuous displacement along x axis
- 55 pressure holes on each adaptive wall (5 files, one between two consecutive jacks, one at the end. 10 jacks per file.)
- the accuracy of the position of the controlled points is 0.1 mm
- the data acquisition, with direct digital recording on perforated tape gives general uncertainties of some thousandth.
- all the pressure measurements are not strictly independent by the using of only one transducer with scanivalves.
There are some redundant measurements on the wall shape: jacks position (X) and more or less continuous recording of the wall profile, data being numerically treated to obtain smooth values of the slopes (Q).

3.1.c. There is no filter on the pressures measurements except the natural one due to the comparatively long tubes to the transducer, but the data used is the mean value between the five holes at the same abscissa.

3.2.a. It is assumed that the external flow field is purely 2 D and extended at infinity in all directions around the quasi - rectangular internal flow field.

3.2.b. Q_j is generally the normal component of perturbation on the control surface deduced from the wall slopes corrected for boundary layer displacement thickness computed with th e measured speed distribution, this condition being in fact used on straight lines, near the wall. P_i^m is generally the longitudinal component of the perturbation speed on the wall, deduced from the static and reservoir pressure measurements (and stagnation temperature).

3.2.c. The functional $P_i\ [\ Q_j^m\ ]$ is computed according to the Mach number ($M < 1$ - subcritical) with linear formulation and the Prandtl Glauert transformation to take account for compressibility, the curvilinear integrals are numerically computed, splitting the contour into 4 parts : the real data being used on top and bottom limits and, upstream and downstream interpolated values which give very small contribution.
($M > 1$ supercritical), when some local Mach number is greater than one a small transonic perturbation method is used to numerically obtain $P_i\ [Q_j^o\ ]$ without need for extrapolation of the measured data due to the change of variable $\bar{x} = \text{arctg } x/h$

3.2.e. HP 2100 except for small transonic perturbation code.

3.3 Various initialisations were used during this early period to test the adaptation process.

3.3.a. Start with straight wall diverging by the small angle-accounting for the boundary layer growth. (NACA 64 A OIO . $\alpha = 0$)

3.3.b. With the same aerofoil at $\alpha = 6°$ a computed curvature is added at the shapes previously obtained to eliminate the obstruction effect

3.3.c. To eliminate the obstruction effect a constant area around the airfoil is also a good starting point at small angle of attack. In the same way the theoretical shapes of the wall were computed for an inviscid flow at different distances of the airfoil for the design of the adaptive wall (small transonic perturbation with model definition (fig.3-37-)) An idea of the conventional use of this test section is given with straight wall.

3.4.a. X = jacks position
P = local longitudinal speed related to Mach number deduced from wall pressure measurements
Q = local tranverse component of the speed deduced from the longitudinal one according to the slope.

3.4.b. Despite the fact that some theoretical attemps were made to determine theoretically $\partial Q_k / \partial X_j$

3.4.c. and experimentally $\partial P_i / \partial X_j$ the adjustment process by hand was so much time consuming that linearisation and matrices determination and inversion were not used but we begin to split the X_j distributions according to the ideas applied later in T2

3.4.d. but using at that time only one relaxation factor taking account of the known global sensitivities of the internal and external flow in terms of divergence, enlarging, orientation and curvature of the section and its midline.

3.4.e. It was recognized that the effective Mach number of a given test was more accurately determined by several local values than by one for upstream reference. An arbitrary weighting function (inverse of the square of the distance to model center) was applied to the difference $P_i^m - P_i [Q_j, M] ; M_\infty$ resulting from the minimisation of the sum of these weighted differences with M as variable. It is only after 1977 that a theoretically justified weighting function was applied and that the effective flow direction was determined according to all the local slopes - Before 1975 the flow direction at the infinity was taken as the general direction of the chords of the mid line between the walls.

3.4.f. fig.6 - citation (37)/

3.4.g. iterations according to (37)

3.4.h. Absolutely zero level of automation.

3.5.a. After the minimisation versus M to obtain M_∞, the weighted (by inverse square distances at the test section center) differences summation $\Sigma (P_i^m - P_i [Q_j, M_\infty])$ gives a figure of merit corresponding to a mean value $P_i^m - P_i [Q] < 3.10^{-3} \bar{P}_i$ According to the internal sensitivity of the transonic flow it gives $\Delta X_j / 2h < 10^{-3}$ The technical means used at that time as well for position (before and after but not during the run). Those for pressure measurements are coherent with this matching error.

3.5.b. No residual interferences perturbation level were determined but on a given airfoil. Comparisons were made with a bad or good adaptation to justify the end of the loop criteria $\Delta \bar{X}_j = \pm 0.1$ mm.

3.6 The lack of an easy to use method to compute the residual interference was the real motivation to develop later the CCB method cit. (63)

3.7.a. Two models 2 D

3.7.b. 2 D - NACA 64 A 010
blockage 0,044
chord length / test section height = 80 / 180 = 0.45
M < 0.866 α = 0
M = 0.85 α = 0 and 6°

2 D NACA 0012
blockage : 0.053 chord/t.sh. = 0.45
M < 0.88 α = 0
M = 0.86 α = 4°
3 D. Just a small touch with a wing body model showing how small are the perturbations to be measured.

3.8 Nothing, according to the aim of this first attempt.

3.9.c The corner flows are ignored but the boundary layer displacement variations due to the airfoil perturbation field are taken into account.

3.9.d. Some comparisons were made between pressure distributions on the 64 A 10 airfoil without or with adaptation.

3.10.a. Published papers listed by Tuttle and Mineck (NASA TM 87 639) No 27 - 31 - 35 - 37 - 40 - -56 - 57.

3.10.b. J.P. CHEVALLIER - Soufflerie transsonique autocorrectrice. Paper for Mini Laws Meeting 5 - 6 Sept. 1974.

3.10.c. J.P. CHEVALLIER Correction de parois en transsonique Internal Report ONERA NT 4/1865 AN Jul. 1972.

1.1 CHALAIS MEUDON ONERA

1.2 Yves LESANT, Research Engineer
B.P. 72 92322 CHATILLON Cedex FRANCE
phone (1) 45 34 75 01 ext 44 28

1.3 S5 Ch

1.4 Research wind tunnel with 2 test sections

1.5 Used for research - Adaptive test section is available

2.1 Continuous, closed return, ambient temperature

2.2 0.220 m * 0.180 m ; 0.3 m long

2.3 M = 1.2 T = 315 K P = 0.6 b Re = 7.4510 (ℓ = 1 m)

2.4 Solid side walls - Top and bottom walls adjusted by 151 transverse sliding plates (180 mm * 1.5 mm) positioned on special profiles

2.5.a. 2 D, 3 D models at high angle of attack are used when strong shock waves reach top and bottom walls.

2.5.b. pressure measurement on the model and on straight lines in the test section measured by scanivalve and a five hole probe.

2.5.c. time for adaptation: one week.
- computation with an Euler code
- wall deflection by machining special profiles for each form, the test section is completly removed.

3.1 pressures measurements on 2 lines near the model (about 60 measurements)

3.2.a. the external flow field is computed with a 2 D Euler code

3.2.b. comparison is performed on the flow

deviation near the upper and lower walls.

3.3 Computation on a CYBER 750, time 30 min

3.4 not iterative : the first computation gives the right shape. This shape is the computed wall shape, not an average with shape. This is because the control surface is in the vicinity of the model, and not in the vicinity of the walls.

3.5 no variations of pressure measured on the model

3.6 too small regarding the aim

3.7 2 D : 21 mm diameter cylinder and 10 mm cylinder
3 D : 15 delta wing 100 * 60 mm

3.9 no comparison because no exterior data

3.10 Y. LESANT essais 2 D et 3 D à M - 1.2 dans une veine adaptable ONERA RTS No 39/3075 AY Decembre 1987

1.1 ONERA/CERT, 2 AVENUE EDOUARD BELIN
31055 TOULOUSE CEDEX
FRANCE

1.2 MIGNOSI André Engineer, Head T2 group
ARCHAMBAUD Jean-Pierre, Research engineer
CERT ; telephone : 61 55 70 44
telex ONECERT 521596 F
Telecopy : 61.55.71.72

1.3 T2 wind tunnel

1.4 Research (ONERA and industrial firms)

1.5 Operational activity since 1975
With adaptive walls since 1978
Cryogenics activity since 1981

2.1 Closed return ; induction driven ; blowdown duration $\lesssim$120 s ; cryogenic; pressurised ($\lesssim$5 bars)

2.2 Rectangular test section length 1.4 m * width 0.39 m * height 0.37 m

2.3 Mach number 0.3 to 0.9
Pressure 1 to 5 bars
Temperature 100 to 300 K
Reynolds number 3 to 40 million (C = 0.2 m)

2.4.a. Solid flexible walls (2D deflection)

2.4.b. Wall deformation (upper and lower walls) ; fixed plan and solid lateral walls.

2.5.a. 2D and 3D tests
Profiles, swept models fixed on sidewall, centered symmetrical models fixed on a sting.

2.5.b. Pressure : two or four walls + model.
Shape : top and bottom walls (2 * 16 jacks and potentiometric comparators).
Forces : wall or sting balances.
Wake : probed with a sting (pressure and temperature).
Temperature : safety control, flow and model (over and inside)
Special devices : strain gauge, accelerometer, optical fibers for the control of the model aeroelastic behavior, unsteady pressure.

2.5.c. Blowdown stabilization 20 to 40 s adaptation with a model data acquisition per iteration 20 s (3 iterations) 3D adaptation with a model data acquisition per iteration 60 s (3 iterations). Model data acquisition 3 s.

3.1.a. 2D - The control surface consists of two fictitious horizontal planes. These planes extend from - 100 H to + 100 H (H, test section height). They are placed near the highest and lowest points of the top and bottom wall streamlines (wall streamlines are the outher limits of the test section inviscid flow) in order to minimize the projection errors (sec 3.1.c).
3D - The 3D adaptation process at T2 wind tunnel is not a real adaptation like in the reference. We use the "Wedemeyer - Lamarche" method. It is a method which computes wall deflections in order to minimize the corrections of the velocity and the flow angle on the model axis. Although we don't calculate an external flow we need a kind of reference surface which consists of four flat walls and extensions on the test section length.

3.1.b. Top and bottom walls are equipped with three pressure tap rows; one on the centerline, two on the sides (symmetry with respect to the centerline). The number of taps and their use are presented in the following table (58,23 : pressure hole numbers) :

	Centerline	Left	Right	
Top	58-2D,3D	23-3D	23-3D	0.4 mm diameter
Bottom	58-2D,3D	23-3D	23-3D	scanivalves or PSI(in progress)

In 3D case, the more interesting row is chosen depending on the model location and after an influence coefficient matrix is defined.
Movement of each flexible wall is carried out by sixteen hydraulic jacks which are moved step by step (unit step = 0.2 mm). A system of close-fitting link rods (less than 0.1 mm play) insures a good 2D movement (vertical, longitudinal to avoid local wall steps and large strain level). The displacement of the flexible wall is realized by successive homothetic shapes. The wall shapes are measured by potentiometric comparators (accuracy 0.05 mm) aligned with the jacks.

3.1.c. Here are presented the different steps occuring between the data acquistion and the begining of the external flow calculation (2D) or the correction determination (3D).
2D -
- Data acquisition on top and bottom walls. Each measure is an average of sixty values. (See 3.1.b)
- Correction coefficients for each pressure measurement

$$\frac{\Delta U}{U} = \frac{(K_1 C_p l_M}{\beta_i}$$

- Change of grid : data grid (58 points) calculation grid (70 points).
- Determination of the velocity components (Q^m, longitudinal and P^m, vertical with the velocity magnitude and the wall streamline local slope (previous iteration)

- Projection of $\bar{Q}^m$ and $\bar{P}^m$ on the flat control surface taking into account the local vertical gradients of the velocity components (deduced from the horizontal gradients).

3D -

A gradient method allows to know the velocity on the reference surface, starting from the velocity measurements on the deflected walls.

3.2.a. There are two options :
- 2D : without particular assumption
- 3D : the model is assumed to be symmetrical with respect to the vertical plane of symmetry of the test section, and to have small lateral extent.

3.2.b. 2D - Q and P are the longitudinal and the vertical components of the perturbation velocity.
3D - The adaptation is the result of two separated calculations respectively linked to the symmetrical and the antisymmetrical effects.

$$Q\begin{cases}\text{Symmetrical velocity (doublet, source effects)} = [U(x)+U(x)]_{top}/2 - [U(x)]_{bottom}/2 \text{ symmetrical deflections} \\ \text{antisymmetrical velocity (vortex effect)} = [U(x)-U(x)]_{top}/2 - [U(x)]_{bottom}/2 \text{ antisymmetrical deflections}\end{cases} \quad \text{X=sum of deflections}$$

3.2.c. 2D - starting point : P^m and $\bar{Q}^m$ on the control surface (see 3.1.c.).
- Determination of the longitudinal velocity component Q_i of the external flow (Green function based on P^m) and the infinite velocity $\bar{Q}_\infty$ (see 3.4.e).
- Change of $\bar{Q}_i^m$ in $Q_i^m = \bar{Q}_i^m - \bar{Q}_\infty$; extrapolation of Q_i^m from the four test section edges to ± 100 H (99 points) P is also extrapolated.
- Q^m and P^m are divided in four terms : $Q_i^m = \sum_{t=1,4} Q_{i,t}^m$ corresponding to the four effects : source doublet, doublet of vortices, vortex.
- For each term, computation of P by a Green function

$$P_{i,t}(x) = \frac{\beta}{\pi} \int_{-100\,H}^{+100\,H} \frac{Q_{j,t}(\xi)}{\xi - x}\, d\xi, \quad \beta = \text{compressibility factor.}$$

- Relaxation of each term with its own relaxation factor ω_t^J $P_{i,t} = \omega_t^J P_{i,t} + (1-\omega_t^J) P_{i,t}^m$
- Combination of the four terms $P_{i,t}$ which gives the vertical velocity component of the external flow P .
- At the end of the external flow computation, we know the velocity components Q_i and P_i (both relaxed) on the control surface.

Remarks

This method has been tested in analytical cases (singularities). So, the calculation grid has been optimized.
The projection from the wall streamlines to the flat control surface and vice versa allows to increase the accuracy of the result of a few per cent.
The extrapolations of Q^m and P^m improve the quality of the Green function computations (8 % up to 15 % according to a single analytical effect like source, vortex ...).

The method that is presented above is in good agreement with the analytical results (≃ 1‰ of accuracy).
This procedure has been applied up to M = 0.8 with a large profile (0.2 m chord ; 12% relative thickness, 6.5 % blockage ratio).

3D -
The velocity on the reference surface gives access to a model representation (singularities distributed on the model axis). The velocity induced by images of these singularities constitutes the part we have to correct. Practically, the wall shape corrections (symmetrical and antisymmetrical, see 3.2.b) are straight deduced from the data on the control surface by means of two linear operators.
This process can start from any wall shape and is fast converging (2 iterations with a good initial wall shape).
This method has been successfully applied up to M = 0.95 with an axisymmetrical model (blockage ratio 2%) and up to M = 0.8 with airplane half models.

3.2.d. 2D - The outputs of the external flow calculation are relaxed velocity components $Q_i + \bar{Q}_\infty$ and P_i on the flat control surface.
- These components are projected on the new wall streamlines (see 3.1.c.)

- The integration $y(x) = \int_{\text{entry}}^{x} \frac{P_i}{Q_i + \bar{Q}_\infty}\, d\xi$

fits two new wall streamline shapes.
- The viscous layer is added to these wall streamline shapes to get the new wall shapes. The viscous layer of each flexible wall is composed of the displacement thickness of its own boundary layer (calculated with pressure distribution) and the displacement thickness of one sidewall boundary layer (considered as a flat plate)
- Finally, an interpolation from the calculation grid to the jack grid gives the flow control variable X_j (J = 1,2 ...32)

3D - The wall shape corrections issue of the wall interference free flow 3.2.c. are directly added to update the wall streamlines.
The processing leading to the control flow variable X is identical to the 2D one described above.

3.2.e. 2D : HP F 1000 Cpu time = 2 s.
3D : HP A 900 Cpu time = 4 s.

3.3.a. Usually, the result of a previous test is taken to initialize the control variables. The best way is to realize a M sweep for the same angle of attack.

3.3.b. 2D -
For a 2D case, estimated wall shapes can be computed by a singularity method which is coupled with the blowdown program set. Singularities are distributed on the model (doublets) and the approximate aerodynamic coefficients (drag → sources ; lift → vortices).

3.3.c. Since 1982, all tests are carried out with the adaptation processing (2D or 3D).

3.4.a. See 3.2.b, 3.2.c, 3.2.d.

3.4.b. In the T2 adaptation procedures (2D and 3D), there is no adjustment of the control variables in terms of control effect matrices.
2D - The velocity component P_i and Q_i are relaxed between the measured value (internal flow) and the external computed flow (see 3.2.c). Relaxation factors have been optimized for each effect (doublet, source ...)
3D - In 3D case, a simple relaxation between the two jack position sets (measured data and computed by the external flow) is sometimes used (relaxation factor = 0.5).

3.4.c. No influence function used.

3.4.d. 2D -
As noted in 3.2.c., the velocity components P and Q are divided in four terms (source , doublet, vortex, doublet of vortices) and each term has its own relaxation factor (see 3.10)ω.
A numerical simulation of this relaxation process, made for each term with a linear internal flow calculation, fits an optimized set of relaxation factors.

	Doublet	Source	Vortex	Vortex doublet
ω_p	0.5	0.25	0.65	0.6
ω_q	0.5	0.75	0.35	0.4

These factors are currently used for the test.
We can demonstrate the two relations :
$\omega_p = 1 - \omega_q$ for each effect.

$$\underset{4 \text{ terms}}{\Sigma\, \omega_p} = \underset{4 \text{ terms}}{\Sigma\, \omega_q} = 2$$

(cancellation of a local deflection).
3D - see 3.4.b.

3.4.e. 2D -
The prescribed value of α(angle of attack) is the real free-stream value at the completion of the adaptation. Indeed, the adaptation method drives local $P_i - P_i^m$ toward zero at the convergence.
- During the blowdown, the computer is adjusting a second throat located downstream the test section and so holds the upstream Mach number close to the prescribed value.
But the free-stream Mach number used in the adaptation process is calculated by the following correction formula deduced from the Capelier - Chevallier - Bouniol correction method:

$$\int_{\text{top and bottom control surface}} [\bar{Q}_i^m - (\bar{Q}_\infty + Q_i)]\, W(x)\, dx = 0$$

where:
$\bar{Q}^m$ is the longitudinal velocity measurement projected on the control surface.
Q_i is the longitudinal perturbation velocity calculated by an external flow calculation with P_i^m as boundary condition (like in 3.2.c., for the determination of P_i (Q_i^m)).
W(x) is a weighting function which gives heavy weight at the vicinity of the model.
$\bar{Q}_\infty$ is the unknown free-stream velocity.
The free-stream Mach number calculated like this is more coherent with the flow surrounding the model.
At the completion of the adaptation, we observe that upstream measured Mach number and free-stream calculated one are very close to each other (difference $\leq$ 0.005) independently of the weighting function.
3D -
After each test, free-stream values (M, α) are adjusted by a correction method (see 3.6).

3.4.f. Flow chart
2D 3D

3.4.g. 2D - 3 to 5 iterations (5 when test starts from flat wall streamlines).
3D - 2 to 3 iterations.

3.4.h. During the first part of a test, wall shapes are initialized and parameters are prescribed (notably the free-stream Mach number and the total number of iterations). After that, all the adaptation procedure is automatic.

3.5.a. Not used.

3.5.b. The control of the convergence process needs 3 or more iterations. This control can be made on the successive wall shapes, the Mach number distribution at the walls and the measurements on the model (strong weight). Usually the test section is considered to be adapted if two successive wall shapes are identical.

(unit jack step = 0.2 mm. $|X - X| \leq 0.1$ mm)
calculate Jack

Generally, if this criteria is verified, the others are also correct, because the blowdown regulation insures a good stabilization of the flow parameters.

3.5.c. Not used.

3.5.d. The convergence of the Mach number distribution on the model is used to control that the adaptation is correctly reached. Generally we can observe an alternate and well damped convergence.

3.5.e. Usually 4 iterations are fixed.

3.6.a. 2D -
Assessment of residual interferences (for $M<1$) gives $\Delta M \cong \pm 0.002$ and $\Delta\alpha \cong \pm 0.020°$ (approximations).
Sidewall boundary layer effect (0.1 to 0.2°) is studied (visualizations, sidewall deflection, sidewall removal).
3D -
The adaptation method is based on a 3D calculation but the control is made by a 2D wall deflection.
After each test, a correction calculation gives local residual corrections of M and α. The method (ONERA - Le Sant) uses a model representation (singularities) which is computed with the wall signatures. (The four tap rows on each flexible walls).
For an airplane half model (swept size/test section width = 80 %) the infinite Mach number correction after adaptation has the same order of magnitude than the 2D discrepancy ($\pm$ 0.002) while the gradient $\partial M/\partial X$ is negligible. The angle of attack correction is approximately 0.2° in the middle of the wing, at great lifting case.

3.6.b. See 3.6.a.

3.7.a. Articles tested:
- 6 airfoils
- 5 symmetrical centered models
- 1 swept wing
- 2 half models fixed at a sidewall.

3.7.b

2D

	Blockage(%)	Chord Height(%)	M_∞	α	Cryogenic tests
NACA 12	4.9	40	0.6/0.85	-2/+6	NO
CAST 7	3.9	32	0.76	-2/+3	NO
CAST 7	4.9	40	0.7/0.78	$-2/^{+2.5}_{+4.5}$	YES
CAST 7	6.5	54	0.6/0.8	-2/+3.5	NO
CAST 10	5.8	49	0.7/0.765	-2/+2	YES
Industrial airfoil	5.0	40	0.73	0/+4	YES

3D

Name	Type	Blockage (%)	Wing span / Test section width (%)	Body lenght / Test section lenght (%)	Total planform area / Test section cross section area (%)	M	α(°)	Cryogenic tests
C5	axisymmetric body	0.3	.	12	.	0.6/0.97	0	NO
C5	"	1.8	.	29	.	0.6/0.95	0°and8°	NO
F4	Airplane	0.25	15	9	.	0.7	-3/+6	NO
Canard model	Airplane	.	.	.	.	0.7/0.85	$0/^{+3}_{+6}$	NO
Cylinder	axisymmetric body	3.5	.	57	.	0.4/0.8	0	NO
Industrial model	swept wing	5.7	100	.	.	0.8	-2/+3	YES
AS07	wing/body	2.0	86	47	.	0.6/0.8	-2/+2	NO
Industrial model	wing/body	1.8	80	53	.	0.78	+1.5/+4	YES

3.8.a. Empty tunnel calibration consists of two tests :
- First, a local treatment of the wall pressure allows to smooth some bump effects near the test section ($\Delta u = (K_1 C_p)_{ref} / \beta_1$).u This treatment is then applied during real tests.
- Secondly, an adaptation of the empty test section leads to diverge flexible wall shapes and zero gradient of velocity versus longitudinal direction. This shows the good accounting of the boundary layers.

3.8.b. The boundary layer noise is approximately $\frac{\sqrt{p'^2}}{q} = 3*10^{-3}$ in the range 1 Hz to 20 kHz.

The turbulence level $\frac{\sqrt{u'^2}}{U_\infty} \neq 10^{-3}$

3.8.c. - We have no experience with calibration model.
- We carry out some tests

Same airfoil located in the test section { - at mid height; - at H/4 beneath the mid height } Same result on the airfoil; good check of the entire adaptation process.

Same airfoil Chord = 120, 150, 200 mm } evolution of the lateral effects.

Test of an airfoil at Reynolds=6*10^6 { Total pressure 3b; Total temperature = 290 K; Total pressure 1.7b; Total temperature = 190 K

-same result on the airfoil-

3.8.d. The repeatability on the measured lift coefficient (deduced from the pressure) is equal to ± 0.01 between tests separated by a taking to pieces.

3.8.e. A lot of tests with the CAST 7 airfoil allows to determine an example of limitations in M, α for $\frac{\text{chord}}{\text{weight}} = 54\%$.

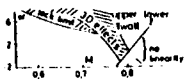

The airfoil is placed at H/4 beneath the mid height.

It is interesting to point out that the 3D effects are more restrictive than the non-linearity limit.

3.9.a. Some tests on nonstationary phenomena have been carried out.
- The oscillation shock wave on an airfoil in buffeting configuration has been characterized with pressure and laser measurements.
- The buffeting phenomena on a body-wing model has been studied with nonstationary pressure transducers, an accelerometer, a strain gauge and optical fibers.

3.9.b. No experimental study of real gas effects in cryogenic operation.

3.9.c. Several series of tests led to the knowledge of the lateral boundary layer by means of probing and visualizations. These tests have been carried out with an airfoil and a wing-body model, in unadapted and adapted test sections. The deformation of the lateral walls as well as the suction of the side wall boundary layer and the corner flow around the airfoil root is also studied.

3.9.d. Comparisons :
- GATEur WG07. - CAST 7 airfoil tested in seven varied facilities. - CAST 10 airfoil - DFVLR ; NASA; ONERA cooperation.

3.9.e. Simulation of lateral deflections by singularity computation (linear 3D) in progress.

3.10.a. Selected bibliography (Tuttle and Mineck; NASA-TM-87639) ONERA/CERT
T2 transonic, cryogenic.
80,115,121,123,127,128,130,132,151,165,168
173,174,179,189,190,203,208,212,213.
Adaptive wall newsletter updates

ARCHAMBAUD J.P.
DOR J.B.
PAYRY M.J.
LAMARCHE L.
Iterative adaptation of the 2D walls of the T2 wind tunnel around an axisymmetric C5 model with variation of Mach number at zero incidence and one test with indicence.
ONERA/CERT R.T. OA No 35/3075 AND - March 1986-

SERAUDIE A.
BLANCHARD A.
BREIL J.F.
Report on tests of a CAST 10 airfoil with fixed transition in the T2 transonic cryogenic wind tunnel with self adaptive walls.
ONERA R.T. OA No 63/1685.

ARCHAMBAUD J.P.
DOR J.B.
MIGNOSI A.
LAMARCHE L.
Initial testing of the adaptation of the two dimensional self-adapting walls of the French T2 wind tunnel around three-dimensional models.
ONERA R.T. OA No 33/7075 - September 1985-

BLANCHARD A.
PAYRY M.J.
BREIL J.F.
Tests with three-dimensional adaptation using the rectangular working section of the French T2 wind tunnel with a type AS07 swept wing half model installed.
ONERA R.T. OA No 34/3075 - November 1985 -

3.10.b. Nothing

3.10.c. Nothing

4.1 No

4.2 Improvements of lateral boundary conditions.

4.3 3D method. Lateral boundary layer accounting.

4.4 It will be useful to carry out some calibration tests with 3D reference models in the framework of cooperative program.

4.5 Use of adaptation processes (2D and 3D) for current studies (see 1.4)

2D

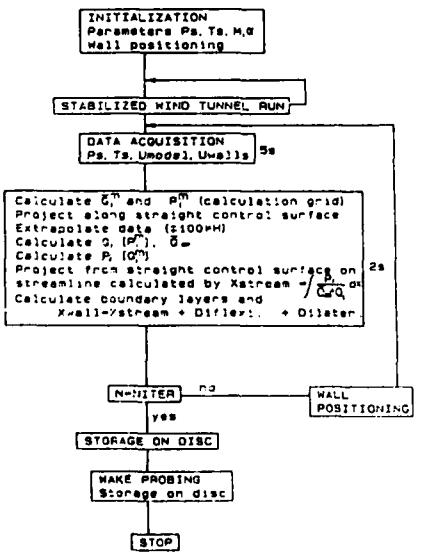

3D

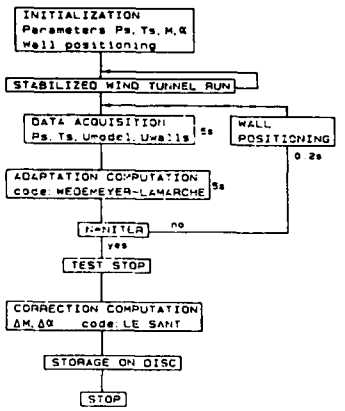

GERMANY

1.1 DFVLR GÖTTINGEN

1.2 E.Wedemeyer, DFVLR, Bunsenstrasse 10, 3400 Göttingen

1.3 Rubber Tube Test Section of High Speed Wind Tunnel

1.4 Research, Industrial Operation

1.5 Used for Research

2.1 Vacuum storage blowdown wind tunnel

2.2 0.8 m diameter, 2.4 m long cylindrical rubber tube

2.3 $0.2 \leq M \leq 0.93$; $0.4 \cdot 10^6 < Re_\ell < 10^6$ ($\ell = 0.1 \sqrt{A_T}$)

2.4.a. Impermeable walls

2.4.b. Wall deformation by 64 jacks

2.5.a. 3-D test; models with sting support

2.5.b. Pressure measurement on the model and on the walls by PSI-system and model force measurement with internal balances.

2.5.c. Time for adaptation 2-10 minutes depending on initial wall setting. Time for model data acquisition ca. 5 seconds.

3.1.a. The cylindrical walls are used as control surface, closure by extrapolation of wall-data at the entrance-and exit plane of test section

3.1.b. Wall displacement and wall pressure are measured at the stations of the 64 jacks. Of 128 pressure taps each two pressures are averaged to give the 64 pressures at the jack stations. Wall displacement is measured by counting the steps of the 64 stepping motors and as a check, by potentiometers.

3.1.c. Wall pressures (C_p - values) are corrected by subtracting the corresponding C_p values of the straight empty test section.

3.2.a. 3-dimensional flow field

3.2.b Variables P = wall pressure, Q = wall displacement

3.2.c. Numerical evaluation. For subcritical conditions at the wall linearized flow is assumed (one step method).

3.2.d. The output "wall displacement" is identical with the control variable "jack position"

3.2.e. IBM 4381, CPU-time: 2 sec.

3.3.a. Previous test

3.3.b. Computation based on wall data

3.3.c. Wall setting so as to compensate boundary layer growth.

3.4.a. Q = wall pressure, P = X = wall displacement

3.4.b. Approximations equivalent to Eq. (8) of reference

3.4.c. Influence functions by computation

3.4.d. -

3.4.e. (M, α) are prescribed and determined by flow conditions at nozzle exit

3.4.f.

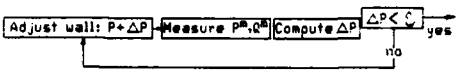

3.4.g. Depending on Mach number 1 to 2 iterations

3.4.h. Fully automatic

3.5.a. End of iteration if $(\Delta C_p)_{max} < 0.005$

3.5.b. -

3.5.c. Residual interferences not calculated and assumed to be negligible.

3.5.d. not applicable

3.5.e. not applicable

3.6.a. not applicable

3.6.b. not applicable

3.7.a. Number of articles tested: 10

3.7.b.
1. FFA-Spindle, 3.1 % blockage
2. ONERA-C5, 3.6 % blockage
3. AGARD Calibration models, 3.5% and 1 % blockage
4. Standard Dynamics Model (non stationary testing)
5. 65° swept Delta wing (VOMO), $A_w/A_T = 0.16$
6. ONERA-M3, span / $\sqrt{A_T}$ = 0.67
7. 30° swept wing pressure distr. model, span/$\sqrt{A_T}$ = 0.76
8. Fighter model; A_w/A_T = 0.23
9. Fighter model; A_w/A_T = 0.13
10. 20° cone-cylinder-model for supersonic testing, 2 % blockage

A_w = Wing planform area
A_T = Tunnel cross section area
$0 < \alpha < 20°$; $0.4 < M < 0.94$

3.8.a. Empty tunnel was calibrated up to M =0.95

3.8.b. Turbulence level not known

3.8.c. Calibration models used to compare data with interference free reference data

3.8.d. Repeatability was tested

3.8.e. Mach number is limited to $M < 0.95$ because of wavyness of walls

3.9.a. Dynamic model testing: Wall adaptation stationary flow. Non stationary wall pressure measurements from which dynamic wall interferences were calculated

3.9.b. not applicable

3.9.c. Calibration of empty test section, taking into a account b/ℓ displacement thickness. Change of boundary layer due to model flow was not taken into account and is assumed to be negligible.

3.9.d. not applicable

3.9.e. not applicable

3.10.a. Papers in Bibliography (Tuttle and Mineck):
No.197,200,201,216,220,221.
Adaptive wall Newsletter No.5, page 6.

3.10.b. -

3.10.c. -

4.1 A new planned facility (GAM) is listed in Questionnaire for DFVLR 2-D test section (Described in Adapted Wall News letter No.6, page 6.)

4.2 -

4.3 -

4.4 -

4.5 Yes

1.1 DFVLR GÖTTINGEN

1.2 J. Amecke, DFVLR, Bunsenstrasse 10, 3400 Göttingen

1.3 Transonic Wind Tunnel Göttingen

1.4 Industrial operation, research

1.5 Industrial operation, research

2.1 Continuous, closed circuit

2.2 H: 1.0 m; W: 1.0 m; L: 3.1 m

2.3 $0.5 \leq M_\infty \leq 2.0$; $0.3 * 10^6 <$;
$Re_\ell < 1.8 \cdot 10^6$ ($\ell = 0.1 \sqrt{A_T}$)

2.4.a. Horizontal walls with 4 slots, vertical walls closed

2.4.b. All slots independent adjustable

2.5.a. 3-D tests: sting support
2-D and half-model tests: turn-tables in the side walls

2.5.b. Pressure measurement on the model, on the walls and in the wake by PSI-system. Force measurement with 3-D model by internal balance. Force measurement with half-model by external balance. Flow field survey by advanced optical systems (Laser Doppler etc.)

2.5.c. Adaptation: 120 s
data acquisition: 20 s

3.1.a. The walls are used as control surfaces, closure by extrapolation of wall data at the entrance-and exit plane of the test section

3.1.b. X = P = slot width (top and bottom wall independent: 4 slots each)
Q = pressure (top and bottom wall center line; 32 pressure orifices in 1 row)

3.1.c. Wall pressures (C_p - values) are corrected by subtracting the corresponding C_p - values of the straight empty test section

3.2.a. 2-dimensional flow field

3.2.b. Wall pressure and slot width

3.2.c. Numerical evaluation. For supercritical conditions at the wall linearized flow is assumed (one step method)

3.2.d. Residual interferences as function of the slot width

3.2.e. IBM 4381, CPU-time: 10 s

3.3.a. Closed slots

3.3.b. Computation based on wall data

3.3.c. Constant slot width. Boundary layer compensation by divergent side walls or/and suction

3.4.a. Not applicable

3.4.b. Not applicable

3.4.c. By experiment

3.4.d. Not applicable

3.4.e. (M_∞ and α) are prescribed and determined by flow conditions at nozzle exit

3.4.f. Flow chart see enclosure

3.4.g. 2 to 3 iterations

3.4.h. Slot adjustment remotely controlled

3.5.a. Minimum residual interferences

3.5.b. Not applicable

3.5.c. Minimum $\partial M / \partial x$ and $\partial \alpha / \partial x$ in model center location

3.5.d. Not required for adaptation

3.5.e. Number of iterations not fixed

3.6.a. 2-D adaptation for 2-D and 3-D flows

3.6.b. ΔM and $\Delta \alpha$

3.7.a. Number of articles tested: 2

3.7.b. NACA 0012 profile: and scripl. = 0.2 m:
2.4 % blockage
NACA 0012 profile: and scripl. = 0.3 m;
3.6 % blockage
$0 \leq \alpha \leq 10°$; $0.60 \leq M_\infty \leq 0.85$

3.8.a. Empty wind tunnel is calibrated in the operating range (see 2.3)

3.8.b. Flow quality not known

3.8.c. Comparison with interference free reference data

3.8.d. Repeatability was tested

3.8.e. Not known

3.9.a. None

3.9.b. Not applicable

3.9.c. Calibration of empty test section, taking into account boundary layer displacement thickness. Change of boundary layer due to model flow was not taken into account and is assumed to be negligible

3.9.d. Not applicable

3.9.e. Not applicable

3.10.a.-

3.10.b. DFVLR Report IB 222 - 85 A 32 (1986)

3.10.c. -

4.1 -

4.2 -

4.3 Extension for 3-D tests

4.4 Low Speed Wind Tunnel, DFVLR Braunschweig (NWB) German Dutch Wind Tunnel (DNW)

4.5 Yes

Measurement	1	2
Measurement Wall	Closed	Slotted Wall
Measurement Quantity	Wall Pressure Distribution	Wall Pressure Distribution

Input to Computation	u_g, ($v_g \equiv 0$)	u_s
Computation of Wall Interference	u_g^i, v_g^i	
Calculation of Model Induced Velocities	$u^m = u_g - u_g^i$ $v^m = - v_g^i$	
Calculation of Wall Induced Velocity		$u_s^i = u_s - u^m$
v - Component from Vorticity Model		v_s^i
Superposition of Model Induced Velocity		$v_s = v^m + v_s^i$
Effective Wall Contour		$\Delta H = \int v_s \cdot dx$

1.1 DFVLR GÖTTINGEN

1.2 E. Wademeyer, DFVLR, Bunsenstrasse 10, 3400 Göttingen

1.3 2-D adaptive Test Section of High Speed Wind Tunnel

1.4 Research, Industrial Operation

1.5 Used for Research

2.1 Vacuum storage blowdown wind tunnel

2.2 0.67 m * 0.72 m; 2.2 m long

2.3 $0.5 \leq M \leq 0.90$; $0.4 * 10^6 < Re_\ell < 10^8$ ($\ell = 0.1\sqrt{A_T}$)

2.4.a. Solid sidewalls, flexible top and bottom wall.

2.4.b. Wall deflection by 9 pairs of jacks on each flexible wall

2.5.a. 3-D test; models with sting support

2.5.b. Pressure measurement on the model and on the walls by PSI-system and model force measurement with internal balances.

2.5.c. Time for adaptation 10 minutes. Time for model data acquisition ca. 5 seconds.

3.1.a. The flexible walls are used as control surfaces, closure by extrapolation of wall-data at the entrance-and exit plane of test section

3.1.b. Wall displacement is measured at the stations of the 2 * 9 pairs of jacks 24 wall pressures along centreline of each flexible wall.

3.1.c. Wall pressures (C_p - values) are corrected by subtracting the corresponding C_p - values of the straight empty test section.

3.2.a. 3-dimensional flow field

3.2.b. Variables are wall pressure and wall displacement.

3.2.c. Numerical evaluation. For subcritical conditions at the wall linearized flow is assumed (one step method).

3.2.d. The output "wall displacement" is identical with the control variable "Jack position"

3.2.e. IBM 4381, CPU-time: 2 sec.

3.3.a. Previous test or straight walls.

3.3.b. Computation based on wall data

3.3.c. Wall setting so as to compensate boundary layer growth.

3.4.a. Method of 2-D adaptation for 3-D flows.

3.4.b. not applicable

3.4.c. Influence functions by computation

3.4.d. not applicable

3.4.e. (M, α) are prescribed and determined by flow conditions at nozzle exit

3.4.f.

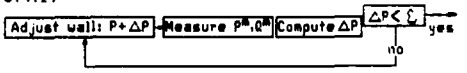

3.4.g. Depending on Mach number 1 to 2 iterations

3.4.h. Wall adjustment manually.

3.5.a. End of iteration if $(\Delta C_p)_{max} < 0.005$

3.5.b. -

3.5.c. Residual interference can be calculated on the basis of wall pressure measurements. 288 pressure orifices are on all four walls.

3.5.d. not necessary

3.5.e one step method

3.6.a. 2-D adaptation for 3-D flows. Residual interferences computed by method of Holst.

3.6.b. no results so far

3.7.a. Number of articles tested: 3

3.7.b. 1. FFA-Spindle, 3.1 % blockage
2. 30° swept wing pressure distr. model, span/ $\sqrt{A_T}$ = 0.76
3. Force measurements on blunt missile body.

A_T = Tunnel cross section area
$0 < \alpha < 20°$; $0.4 < M < 0.94$

3.8.a. Empty tunnel was calibrated up to M = 0.90

3.8.b. Flow quality not known

3.8.c. Calibration models used to compare data with interference free reference data (see 3.7.b)

3.8.d. Repeatability was tested

3.8.e. not known

3.9.a. none

3.9.b. not applicable

3.9.c. Calibration of empty test section, taking into account b/ℓ. displacement thickness. Change of boundary layer due to model flow was not taken into account and is assumed to be negligible.

3.9.d. not applicable

3.9.e. not applicable

3.10.a. DFVLR Report, IB 29112-88 A 03

3.10.b. -

3.10.c. -

4.1 A new planned facility (GAM) described in Adapted Wall News letter No. 6, page 6.

4.2 The GAM will be installed into the 1 m 1 m transonic wind tunnel of the DFVLR Göttingen

4.3 Quasi wall adaptation by use of variable slots in side walls

4.4 -

4.5 -

1.1 TECHNICAL UNIVERSITY OF BERLIN
INSTITUT FUR LUFT-UND RAUMFAHRT
MARCHSTRASSE 14
1000 BERLIN 10

1.2 Prof.Dr. Ing. Uwe Ganzer, Director of Development
Messerschmitt-Bölkow-Bloha GmbH.
Postfach 95 01 09
2103 Hamburg 95
Germany
telephone: (040) 7437-2741
telex: 21950-0 mbb d

1.3 TUB 2D and TUB 3D

1.4 Active

2.1 Continuous, open, atmospheric stagnation conditions

2.2 2D: 150 mm * 150 mm square section, length 690 mm
3D: Octagonal 225 cm² section, length 830 mm

2.3 2D: M = 0.3 to 0.95
Re/l_m 7.10^6 to 15.10^6
3D: M = 0.3 to 1.3

2.4.a. Impermeable, flexible

2.4.b. Wall deformation

2.5.a. 2D: Airfoil model mounted in side wall
3D: Model mounted on sting and quadrant

2.5.b. Model pressure tapping, sting mounted force balance, Laser Anemometer

2.5.c. 2D: for one adaptation:
3D: for one adaptation:
Automatic model data acquisition

3.1.a. 2D: Rectangular at the undeflected wall position, extrapolated,
3D: Circular at the mean radius of the octagonal test section, extrapolated

3.1.b. 2D: Control variable : wall deflection at the jacks (13 jacks at each wall)

Control surface variables P,Q : tangential and normal velocity component (wall deflection)

3D: Control variables: wall deflection at the 78 jacks (10 jacks at each wall except top and bottom wall, there 9 jacks)

Control surface variables P.Q : tangential and normal velocity component (wall deflection)

3.1.c. 2D: Filtering versus time, extrapolation, correction of freestream Mach number

3D: Filtering versus time, extrapolation, correction of freestream Mach number, interpolation

3.2.a. 2D : 2D
3D : 3D, no yaw angle (Symmetric about vertical axis)

3.2.b. 2D: P ≙ normal velocity component
Q ≙ tangential "
3D: P ≙ normal velocity component
Q ≙ tangential "

3.2.c. 2D (Subcritical) analytical (M < 1)
2D (Supercritical) numerical Full-Potential code (M < 1)
3D (Subcritical) numerical Panel-method (M < 1)
3D (Supercritical) numerical Full-Potential code (M < 1)
3D (Supersonic) numerical, wave relation (M > 1)

3.2.d. 2D: new wall deflection, new normal velocity component
3D (Subcritical): as 2D but also residual interferences
3D: as 2D

3.3.a. 2D } Previous test
3D }

3.3.b. -

3.3.c. -

3.4 Iteration process

3.4.a. 2D P ≙ normal velocity
3D Q ≙ tangential
x ≙ wall deflection

3.4.b. 2D: Scalar relaxation factor
3D (Subsonic) : no approximation
3D (Supersonic) : Scalar relaxation factor

3.4.c. 2D --
3D (Subsonic) computation

3.4.e. 2D measurement by pressure taps
3D far upstream and correction

3.4.f. 2D See publications.
3D

3.4.g. 2D 2 to 4
3D 1 to 4

3.4.h. 2D totally automated
3D

3.5.a. 2D, 3D } Convergence of tangential velocity component of exterior and interior flow

3.5.b. 2D, 3D } End of loop if movement of the walls goes to zero

3.5.c. 2D Cauchy-Integral, on axis of test section
3D (Subcritical): Calculated but not used

3.5.d. --

3.5.e. --

3.6.a. 2D: Cauchy-Integral, (M<1), 2D test in 2D test section
3D: Panel method (M<1) 3D tests in 3D test section

3.6.b. 2D, 3D } Check for convergence of the adaptation procedure

3.7.a. 5

3.7.b. 2D: CAST 7, blockage
chord length/test section height:0.67
M : 0.6 to 0.85
α : 0° to 6°
3D: Body (axisymmetric), blockage 2% body length/test section length : 0.2

wing/body, blockage 1.2 %
wing span/test section width: 0.67
body length/test section length : 0.144
cross wing area/test section cross-section : 0.067
M : 0.7 to 0.8
α : -3° to 2°

Wing/body/tail, blockage 1.3 %
wing/span/test section width : 0.67
body length/test section length : 0.175
gross wing area/test section cross-section : 0.280
M : 0.7 to 1.2
α : -3° to 8°

3.8.a. Empty tunnel calibrated for effects of boundary-layer thickness

3.8.b. Flow quality : $\Delta M = 0.002$, $\Delta\alpha = 0.1°$, turbulence level $T = 0.8$ % $E = 0.8$ %

3.8.c. none

3.8.d. good repeatability

3.8.e. dependent on the wall deflection
2D : ± 20 mm 3D : ± 10 mm

3.9.a. none

3.9.b. none

3.9.c. none

3.9.d. none

3.9.e. Simulation of 2D and 3D sub- and supersonic adaptation, study of optimal convergence

3.10.a. Ziemann,J. Convergence behaviour that controls adaptive wind tunnel walls near the test section in the high angle of attack range.
NASA TM-77006, Nov. 1982, 80pp

Ganzer, U. Stanewsky,E. Ziemann,J. Sidewall effects on airfoil tests. ICAS Journal, vol. 22, Febr. 1984.

Ganzer,U. Igeta, Y. Ziemann, J. Design and operation of TU-Berlin wind tunnel with adaptable walls. ICAS, vol.1, 1984

Ganzer, U. Igeta, Y. Transonic tests in a wind tunnel with adapted walls. ICAS, vol. 1, 1982.

Ganzer, U. Igeta, Y. Kleemann,E. Rebstock,R. Development of a wind tunnel test section with adaptive flexible walls for three-dimensional flow-final report.
BMFT-FB-W-83-026, Oct. 1983.

Ganzer, U. Rebstock,R. Flexible, adaptive walls for transonic wind tunnels in the subsonic and supersonic regions, DGLR Paper 84-108a.

Barg, J. The development of computer control for application to flexible wind tunnel walls.
ILR Mitt. 70, Technical Univ. Berlin, 1980.

Barg, J. Setup for fast automatic adaptation of flexible wind channel walls
ILR-53, Technical Univ. Berlin, 1982

Ganzer, U. Wind tunnels with adapted walls for reducing wall interference.
Zeitschrift für Flugwissenschaften und Weltraumforschung, vol. 3, No.2, 1979.

Ganzer, U. Adaptable wind tunnel walls for 2D and 3D model tests.
Proceedings (A81-11601), ICAS Paper 23-3

Ganzer, U. On the use of adaptive walls for transonic wind tunnel testing.
AGARD-CP-335 (N 83-20957)

Ganzer, U. The technology of adaptive wind tunnel walls. 3 BMFT Statusseminar, Hamburg, May

2-4, 1983

Ganzer ,U. A short note on recent advances in the adaptive wall technique for 3D-model tests at the TU-Berlin. AGARD-CP-348, Febr. 1984, Paper No.6A

Ganzer, U A review of adaptive wall wind tunnel. Progress in Aerospace Sciences, vol. 22, Pergamon Press, 1985

3.10.b. none

3.10.c. none

4.1 none

4.2 none

4.3 none

4.4 none

4.5 Routine operational testing.

ITALY

1.1 ISTITUTO DI AERODINAMICA "UMBERTO NOBILE" - FACOLTA' DI INGEGNERIA - UNIVERSITA' DEGLI STUDI DI NAPOLI - NAPOLI - ITALIA

1.2 Giuseppe P. Russo
Associate Professor
Chair of Experimental Gasdynamics
Istituto di Aerodinamica "Umberto Nobile"
Piazzale Tecchio 80
80125, Napoli
Italia

Tf. 39-81-768-3360
Tx. 722392 INGENA (I)
Fax 39-81-632044

1.3 Adaptive Walls Wind Tunnel (AWWT)

1.4 Research, pilot wind tunnel

1.5 Adaptation is still manually operated; an automated data acquisition and control system is in preparation

2.1 Continuous, open return, indraft wind tunnel

2.2 0.2m * 0.2m * 1m

2.3 Mach number is continuously variable from 0 to 0.55; maximum unit Reynolds number is 10^7 m^{-1}

2.4.a. Impermeable walls

2.4.b. Wall deformation (2*16 jacks)

2.5.a. 2D test; model supported between windows

2.5.b. 2 16 pressure and displacements are measured on the walls and 30 pressures on the model; total and static pressures of the free stream are measured upstream of the model.

3.2.e. IBM Personal System 2/60

3.10.b. G.P. Russo-M. Basciani: "Design, Calibration and Preliminary Tests of a Pilot Flexible-Walled Adaptive Wind Tunnel" - Presented at the IX Congresso Nazionale della Associazione Italiana di Aeronautica ed Astronautica - Palermo, 26 - 29 Ottobre, 1987.

4.1 By the end of 1988 a personal computer controlled data acquisition and control system will be readied. Preliminary tests will be performed on a NACA 0012 airfoil. Work is in progress in order to test the effectiveness of software found in the open literature i.e. FLEXWALL by Everhart and Goodyer and Wolf's approach to wall adaptation. The ONERA computer program is not yet available.

PEOPLE'S REPUBLIC OF CHINA

1.1 NPU, XIAN, CHINA

1.2 Prof.He, Jia Ju Northwestern Polytechnical University, Xian, China

1.3 NPU Adaptive Wall Wind Tunnel

1.4 Research

1.5 Most recent use: Sept. 1988

2.1 Continuous, blowdown

2.2 b = 23.8 cm, h = 25.6 cm

2.3 low speed, U < 45 m/sec
Re/m < $3*10^6$ /m

2.4.a. 2 flexible, 2 solid walls

2.4.b. wall deformation

2.5.a. 2D and 3D tests; sting mounted models

2.5.b. one row of pressure taps on each flexwall

2.5.c. 30 min for adaptation, 10 min for model data acquisition

3.1.a. Upper and lower wall and upstream-and downstream cross section

3.1.b. 21 pressure taps and 21 screwjacks per flex. wall

3.1.c. extrapolation

3.2.a. 2D iterative and 2D adaptation for 3D flows. (elimination of interferences at tunnel centreline)

3.2.b. 2D: P = wall displacement, Q = wall pressure

3.2.c. numerical, low speed

3.2.d. wall displacement P = X

3.2.e. IBM, PC/XT : 3 min cpu-time

3.3.a. straight wall or previous test

3.3.b. input from measured wall pressure and wall displacement

3.3.c. solid walls

3.4.a. P = X = wall displacement, Q = wall pressure

3.4.b. linearization

3.4.c. computed influence function

3.4.d. relaxation factor < 0.5

3.4.e. Prescription of free stream velocity and angle of attack

3.4.f. usual iterative procedure

3.4.g. 2-3 iterations for 2D adapt. for 3D flow: one step

3.4.h. no automation

3.5.a. wall displacement < 0.4 mm

3.5.b. -

3.5.c. -

3.5.d. -

3.5.e. -

3.6.a. 2D adaptation for 2D tests; 2D adaptation for 3D tests

3.6.b. -

3.7.a. 3 articles tested

3.7.b. 2D:1. Cylinder model (13,7 % blockage), 2.NACA 0012 airfoil (ℓ = 20 cm)
3D:wing-body pressure model.

3.8.a. empty tunnel calibration

3.8.b. uniformity of velocity

3.8.c. none

3.8.d. unknown

3.8.e. unknown

3.9.a. none

3.9.b. none

3.9.c. none

3.9.d. Relation to unadapted results and interference free data of 1.5 m tunnel

3.9.e. none

3.10.a. Adaptive Wall Newsletter Nr.5

3.10.b. AIAA 88-2040 and references in AIAA 88-2040

3.10.c. Goodyer, Southampton ; Kilgore, Wolf, NASA Langley; Ganzer, TU Berlin

4.1 2D flex. wall test section in low turbulence wind tunnel (TU <.05%) 1 m * 0.4 m, V = 75 m/sec, 1989 finished.

4.2 0.3 m * 0.3 m high speed tunnel adapt. test section designed.

4.3 Improvement of methods

4.4 -

4.5 -

UNITED KINGDOM

1.1 DEPARTMENT OF AERONAUTICS AND ASTRONAUTICS,
THE UNIVERSITY,
SOUTHAMPTON, S09 5NH
HAMPSHIRE, ENGLAND

1.2 Dr. Michael Goodyer,
Reader in Experimental Aerodynamics,
(above address)
Phone (44) (0) 703 559122 X 2374/2324
Telex 47661
Fax (44) (0) 703 671778

1.3 Low speed self-streamlining tunnel

1.4 The development of adaptive wall test techniques

1.5 Operational, with swept wing panel.

2.1 Continuous, open return, fan driven.

2.2 Rectangular in cross-section, 30.48 cm wide * nominal 15.24 cm deep. The length of top and bottom walls controlled by jacks is 127.3 cm.

2.3 Low speed (Mach 0.1). Speed 33m/s. Chord Reynolds number about 290,000.

2.4.a. All walls are impermeable.

2.4.b. Deformation of top and bottom walls.

2.5.a. Initial tests were 2D with models supported from the sidewalls. Current tests are 3D with a swept wing panel of constant chord supported from the sidewalls.

2.5.b. Models: pressure distributions, wake surveys.
Walls: longitudinal pressure and shape distributions of the flexible top and bottom walls. Some sidewall pressure measurements.

2.5.c. Initially (in 1973) very slow for adaptation, around 1 week because of manual operation, the absence of a predictive wall setting strategy and the use of a remotely situated terminal to an old computer, although model data acquisition was relatively quick: as long as it took to write down the readings of a bank of manometer tubes. Latterly adaptation with this manually operated operated test section is taking less than 1 day still using a remote but modern computer and a predictive wall setting strategy.

3.1.a. The entire length of the flexible walls of the test section (dimensions in Q2.2) are used as control surfaces. Sidewalls are flat. The wall adjustment algorithm assumes straight extensions of the walls upstream and downstream.

3.1.b. Up to 18 jacks position each flexible wall but nearer 16 (depending on the stage of development of the test section, which has been used periodically for 15 years) are used in the adaptation process to control the Q and X variables. Similarly up to 16 wall static pressure tappings (one at each jack) provide P. All are independent except as coupled by aerodynamics, imaginary and real, and the structural stiffnesses of the flexible walls. Accuracy is not good: wall pressure coefficient resolution is about 0.01 and movement of a jack is uncertain to about 0.15 mm.

3.1.c. No pre-processing.

3.2.a. 2D for 2D models. 2D in the flow component at right angles to the leading edge of the swept wing.

3.2.b. P: static pressure at most jack position on the flexible walls.
Q: Positions of the jacks.

3.2.c. Analytical, M < 1 subcritical.
Output includes next required wall shapes (jack settings, variables Q and X) and associated exterior velocity distributions, also estimates of the quality of the current "streamlining".

3.2.d. In the earliest days on an unknown HP around 1 hour per iteration, up to 10 iterations per streamlining. Now 10 seconds per iteration using DEC PDP 11-84, 2 iterations per streamlining.

3.3.a. Either (i) Straight walls with empty test section, or (ii) Any convenient set of curved walls over which the imaginary side velocity or pressure distributions are known.

3.3.b. Potential flow predictive using wall shapes, velocity distributions of both sides. No model input.

3.3.c. Not applicable.

3.4.a. Pressure at jack, jack displacement from the straight, P and Q respectively. Displacement is also X.

3.4.b. No comment.

3.4.c. Experiments and computations.

3.4.d. No comment.

3.4.e. No corrections are made: the values existing during the test are not modified.

3.4.f. Enclosed separately.

3.4.g. 2.

3.4.h. No automation aside from the processing of data by computer.

3.5.a. Not used.

3.5.b. Not used.

3.5.c. Residuals are computed from the vorticity existing in the walls after the streamlining process is terminated, using potential flow theory to give two components of wall-induced interference. Calculated along the complete centreline of the test section, although only the model region is of any real interest.

3.5.d. Not used in iterating.

3.5.e. Typically 2 in this tunnel. Experience has shown that attempts at further streamlining do not result in significant sustained improvements in quality as judged by the residuals.

3.6.a. See 3.5.c. Method is applicable only to incompressible speeds and untapered aerofoil sections. Variations in the thicknesses of the boundary layers on the two flexible walls may be taken into account. No allowance is made for

variations in the states of the sidewall boundary layers.

3.6.b. Residuals are usually so small that corrections to model performance data are meaningless in relation to other measurements such as α.

3.7.a. 3 models.

3.7.b. 2D.(i) High blockage (30 % nominal with straight walls) circular cylinder.
(ii) Aerofoil section NACA 0015-64 blockage 9.7 % with straight walls, chord: height 0.645 . M = 0.1 α = 0 and 10 degrees. The photograph on page 139 of reference (i) in 3.10.b shows this model and tunnel.
(iii) Aerofoil section NACA 0012-64 blockage 10.8 % and chord: height 0.9 .M = 0.1 . α range -6 degrees to + 12 degrees.

3D. NACA 0012-64 section at right angles to the leading edge, swept at 40 degrees, Nominal blockage is 10.8 %. Chord: nominal height is 1.17 streamwise. M = 0.1 . Span = test section width, Ratio of streamwise chord to test section length is 0.196 . Planform to test section area ratio is 1.17. Mach 0.1. α range -2 to 12 degrees.

3.8.a. Walls streamlined empty to give zero pressure coefficients at all jack pressure tappings (to C tolerance 0.01) along both flexible walls. This accounts to a first order for the development of the boundary layers along the four walls.

3.8.b. Not measured.

3.8.c. Aerofoil model was calibrated at duplicated Mach and Reynolds numbers *and zero* sweepback by NASA LRC in their Low Turbulence Pressure Tunnel at a blockage of 0.7 %.

3.8.d. No comment.

3.8.e. M: not applicable to this tunnel.
α, size limits: not yet determined.

3.9.a. Curved and streamlined walls have been used to simulate steady pitching of an aerofoil (reference 66).

3.9.b. Not applicable.

3.9.c. See 3.6.a and 3.8.a.

3.9.d. Depending on the blockage and perhaps more so on the lift the effects can be profound when comparing straight wall data with streamlined.

3.9.e. The influence on the flow at the position of the model arising from an error in setting the displacement of a wall jack has been analysed.

3.10.a. 33,38,47,62,66,75,86,95.

3.10.b. (i) D. Baals and W.R. Corliss. "The wind Tunnels of NASA." NASA SP-440, 1981.
(ii) M.J. Goodyer. "A swept wing panel in a low speed flexible walled test section". March 1987. To be published as a NASA CR.

3.10.c. (i) M.J. Goodyer. "Self-adapting flexible test-section walls". 14 July 1972. Witnessed notes on the principles of adaptive walls, made while working at NASA Langley Research Center, Hampton Virginia.
(ii) M.J. Goodyer. "Flexible-wall wind tunnels". April 1973, an expansion of 3.10.c (i) which mentions the NPL work and includes the suggestion that any new tunnel should first explore 2D testing.
(iii) P.E. Rubbert. Notes on adaptive walls dated 4 September 1973 to Dr. Goodyer with copies in the ETB Library at NASA LRC.

4. No comment.

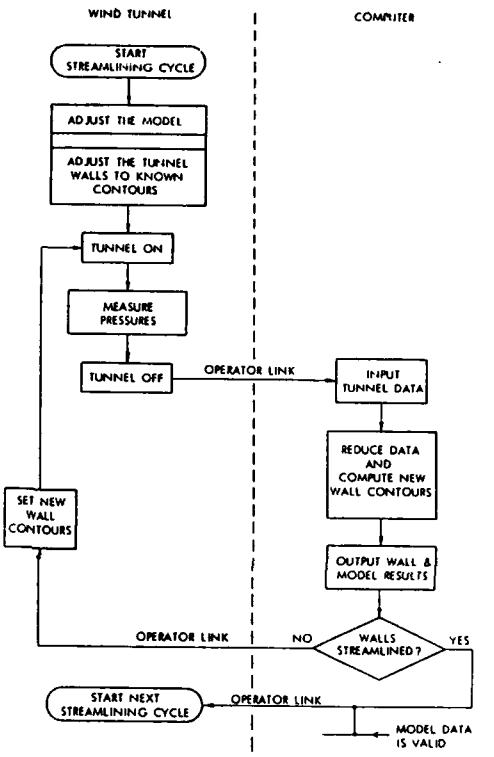

SELF STREAMLINING WIND TUNNEL MANUAL OPERATING PROCEDURE

1.1 DEPARTMENT OF AERONAUTICS AND ASTRONAUTICS,
THE UNIVERSITY,
SOUTHAMPTON, SO9 5NH
HAMPSHIRE, ENGLAND

1.2 Dr. Michael Goodyer,
Reader in Experimental Aerodynamics,
(above address)
Phone (44) (0) 703 559122 X2374/2324
Telex 47661
Fax (44) (0) 703 671778

1.3 Prototype cascade-blade flexible walled wind tunnel

1.4 The development of adaptive wall test techniques.

1.5 Dismantled.

2.1 Continuous, fan driven, open return.

2.2 Rectangular, 76.2 mm in the spanwise direction, by 55.9 mm.

2.3 Mach 0.1 typical. 33 m/s. Chord Reynolds number 232,000.

2.4.a. All walls are impermeable.

2.4.b. Wall deformation.

2.5.a. 2D testing of a single untwisted constant-chord highly cambered turbine blade model mounted between flat rigid sidewalls, reproducing cascade flow.

2.5.b. Model surface pressures. Streamwise distributions of static pressures along both flexible walls. Positions of walls. Flow deflection from measured streamtube boundaries after streamlining. Reference speed from pitot-static measurements approximately two chords upstream of leading edge of model.

2.5.c. About 6 working days. Slow because this was a manually operated tunnel using an undeveloped streamlining algorithm.

3.1.a. The flexible walls were highly cambered, extending approximately 2 chords upstream of the model and 1.5 chords downstream. The model chord was 10.16 cm and the span 7.62 cm. The depth of the test section after streamlining was one blade pitch (55.9 mm) measured in the plane of the leading edges of the simulated cascade.

3.1.b. Wall shapes were controlled by 14 screw jacks on the wall passing the suction surface of the model and 12 screw jacks on the wall passing the pressure surface. These provide Q and X variables. Wall static pressures, measured near each jack, provide the P variables. All are independent except as coupled by aerodynamics and the stiffness of the flexible walls. Accuracy was not good: wall pressure coefficient resolution was about 0.01 and movement of a jack uncertain to about 0.15 mm.

3.1.c. The jacks and wall pressure tappings were irregularly spaced introducing the need to interpolate measurements to allow pressure matching at appropriate points around the flexible walls. No filtering or extrapolation.

3.2 There is no external flowfield to be calculated. The streamlining criterion to be used in cascade flow is quite different from unconfined flow.

3.3.a. Initially the walls are set very approximately to streamlines.

3.3.b. All tunnel runs are with the model present, but no assumptions are made about model behaviour. The computations which follow a run are mostly geometric and interpolative in order to provide information allowing the tunnel operator to manoeuvre the walls towards streamlines, that is to the condition where the same C_p exists at appropriate opposite points (in the plane of the cascade) across the test section: the cyclic property of cascade flows.

3.3.c. Not applicable.

3.4.a. Pressure along the flexible walls is P; wall position is Q and X.

3.4.b. A predictive algorithm was not available. Wall movement was made proportional to the differences between pressures measured at opposite sides (as defined in 3.3.b) of the test section.

3.4.c. The constants of proportionality for 3.4.b. were determined independently for each jack using the most recent experience at the jack during the iterative process.

3.4.d. Not used.

3.4.e. No corrections are made: the values existing during the test are not modified.

3.4.f. Not avaliable.

3.4.g. About 13.

3.4.h. No automation.

3.5.a. Iterations were stopped when the average modulus of the differences in C_p measured on opposite sides (12 points per side) of the test section appeared to reach a minimum. The limited experience with this tunnel showed this modulus to be about 0.05 which was 10 % of the value existing at the beginning of the streamlining cycle. 0.05 is high compared with values attainable with normal flexible-walled tunnels which simulate unconfined flows but should be viewed in context with the C_p's existing after streamlining. Along both walls of the cascade tunnel these were: 0 at inlet, peak suction C_p = -2, outlet C_p = -1.7.

3.5.b. See 3.4.c.

3.5.c. Not used.

3.5.d. Surface pressure distribution.

3.5.e. No comment.

3.6 Not estimated in these tests.

3.7.a. One model.

3.7.b. Large scale 2D plastic model of untwisted turbine blade supplied for these tests by the British National Gas Turbine Establishment. Blockage 27 %, spanning the test section. Chord: height 1.82, Mach 0.1. Incidence was zero relative to the leading edge, 41.6 degrees relative to the mean chord line (this is the stagger angle). Flow turning angle was 71 degrees.

3.8.a. Not applicable.

3.8.b. Not measured.

3.8.c. Not available.

3.8.d. No comment.

3.8.e. No comment

3.9.a. None.

3.9.b. Not applicable.

3.9.c. Allowances were made for the variations of the boundary layer displacement thicknesses along the two flexible walls, using their pressure distributions (nominally the same after streamlining) for the computations.

3.9.d. Not applicable.

3.9.e. None.

3.10.a.30,38,66.

3.10.b. None.

3.10.c. None.

4. None

1.1 DEPARTMENT OF AERONAUTICS AND ASTRONAUTICS,
THE UNIVERSITY,
SOUTHAMPTON, SO9 5NH
HAMPSHIRE, ENGLAND

1.2 Dr. Michael Goodyer,
Reader in External Aerodynamics,
(above address)
Phone (44) (0) 703 559122 X2374/2324
Telex 47661
Fax (44) (0) 703 671778

1.3 Transonic Self-streamlining Wind Tunnel TSWT.

1.4 The development of adaptive wall test techniques.

1.5 Operational for 2D and 3D testing.

2.1 Intermittent, closed return, induced flow, atmospheric stagnation conditions.

2.2 Rectangular in cross-section, 15.24 cm wide by a nominal 15.24 cm deep. The length of the top and bottom walls controlled by jacks is 111.8 cm.

2.3 Subsonic/transonic/supersonic to about Mach 1.8. Chord Reynolds number up to about 2 millions.

2.4.a. All walls are impermeable.

2.4.b. Deformation of top and bottom walls.

2.5.a. 2D: models span the test section and are supported from the sidewalls.
3D: half models are mounted on one sidewall. Full models are sting mounted.

2.5.b. Models: varied. including pressure distributions (to transducer through Scanivalve), wake surveys, six component force balance for sting mounting.
Walls: longitudinal and transverse pressure distributions of the flexible top and bottom walls, and one sidewall (to transducers through Scanivalve) giving about 300 pressure inputs. Contours of the two flexible walls. Flow angles for measurement of influence coefficients from CEA High Sensitivity Yawmeter.

2.5 c. In 2D testing: Using our predictive wall setting strategy (generally satisfactory up to Mach 0.85) about 2 minutes for one streamlining cycle of three iterations, which is typical number of iterations when the delta (α or M) is typical for a sweep. Slowest process is jack movement, followed by time to scan pressures. Time for acquisition of model data is short, typical of modern data logging, and is included in above times as we monitor model behaviour during every iteration. Breakdown of typical time for one iteration: jack movement 20 seconds, pressure scan 10 seconds, measure tunnel reference conditions 6 seconds, computation 4 seconds.

In 3D testing: Slower than 2D. Breakdown of one typical iteration is:
computations about 3 minutes, jack movement 20 seconds, pressure scan and force measurement 20 seconds. 3 to 4 iterations are required typically at around Mach 0.7 .

3.1.a. Almost the entire lengths of the flexible walls of the test section (dimensions in Q2.2) are used as control surfaces. Sidewalls are flat. The various wall adjustment strategies developed for this tunnel assume straight extensions of the walls upstream and downstream, varying between algorithms from 6 inches to infinity.

3.1.b. 20 jacks are used for positioning each flexible wall but only the upstream 19 are used in the adaptation process to control the Q and X variables. Similarly the wall static pressure tappings provide P. All are independent except as coupled by aerodynamics, imaginary and real, and the structural stiffnesses of the flexible walls. Wall pressure resolution is about 0.3 mm. Hg and movement of a jack is uncertain to about 0.13 mm.

3.1.c. Measured wall pressure data is extrapolated downstream along the extensions. Some codes require wall data to be interpolated between measuring points.

3.2.a. 2D for 2D models. Several codes have been developed and cross-checked. Two codes are under development/use 3D testing:
(i) U. of S. method. To simplify computations the external flowfield which completely surrounds the test section is partitioned in such a way that the exterior flow is entirely two-dimensional. Singularities are avoided which would otherwise exist along the four corners of the velocities, also all three interference velocity components arising from the loadings on all partitions. Applicable to straight or curved walls.
(ii) Ashill and Weeks' 3D interference assessment method is being used as a check for the straight-wall cases and is being extended to cope with curved walls. The method involves no explicit external flowfield computation.

3.2.b. P: static pressure at 19 jack positions on each of the two flexible walls. Q: positions of these jacks.

3.2.c. Varied, analytic, numerical and mixed.
2D tests:
(i) Analytic linearised one-step for the exterior flows and also the selection of new wall contours. $M < 1$. Flex walls subcritical, test section can contain supercritical flow. CPU time per iteration 3 seconds with our strategy 1 and 6 seconds with strategy 2.

(ii) Numerical TSP code for exterior flows. $M < 1$. Model, flex walls and exterior flow all may be supercritical. Uses analytic method for selecting new wall contours. CPU time per iteration 6 to 12 minutes at up to about Mach 0.8 sometimes rising to as much as 25 minutes at Mach 0.95.

3D tests:
(i) U. of S. method. Analytic, linearised, subcritical walls. All components of exterior flow are two-dimensional.

(ii) Ashill and Weeks' method. Linearised subcritical flow. CPU time 60 second for the targetted line only.

3.2.d Output includes the next required wall shapes (jack settings, variables Q and X) and associated exterior velocity distributions if required, also estimates of the current "streamlining".

3.2.e. DEC PDP 11-84. CPU times in 3.2.c. Operating system is RT-11.

3.3.a. Either (i) Aerodynamically straight walls (determined with empty test section), or (ii) Any convenient set of walls curved away from (i) over which the imaginary-side velocities or pressure distributions are known or may be computed.

3.3.b. See 3.2.c. The streamlining process does not require any model inputs.

3.3.c. Not applicable. Straight walls

3.4.a. Wall pressures, jack displacement from the aerodynamically straight, P and Q respectively. Displacement is also X.

3.4.b. No comment.

3.4.c. Computations and experiments. Bibliography item 218 and reference (iv) below respectively.

3.4.d. Our first 2D predictive strategy (strategy 1) uses empirically determined factors to allow for the effects of aerodynamic coupling between the two flexible walls, and other factors to scale the wall movements demanded by the algorithm to encourage more rapid convergence to streamlines.

3.4.e. No corrections are made: the values existing during the test are not modified.

3.4.f. Enclosed separately.

3.4.g. Average about 1.5 in 2D testing with a well designed test programme.
Average about 3.5 in 3D testing to date.

3.4.h. Fully automatic.

3.5.a. An indicator of the quality of streamlining used in 2D testing for 15 years at Southampton is based on a measure of the pressure imbalance across a flexible wall determined in the following way. The measure, E, is the average of the modulus of the pressure imbalances (the imbalance is between the real and imaginary components of the flow either side of a wall and is expressed as a pressure coefficient) existing at the jacks along one wall. E is determined separately for each flexible wall.

3.5.b. Not used.

3.5.c. Residuals are computed from the vorticity existing in the walls (and partitions when invoked) after the streamlining process is terminated, using linearised theory to give two or three components of wall-induced interference. These can be calculated for any region of the test section, although only the model region is of any real interest. Streamlining ceases when the residuals are nominally zero. Typical levels of residual wall-induced velocity perturbations normalised with respect to the free stream velocity are, for 2D testing at the chord line and for 3D testing at the line targetted for zero perturbation, at about Mach 0.7,
streamwise perturbation 0.001 to 0.002
vertical (upwash) component 0.001
Typically these perturbations convert to errors in C_L of less than 0.008, $\alpha < 0.015$ degrees and induced camber < 0.07 degrees. In 3D testing away from the targetted line the maximum perturbation is in the upwash, typically peaking at 0.01.

3.5.d. Not used in iterating.

3.5.e. Not fixed. Typically 3 in this tunnel at speeds up to one wall (one of the flexible pair in 2D testing, any wall in 3D) becoming sonic. Experience has shown that attempts at further streamlining do not result in consistently sustained improvements in quality as judged by the residuals or E.

3.6.a. See 3.5.c. $M < 1$. In 2D tests the variations in the thicknesses of the boundary layers on the two flexible walls may be taken into account. No allowance is made for variations in the states of the sidewall boundary layers at present. No boundary layer effects are included in 3D testing aside from the growth in the empty test section.

3.6.b. For 2D tests the residuals are usually so small that corrections to model performance data are meaningless in relation to other measurement errors such as in α. Output is in the form $\delta\alpha$, δM . $\partial\alpha/\partial x$ converted to an induced camber.
For 3D tests the residuals are presented as contour plots for each of the three components of wall-induced perturbation. Corrections for the residuals are not made at present.

3.7.a. Six models plus yawmeter and wake traverse probe.

3.7.b. 2D
(i) Aerofoil section NACA 0012-64. With straight walls. blockage 8 %, chord: height 0.67. Speed range from low subsonic to Mach 0.96. α range -4 to + 6 degrees.

(ii) Aerofoil section NPL 9510. With straight walls. blockage 11 %, chord:height 1.0. Speed range from low subsonic to Mach 0.87. α range 0 to 6 degrees.

(iii) Aerofoil section CAST 7. With straight walls. blockage 8 %, chord: height 0.67. Speed range from low subsonic to Mach 0.82. α range -2 to +3.5 degrees.

3D
(i) Sidewall mounted aspect ratio 2 cropped delta wing. Ratio of tip chord to root chord 0.143. Leading edge sweep 56 degrees. Zero trailing edge sweep. Straight wall blockage 4.1 % . Ratio of semi-span to width of test section 0.58. Ratio of root chord to length of test section is 0.14. Ratio of planform area to test section flow area is 0.34. Mach range 0.3 to 0.9. α range -11 to + 10.4 degrees.

(ii) Sidewall mounted aspect ratio 2.64 swept wing. Ratio of tip chord to root chord 0.38. Leading edge sweep 49 degrees. Trailing edge sweep 27 degrees. Straight

wall blockage 3.4 %. Ratio of semi-span to width of test section 0.67. Ratio of root chord to length of test section is 0.091. Ratio of planform area to test section flow area is 0.28. Mach range 0.6 to 0.9 . α range -8 to + 10 degrees.

(iii) Sting-mounted aspect ratio 3.2 wing-body force model. Straight wall blockage 2.6 %. Ratio of wing span to width of test section is 0.214. Mach range 0.3 to 0.7. α range -1 to + 9 degrees.

3.8.a. Walls are streamlined empty to give zero pressure coefficients at all jack centreline pressure tappings (to an indicated C standard deviation of less than 0.003) along both flexible walls. This accounts to a first order for the development of the boundary layers along the four walls. The three estimated wall-induced non-dimensional perturbation components at the model position when thus streamlined but empty are typically < 0.001.

3.8.b. The turbulence level measured in a very similar NPL tunnel to TSWT was typically 0.3 %.

3.8.c. All 2D aerofoil models were tested at duplicated Mach and Reynolds numbers in at least one other tunnel providing other sources of performance information, but whether these can be regarded as providing sources of reliable calibration data is questionable. Only 3D model (iii) has been calibrated, in the NASA 7X10 foot High Speed Tunnel at Langley Research Center at duplicated Mach and Reynolds numbers.

3.8.d. A number of tests of a 2D model in *TSWT* using several streamlining algorithms, from the first NPL algorithm to the most modern, have shown excellent repeatability and uniqueness of solution (reference (iii) below). Tests on half-wing (i) of 3.7.b. have shown a repeatability of about 0.002 in wall-induced non-dimensional perturbations.

3.8.e. The practical limits of jack movement have been reached in 2D tests at high α and M. The fundamental limits have not been explored.

3.9.a. None.

3.9.b. Not applicable.

3.9.c. See 3.6.a. and 3.8.a. In 2D tests at M < 0.85 the effects of variations in flexible wall boundary layer thicknesses between the empty test section case and a model test have been shown to be insignificant in terms of model performance.

3.9.d. Information for 2D tests is in citations 33,38,62,95,114,125,133,149,178,188 of the bibliography plus references (iii) and (iv) below.

3.9.e. Computations of jack-movement influence coefficients (Bibliography item) backed by experimental verification, ref. (iv) below.

3.10.a. Citations 62,66,75,86,90,95,104,114,125, 133,138,143,145,146,149,153,178,187,188,217 218.

3.10.b. (i) Goodyer, M.J. "Predictive Wall Adjustment Strategy for Two-Dimensional Flexible Walled Adaptive Wind Tunnel. A detailed Description of the first One-Step Method." Southampton University Memo AASU 85/12 January 1986. To be published as a NASA CR.
(ii) Lewis, M.C. "Empty Test Section Streamlining of the Transonic Self-streamlining Wind Tunnel fitted with New Walls." Southampton University Memo AASU 86/10, June 1986. To be published as a NASA CR.
(iii) Lewis, M.C. "An evaluation in a Modern Wind Tunnel of the Transonic Adaptive Wall Adjustment Strategy Developed by NPL in the 1940's." Southampton University Memo E.AASU 86/11. December 1986. To published as a NASA CR.
(iv) Neal, G. "The experimental verification of the wall movement influence coefficients for an adaptive walled test section." Southampton University Memo AASU 87/4, March 1987. To be published as a NASA CR.
(v) Lewis, M.C. "The Status of Three-Dimensional Testing in the Transonic Self-Streamlining Wind Tunnel at the University of Southampton." Southampton University Memo AASU 87/11, July 1987.
(vi) Lewis, M.C. "Aerofoil Testing in a Self-streamlining Flexible-walled Wind Tunnel." Ph.D. Thesis, University of Southampton, July 1987.

4.1 None.

4.2 None.

4.3 Continuous. Main emphasis is on 3D testing in this 2D tunnel and 2D testing in the Mach range 1 to 1.2 .

4.4 None

4.5 none.

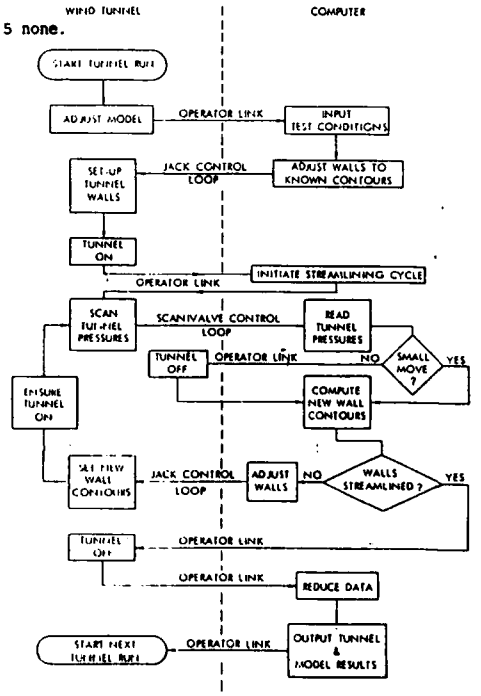

SELF STREAMLINING WIND TUNNEL AUTOMATIC OPERATING PROCEDURE

1.1 NATIONAL PHYSICAL LABORATORY, TEDDINGTON, MIDDLESEX, ENGLAND DEPARTMENT OF SCIENTIFIC AND INDUSTRIAL RESEARCH.

1.2 Dr. M.J. Goodyer, Reader in Experimental Aerodynamics, Department of Aeronautics and Astronautics, University of Southampton, Southampton SO9 5NH.

1.3 5 in * 2 in High Speed Wind Tunnel, Aerodynamics Division, NPL.

1.4 Prototype adaptive wall tunnel, used to develop the technique. Some 2D aerofoil testing.

1.5 Inactive. Tunnel dismantled.

2.1 Dry air injector driven. Intermittent, but up to several minutes run time. Open circuit.

2.2 5 in * 2 in nominal (12.7 cm * 5.1 cm), rectangular. Length about 10 in (0.25 m).

2.3 Normal operation up to choking speed with 2D model (say M = 0.93) giving Re ≈ $0.75 * 10^6$ (max) based on 2 in (5.1 cm) aerofoil chord. Has been run supersonic.

2.4 Control of speed through pressure of air in chamber around fixed blowing slot.

2.4.a. Rigid sidewalls. Flexible wall 0.015 in. (0.38 mm) thick formed the narrower walls. All walls impermeable.

2.4.b. Wall deformations, via screw jacks (6 on each wall at 1½ in. (3.8 cm) spacing). These penetrated the outer wall of tunnel and were hand-operated.

2.5.a. 2D Aerofoil Sections. Pressure plotting models normally. Generally aerofoils had up to 2 in. (5.1 cm) chord and spanned the 2 in (5.1 cm) dimension. No boundary layer diversions, suction slots or end plates, on side-walls.

2.5.b. Models, see 2.5.a. Wall pressures measured along central line of both flexible walls over full length of tunnel. Wake traverse apparatus downstream of model. Hence the normal practice for 2D models was to determine drag from wake traverses; lift from pressure integration.

2.5.c. Not known.

3.1.a. Wall shape via micrometer settings on external walls of tunnel. Setting accuracy about 0.001 in (0.025 mm).

Extent: whole test section.

3.1.b. Tunnel total pressure + wall static pressures constitute P. Accuracy about 0.05 in (1.3 mm) Hg. Wall shape data constitutes Q. Streamwise position of data is X.

3.1.c. No comment.

3.2.a. 2D (see ref. 8).

3.2.b. In 3.1.b.

3.2.c. Analytic, M < 1 subcritical

3.2.d. A relationship between the constant pressure and streamlined profiles.

3.2.e. Sliderule and mechanical desk calculator (Brunsviga and Marchant)

3.3.a. Not relevant.

3.3.b. Walls set 60 % of way from "straight" to constant pressure. No model inputs used.

3.3.c. Allowance for BL growth on all 4 walls by divergence of flexible walls.

3.4.a. See 3.1.b.

3.4.b. No comment.

3.4.c. and 3.4.d. The human being quickly learned to respond in magnitude and direction to the changes in wall setting required to achieve constant pressures.

3.4.e. From total head (H) and static pressure (p) at a position on the sidewall 2 chords upstream of a 5.1 cm chord aerofoil model.

3.4.f. Not available.

3.4.g. One iteration at all times.

3.4.h. No automation.

3.5.a. The control surface shape was based on achieving constant pressure walls to within 0.05 in (1.3 mm) Hg. Stagnation pressure was 1 atmosphere.

3.5.b. Not relevant.

3.5.c. Not calculated.

3.5.d. Model measurements not used.

3.5.e. One. See 2.5.c.

3.6 Not attempted.

3.7 Several aerofoils including NACA 0020, Joukowski sections. Blockage up to 4.8 %.

3.8.a. Measurements of static pressures along the centrelines of the flexible walls and on the sidewalls in the plane of symmetry showed good Mach number distributions up to Mach 0.95, test section empty.

3.8.b. No information.

3.8.c. None.

3.8.d. No information.

3.8.e. Tests are reported to :
M = 0.93 on 4.8% blockage aerofoil at α=0
M = 0.97 on 2.5% blockage aerofoil at α=0
M = 0.90 on 4.8% blockage aerofoil at α=10°

3.9.a. None.

3.9.b. N/A

3.9.c. No comment.

3.9.d. No comment.

3.9.e. This whole concept of streamlining is based on theoretical analysis.

3.10 NASA TM 87639 citations are:
Adaptive Wall Newsletter No.4 - update 3
No.5 - updates 1,2

Further references are:

A. Fage, A. and Sargent, R.F. Effect on Aerofoil Drag of Boundary-Layer Suction Behind a Shock Wave. ARC R&M 1913,

October 1943.

B. Research Programme of Aerodynamics Division, N.P.L. AC 19, 9138, November 1945

4. Tunnel now dismantled.

1.1 NATIONAL PHYSICAL LABORATORY, TEDDINGTON, MIDDLESEX, ENGLAND. DEPARTMENT OF SCIENTIFIC AND INDUSTRIAL RESEARCH (UP TO ABOUT 1965), THEN MINISTRY OF TECHNOLOGY. NOW DEPARTMENT OF TRADE AND INDUSTRY

1.2 (i) Dr. E.W.E. Rogers (Retired: Ex Deputy Director, RAE, Farnborough) 64 Thetford Road, New Malden, Surrey, England KT3 5DT. Tel: 01-942-7452

(ii) Mr. H.H. Pearcey (Visiting Professor, Aeronautics Department, City University; Consultant on Aerodynamic and Marine Flow Problems. Ex Head of Research, National Maritime Institute).

4/4 Church Road, Teddington, Middlesex, England. Tel: 01-997-5535.

Both the above were members of Aerodynamics Division, NPL until October 1970.

1.3 20 in * 8 in High Speed Wind Tunnel, Aerodynamics Division, NPL.

1.4 Mainly research on aerofoils at subsonic, and later, transonic speeds. At the time that this wind tunnel was operational there were no computational results for compressible flow with shock waves and hence no absolute criteria of accuracy (but see results on models of different size, comparison with flight tests etc.). We were more concerned with establishing physical understanding of transonic flow phenomena (e.g. shock-induced separation and its effects) and hence of ensuring appropriate qualitative nature of the flow, e.g. thin turbulent boundary layers to represent high Reynolds numbers. We were particularly reassured by reproducing the qualitative effects of shock-induced separation as observed on X-1 aircraft in flight, and typified by shock-wave movements.

1.5 Inactive. "Solid" flexible walls replaced by slotted walls in 1954. Tunnel dismantled c. 1971.

2.1 Dry air injector driven. Intermittent, but up to several minutes run time. Closed circuit from June 1954.

2.2 17 1/2 in * 8 in nominal (44.5 cm * 20.3 cm), Rectangular. Length about 48.5 in (1.23 m). Glass windows on 2 wider walls; flexible walls of 0.02 in (0.51 mm) spring steel on narrower width.

2.3 Normal operation up to choking speed with 2D model (say M = 0.90) giving Re ≈ $1.9 * 10^6$ (max) based on 5 in (12.7 cm) aerofoil chord. Has been run supersonic.

2.4 Control of speed through pressure of air in chamber upstream of fixed blowing slot. Supply pressure 350 psi max (25 Bars). "Machmeter" used to sense relationship between (atmospheric) total pressure + test section static pressure (see 'Pankhurst and Holder' (ref.12) for details of Machmeter).

2.4.a. Flexible steel plate, in three sections with 2 small gaps of width about 1 mm, and large 'plenum chamber' to rear of wall providing space for screw jacks. These penetrated to outer wall of tunnel and were hand-operated.

2.4.b. Wall deformations, via screw jacks (19 on each wall)

2.5.a. 2D Aerofoil Sections, but some early work on 3D models (such as the Meteor jet fighter) and some on instruments (probes, including full-scale Mark VII Pitot-Static head, blast gauges). Pressure plotting models normally. Generally aerofoils had 5 in (12.7 cm) chord and spanned the 8 in (20.3 cm) dimension. Supported usually via 3 pins entering holes in each glass window; these pins served to lead out the pressure tubes. However other aerofoil sizes (e.g up to 12 in (30.5 cm) chord) were used and occasionally the model was supported from metal side-walls. No boundary layer diversions, suction slots or end plates, on side-walls.

2.5.b. Models, see 2.5.a. Wall pressures measured along central line of both flexible walls over full length of tunnel (48.5 in, 1.23 m.). Wake traverse apparatus downstream of model position, with fitted static, total-head and yaw probes to vary region of exploration.

Schlieren and shadowgraph photography used extensively.

Direct force measurement not usual. An air-bearing balance was developed for the tunnel in about 1947 but was not used significantly. Hinge-moment balances were used in tests on aerofoils with control surfaces.

Hence the normal practice for 2D models was to determine drag from wake traverses; lift from pressure integration.

2.5.c. Stages of adaptation were:-
a) Adjustment of wall to get uniform ('open jet') wall pressures- say 1 to 3 minutes running time for each α and M.
b) Calculations of wall settings required for minimum interference condition, approximately 5 minutes.
c) Setting walls to required shape, approximately 3 minutes.

Time to acquire pressure distribution on aerofoil: typically 1 minute to ensure steady mercury manometer readings.
Wake Traverse: up to 7 minutes in difficult high M, high α case with rather unsteady wake flow.
Data taken at one M and one α for each run.

3.1.a. Wall shape via micrometer settings on external walls of tunnel. Extent: whole test section.

3.1.b. Tunnel total pressure + wall static pressures constitute P. Accuracy about 0.05 in (Hg. Wall shape data constitutes Q. Streamwise position of data is X.

3.1.c. Smoothing and fitting done by eye and judgement!

3.2.a. 2D (see ref.8).

3.2.b. In 3.1.b.

3.2.c. Analytic, M < subcritical

3.2.d. A relationship between the constant pressure and streamlined profiles.

3.2.e. Sliderule and mechanical desk calculator (Brunsviga and Marchant)

3.3.a. See 2.5.c. Knowledge of wall shapes.

3.3.b. Wall set 60 % of way from "straight" to constant pressure. No model inputs used.

3.3.c. Allowance for BL growth on all 4 walls by divergence of flexible walls.

3.4.a. See 3.1.b.

3.4.b. No comment.

3.4.c. and 3.4.d. The human being quickly learned to respond in magnitude and direction to the changes in wall setting required to achieve constant pressures.

3.4.e. From total head (H) and static pressure (p) at reference position at jack p/H = f(M). Reference position initially at Jack 5 but later moved to start of test section.

3.4.f. Not available.

3.4.g. One iteration at all times.

3.4.h. No automation.

3.5.a. The control surface shape was based on achieving constant pressure walls to within 0.05 in (1,3 mm) Hg. Stagnation pressure was 1 atmosphere.

3.5.b. Not relevant.

3.5.c. Not calculated.

3.5.d. Model measurements not used.

3.5.e. One. See 2.5.c.

3.6 Not attemped

3.7.a. At least 50 aerofoils; a few 3D models. (See Adaptive Wall Newsletter No.4 update 3).

3.7.b. 2D Aerofoils include NACA 0012, 0015, 0020, 64 series, NACA 2218 (Typhoon section), Clark Y, EC 1250, RAE series 102, 104, Mustang airfoil, Goldstein Roof-Top aerofoil) and propeller sections. Griffith section aerofoil. Standard model had 5 in (12.7 cm) chord, thickness up to 15 % (ie 0.75 in (1.9 cm)) or 3.75 % blockage. More usually 10-12 % thickness. Range of chords used was 2 in (5.1 cm) to 12 in (30.5 cm). c/h = 5/17.5 = 0.29 as standard, but varying from 0.11 to 0.69. M:0.4→choking speed (say 0.90 at low α). α : -5° to + 15° typically

3D only a few geometries tested. Axisymmetric bodies, bombs, probes, Meteor clipped wing model, blast gauges, swept wing.

3.8.a. Variation in H and p were measured and were good, but no data is available.

3.8.b. (i) Turbulence measurements using spheres were carried out in 1942. The critical Reynolds number (M < 0.4) was $2.86 * 10^5$. This compares with a range of $1.5 * 10^5$ to $3.6 * 10^5$ for various contemporary tunnels and $3.85 * 10^5$ for free air.
(ii) Relatively low turbulence was inferred from the ability to sustain laminar flow on low-drag aerofoils up to a Reynolds number of at least $4 * 10^6$.

3.8.c. No tests. (Tunnel used towards the end of its life to calibrate slotted test sections).

3.8.d. See 3.2.c.
Normal 2D operation was:
1) 'Straight' wall data up to about M = 0.75 (or lower at higher α).
2) 'Streamlined' wall data from about M = 0.7 to choking speed.

The practice was to correct the 'straight' wall data by standard methods for lift and blockage effects and to check that the corrected data overlapped the 'streamlined' wall data (in the M = 0.7 to 0.75 range).

Tests stopped when tunnel choked and/or shockwaves reached the wall. Acceptance that 'streamline' theory was thought by some to be increasingly inappropriate as supersonic flow region grew, but there were no obvious discontinuities in results. There were unsuccessful attempts to apply ΔM corrections along the lines of the empirical corrections used by Evans in the late 40s for RAE fixed wall High Speed Tunnel.

3.8.e. Comments in 3.8.d apply to standard model.

3.9.a. None.

3.9.b. N/A

3.9.c. See 3.3.(c). Dr. Rogers is convinced that thick sidewall boundary layers induced an incidence change at the aerofoil centre giving an effective finite span model. He found that integrated X-force (along chord) and Y force from pressure distributions when resolved were much less than wake traverse drag indicating an actual flow incidence greater than the geometric incidence.

3.9.d. No comments beyond those in 3.8.d.

3.9.e. This whole concept of streamlining is based on theoretical analysis.

3.10 NASA TM 87639 citations 4,6,7,8,11,12
Adaptive Wall Newsletter No.4 - update 1,3
No.5 - update 4
No.6 - update 1,2, 3,4.

There are many published papers of data from 20 in * 8 in tunnel, also many unpublished papers, and (now-lost) data. A selection of references appears in Chapter 1. Further references are:

A. Hyde, G.A.M. Turbulence Measurements with Spheres in the N.P.L. High Speed Tunnels. ARC R and M 1959, September 1942.

B. Beavan, J.A. and Hyde, G.A.M. Examples of Pressure Distributions at Compressibility Speeds on EC 1250. ARC R and M 2056, September 1942.

C. Pearcey, H.H. Drag Measurements on NACA 2218 Section at Compressibility Speeds for Comparison with flight Tests and Theory. ARC R and M 2093 April 1943.

D. Pearcey, H.H. Profile Drag Measurements at Compressibility Speeds on Aerofoils with and without Spanwise Wires or Grooves. ARC R and M 2252, August 1943.

E. Fage, A. and Sargent, R.F. An Air-injection Method of Fixing Transition from Laminar to Turbulent Flow in a Boundary Layer. ARC R and M 2106, June 1944.

F. Beavan, J.A., Hyde, G.A.M. and Fowler, R.G. Pressure and Wake Measurements up to Mach Number 0.85 on an EC 1250 Section with 25 per cent. Control. ARC R and M 2065, February 1945.

G. Holder, D.W. Transition Indication in the National Physical Laboratory 20 in. 8 in. High-Speed Tunnel. ARC R and M 2079, July 1945.

H. Research Programme of Aerodynamics Division, N.P.L. AC 19, 9138, November 1945.

I. Pearcey, H.H. and Rogers, E.W.E. The Effect of Compressibility on the Performance of a Griffith Aerofoil. ARC R and M 2511, November 1946.

J. Pearcey, H.H. and Beavan, J.A. Force and Pressure Coefficients up to Mach Number 0.87 on the Goldstein Roof-Top Section 1442/1547. ARC R and M 2346, April 1946.

K. Beavan, J.A., Rogers, E.W.E. and Cartwright, B.E. High Speed Wind Tunnel Tests on an Aerofoil with and without Two-Dimensional Spanwise Bulges. NPL Aerodynamics Division CP no. 78, February 1951.

4. Tunnel now dismantled.

UNITED STATES

1.1 UNIVERSITY OF ARIZONA, TUCSON, ARIZONA

1.2 Professor W.R. Sears
Dept. of Aerospace and Mechanical Engineering
University of Arizona
Tucson, AZ 85721
(602) 621-6107

1.3 Arizona Adaptable-Wall Wind Tunnel

1.4 Research

1.5 Operational (most recent used: December 1987)

2.1 Open Return

2.2 Rectangular 50.8 cm * 50.8 cm * 144.8 cm

2.3 Up to M = 0.09, Re = 1,000,000

2.4.a. Venetian blind louvers

2.4.b. Segmented rotation of louvered vanes

2.5.a. 3D test, Generic V/STOL Transport Model, Single Strut Support

2.5.b. LDV velocity measurement

2.5.c. 45 min for each iteration, typical run requires 7 iterations

3.1.a. 5 sided rectangular box 3/4 size of working section,

3.1.b. Flow control: percent of opening of venetian blind louvers, Control surface flow variables: tangential and normal velocities, 32 field points.

3.1.c. Time average of data

3.2.a. 3D panel method

3.2.b. Q = tangential velocity
P = normal velocity

3.2.c. Numerical

3.2.d. Output = mismatch in normal velocity; related to X according to equation (5)

3.2.e. Micro-computer (osborne 1) ; CPU time: 1 minute

3.3.a. Previous test

3.3.b. None.

3.3.c. None.

3.4.a. P = normal velocity
Q = tangential velocity
X = percent of opening of venetian blind louvers

3.4.b. dQ/dX ignored

3.4.c. Experimental determination of influence coefficient in the presence of model

3.4.d. Relaxation factor = 0.15

3.4.e. Prescribed and search for best fit

3.4.f. See diagram 1

3.4.g. 7 iterations

3.4.h. Manual operation

3.5.a. R.M.S. of velocity mismatch; uniform weighing

3.5.b. See 3.2.d.

3.5.c. Calculation of residual velocity error at model location

3.5.d. None

3.5.e. Variable number of iterations according to mismatch

3.6.a. 3D adaptation for 3D test

3.6.b. Residual error at model

3.7.a. One model only

3.7.b. 3D: wing/body/tail
1:2 wing span to test section width
1:20 platform area to test section cross-section area; Lower surface blown flaps
M = 0.006 - 0.02
Angles of attack = 4 - 23 degrees

3.8.a. Total head survey only

3.8.b. No data; turbulence level probably high

3.8.c. None

3.8.d. Repeatability varies according to position in working section; typically 1 %

3.8.e. Low speed only

3.9.a. N.A.

3.9.b. N.A.

3.9.c. N.A.

3.9.d. N.A.

3.9.e. See Lee, D.C.L. and Sears, W.R. "Experiment with Adaptable-Wall Wind Tunnel for Large Lift", Journal of Aircraft, Vol 24, June 1987, pp. 371-376.

3.10.a. Sears, W.R., "On the Definition of Free-stream Conditions for Wind-Tunnel Testing", Presented at the Symposium on Numerical and Physical Aspect of Aerodynamic Flow, Long Beach, Calif., Jan 19-21, 1981, 4 pp. In: Proceedings (A81-32571) California State University 1981.

Sears, W.R., "Wind Tunnel Testing of V/STOL Configuration at High Lift", Presented at the 13th Congress of International Council of the Aeronautical Science (ICAS)/AIAA Aircraft Systems and Technology Meeting, Seattle Washington, Aug 22-27, 1982. In: Proceedings Vol 1 (A82-40876), AIAA 1982, pp. 720-730.

Sears, W.R., "A Wind-Tunnel Method for V/STOL Testing", In: Recent Advance in Aerodynamics, pp. 547-766, Springer-Verlag, 1986, (A87-15463).

Sears, W.R., and Lee, D.C., "Experiments in an Adaptable-Wall Wind Tunnel for V/STOL Testing, AD-A174900, AFOSR-86-2088TR, September 1986, N87-19412f.

3.10.b. Lee, D.C.L. and Sears, W.R., "Experiment with Adaptable-Wall Wind Tunnel for Large Lift", Journal of Aircraft, Vol 24, June 1987, pp.371-376.

3.10.c. None.

4.1 N.A.

4.2 N.A.

4.3 Presently studying improvement of method and special applications.

4.4 N.A.

4.5 N.A.

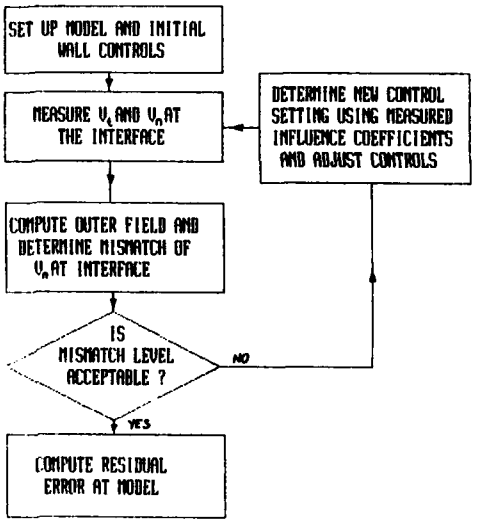

1.1 ARNOLD ENGINEERING DEVELOPMENT CENTER
ARNOLD AFB, TN 37389
USA

1.2 Dr. H.L. Laster
AF/DOT
Arnold AFB, TN 37389
USA
Telephone: (615) 454-7608
Telex: 554435

1.3 One-Foot Aerodynamic Wind Tunnel (1T), 3D Adaptive-Wall Test Section.

1.4 Research.

1.5 Inactive since June 1985; test section and control system in storage.

2.1 Continuous-flow, nonreturn tunnel with 2D flexible nozzle and test section ventilated to auxiliary plenum evacuation system.

2.2 0.305 m height and width of square cross section, 0.953 m long.

2.3 0.5 $\leq M_\infty \leq$ 1.0 with adaptive-wall instrumentation (static pipes)installed; unit Reynolds number varies with Mach number in range of $11.5 * 10^6$ to $17.2 * 10^6$ per meter.

2.4.a. Perforated wall with 60 inclined holes and porosity variable from 0 to 10 % .

2.4.b. Walls divided into 64 segments, each with independently-controlled variable porosity plus global plenum-pressure control, see Fig. 1.

2.5.a. 3D testing with sting support for wing/body/tail models, see Fig.2.

2.5.b. Wall Interference Model: Surface pressures at 134 static orifices, see Fig. 3; lift by strain gages on sting.

Interface Surface: Static pressure, C_p , and its radial derivative, $\partial C_p / \partial r$, measured by two-component differential static pipes mounted on a rotating mechanism to sweep out a cylindrical surface with circular cross-section of 0.254 m diameter, see Fig. 2.

2.5.c. No attempt made to adapt in a short time during research investigation; model data acquisition by electronically-scanned pressure modules takes a fraction of a second.

3.1.a. Circular-cylindrical surface (see 2.5.b); measurements from 0.625 body lengths upstream of nose to 0.375 body lengths downstream of tail; $Q = \partial C_p/\partial r$ data extrapolated to 1.375 body lengths upstream and 0.958 body lengths downstream for exterior-flow calculations, see 3.1.c.

3.1.b. Control variables: X_1 is ratio of upstream sidewall static pressure to tunnel stagnation pressure (P_s/P_T) and is controlled by the valve adjusting global plenum pressure; X_j, $2 \le j \le 15$, are porosity of selected groupings of segments, with all segments in each group of constant porosity, $\bar{c}_j$.

Flow Variables: Each pipe has 40 pairs of diametrically-opposed orifices which are spaced nonuniformly in the axial direction to accommodate the disturbance signatures of typical models; data obtained typically at 8 azimuthal positions, Θ, of the pipes between 15° from vertical (below the model) and 165° (above it), with the assumption of lateral symmetry for laterally symmetric models; total of 640 data points, of which 320 are $P = C_p$ and 320 are $Q = \partial C_p/\partial r$, to provide the data required for adaptation.

3.1.c. No filtering or smoothing of data was used; interpolation by spline fitting; extrapolation of Q beyond the measurements accomplished by assuming $Q = 0.0$, which is indicated by the measured data and by model flow field predictions.

3.2.a. Fully 3D in cylindrical coordinate system (x,r,Θ); assume lateral symmetry.

3.2.b. $P = C_p = -2v_x$, $Q = \partial C_p/\partial r = -2\,\partial\psi/\partial x$ as in 3.1.b, where v_x and v_r are perturbation velocity components in the axial direction and normal to the interface.

3.2.c. Numerical solution of transonic small disturbance equations written in terms of the acceleration potential, which is interpreted here as C_p ; applied for $M_\infty < 1$ but with locally supersonic flow existing at the interface.

3.2.d. Output is $P = C_p$, which is related indirectly to the control variables X_j (plenum pressure and wall segment porosity); relationship must be found by experimental measurement of influence functions $\partial P_i^m / \partial X_j$, see 3.4.b.

3.2.e. PDP 11/73 minicomputer dedicated to adaptive-wall tunnel; approximately 7 minutes for exterior flow calculation at $M_\infty \le 0.90$, 15 minutes at $M_\infty = 0.95$.

3.3.a. Not used to date.

3.3.b. Not used to date.

3.3.c. Experiments to date have begun with uniform porosity and the empty tunnel calibration value of the ratio of plenum pressure to stagnation pressure.

3.4.a. P,Q and X are defined above in 3.1.b and 3.2.b.

3.4.b. Equation (8) is used with an entirely different procedure from that in the terms of reference. First, the matrix inversion in Eq. (8) is replaced by a constant relaxation factor, so $\Delta P_j = k\, DP_j$. Then a normalized merit function Ψ is defined by

$$\Psi = \int_S W(x)\,[\,\Delta P(x,\Theta_1)]^2 ds \;/\; \int_S W(x)\,ds$$

where W(x) is a weighting function and S is the interface surface. For efficiency, the integration was limited to the x-integration at two representative Θ values namely $\Theta = 65°$ and $115°$. Next, each X_j is perturbed, in turn, and $\partial P_i^m / \partial X_j$ is measured at the representative Θ. These data are used to replace P_i^m with $P_i^m + (\partial P_i^m / \partial X_j)\,\Delta X_j$ to reevaluate Ψ so that the gradient $\partial\Psi/\partial X_j$ can be calculated. The gradient projection method for optimization is used to determine a one-dimensional search direction in terms of the X_j . A sequence of successively larger steps is performed in this search direction to find the minimum Ψ , which is the best fit of a revised P_i^{m+1} to the target distribution $P_i^m + kDP_i$. The iteration continues by repeating the entire procedure, see Fig. 4 and 3.4.f below.

The iteration strategy which worked best is as follows:
1) In first iterative step, only $X_1 = P_s/P_T$ control variable is active with the weighting function $W(x) = 0.0$ everywhere on the interface along x except in the immediate vicinity of the tail where $W(x) = 1.0$.

2) In succeeding iterative steps, X_1 is inactive and the various wall segment grouping porosities $X_j = \bar{c}_j$ are active with $W(x) = 0.0$ on the interface except in the vicinity of the wing where $W(x) = 1.0$.

3.4.c. Influence functions measured experimentally at each iterative step, see 3.4.b. and Fig. 4.

3.4.d. Uniform relaxation factor of $k = 0.75$ was used.

3.4.e. M_∞ and α are prescribed; the iteration drives $P = C_p$ to the distribution which satisfies the exterior flow condition (Eq. (1) in terms of reference) subject to the approximations discussed in 3.4.b; flow-

angle probes on upper and lower walls at beginning of perforated segments, see Fig. 2, verify that no flow inclination relative to the empty tunnel calibration has been introduced.

3.4.f. See Fig. 4; in procedure described in 3.4.b, there are no constraints, so only the optimization search branch is used.

3.4.g. Two or three.

3.4.h. Fully automated and controlled by dedicated PDP 11/73 minicomputer; operator intervention possible to inspect and check data and to revise parameters involved in iteration procedure.

3.5.a. See 3.4.b.

3.5.b. In experiments to date, iteration continued until limit of porosity control, X_j , was reached while searching to achieve minimum Ψ.

3.5.c. Merit function, Ψ , was reduced, as described in 3.4.b, until the limits of 3.5.b. were reached.

3.5.d. Model surface pressures were monitored along a row of orifices on the fuselage and along rays at 3 semispan stations on the wing and 2 on the tail, see Fig. 3, but not used as criteria for ending iteration.

3.5.e. Not used.

3.6.a. Wall interference assessment and correction (WIAC) procedures are currently under development at AEDC for fully 3D configurations; $M_\infty < 1$, but with supercritical flow present, in general, at model and interface, using numerical solution of both the transonic small disturbance theory equations and the Euler equations.

3.6.b. Output in two forms is being investigated; first, ΔC_p is evaluated everywhere on model and is integrated to obtain ΔC_L and ΔC_m at the tunnel test conditions of M_∞ , α; second, ΔM_∞ and $\Delta\alpha$ as well as residual ΔC_p , ΔC_L and ΔC_m at the corrected Mach number $M_\infty + \Delta M_\infty$; contour plots of interference on the model or throughout the flow field are possible.

3.7.a. One test article to date.

3.7.b. 3D: Wing/Body/Tail configuration shown in Fig. 3; in 1T, blockage = 2.50 %, wing span/tunnel width= 0.7000, body length/test section length = 0.320, and total planform area/tunnel crosssection area = 0.160; negligible or correctable interference for $M_\infty \leq 0.80$, adaptations carried out for $M_\infty = 0.90$, $\alpha = 0°$ and 4°, and $M_\infty = 0.95$, $\alpha = 4°$.

3.8.a. Empty tunnel was calibrated to give ratio of plenum pressure to stagnation pressure as a function of uniform porosity - results agreed with earlier data similar, but non-segmented walls.

3.8.b. Not investigated.

3.8.c. All adapted data in 1T were compared with reference data obtained on the same model in the AEDC Four-Foot Aerodynamic Wind Tunnel (4T); in 4T, the blockage = 0.16 %, wing span/tunnel width = 0.175, body length/test section length = 0.080, and total planform area/tunnel cross-section area = 0.010.

3.8.d. Limited repeatability studies were satisfactory.

3.8.e. Insufficient data available at this time.

3.9.a. None.

3.9.b. Not applicable.

3.9.c. Not investigated.

3.9.d. Initial conditions were unadapted results at calibration conditions, see 3.3.c; adapted results were superior to the unadapted.

3.9.e. None.

3.10.a. References 135, 155, and 184 in NASA-TM-87639; Reference 9 in Adaptive-Wall Newsletter No.4 bibliography update.

3.10.b. A recent paper concerning wall-interference calculations for the model of Fig. 3 using numerical solution techniques for the Euler equations is:
Donegan, T.L., Benek, J.A., and Erickson, J.C., Jr. "Calculation of Transonic Wall Interference." AIAA Paper No. 87-1432, June 1987.

3.10.c. None.

4.1 None planned.

4.2 None planned.

4.3 None planned for about 2 years.

4.4 A cooperative program with NASA Langley Research Center, DFVLR, and Dornier will include measurement of interface data during 4T testing for WIAC purposes.

4.5 None planned.

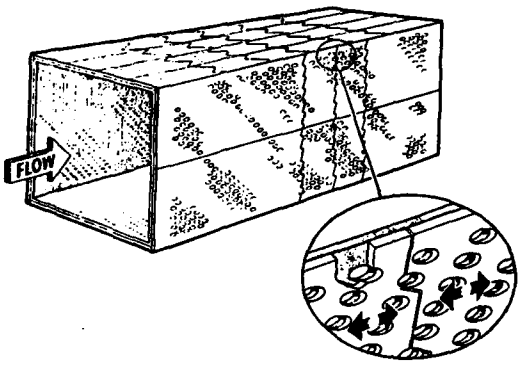

Figure 1. Segmented, Variable Porosity Wall Test Section

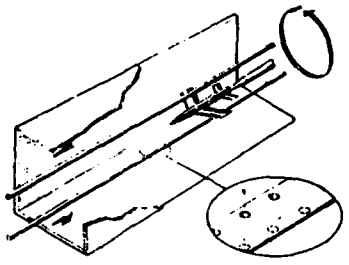

Figure 2. Interface Measurement System

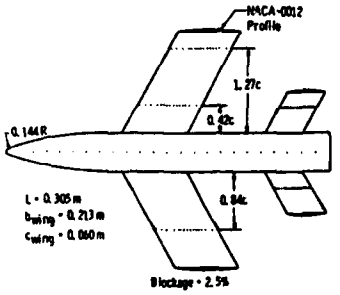

Figure 3. Generic Wall Interference Model.

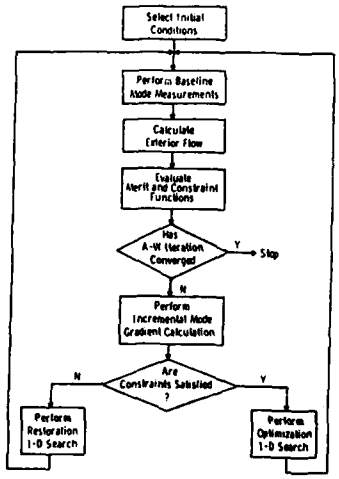

Figure 4. Automated Adaptive-Wall Iterative Procedure.

1.1 CALSPAN CORP. ADVANCED TECHNOLOGY CENTER
P.O. BOX 400
BUFFALO, NY 14225

1.2 J.C. Erickson, Jr.
Calspan Corp./AEDC Operations
MS600
Arnold AFB, TN 37389
USA
Telephone: (615) 454-6691
Telex: 554435

1.3 Calspan One-Foot Tunnel.

1.4 Research.

1.5 Inactive since 1980; test section and most of tunnel circuit dismantled and in storage.

2.1 Continuous-flow, closed-return, variable-density wind-tunnel (see Refs. 36 and 64 in NASA-TM-87639).

2.2 0.305 m height by 0.254 m width rectangular cross section, 1.676 m long.

2.3 $0.55 \leq M < 1.0$ with adaptive-wall instrumentation (static pipes) installed; unit Reynolds number for adaptive-wall experiments was $6.56 * 10^6$ per meter.

2.4.a. 2D with solid sidewalls; perforated upper and lower walls, 0.00159 m thick, with normal holes of 0.00159 m diameter on 0.00318 m centers and nominal porosity of 22.5 %.

2.4.b. 10 independently-controlled, segmented plenum chambers beyond upper wall; 8 beyond lower wall; each plenum chamber controlled by a valve to the tunnel stilling chamber for pressure and to an auxiliary compressor for suction.

2.5.a. 2D experiments only; airfoils supported by sidewalls.

2.5.b. Two NACA 0012 models:
0.152 m chord with 0.064 m wide metric section with a three-component force balance at tunnel centerline and an adjacent row of static pressure orifices.

0.102 m chord with centerline row of static pressure orifices. Experiments were performed in two basic phases:

Phase I: Mildly supercritical flow with weak shocks at the model, but subcritical flow at the interface; 0.154 m chord model (Refs. 36 and 64).

Phase II: Strongly supercritical flow with strong shocks at the model, and supercritical flow at the interface; 0.102 m chord model (Refs. 78, 100, 110, and 135).

Interface measurement capability:

Phase I: static pressure, C_p, measured by upper and lower static pipes, each of 0.0127 m diameter with a single row of 52 static pressure orifices; normal velocity, v_n, measured by 18 flow-angle probes, one above the center of each plenum chamber.

Phase II: C_p and the longitudinal derivative, $\partial v_n / \partial x$, measured by upper and lower two-component differential static pipes, each of 0.0159 m diameter with 18 pairs of differential orifices and 15 single orifices; 15 flow-angle probes retained to measure v and fix constants of integration (Refs. 100, 110, and A16).

2.5.c. Totally manual operation with exterior-flow calculations performed off-line; all pressure data acquired via Scanivalves, but with manual reading from a digital voltmeter.

3.1.a. Doubly-infinite lines above and below model; data extrapolated up-and downstream of measurements based on theoretical considerations.

3.1.b. Control variables: X_j, $1 \leq j \leq 18$, were the valve settings controlling the pressure/suction level in plenum j; throughout the adjustment process, a representative C value upstream was held fixed (see 3.4.e). Flow variables:

Phase I: $P = v_x = -C_p/2$ as measured on each pipe; and $Q = v_n$ as measured by each flow-angle probe (see 2.5.b).

Phase II: $P = v_x = -C_p/2$ as measured on each two-component pipe; and $Q = v_n$ as integrated using the probes and pipes (see 2.5.b).

3.1.c. No filtering or smoothing of data.

Phase I: Interpolation and extrapolation by multipole-expansion technique (see 3.2.c and Refs. 23, 36, and 64).

Phase II: Interpolation by cubic splines; extrapolation of v_n by fairing to zero as indicated by the measured distributions and model flow field predictions at $M \geq 0.90$.

3.2.a. 2D flow:
Phase I: Prandtl-Glauert (P-G) equation, linearized compressible flow.

Phase II: Transonic small disturbance equations (TSDE).

3.2.b. $P = v_x = -C_p/2$
$Q = v_n$

3.2.c. Phase I: v measurements fit by least squares to obtain coefficients in a multipole expansion (MPE) techniques; v then evaluated from MPE procedure (see Refs. 23, 36, and 64); used for $M \leq 0.725$.

Phase II: v_n measurements interpolated and extrapolated as boundary conditions for numerical finite-difference solutions to the TSDE for the velocity potential, which is differentiated numerically to determine v_x; used for $M \leq 0.95$.

3.2.d. Output is $v_x = P$, which is related to the valve settings X by means of influence functions resulting from the response of v_x everywhere along the interfaces to individual plenum pressure changes (see 3.4.c).

3.2.e. IBM 370/165 central computer at Calspan/ATC.

3.3.a. Phase I: not used.

Phase II: After successful iteration at $M = 0.9$, $\alpha = 3°$ (see 3.3.b), $\alpha = 2°$ was set with valve settings unchanged; same procedure used successively to reduce α to 1°.

3.3.b. Phase I: Computational results for v_x from P-G representation of airfoil by a vortex, source, and streamwise doublet.

Phase II: Computational results for v_x from TSDE numerical solution for M = 0.9, α = 3° case (see 3.3.a).

3.3.c. Phase I: Not used.

Phase II: Not used.

3.4.a. $P = v_x = -C_p/2$
$Q = v_n$
X = valve settings to achieve desired pressure in each plenum.

3.4.b. The entire term $\{\quad\}^{-1}$ in Eq.(8) was replaced by a constant relaxation factor, k.

3.4.c. Influence functions between ΔX and $\Delta P = \Delta v_x$ were investigated experimentally; basically, if an upstream C_p were held fixed, adjusting the valve setting of each plenum had the effect that Δv_x was approximately zero upstream of that plenum and constant downstream; hence, adjacent upper and lower plenum valves were adjusted simultaneously beginning at the upstream end and sweeping sequentially downstream setting v_x immediately downstream of the plenum being adjusted; two or three sweeps were sufficient.

3.4.d. Phase I: k = 0.25

Phase II: k = 0.50

3.4.e. An upstream pipe orifice was correlated with a sidewall orifice farther upstream to maintain C_p = 0 there; angle of attack was set geometrically, but care had to be exercised during the valve adjustment process (upper and lower) at the upstream end of the test section to avoid an unintentional, uniform crossflow component.

3.4.f. See attachment for simplified version.

3.4.g. Phase I: 6 or 7 .

Phase II: 3.

3.4.h. None.

3.5.a. None, only a qualitative measure of agreement between P_m and P [Q_m] was assessed and iteration terminated when improvement was no longer possible.

3.5.b. Not used, unless available control limits were reached, whereupon iteration was terminated.

3.5.c. Not used.

3.5.d. Not used, but monitored.

3.5.e. Not used.

3.6.a. Not used.

3.6.b. Not used.

3.7.a. 2, see 2.5.b.

3.7.b. 2D: NACA 0012 sections, see 2.5.b.
Phase I: 6 % blockage, chord/tunnel height = 0.5;
M = 0.55, α = 4° and 6°
M = 0.725, α = 2°
Phase II: 4 % blockage, chord/tunnel height = 0.333;
M = 0.90, α = 1° , 2° , and 3°

3.8.a. Empty tunnel calibration without active wall control showed a 20 % acceleration of the flow over the length of the test section; active wall control removed this acceleration (Ref. 36).

3.8.b. Not investigated.

3.8.c. All data were compared with data on the 0.152 m chord model in a dedicated test program in the Calspan Eight-Foot Tunnel; both One-Foot and Eight-Foot testing was at the same Reynolds number with fixed transition (Ref. 24).

3.8.d. Not investigated.

3.8.e. Not investigated thoroughly, but smaller 0.102 m chord model was built to overcome a perceived lack of control at M ≥ 0.75 (Refs. 70 and 78).

3.9.a. None deliberately, but at M = 0.85, α = 1° it was not possible to achieve a steady flow (Ref. 78).

3.9.b. Not applicable.

3.9.c. Boundary layers on perforated walls were investigated (Refs. 36, 64, and 137).

3.9.d. Not investigated.

3.9.e. Numerical simulations of the basic iterative procedure were performed for subcritical flows (Refs. 23 and 36) and for supercritical flow (Ref. 36 and unpublished STA paper in 3.10.b). Numerical simulations of segmented-plenum, perforated-wall test section were made (Ref. 137); semi-emprical model of entire tunnel, including auxiliary pressure and suction systems, was developed (Refs. 70 and 78).

3.10.a. Of many papers and reports in NASA-TM-87639, most important and accessible are Refs. 23-25, 36, 53, 64, 70, 78, 100, 110, 135, 137, and A16.

3.10.b. Erickson, J.C., Jr. "The Concept of a Self-Correcting Wind Tunnel", Presented at the 42nd Semiannual Meeting of the Supersonic Tunnel Association, Buffalo, NY, October 1-2, 1974 (see 3.9.e).

3.10.c. None.

4.1 None

4.2 None

4.3 None

4.4 None

4.5 None

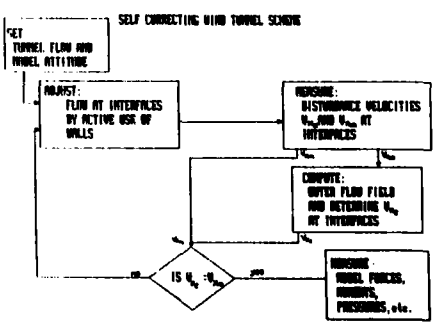

1.1 NASA AMES RESEARCH CTR.
MOFFETT FIELD, CA 94035

1.2 Edward Schairer, Aerospace Engineer
M.S. 260-1
NASA AMES Research Center
Moffett Field, CA 94035
(415) 694 - 4143

1.3 25*13 cm Indraft Tunnel

1.4 Research

1.5 Inactive (1980)

2.1 Indraft, Choked Nozzle Downstream, continuous

2.2 Rectangular
13 cm
25 cm
74 cm

2.3 M < 0.80 Atmospheric total pressure

2.4.a. Slotted top and bottom; solid side-walls

2.4.b. Plenum pressure, segmented (10 upper, 10 lower)

2.5.a. 2-D Airfoil spanning test section, supported by side-walls

2.5.b. Surface pressures measured at orifices with scanivalve pressure transducer.
1 - Component LV
Scanivalve Press. Transducer

2.5.c. ~ 1 Hour
~ 10 Sec

3.1.a. 2-Level interference assessment. Levels were at ± 0.4 C and ± 0.67 C and extended 2.3. C upstream and downstream of model quarter-chord. No extrapolation.

3.1.b. X 20 Plenum compartment pressures. Strongly coupled.
P Upwash
N_p 10 at 0.33c intervals
Accuracy ~ ± 0.3 m/sec
Q upwash
N_q 15 at 0.33 c intervals
Accuracy ~ ± 0.3 m/sec

3.1.c. Filtering : None
Smoothing : None
Extrapolation : None

3.2.a. 2-D Prandtl - Glauert

3.2.b. P : upwash
Q : upwash

3.2.c. Analytic solution integrated numerically

3.2.d. Upwash, related to X by empirical influence coefficients

3.2.e. Data General Eclipse S 200
~ 1 sec

3.3.a. All tests begun with "Passive" walls- no mass flow through walls

3.3.b. Not applicable.

3.3.c. Unknown

3.4.a. See 3.1.b.

3.4.b. $\Delta X_j = \{ \partial P_i / \partial X_j \}^{-1} DP_i$

3.4.c. Experiments

3.4.d. 0.5

3.4.e. Mach No. determined from upstream side-wall pressure tap, total press, and total temp. Free-stream direction assumed to coincide with tunnel axis.

3.4.f. See attachment.

3.4.g. 3

3.4.h. All processes automated except for adjustment of plenum pressures which was done manually following computer instructions.

3.5.a. RMS difference between theory and exp. at control points. Equal weights.

3.5.b. Arbitrary decision of operator.

3.5.c. Not used

3.5.d. Not used.

3.5.e. Not used. Iteration continues until figure of merit shows no further improvement

3.6.a. Not used.

3.6.b. -

3.7.a. 1

3.7.b. NACA 0012
Blockage 7 %
C/H 0.586
M range 0.6→0.8
α range 0°, 2°
b/w -
Sw/(hxw)-

3.8.a. Axial Mach distribution measured using side-wall pressure taps. Standard deviation typically 0.006.

3.8.b. Unknown

3.8.c. Airfoil pressure distribution compared with Calspan 8' W.T. data

3.8.d. Not determined

3.8.e. Mach limited to ~ 0.80 : condensation at higher Mach interfered with LV

3.9.a. Not applicable

3.9.b. Not applicable

3.9.c. Not investigated

3.9.d. Not applicable

3.9.e. None

3.10.a.1. BODAPATI, SCHAIRER, DAVIS, "Adaptive-Wall Wind Tunnel Development for Transonic Testing", J. of Aircraft Vol 18, No 4 , April 1981.

2. DAVIS, "A Compatibility Method for Adaptive-Wall Wind Tunnels", AIAA J., Vol 19, Sept. 1981.

3. SCHAIRER and MENDOZA, "Adaptive-Wall Wind Tunnel Research at Ames Research Center", AGARD CP 335, Sept. 1982.

1.1 NASA AMES RESEARCH CTR.
MOFFETT FIELD, CA 94035

1.2 Edward Schairer, Aerospace Engineer
M.S. 260-1
NASA AMES Research Center
Moffett Field, CA 94035
(415) 694 - 4143

1.3 25*13 cm Indraft Tunnel

1.4 Research

1.5 Inactive (1981)

2.1 Indraft, Choked nozzle downstream, continuous

2.2 Rectangular
13 cm
25 cm
74 cm

2.3 M < 0.80
Atmospheric total pressure

2.4.a. Slotted top and bottom; solid side-walls

2.4.b. Plenum pressure, segmented (18 upper, 18 lower)

2.5.a. 3-D sidewall mounted semi-span wing (tapered, unswept)

2.5.b. Model loads measured by 6 - component balance
1 - component LV
Scanivalve Press. Transducer

2.5.c. ~ 1 Hour
~ 1 sec

3.1.a. 2 - Surface interference assessment. Each surface was a right rectangular prism extending 2.3 mean aero. chords upstream and downstream of model quarter-chord. No extrapolation.

3.1.b. X 36 Plenum compartment pressures. Strongly coupled
P Upwash
N_P 49
Accuracy ~ ± 0.3 m/sec
Q Upwash
N_Q 49
Accuracy ~ ± 0.3 m/sec

3.1.c. Filtering : None
Smoothing : None
Extrapolation : None

3.2.a. 3-D Linearized, Compressible.

3.2.b. P : upwash
Q : upwash

3.2.c. Finite differences

3.2.d. Upwash, related to X by empirical influence coefficients

3.2.e. Data General Eclipse S 200
~ 30 sec

3.3.a. All tests begun with "Passive" walls - no mass flow through walls

3.3.b. Not applicable

3.3.c. Unknown

3.4.a. See 3.1.b.

3.4.b. $\Delta X_j = (\partial R_i / \partial X_j)^{-1} DR_i$

3.4.c. Experiments

3.4.d. 0.5 → 1.0

3.4.e. M: Mach No. determined from upstream side-wall pressure tap, total pressure, and total temperature.
α: Free-stream direction assumed to coincide with tunnel axis.

3.4.f. See attachment

3.4.g. 3

3.4.h. All processes automated except for adjustment of plenum pressures which was done manually following computer instructions

3.5.a. RMS difference between theory and exp. at control points. Equal weights.

3.5.b. Arbitrary decision of operator.

3.5.c. Not used

3.5.d. Not used

3.5.e. Not used. Iteration continues until figure of merit shows no further improvement.

3.6.a. Not used

3.6.b. -

3.7.a. 1

3.7.b. Semi-span wing
Blockage 2.67 %
M range 0.6 → 0.7
α range 0° → 5.3°
b/w 0.678
Sw/(hxw) 0.44

3.8.a. Axial Mach distribution measured using side-wall pressure taps. standard deviation typically 0.006.

3.8.b. Unknown

3.8.c. Model lift-curve compared to experimental "Free-Air" data. Velocities compared to CFD result.

3.8.d. Not determined

3.8.e. Mach limited to ~0.80 : Condensation at higher Mach interfered with LV.

3.9.a. Not applicable

3.9.b. Not applicable

3.9.c. Corner-flow observed during calibration. Effect on test was unknown.

3.9.e. Results correlated with numerical simulations of J.P. Mendoza.

3.10.a. 1. SCHAIRER, "Experiments in a Three-Dimensional Adaptive-Wall Wind Tunnel", NASA TP 2210, Sept. 1983.

2. DAVIS, "A Compatibility Method for Adaptive-Wall Wind Tunnels", AIAA J., Vol 19 No 9, Sept. 1981.

3. SCHAIRER and MENDOZA. "Adaptive-Wall Wind Tunnel Research at Ames Research Center", AGARD CP 335, Sept. 1982.

4.MENDOZA,"A numerical Simulation of Three-Dimensional Flow in an Adaptive-Wall Wind Tunnel", NASA TP 2351, Aug. 1984.

SCHAIRER, "Assessment of Lift and Blockage - Induced Wall Interference in a Three-Dimensional Adaptive-Wall Tunnel", in NASA CP-2319, 1984.

1.1 NASA AMES RESEARCH CTR.
MOFFETT FIELD, CA 94035

1.2 Edward Schairer, Aerospace Engineer
M.S. 260-1
NASA AMES Research Center
Moffett Field, CA 94035
(415) 694 - 4143

1.3 2 By 2-Foot Transonic Wind Tunnel

1.4 Research to Industrial Operation

1.5 Integrated systems test nearly completed (Mar 1988)

2.1 Continuous, Closed return

2.2 Square
0.61 m
0.61 m
0.52 m

2.3 $0.2 \leq M \leq 1.0$
Atmospheric total pressure

2.4.a. Slotted top and bottom; solid side-walls

2.4.b. Plenum pressure, segmented
(32 upper, 32 lower)

2.5.a. 2-D Airfoil spanning test section, supported by side-walls

2.5.b. Surface pressures to be measured at orifices with scanivalve pressure transducer
2-component LV

2.5.c. To be Determined (TBD)
~ 10 sec

3.1.a. Instrumentation and software available for either 1 - or 2 - Component interference assessment. Heights of control levels TBD - LV and glass side -walls allow maximum flexibility in choosing. Software in place to extrapolate.

3.1.b. X 64 plenum compartment pressures. Expected to be strongly coupled
P upwash or axial
N_P 32
Accuracy TBD
Q upwash or axial
N_Q 32
Accuracy TBD

3.1.c. Filtering : None
Smoothing : Smoothing LV velocity distributions avaliable
Extrapolation : Data may be extrapolated using multi-pole at model Quarter-chord to fit data.

3.2.a. 2-D Linear, compressible, 2-D 1-step, and non-linear (transonic small perturbation-TSP)

3.2.b. P : upwash or axial
Q : upwash or axial

3.2.c. Linear analytic solution evaluated numerically TSP equ. solved by finite differences.

3.2.d. Upwash or axial, related to X by empirical influence coefficients.

3.2.e. Data General Eclipse S 200
Linear sol'n: ~ 1 sec
TSP sol'n : ~ 60 sec

3.3.a. TBD

3.3.b. Not applicable

3.3.c. TBD

3.4.a. See 3.1.b.

3.4.b. $\Delta X_j = (\partial P_i / \partial X_j)^{-1} DP_i$

3.4.c. Experiments

3.4.d. TBD

3.4.e. M: To be prescribed

α: To be prescribed

3.4.f. See attachment

3.4.g. TBD

3.4.h. Designed to be fully automated

3.5.a. RMS difference between theory and exp. at control points. equal weights.

3.5.b. User selected pressure change threshold

3.5.c. To be Determined for P and Q using linear WIAC methods

3.5.d. TBD

3.5.e. Not used. Iteration continues until figure of merit shows no further improvement

3.6.a. Linear WIAC methods to be used

3.6.b. TBD

3.7.b. NACA 0012
Blockage 3 %
C/H 0.25
M range TBD
α range TBD

3.8.a. Axial Mach distribution to be measured with LV and static pressure pipe along tunnel centerline.

3.8.b. TBD

3.8.c. Large data-base of pressure distributions available for comparison

3.8.d. TBD

3.8.e. TBD

3.9.a. Not applicable

3.9.b. Not applicable

3.9.c. TBD

3.9.d. TBD

3.9.e. Results to be compared to TSFOIL and other numerical simulations.

3.10.a. 1. SCHAIRER, "Methods for Assessing Wall Interference in the Two-by Two-Foot Adaptive-Wall Wind Tunnel", NASA TM 88252, June 1986.

2. MORGAN and LEE, "Construction of a Two by Two Foot Transonic Adaptive-Wall Test Section at the NASA Ames Research Center, AIAA Paper 86 - 1089, May 1986.

3. SCHAIRER, "Two-Dimensional Wind-Tunnel Interference From Measurements on Two Contours", J. of Aircraft, Vol 21, No 6, June 1984.

4. DAVIS, S.S., "Applications of Adaptive-Wall Wind Tunnels" J. of Aircraft, Vol 23, no 2, FEB 1986.

5. DAVIS, S.S., "The Evolution of Adaptive-Wall Wind Tunnels", NASA TM 84404, Sept. 1983.

3.10.b. Contribution to "Adaptive-Wall Newsletter" No 4 (Feb 1987)

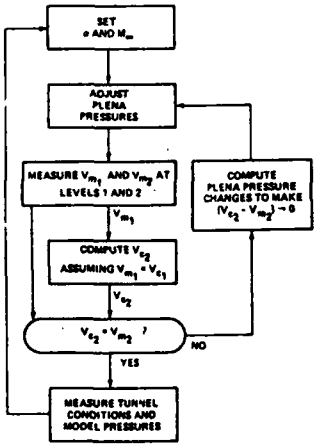

Fig. 2 Adaptive-wall wind-tunnel scheme.

1.1 EXPERIMENTAL TECHNIQUES BRANCH, NASA LANGLEY RESEARCH CENTER, HAMPTON, VIRGINIA, USA

1.2 Dr. Stephen Wolf, Mail Stop 287, NASA Langley Research Center, Hampton, Virginia 23665-5225, USA. Tel.(804)-865-4807. Telex.823405. Fax.(804)-865-2300.

1.3 0.3 m Transonic Cryogenic Tunnel (TCT).

1.4 Research and production type testing.

1.5 Active

2.1 Continuous; Closed Return; Cryogenic; Pressurized

2.2 0.33 m square, 1.417 m long

2.3 Mach 0.2 to 1.1; Unit Reynolds number up to 328 million per meter

3.4.a. Impermeable; flexible top and bottom walls, rigid sidewalls.

2.4.b. Wall deformation.

2.5.a. 2D tests, model supported between rigid sidewalls.

2.5.b. Pressures and wake survey.

2.5.c. Adaptation < 2 minutes; Model data < 20 seconds; Wake Survey < 5 minutes.

3.1.a. Effective test section boundary shape.

3.1.b. Static pressures on the floor and ceiling (Variables Q) - 18 per wall on the tunnel centerline; Position relative to the fixed upstream end of the walls in inches:
4.75,10.5,15.5,19.5,22.5,24.5,26.,27.5,29., 30.5,32.,33.5,35.5,37.5,39.5,42.5,46.5, 51.5;
Accuracy : ± 0.25 % of reading (0 to 20 PSI)
Independence: Aerodynamically linked together;
Redundancy: None.
Local wall deflections at each of the jack locations (Variables X) -18 per wall;
Position as for the static pressure measurements;
Independence: Small mechanical interactions;
Redundancy: None.

3.1.c. Static pressure values are time averaged. Also these pressures are interpolated to determine static pressure values midway between wall jacks during the wall adaptation computations.

3.2.a. 2D, Linearised, Small wall slopes.

3.2.b. Local wall slope and local static pressure on the floor and ceiling.

3.2.c. Analytical adjustment of external flow field pressures on each wall shape from one iteration of the adaptation process to the next. Range of application is limited to where the local wall Mach number is near sonic with the flexible walls adapted or nearly adapted. With a test section height/chord ratio of 1.5, free stream Mach number is restricted to about 0.85. (Note suitable external flow field calculations to raise this Mach number restriction to Mach 1.0 are available when this becomes necessary.)

3.2.d. New external flow field pressure distribution used with the predicted wall shape (Variables X) for the next iteration of the adaptation process.

3.2.e. Modcomp Classic IV (CPU-A) mini-computer; CPU time CPU time- Unmeasurable (nano-seconds).

3.3.a. Automatic selection of experimental wall shapes from a wall library, or calculation of potential flow wall shapes based on expected model lift and drag coefficients, or aerodynamically straight walls. These initial wall shapes are available for any test sweep.

3.3.b. Automatic selection of wall shapes based on operator entered setup parameters, i.e. α, M and Rc.

3.3.c. Test section always active.

3.4.a. Variable Q - Local wall static pressure
Variable P - Local wall slope
Variable X - Local wall deflection

3.4.b. 2D; Linearised; Small wall slopes; Each wall analyzed separately.

3.4.c. We refer to the influence coefficients as coupling factors and scaling factors, which we determine experimentally.

3.4.d. Coupling factors: 35 % of one wall movement fed into the other wall.
Scaling factors: 80 % of the predicted wall movement used.

3.4.e. The free stream Mach number (M) is measured at the test section entrance. The model angle of attack is measured geometrically relative to the tunnel centerline.

3.4.f. See attached sheet number 1

3.4.g. Usually one or two iterations are required.

3.4.h. Complete automation used for production type tests.

3.5.a. The control surface figure of merit we refer to as streamlining quality. We assess this streamlining quality by the magnitudes of the modulus of the local C_p error along each wall, the induced angle of attack at the model leading edge, induced camber along the model chord line and the averaged induced velocity along the model chord line.

3.5.b. The prediction of new wall shapes is based on the imbalance of the internal and external pressure distributions along the floor and ceiling.

3.5.c. Modulus of the local C_p error $<$ 0.01 (Calculated from already known pressure distributions) Induced angle attack $<$ 0.015 degree (Calculated from wall pressure loadings) Induced camber $<$ 0.07 degree (Calculated from wall pressure loadings)
Average induced C_p error $<$ 0.007 (Calculated from wall pressure loadings)

3.5.d. No model measurements used during the adaptation process.

3.5.e. Number of iterations not fixed. However the control system will alert the operator to a convergence problem if more than 6 iterations are attempted in an adaptation process.

3.6.a. Each wall is represented as a vortex sheet in a uniform potential flow field. Linearised theory is then used to calculate the induced effects of this wall vorticity at the model location. The range of application is the same as for external flow calculations, i.e. when the walls are near sonic either adapted or nearly adapted.

3.6.b. We use the residual interferences to decide when to stop the adaptation process. The residual interferences at the end of an adaptation process are considered acceptably small. No classical type corrections are applied to the model data.

3.7.a. Ten 2-D airfoils.

3.7.b. NACA 0012; blockage = 6 %; chord/height ratio = 0.5; M range 0.3 to 0.78; α range - 6° to 8.5°; Rc range 3 million to 30 million.
NACA 0012; blockage = 12 %; chord/height ratio = 1.0; M range 0.5 to 0.76; α range -2° to 6°; Rc range 6 million to 15 million.
CAST 10; blockage $\approx$ 12 % ; chord/height ratio = 0.75; M range 0.3 to 0.8; α range -2.3° to 11.5°; Rc range 6 million to 73.4 million.
CAST 10; blockage $\approx$ 12 %; chord/height ratio = 0.54; M range 0.7 to 0.8; α range -1° to 6.9°; Rc range 4 million to 45 million.
Advanced Cambered Airfoils; blockage $\approx$ 12 %; chord/height ratio = 0.46; M range 0.3 to 0.775; α range -9° to 11°; range 3 million to 24 million.

3.8.a. Empty tunnel calibration over M range 0.25 to 0.95 and Rc range 10 million to 100 million per foot.

3.8.b. Mach number variations of the order 0.004 in the empty test section up to about Mach 0.8. Turbulence data is being analyzed.

3.8.c. We carried out extensive validation tests with the NACA 0012 and CAST 10 airfoils described in answer 3.7.b.

3.8.d. Repeatability of the order 0.001 in normal force coefficient (Cn) and .0005 in drag coefficient (Cd) is possible. We have many data comparisons when models were re-installed in the tunnel for numerous reasons.

3.8.e. Our test envelope is currently bounded by hardware limitations which are very dependent on the model under test. However, we have published a test envelope for a chord/height ratio of 0.71, as shown on sheet number 2. Production testing and research testing envelopes are different because the levels of operator experience determine which hardware problems restrict the envelope. The lowest possible level is assumed for production testing.

3.9.a. N/A

3.9.b. Very small effects observed in data reduction. 0.3 -m TCT data is corrected for real gas effects using the Beattie - Bridgeman equation of state for nitrogen gas.

3.9.c. The spanwise variation of the model wake is small for moderate lifts, indicating good 2-D flow in the test section. Preliminary tests using passive sidewall boundary layer control indicate that the maximum lift of a 2-D model may be sensitive to sidewall boundary layer effects. However, good comparisons of data from different chord models, with the same section, strongly indicates that the sidewall boundary layer effects are minimized in a shallow adaptive wall test section.

3.9.d. Sheet number 3 shows a comparison of uncorrrected data from the 0.3 -m TCT adaptive wall test section and the 0.3 -m TCT ventilated test section. The model section is CAST 10. The chord/height in the flexible walled test section is 0.54 and in the slotted walled test section is 0.127. The data sets are quite different in terms of lift curve slope and maximum lift despite the small size of model used in the slotted walled test section.

3.9.e. We used flow simulations to check our wall adjustment software. Control concepts cannot be simulated with flexible walled test sections since all the wall adjustment procedures are theoretically so-called One-Step methods. Experimental evaluation of all these procedures proves iterations are necessary in the adaptation process because the model flow field changes for each iteration. The wall adjustment procedures cannot take this in to account without detailed knowledge of the model. Indeed if we had this detailed knowledge there would be no need to carry out a wind tunnel test of the model in the first place.

3.10.a. See the subject index in Nasa TM-87639 for 0.3 -m TCT.

3.10.b. Ladson C.L.; and Ray E. J.: Evolution, Calibration, and Operational Characteristics of the Two-Dimensional Test Section of the Langley 0.3 -Meter Transonic Cryogenic Tunnel. NASA TP-2749. September 1987. 170 pp.

Mineck R.E.: Wall Interference Tests of a CAST 10-2/DOA 2 Airfoil in an Adaptive Wall Test Section. NASA TM-4015. December 1987. 98 pp.

Wolf S. W. D. : Evaluation of a Flexible Wall Testing Technique to Minimize Wall Interferences in the NASA Langley 0.3 -m Transonic Cryogenic Tunnel. AIAA Paper 88-0140. Presented at the AIAA 26th Aerospace Sciences Meeting, Reno, Nevada, January 11-14, 1988 11 pp.

3.10.c. None

4.1 None

4.2 We plan to install a 3-D model support system into the 0.3 -m TCT during April 1988. An improved contraction is planned for later in 1988. New flexible walls with increased flexibility and more pressure tappings are planned.
A new drag rake system is being proposed.

4.3 Further investigate effects of sidewall boundary layer control for 2-D testing, as part of the continuing study of residual interferences. Evaluate existing procedures for 2-D testing close to Mach 1.0.
Add to the already extensive documentation of the adaptive wall system to allow easier use of the testing technique by any wind tunnel user.
Evaluate 3-D testing in the 0.3 -m TCT adaptive wall test section.

4.4 Complete CAST 10 tests as part of ONERA, DFVLR. NAE and NASA agreements. With improved flexible walls, we hope to expand our validation testing of large models (chord/height ratio = 1.0). Primarily, we will carry out 3-D validation tests with well known models.

4.5 We will be using the tunnel for numerous research programs not directly related to use of adaptive walls, i.e model surface finish and cryogenic model technology investigations.

ADDITIONAL DETAILS ABOUT 3-D TESTING

1.2 Dr. Rainer Rebstock, Mail Stop 287, NASA Langley Research Center Hampton, Virginia 23665-5225, U.S.A. Tel. (804)-865-4074 Telex 823405, Telefax (804)-865-2300

2.5.a. Half model mounted on side-wall, 3-D sting support will be installed in 1988

2.5.b. Model forces, wall pressures

2.5.c. Information will be available 4/88 (first 3-D test).

3.1.a. Streamtube formed by the aerodynamically straight walls, extended downstream by half the test section length

3.1.b. Variable X : wall deflection at each jack location (18 per wall)
Variable P : Local wall slope
Variable Q : static pressure measured on 7 rows of orifices (3 rows on both top-and bottom walls, 1 row on sidewall) 18 orifices per row at jack locations.

3.1.c. Variables P and Q extrapolated downstream in keeping with the length of the control surface

3.2 The wall adaptation for a 3-D model in a 2-D adaptive wind tunnel does not follow the procedure outlined in the Questionnaire. The strategy is as follows:
In a first step, the wall interference (blockage and upwash) is computed along the model axis. The linearized 3-D potential equation is solved with the measured variables P and Q as a boundary condition. A representation of the tested model is not required. The adaptation of the top and bottom walls is aimed at eliminating the wall interference at the model axis. That is, the deflections are calculated so as to produce equal but opposite blockage and upwash velocities at the model axis. Again, linear potential flow (2-D equation) is assumed.

3.2.c. Numerical; $M < 1$ at the walls.

3.2.d. Wall slope; integrated to obtain deflections at jack positions.

3.2.e. MicroVax II; 30s.

3.3.a. Adapted contour for similar flow case obtained from wall library

3.4.a. P : wall slope
Q : wall static pressure
X : wall deflection

3.4.f. See attached sheet number 4

3.4.h. Fully automated; manual input required to stop wall adaptation

3.5.c. Residual Mach number interference and induced absolute angle-of-attack are calculated along the 1/4 chord line. Their absolute values and/or gradient in spanwise direction will be used to assess the quality of the wall adaptation. No particular limits have been determined yet.

3.6.a. Wall interference assessment in the model region is part of the wall adaptation algorithm (see above).

3.6.b. Averaged values of $\Delta\alpha$ and ΔM are used to correct the freestream parameters.

3.7 No test so far. A side-wall mounted wing will be tested in March 88. Wing span is 50 % of test section width.

3.10.b. Rebstock, R.: Procedures for Computing Transonic Flows for Control of Adaptive Wind Tunnels NASA TM 88530, Jan. 1987.

Rebstock, R.: Capabilities of Wind Tunnels with Two Adaptive Walls to Minimize Boundary Interference in 3-D Model Tests Paper prepared for the Transonic Symposium, to be held at NASA Langley Research Center, April 1988.

4.2 Installation of sting support in test section. Tests with Space Shuttle orbiter models in Summer 88.

4.3 Development of a strategy for near sonic Mach numbers when the supersonic flow regions extend to the tunnel walls.

1.1 ADAPTIVE WALL TUNNEL - PART OF SVERDRUP TECHNOLOGY, ERGINEERING DIVISION FACILITIES LOCATED AT ENGINEERING OFFICES, 600 WILLIAM NORTHERN BLVD.
TULLAHOMA, TENNESSEE

1.2 Contacts:
Dr. Michael O. Varner, Manager Advanced Engineering Applications Branch
600 William Northern Blvd.
P.O. Box 884
Tullahoma, Tennessee 37388
Phone (615) 455-6400, ext. 402

1.3 AWAT (Adaptive Wall Automotive Tunnel)

1.4 Pilot and research facility for automotive testing

1.5 Inactive - most recent tests conducted in March 1987

2.1 Open return circuit

2.2 Rectangular test section, 0.305 mH 0.61 mW 2.44 mL

2.3 $0.05 < M < 0.20$, $1*10^6 < R_c/m < 4*10^6$

2.4.a. Impermeable; 12 longitudinal, individually contourable flexible slats covering sides and top walls. Flat floor.

2.4.b. Flexible slats contoured by 17 manually set screw jacks per slat.

2.5.a. 3D testing of bluff, non-lifting bodies. Test models rigidly fixed to floor.

2.5.b. Model pressure measurements, flow field angularity and pitot pressure.

2.5.c. One wall iteration requires manual adjustment of 204 jacks, approximately 2 hours; model/wall pressure data taken with scanivalve system, approximately 1 minute.

3.1.a. Rectangular, fixed control surface based on undeflected wall position.

3.1.b. 204 first order quadrilateral panels are used to model the exterior flow (influence coefficients). Measured quantities on walls are slat pressures and slope. These are converted to streamwise and normal slat surface velocity consistent with small deflection theory. The interior slat streamwise velocity is combined with the influence coefficients to yield the exterior normal velocity at the slat surface. Relaxation is used to combine the exterior and interior normal velocities yielding the updated slat normal velocity. The normal velocities are streamwise integrated to yield the updated slat position. Iteration is continued until the exterior and interior normal velocities at each jack location converge. In the indicated nomenclature,
P ~ Normal velocity at each jack station
Q ~ Streamwise velocity at each jack station, evaluated from slat pressures
X ~ Slat position relative to undeflected (straight wall) condition.

3.1.c. Pressure data smoothed using averaging of 10 samples, wall position data fit with cubic spline.

3.2.a. 3D, floor is plane of symmetry

3.2.b. See 3.1.6.

3.2.c. Analytical evaluation of influence coefficient using low order panel method, incompressible.

3.2.d. See 3.1.6.

3.3.a. Convergence started from deformed or straight wall positions.

3.3.b. No input required from model measurements.

3.3.c. Rectangular test section.

3.4.a. See 3.1.6.

3.4.b. Exterior flow defined by source distribution over panel representation of test section walls. Small perturbation assumption applied so that influence coefficients are calculated only once for undeflected wall position.

3.4.c. Influence functions determined analytically as in 3.4.b.

3.4.d. $\omega \sim .07$ determined by analytic experiments.

3.4.e. Free stream values based on test section entrance pressures. No corrections applied.

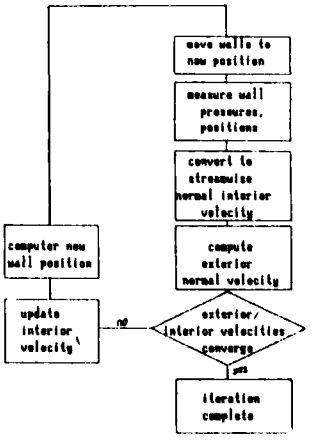

3.4.g. 3 to 7 iterations.

3.4.h. Only data acquisition is automatic.

3.6.a. 3D adaptation for 3D tests.

3.6.b. Model Δc_p .

3.7.a. 3.

3.7.b. 3D articles: 10, 20, 30 % bluff body blockage car models.

3.8.a. Boundary layer profiles at nozzle exit, CMR test section exit.

3.8.b. No flow quality measurements made to date.

3.8.c. Interference free environment confirmed by comparison of flow angularity, wall position and exterior flow calculations for 10 and 20 percent blockage models.

3.9.d. Results of adapted/unadapted are provided in Reference 1 paper (Section 3.10.a).

3.9.e. Numerical simulations on control are discussed in Reference 1 paper (Section 3.10.a).

3.10.a. Whitfield, J.D.,Jacocks, J.L., Dietz, W.E. and Pate, S.R. "Demanstration of the Adaptive Wall Concepts Applied to an Automotive Wind Tunnel," SAE paper 820373.

3.10.b. Starr, Rogers F. and Varner, M.O. "Application of Adaptive Wall to High-Lift Subsonic Aerodynamic Testing - An Engineering Evaluation", AIAA paper 84-0626.

4.3 Plans are now underway to implement the "one step" algorithm in the adaptive wall control algorithm.

4.4 Sensitivity studies were conducted in early 1987 to define wall position and pressure measurement sensitivity requirements for the adaptive wall process. Analysis of the results should be completed during 1988.

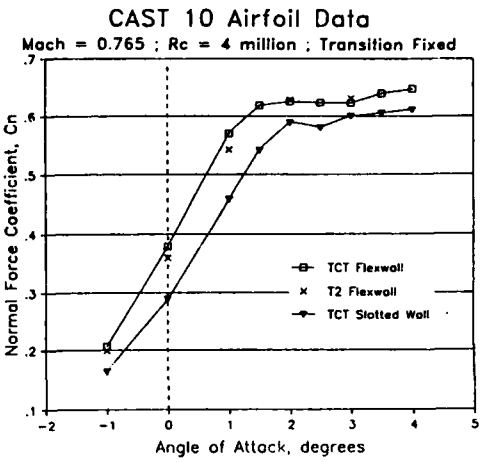

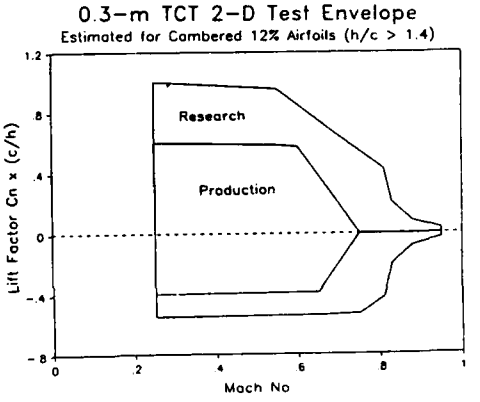

WALL ADAPTATION FLOW CHART

3-D MODEL IN TEST SECTION WITH FLEXIBLE TOP- AND BOTTOM WALLS

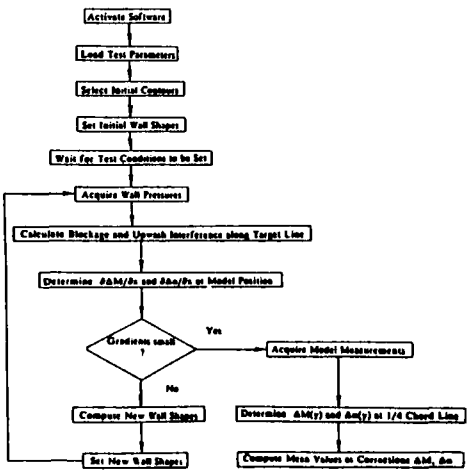

Infinite Flow Streamlining

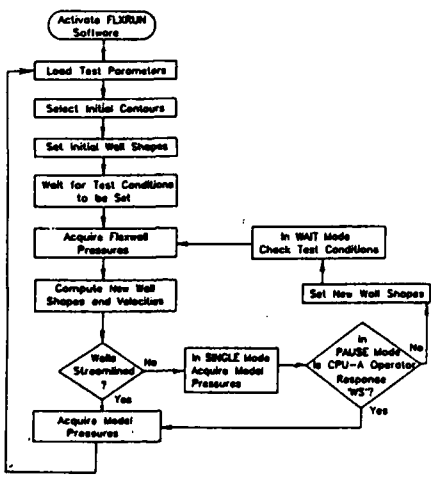

CPU-A Event Flow Chart

A-44

REPORT DOCUMENTATION PAGE

1. Recipient's Reference	2. Originator's Reference	3. Further Reference	4. Security Classification of Document
	AGARD-AR-269	ISBN 92-835-0558-1	UNCLASSIFIED

5. Originator Advisory Group for Aerospace Research and Development
North Atlantic Treaty Organization
7 rue Ancelle, 92200 Neuilly sur Seine, France

6. Title ADAPTIVE WIND TUNNEL WALLS: TECHNOLOGY & APPLICATIONS

7. Presented at

8. Author(s)/Editor(s)	9. Date
Various	April 1990
10. Author's/Editor's Address	**11. Pages**
Various	152

12. Distribution Statement This document is distributed in accordance with AGARD policies and regulations, which are outlined on the Outside Back Covers of all AGARD publications.

13. Keywords/Descriptors

Wind tunnels
Walls
Adaptive systems
Unsteady flow
Algorithms
Streamlining
Aerodynamic characteristics

14. Abstract

This report presents the results of a study by Working Group 12 of the Fluid Dynamics Panel of AGARD on adaptive-wall wind tunnels. This presentation reviews the history and state of the art of adaptive-wall technology, with regard to both the various streamlining algorithms and the existing adaptive-wall facilities; discusses limitations and open questions of adaptive-wall methods and compares them with passive-wall correction techniques; assesses residual wall interferences; presents the prospects for high-productivity and unsteady flow testing with adaptive walls; and makes recommendations for future developments. The participants in WG12 represented Canada, France, Federal Republic of Germany, Italy, Netherlands, Turkey, United Kingdom and United States.

AGARD Advisory Report No.269 Advisory Group for Aerospace Research and Development, NATO ADAPTIVE WIND TUNNEL WALLS: TECHNOLOGY & APPLICATIONS Published April 1990 152 pages This report presents the results of a study by Working Group 12 of the Fluid Dynamics Panel of AGARD on adaptive-wall wind tunnels. This presentation reviews the history and state of the art of adaptive-wall technology, with regard to both the various streamlining algorithms and the existing adaptive-wall facilities; discusses limitations and open questions of adaptive-wall methods and compares them with passive-wall correction P.T.O	AGARD-AR-269 Wind tunnels Walls Adaptive systems Unsteady flow *Algorithms* Streamlining Aerodynamic characteristics	AGARD Advisory Report No.269 Advisory Group for Aerospace Research and Development, NATO ADAPTIVE WIND TUNNEL WALLS: TECHNOLOGY & APPLICATIONS Published April 1990 152 pages This report presents the results of a study by Working Group 12 of the Fluid Dynamics Panel of AGARD on adaptive-wall wind tunnels. This presentation reviews the history and state of the art of adaptive-wall technology, with regard to both the various streamlining algorithms and the existing adaptive-wall facilities; discusses limitations and open questions of adaptive-wall methods and compares them with passive-wall correction P.T.O	AGARD-AR-269 Wind tunnels Walls Adaptive systems Unsteady flow *Algorithms* Streamlining Aerodynamic characteristics
AGARD Advisory Report No.269 Advisory Group for Aerospace Research and Development, NATO ADAPTIVE WIND TUNNEL WALLS: TECHNOLOGY & APPLICATIONS Published April 1990 152 pages This report presents the results of a study by Working Group 12 of the Fluid Dynamics Panel of AGARD on adaptive-wall wind tunnels. This presentation reviews the history and state of the art of adaptive-wall technology, with regard to both the various streamlining algorithms and the existing adaptive-wall facilities; discusses limitations and open questions of adaptive-wall methods and compares them with passive-wall correction P.T.O	AGARD-AR-269 Wind tunnels Walls Adaptive systems Unsteady flow Algorithms Streamlining Aerodynamic characteristics	AGARD Advisory Report No.269 Advisory Group for Aerospace Research and Development, NATO ADAPTIVE WIND TUNNEL WALLS: TECHNOLOGY & APPLICATIONS Published April 1990 152 pages This report presents the results of a study by Working Group 12 of the Fluid Dynamics Panel of AGARD on adaptive-wall wind tunnels. This presentation reviews the history and state of the art of adaptive-wall technology, with regard to both the various streamlining algorithms and the existing adaptive-wall facilities; discusses limitations and open questions of adaptive-wall methods and compares them with passive-wall correction P.T.O	AGARD-AR-269 Wind tunnels Walls Adaptive systems Unsteady flow Algorithms Streamlining Aerodynamic characteristics

techniques; assesses residual wall interferences; presents the prospects for high-productivity and unsteady flow testing with adaptive walls; and makes recommendations for future developments. The participants in WG12 represented Canada, France, Federal Republic of Germany, Italy, Netherlands, Turkey, United Kingdom and United States.

ISBN 92-835-0558-1

techniques; assesses residual wall interferences; presents the prospects for high-productivity and unsteady flow testing with adaptive walls; and makes recommendations for future developments. The participants in WG12 represented Canada, France, Federal Republic of Germany, Italy, Netherlands, Turkey, United Kingdom and United States.

ISBN 92-835-0558-1

techniques; assesses residual wall interferences; presents the prospects for high-productivity and unsteady flow testing with adaptive walls; and makes recommendations for future developments. The participants in WG12 represented Canada, France, Federal Republic of Germany, Italy, Netherlands, Turkey, United Kingdom and United States.

ISBN 92-835-0558-1

techniques; assesses residual wall interferences; presents the prospects for high-productivity and unsteady flow testing with adaptive walls; and makes recommendations for future developments. The participants in WG12 represented Canada, France, Federal Republic of Germany, Italy, Netherlands, Turkey, United Kingdom and United States.

ISBN 92-835-0558-1